

Technology for Development

Dr. Greg Beaucage

Professor of Chemical and Materials Engineering
University of Cincinnati, USA

What types of technology can be used to:

- 1) Solve development needs
- 2) Create Ethiopian businesses

Photovoltaics

Batteries

Non-PV Solar

Two Examples: Soil Moisture Sensors
 Solar Street Lights

35,085 undergraduate students

10,054 full-time graduate

(6,739 part-time undergraduate students

3,366 part-time graduate)

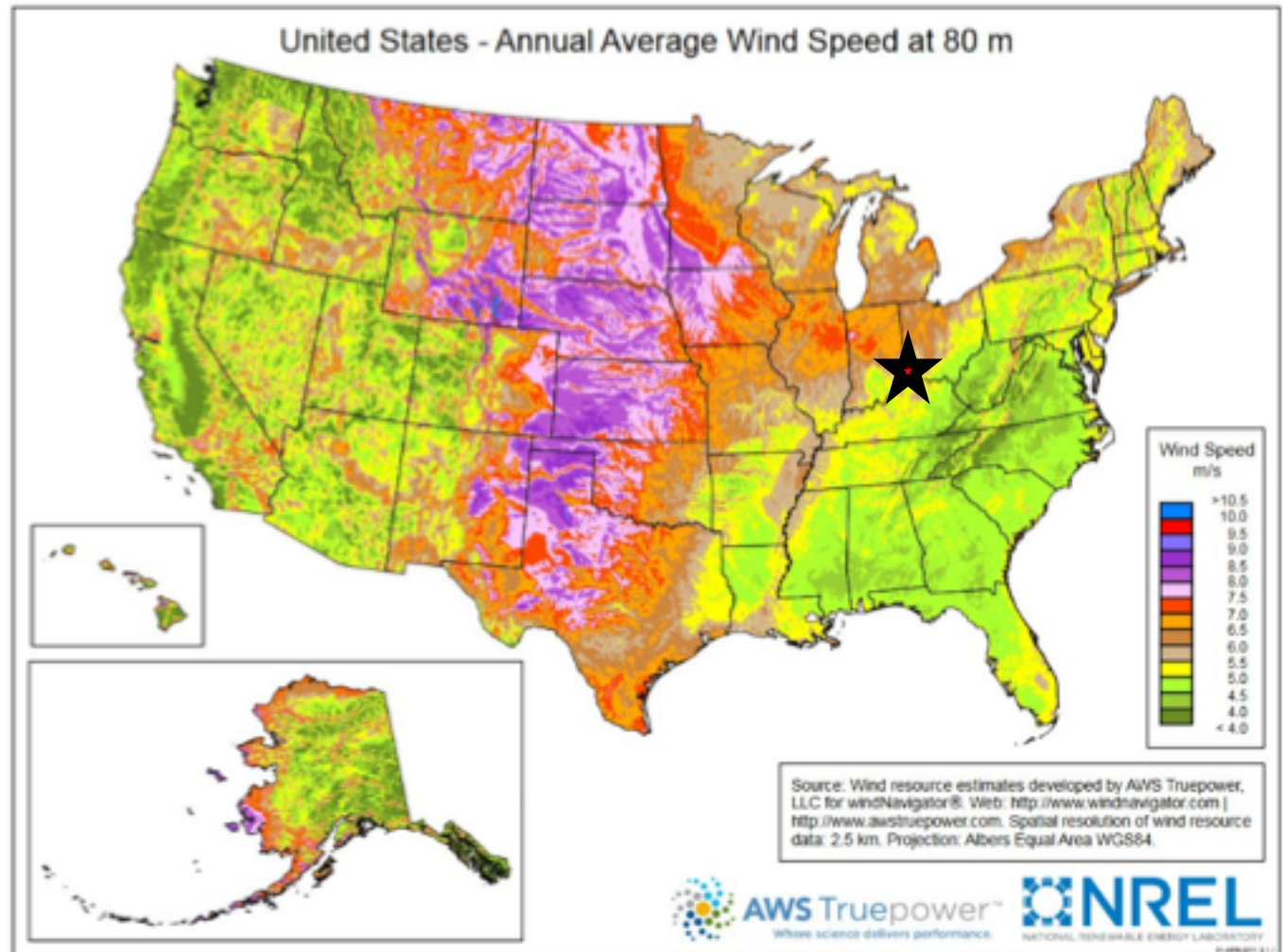
80.9 percent residents of Ohio

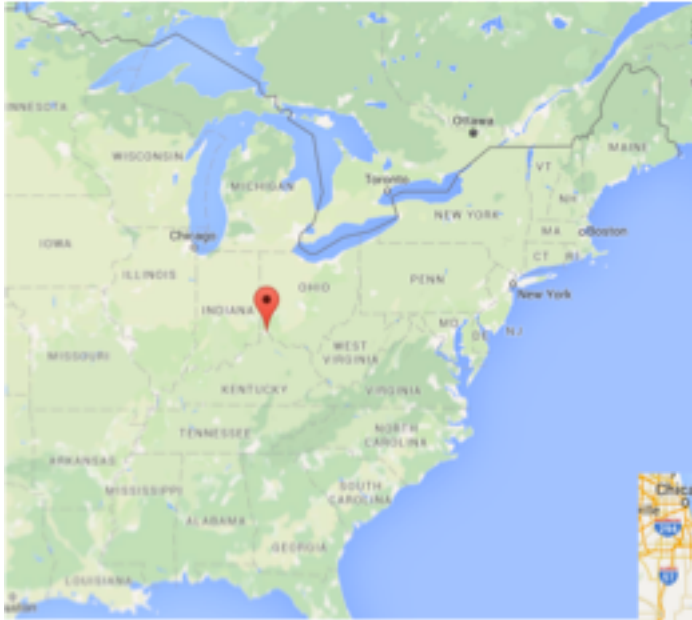
\$532.0 million External Grants (2015)

4,500 full time faculty

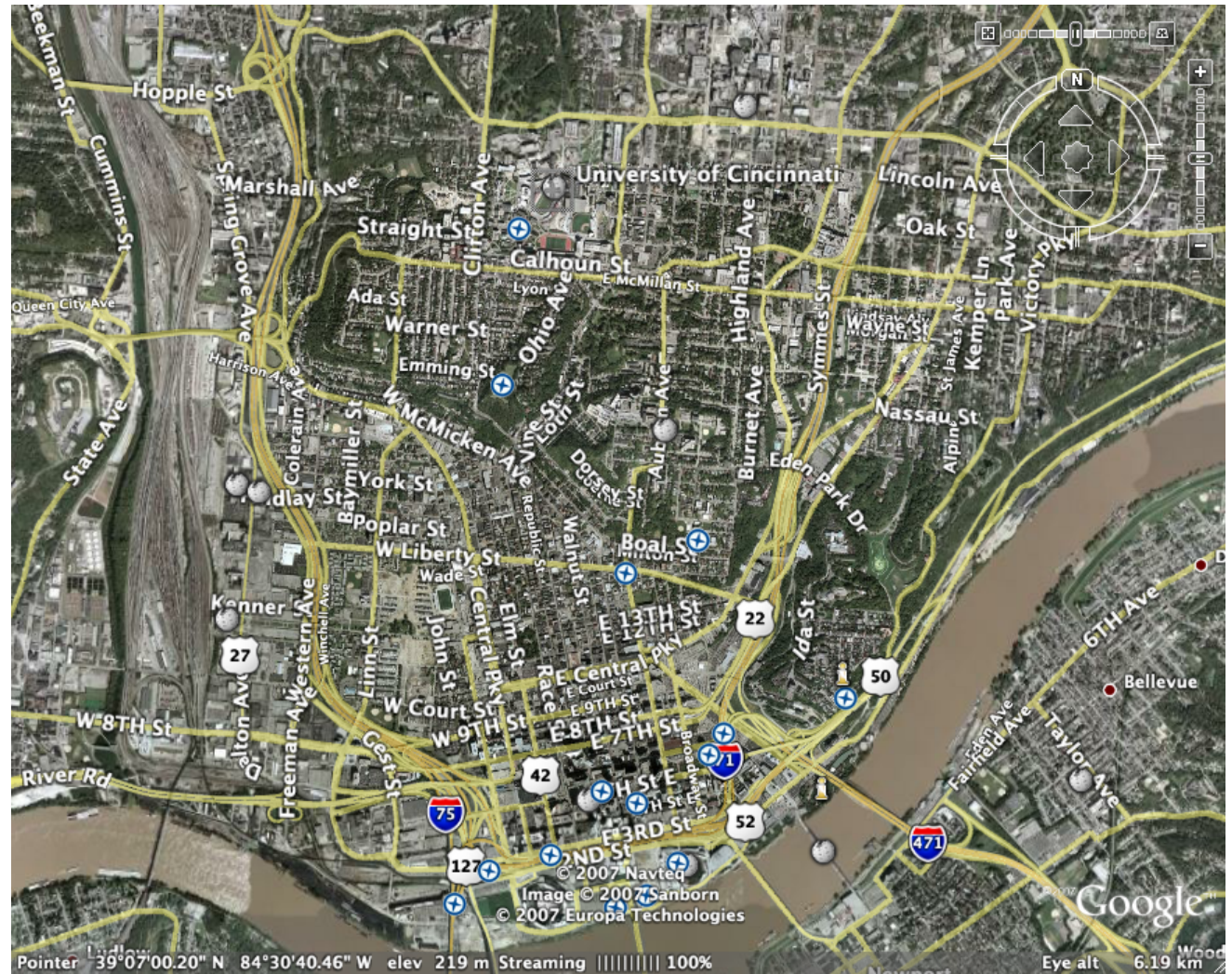


US 325,600,000
Ethiopia ~110,000,000



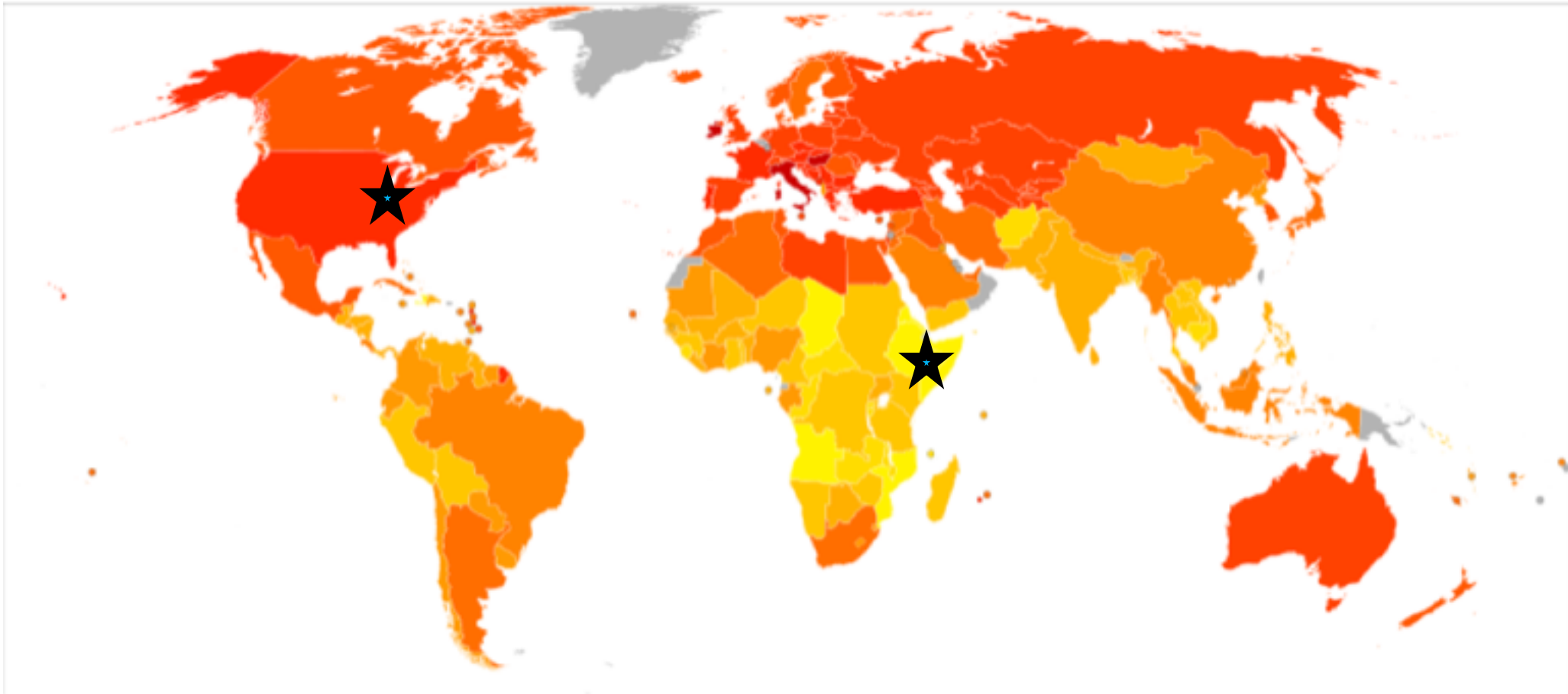


Cincinnati 2,100,000
Addis 3,400,000





Energy Consumption in the World



Most of Africa is near the equator, this distorts the size in a 2d projection.



Energy access in Africa: Challenges ahead

Abeeku Brew-Hammond

The Energy Center, KNUST, Kumasi, Ghana

Household Access, Penetration Rate

Low Income → Poor Energy “Access” → Low Income

What does “Access” mean? (Are we measuring the correct aspect?)

Grid versus “Decentralized Source”

“Modern” versus Traditional Sources of Energy

Selling state subsidized energy below cost can lead to decreased availability.

(Motivation for expansion is lost) Availability versus Affordability

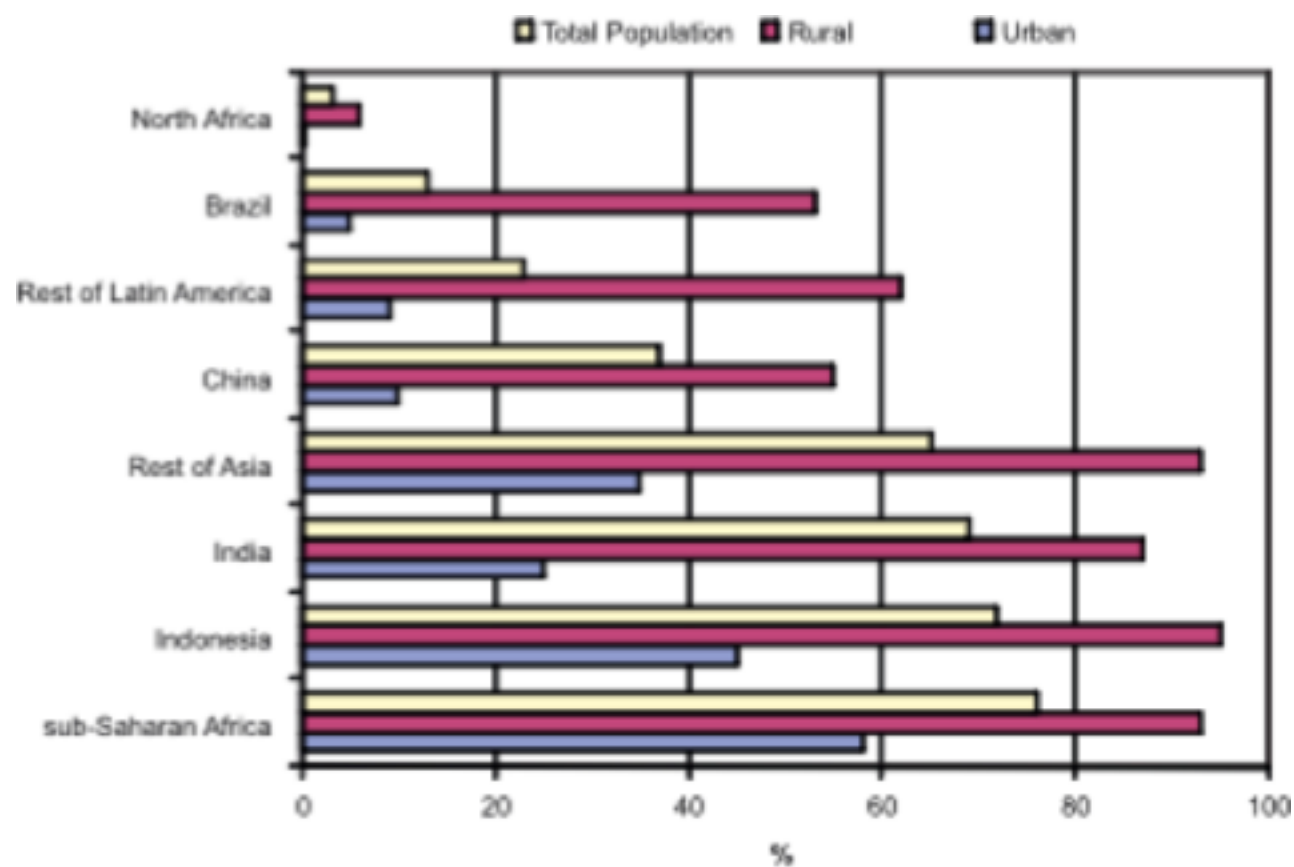


Fig. 1. Proportion of the population relying on traditional biomass for cooking.

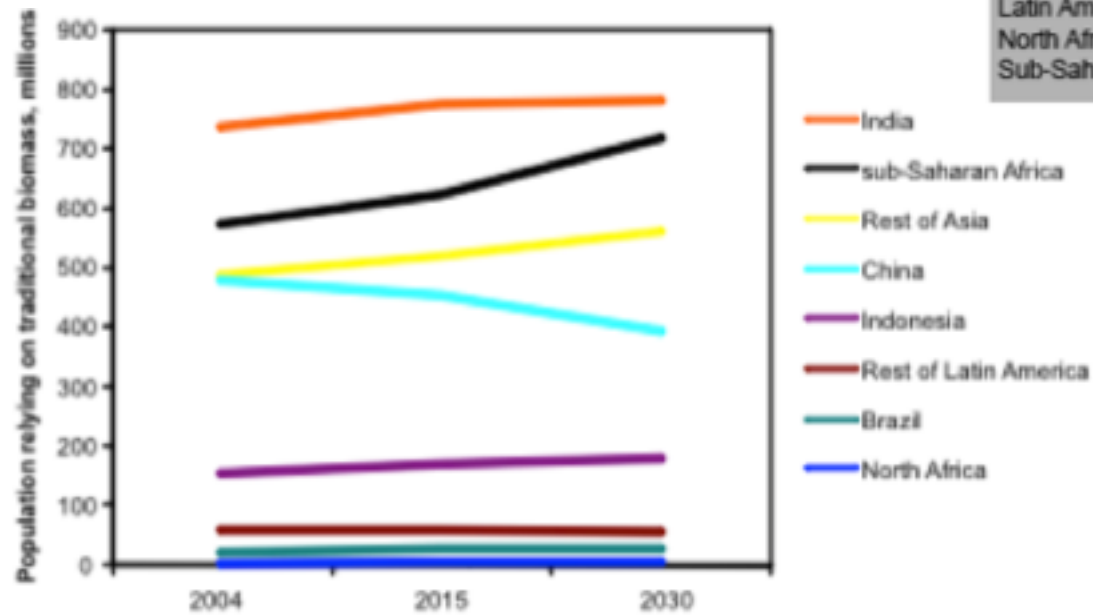


Fig. 2. Projections of people relying on traditional biomass for cooking.
Data Source: IEA (2006).

Table 1 Percentage share of population that depends on traditional biomass

Country/region	Percentage share of population
China	56
Indonesia	74
Rest of East Asia	37
India	58
Rest of South Asia	41
Latin America and the Caribbean	23
North Africa and Middle East	0.05
Sub-Saharan Africa	89

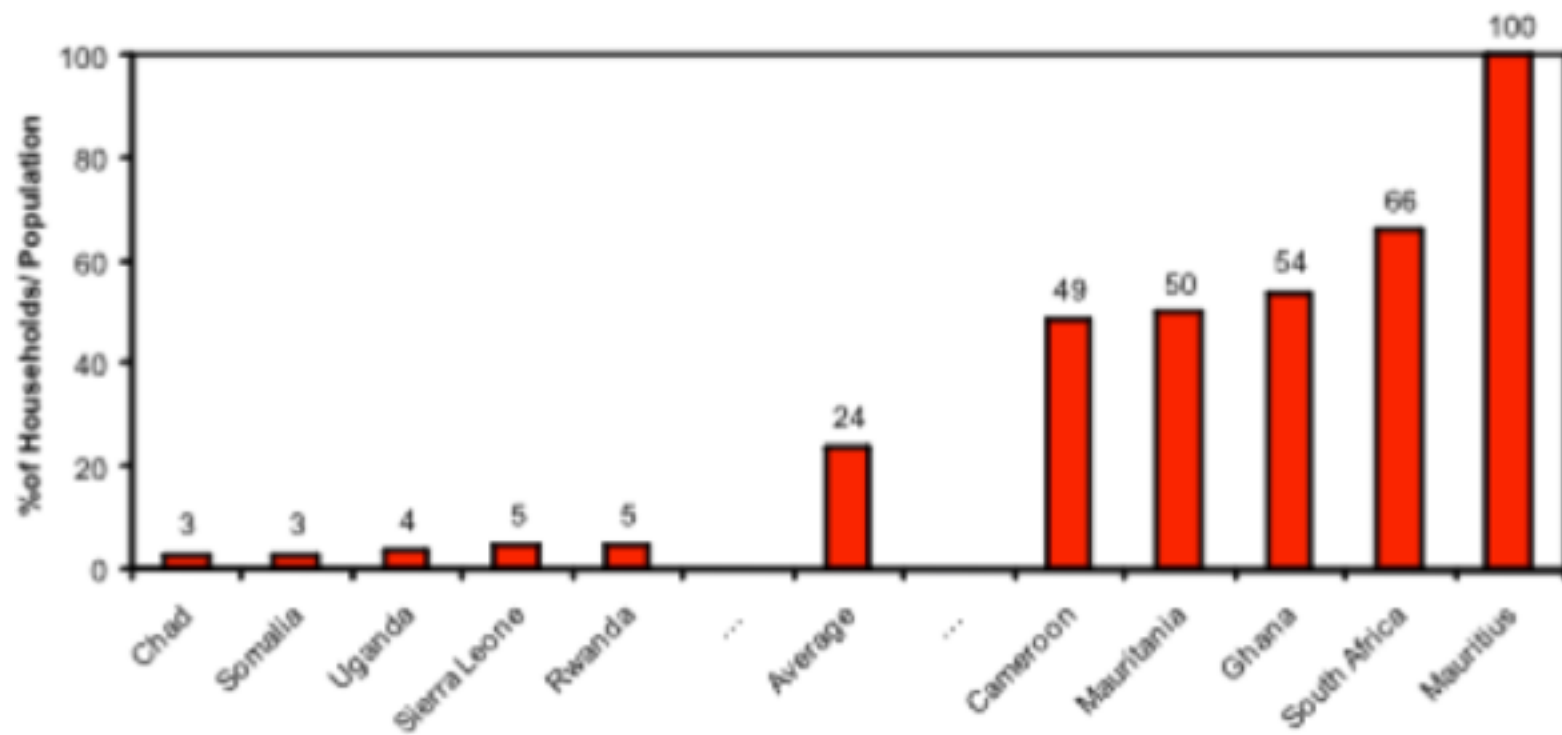


Fig. 3. Access rates for least and most electrified countries in sub-Saharan Africa.

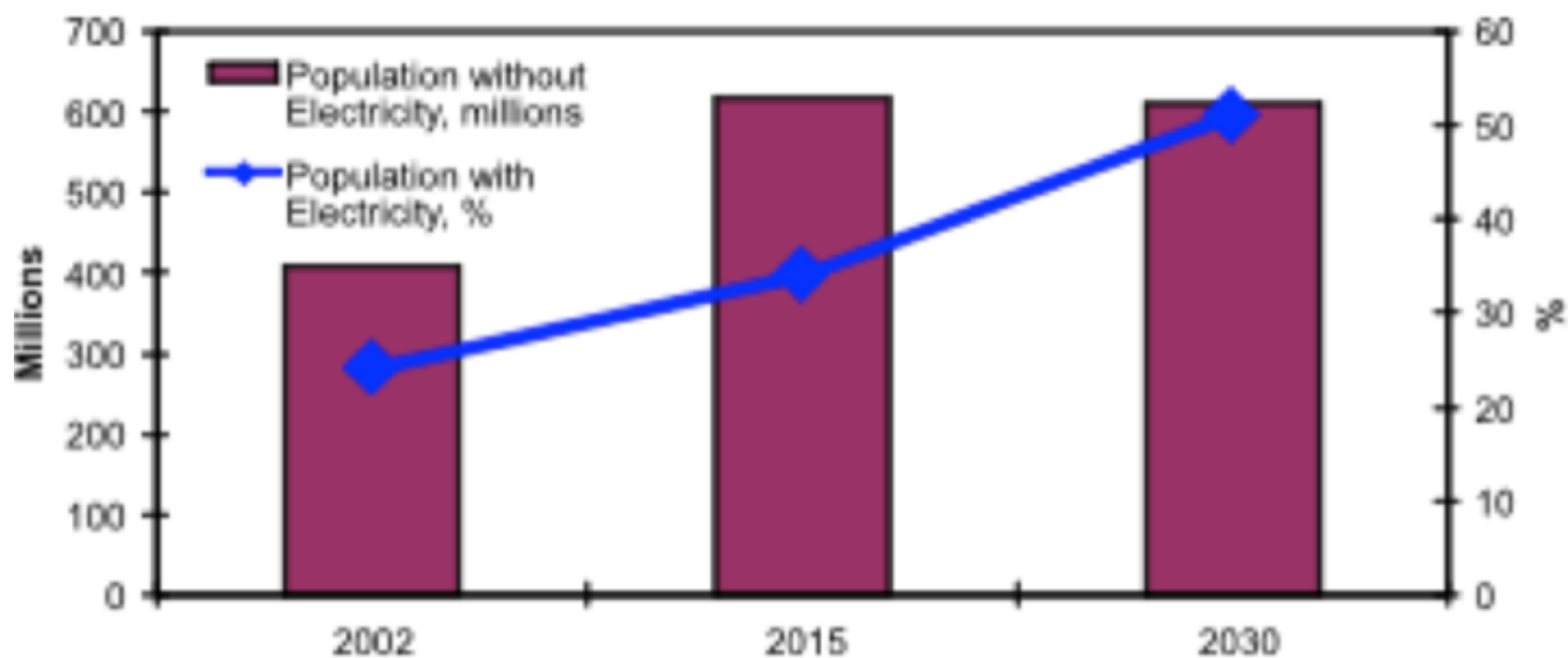
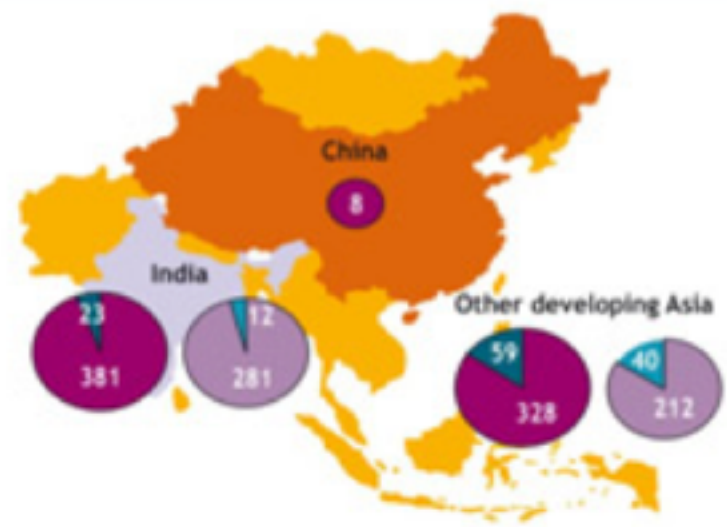
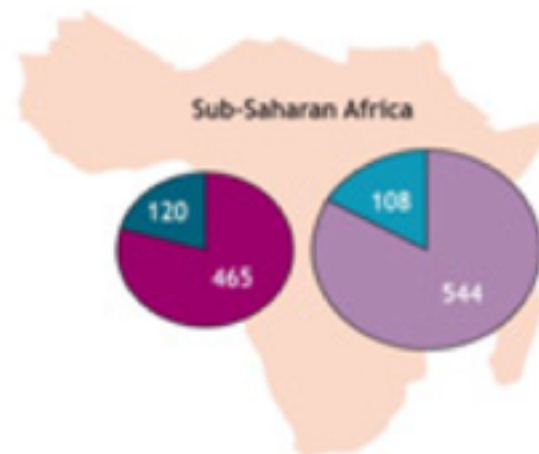
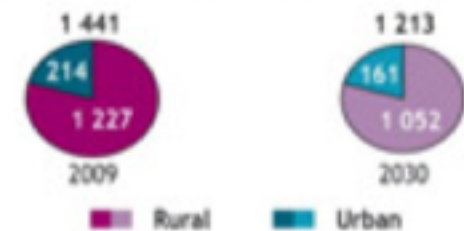


Fig. 4. Projections for population with and without electricity in sub-Saharan Africa.

Population with no electricity (millions)



World population without access to electricity



Note: not to scale

The boundaries and names shown and the designations used on maps included in this publication do not imply official endorsement or acceptance by the IEA.

About 2.8 billion people or close to half of the world's population is estimated to survive on less than US\$ 2 per day³ – the “poor” as defined by international agencies such as the IEA, World Bank, UNDP, UNEP and OECD. A key distinguishing feature of the world's poor is inadequate access to cleaner energy sources. The majority of those earning less than US\$ 2 per day rely on traditional biofuels to meet the bulk of their energy needs and have no access to electricity. Traditional biofuels meet the bulk of the energy needs of an estimated 2.4 billion people. Some 1.6 billion people have no access to electricity and a significant portion have limited or no access to cleaner and more modern fuels such as kerosene, LPG and natural gas.

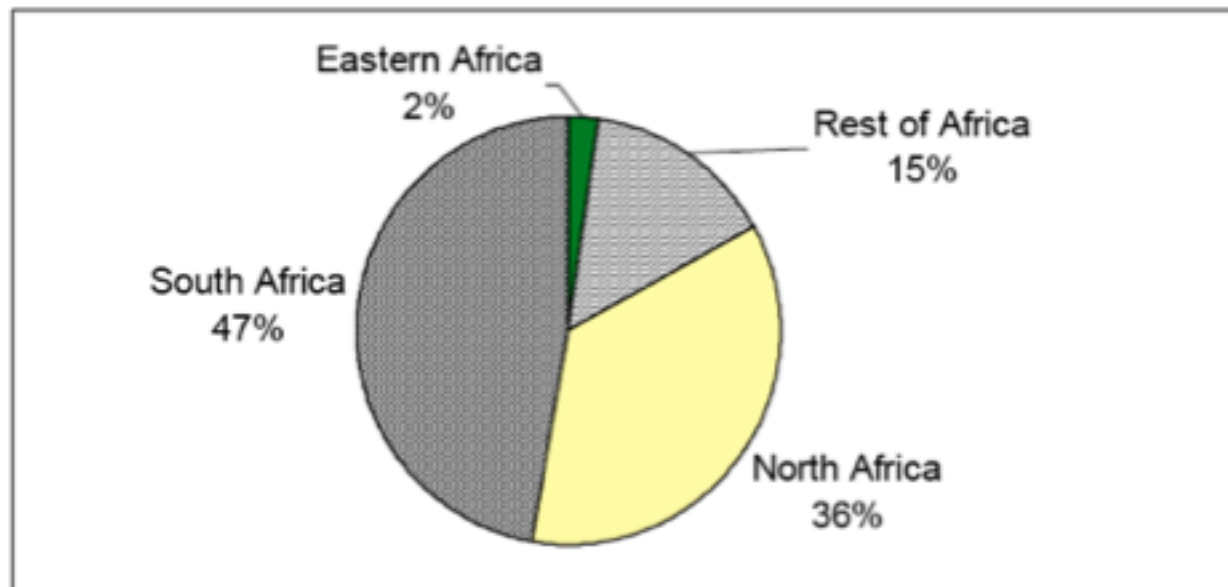
Table 1 Electricity Consumption per capita for Selected Developing Regions of the World

Region	Annual Electricity Consumption per capita (kWh) – 2000
Latin America and the Caribbean	1,528
East Asia and the Pacific	760
South Asia	323
Sub-Saharan Africa ⁹	432
Eastern Africa	60

Sources: World Bank 2003, AFREPREN 2002, UEB 1999, and UNDP 2002.

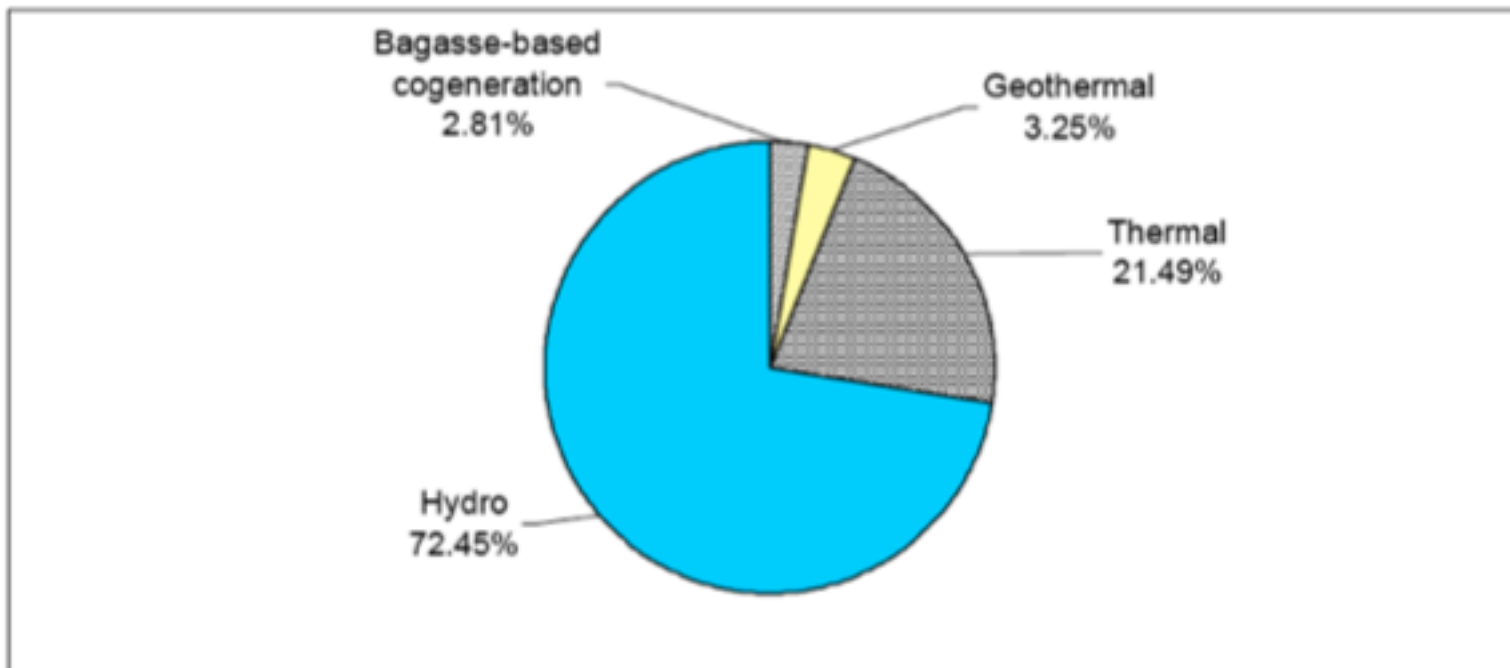
Myth	Reality
The poor do not consider access to energy a priority.	The poor may not use the term 'energy' but they often spend far more time and effort obtaining energy services compared to the richer section of the population. They spend a substantial proportion of their household income on energy for basic survival activities, that is cooking, keeping warm, and so on.
Access to electricity, grid or decentralized, will solve all the energy service needs of the poor.	People need to access a range of energy sources to satisfy their energy needs, that is cooking, heating, transport, and communication.
Poor people cannot pay for their energy services.	Many poor people pay more per unit of energy than the better off, partly due to inefficient conversion and lack of integrated planning.
Only rural areas suffer from lack of access to energy.	Poor people in urban and peri-urban areas also suffer from lack of access to energy services, and their numbers are likely to increase. It is predicted that almost 61% of the world's population will be living in urban and peri-urban areas and services are not expected to grow commensurately.
Commercial energy required to satisfy the needs of the poor is significant with respect to total global energy consumption.	Reaching the poor with basic modern energy services as envisioned in the MDG Energy Vision would increase global commercial energy consumption by about 900 TWh (terrawatt-hour) per year, which is less than 1% of the global energy demand.

Figure 1 **Share of Installed Capacity in Africa (2000).**



Sources: World Bank 2003, IEA 2002.

Figure 2 **Electricity Production in Eastern Africa (2000)**



Sources: Karekezi et al (eds), 2002b, AFREPREN, 2002, IEA, 2002

Table 2 Electrification Levels in Eastern Africa

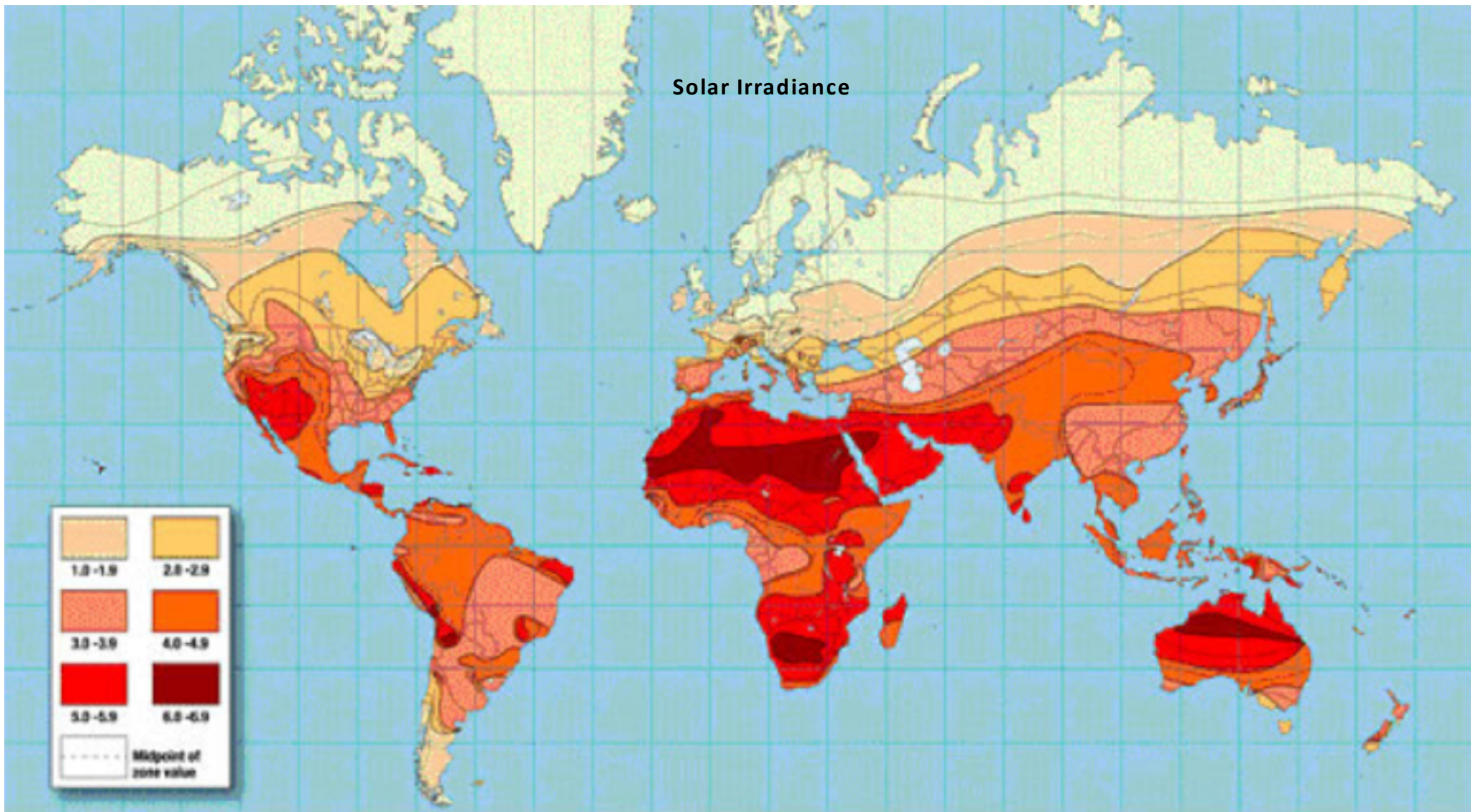
Country	National Electrification levels (%) - 2001
Ethiopia	2
Uganda	4
Kenya	6**
Tanzania	10*
Mauritius	100

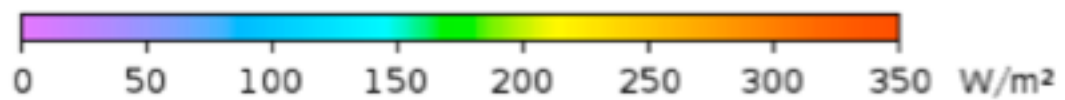
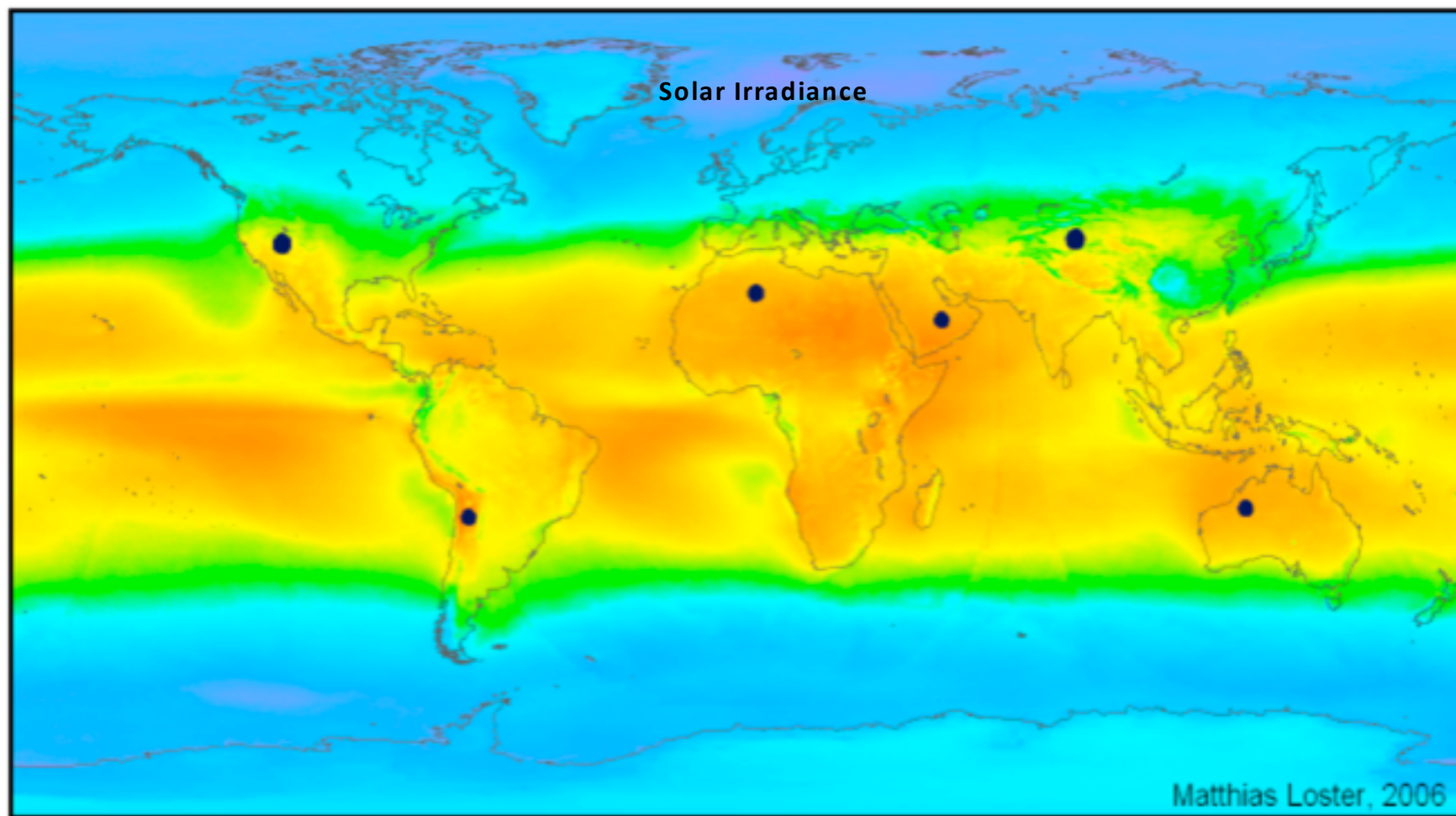
* 2002 data

** This figure only refers to the proportion of households connected to the electricity grid and may differ significantly from other sources which indicate the proportion of electrified population derived from the total number of grid electricity customers.

Sources: AFREPREN, 2002, Karekezi et al (eds), 2002b; Republic of Kenya, 2002; Okumu, 2003; Kinuthia, 2003

Solar Irradiance



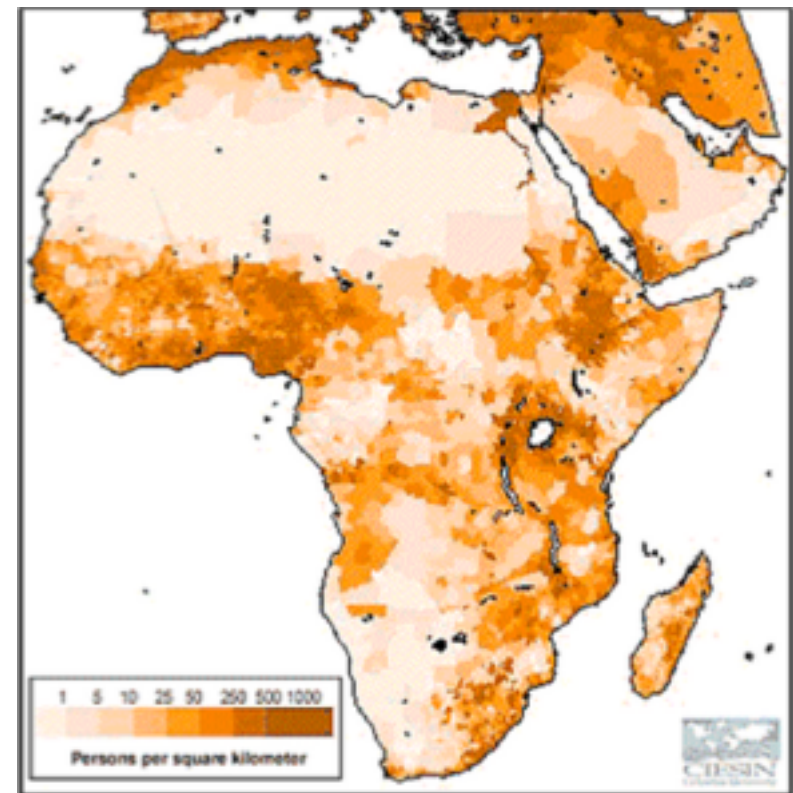
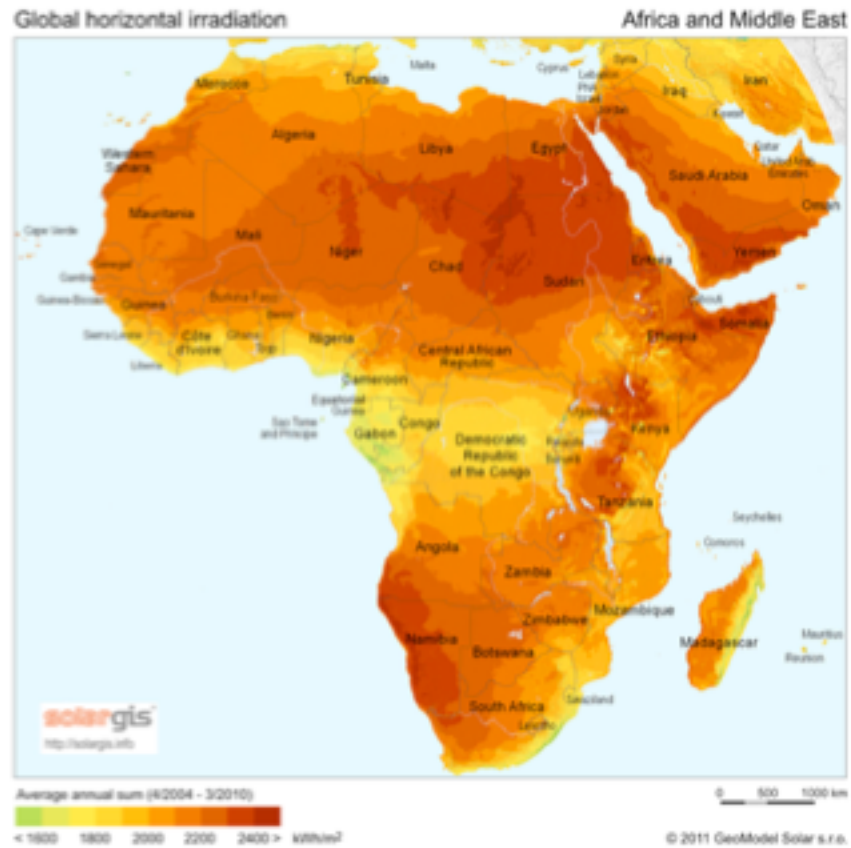


$$\Sigma \bullet = 18 \text{ TWe}$$

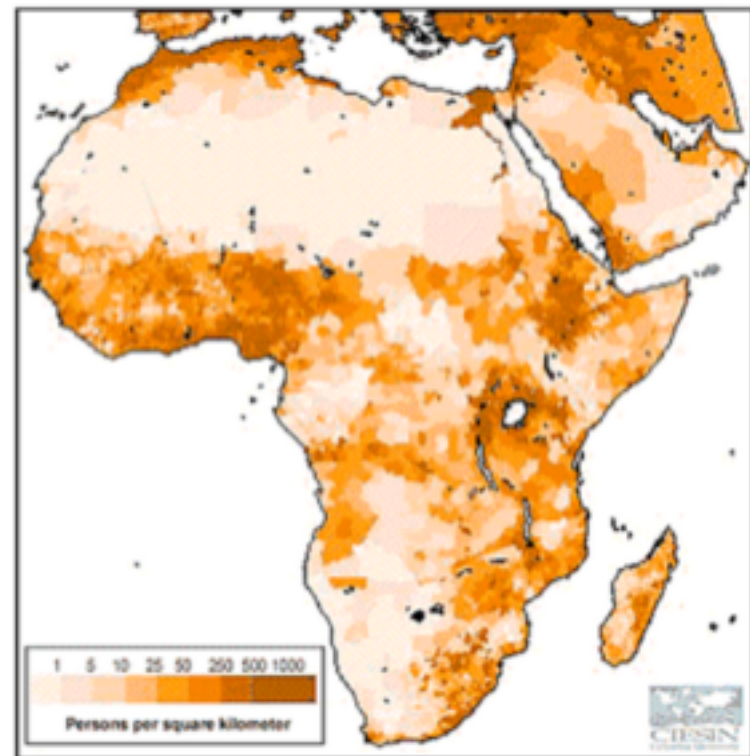
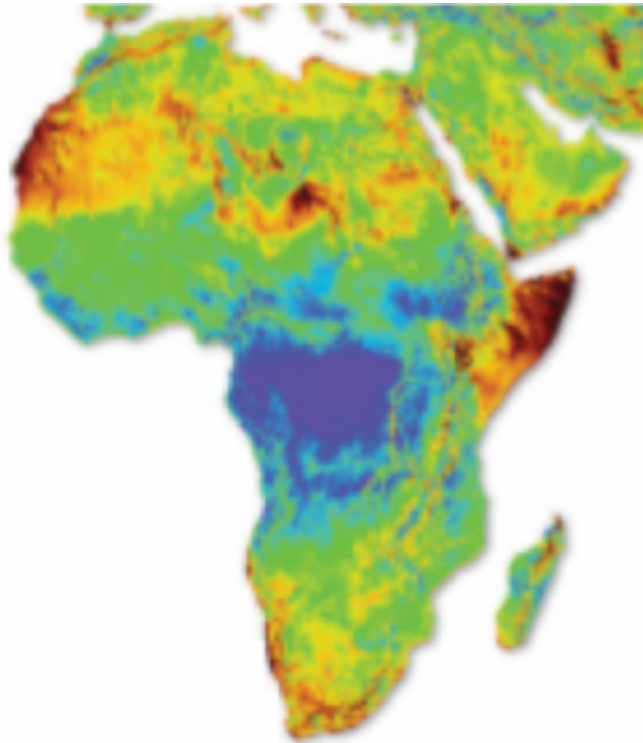
Africa and Middle East



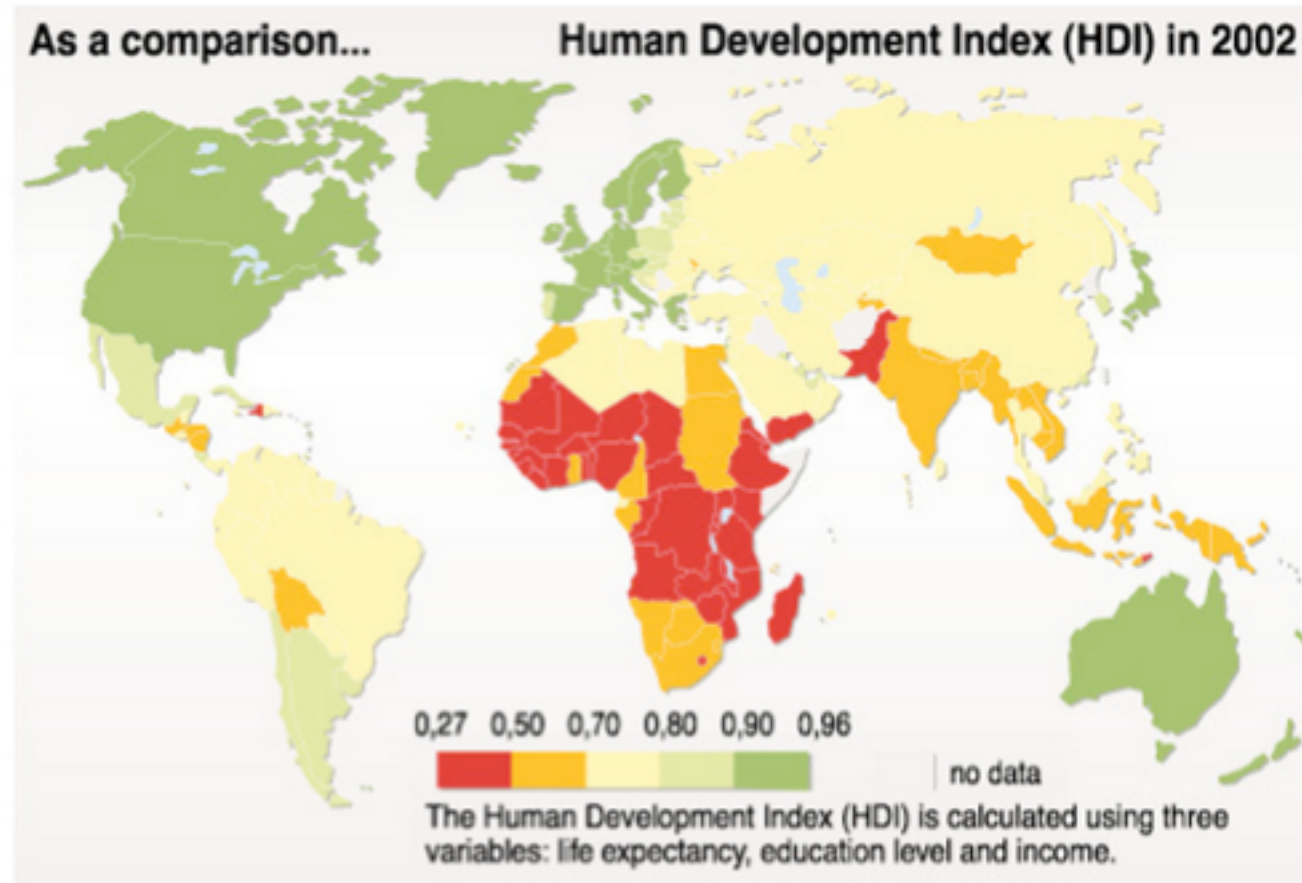
Solar Irradiance compared to Population Density



Average Wind Power Potential compared to Population Density

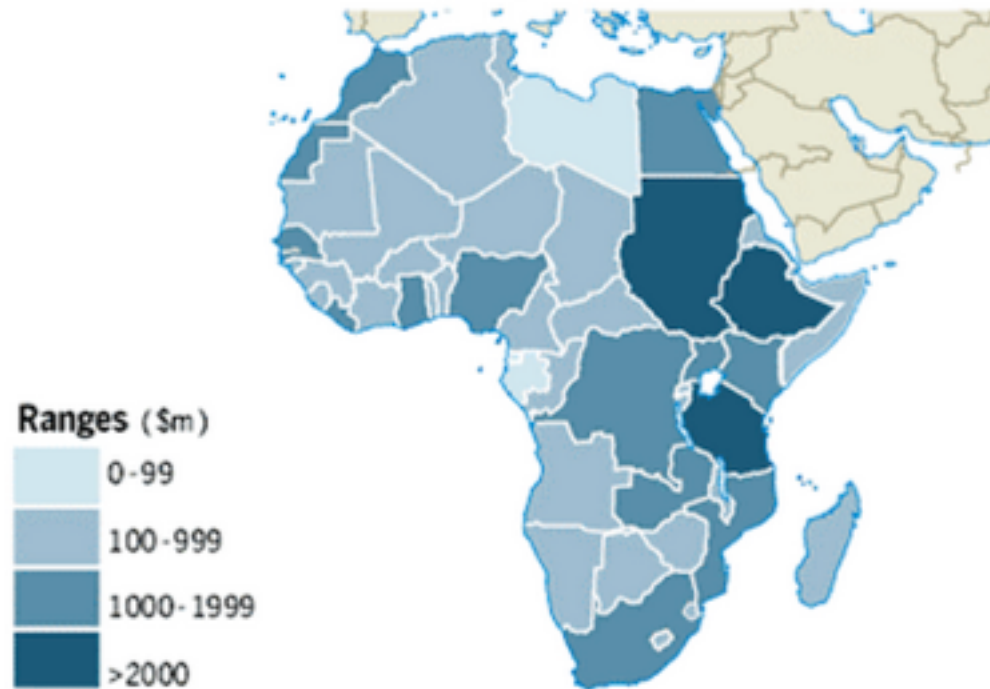


How the west views Africa as a whole.



How the west views Africa as a whole.

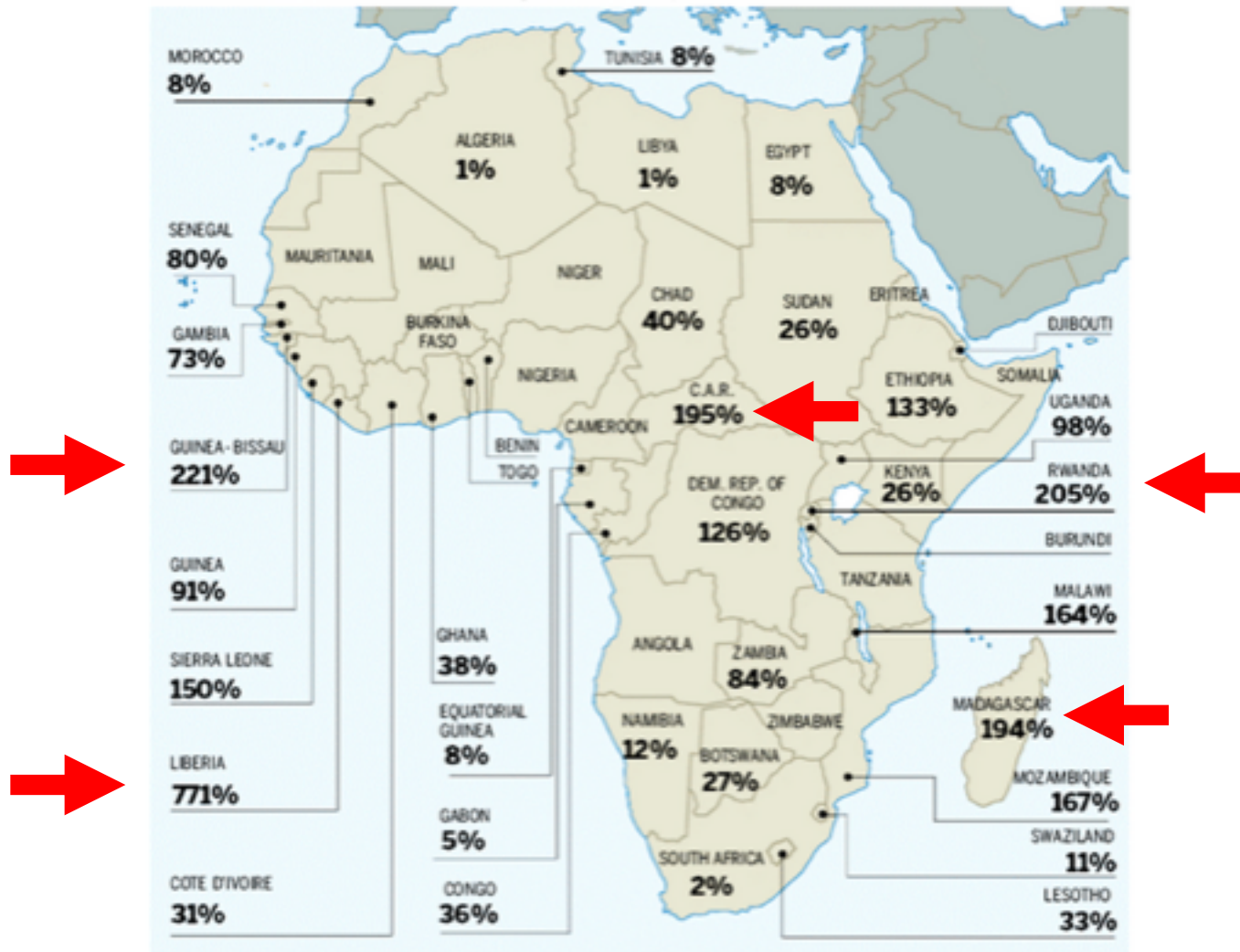
Levels of net official aid received, 2008 (\$m)



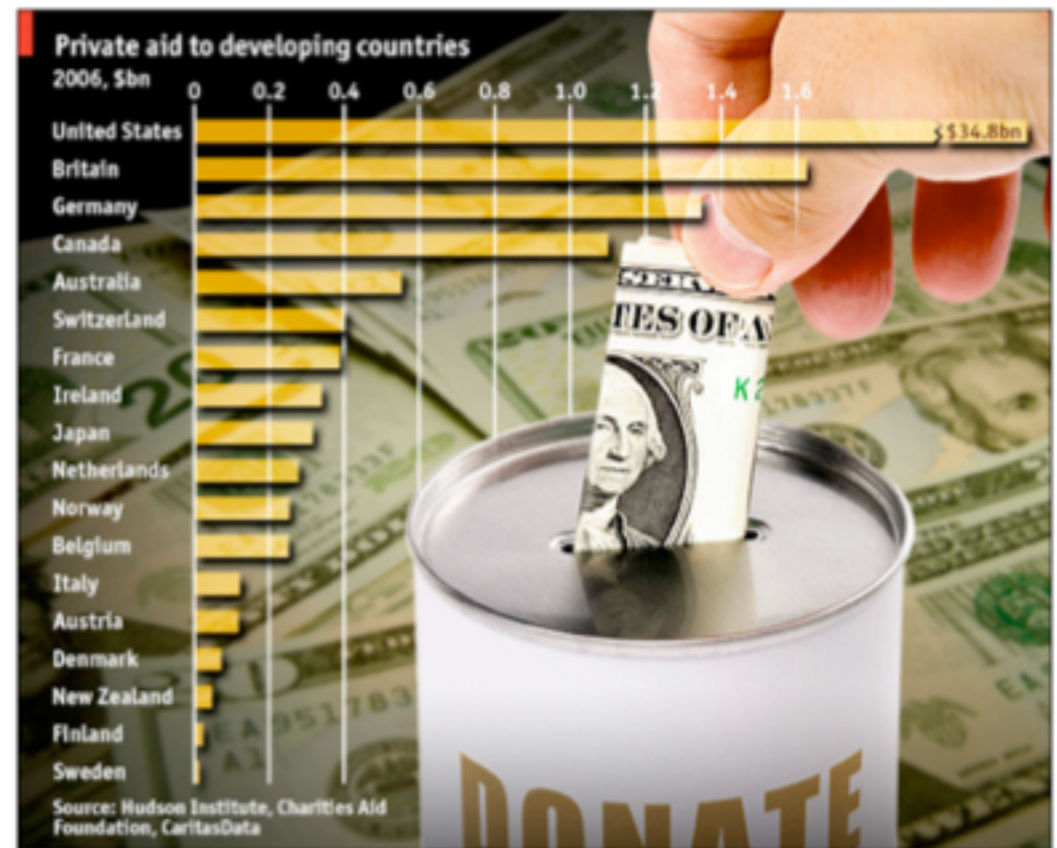
(source)

Africa's dependence on aid

Net official aid received as a % of government expenditures, 2008

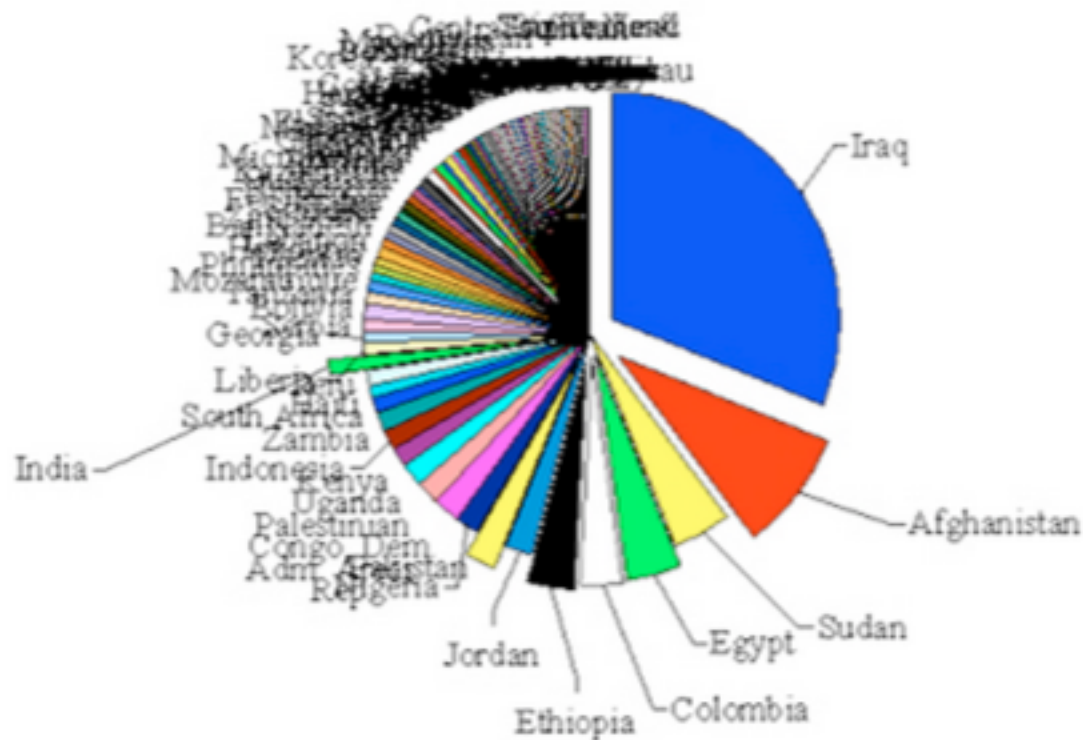


How the west views Africa as a whole.



How the west views Africa as a whole.

Here's a somewhat silly yet telling graph showing US development aid by destination country:



What is Photovoltaic (PV) Solar Energy

A typical off-grid installation

A typical solar well

How to manufacture a solar panel

How silicon PV works



Figure 6.8 Selling solar in Kenya (EPIA/Free Energy Europe).



Figure 5.1 Remote and independent: a stand-alone system for a farmhouse.



Figure 5.1 Remote and independent: a stand-alone system for a farmhouse.

- 1) PV Panels
- 2) Other sources of Power: Wind Turbine, Diesel or Gasoline Generator, Hydropower
- 3) Charge Controllers
- 4) Battery Bank
- 5) AC Inverter/Direct DC systems
- 6) Fuse box(es)
- 7) Appliances/Loads

Process for design of an off-grid PV system

1) Determine the needed AC and DC loads

Typically DC is for lighting and any RV type appliances that inhabitants are willing to accept as substitution for AC appliances (you loose ~50% of the power in conversion to AC)

The entire system is designed around the anticipated load for an off-grid system and typically it is difficult or impossible to increase this load with the existing system once it is built. So off-grid systems are inflexible in terms of the load. Peak load controls the cost of every component in the system.

2) The total cost (including cost to the environment per kW-hr from the PV system needs to be carefully compared to alternatives

Increased insulation and energy conservation

Other solar energy sources of heating

Biomass and wood heat etc.

3) Once the AC and DC loads are determined the voltage of the PV/Battery system is decided based on the load, distance of transmission from PV to batteries, available battery and PV module voltages and associated costs, step-up or step-down needed for appliance voltage and the associated loss, inverter/charge controller costs.

4) Location for the PV modules must be determined and the solar irradiance must be determined to estimate the power output of the PV modules, the optimal location and the optimal tilt of the PV modules. The need for a tower or other support structures, distance of transmission from PV modules to batteries and needed cabling must be determined.

5) A ventilated housing for the battery bank must be constructed (produces H₂ and O₂ and contains sulfuric acid, batteries may require routine maintenance.

Process for design of an off-grid PV system

- 1) Determine the needed AC and DC loads
- 2) Compared to alternatives
- 3) Voltage of the PV/Battery system
- 4) Location for the PV modules
- 5) A ventilated housing for the battery bank must be constructed
- 6) A detailed plan for burying power cables, grounding and other safety issues needs to be developed. PV modules CAN NOT BE TURNED OFF so consideration of means to block the modules during repair and routine maintenance needs to be considered.
- 7) A plan for wiring of the facility needs to be developed and the costs assessed including appropriate circuit breakers and grounds.



Figure 5.1 Remote and independent: a stand-alone system for a farmhouse.

- *Without battery storage or inverter.* A PV module can supply a DC load directly. A simple example is the type of small solar fountain that floats on a garden pond: the PV sends its current directly to a DC motor driving a pump. The fountain plays only when the sun shines. A more serious application is water pumping for village water supply, irrigation, or livestock watering, where a PV array supplies a DC motor driving a pump that delivers water to a holding tank whenever the sunlight is sufficiently strong.
- *With inverter, without battery storage.* This type of system produces AC power from a PV module or array and is appropriate when AC electricity is useful at any time of day. For example, AC motors are sometimes used for pumping schemes in preference to DC motors because of their rugged reliability and cheapness (although this must be set against the cost of inverters).



Figure 5.2 Off the grid: PV water pumping for a Moroccan village (EPIA/Isofoton).



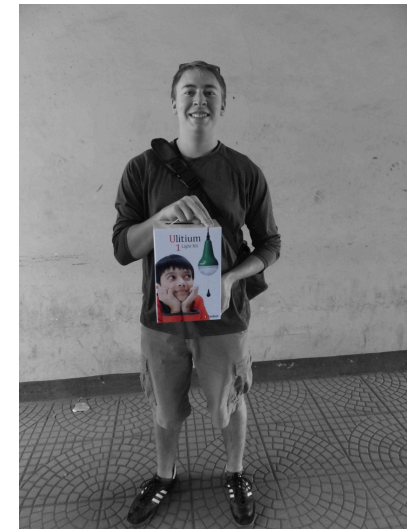
- *With battery storage, without inverter.* Low-power consumer products such as solar calculators and watches come in this category. So do solar-powered garden lights. Moving up the power scale, a variety of electrical loads, including low-energy lights and a small TV, may be run directly from DC batteries. Many of the solar home systems (SHS's) used in developing countries to supply a small amount of PV electricity to individual families are of this type. A typical SHS comprises a battery, a charge controller and a single PV module (see Figure 1.12). Other examples are DC systems for remote telecoms, security systems, and medical refrigeration.

Figure 1.12 This PV module powers a solar home system in Bolivia (EPIA/BP Solar).

Simple Solar Lights at Elementary School 20 km from Haramaya



Simple Solar Lights at Elementary School 20 km from Haramaya



Simple Solar Lights at Elementary School 20 km from Haramaya



Simple Solar Lights at Elementary School 20 km from Haramaya



Solar Well at Elementary School 20 km from Haramaya

Well # 1
10 m, dry



Well # 2
30 m, almost dry



Solar Well at Elementary School 20 km from Haramaya



Batteries

Batteries are the most important component for an off-grid PV system

Deep-Cycle Lead-Acid Batteries are needed
(different than car batteries)

Car Battery: Large current for short times not substantially discharged
PV battery smaller currents for longer times with routine discharge cycles
(In developing countries car batteries are sometimes used due to availability)

Self-discharge rates of 3%/month

Coulombic or charge efficiency 85% percent of charge put in that comes out

Voltage efficiency 90% of voltage when discharged

Energy efficiency 75% Coulombic * Voltage

Flooded or Wet cell: liquid electrolyte must be topped up with DI water, need ventilation for H₂, O₂
versus

Sealed or Valve-regulated cell: gas tight valve allows gas to escape on overpressure H₂, O₂ make water internally
Gel electrolyte sealed battery.

Sealed batteries require low maintenance but are more expensive

Batteries

Battery capacity: Ampere Hours (Ah), product of current supplied and time

12V battery that provides 20 A for 10 hr is a 200 Ah battery (at 20°C at the 10 hour rate)
(slower discharge leads to larger capacity, lower temperature leads to lower capacity 1% per degree)

For PV we are interested in 100 hour rate

A 200 Ah battery at 12V can provide 2.4 kWh total energy storage.

The PV array must produce more voltage than the battery in order for the system to work.
So we need to know how the voltage of the battery varies during charging and discharging.

Batteries

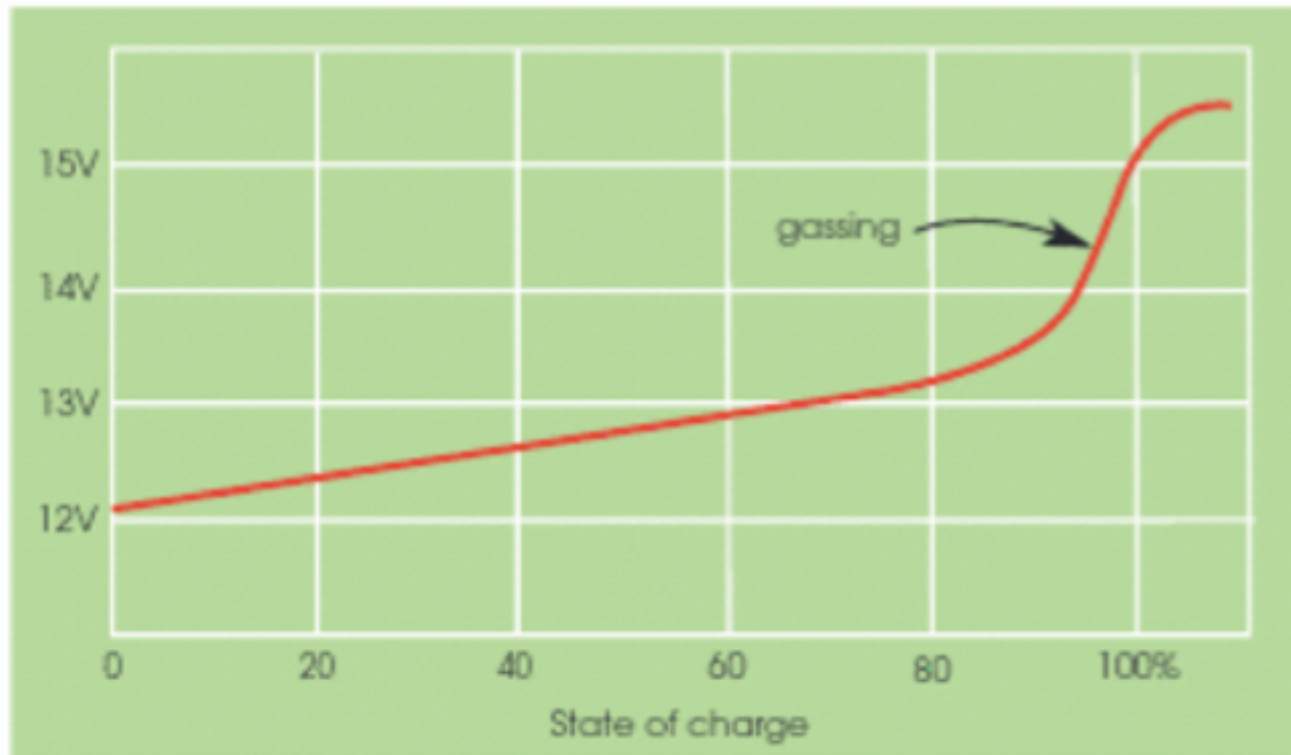


Figure 5.3 Typical charging characteristic of a 12V lead-acid battery.

Batteries

12V 200 Ah battery shown for constant current discharge
20 A for 10 hours or 2 A for 100 hours

11 V is where damage to battery occurs

For extended discharged state sulphation occurs: lead sulphate crystals form on the plates

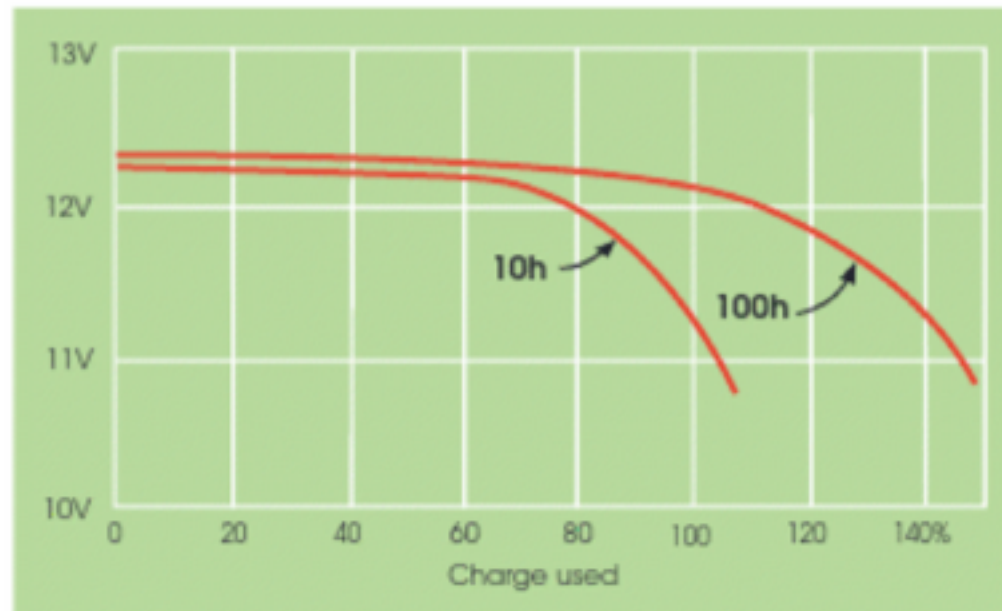


Figure 5.4 Typical discharge characteristics of a 12V lead–acid battery.

Charge Controllers

Control the flow of current from PV array into the battery bank
and from battery bank to loads

Prevent overcharging of the batteries and over-discharging when demand exceeds supply by disconnecting PV array above 14V for float charging, 14.4 for boost charging and 14.7 for equalization charging in a flooded 12 V battery.

Prevent excess discharging by disconnecting the load when voltage falls to 11 V.
Protects the batteries.

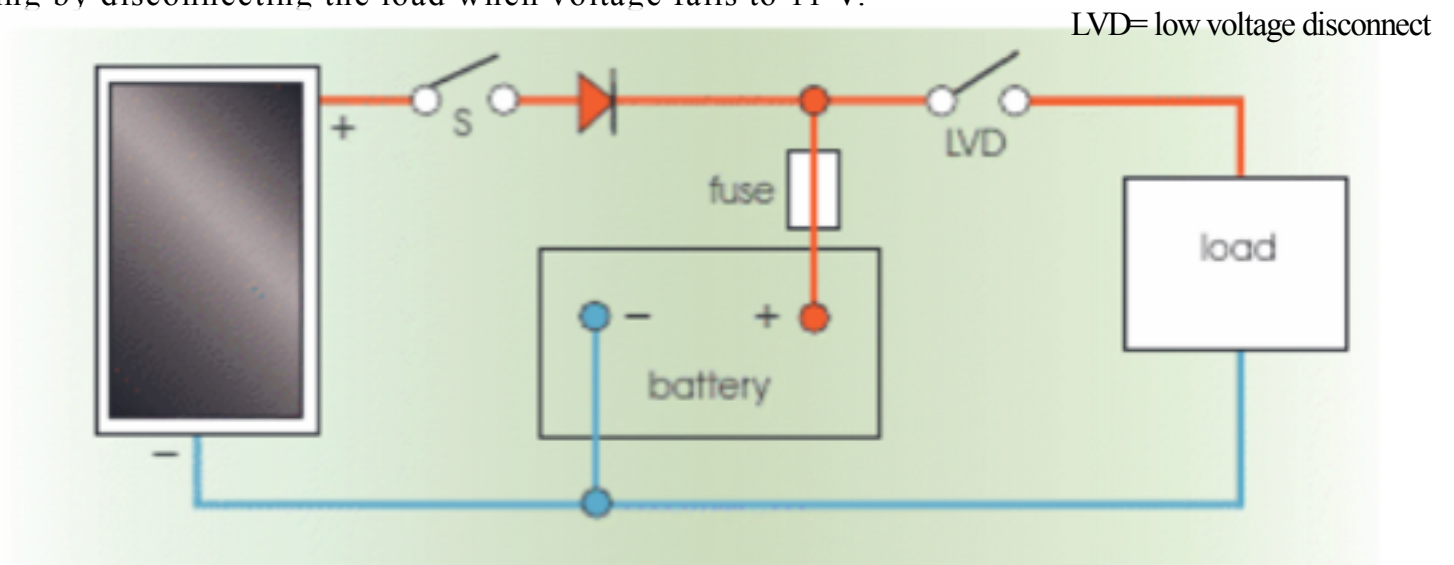


Figure 5.6 Series charge control.

Charge Controllers

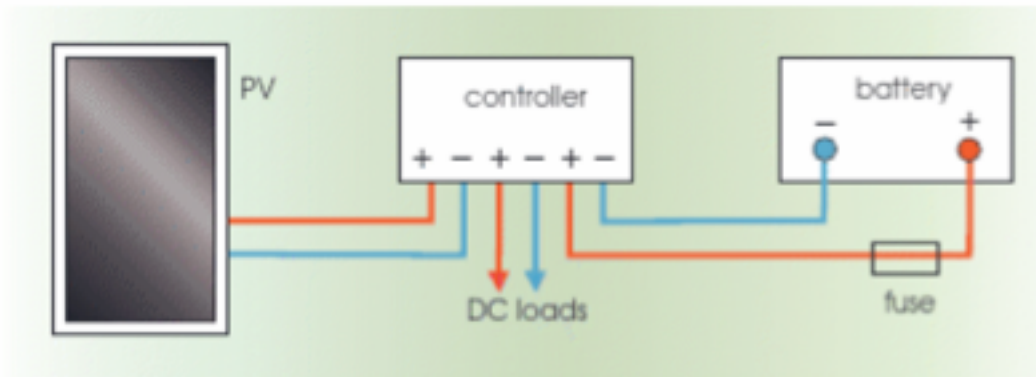


Figure 5.5 A simple scheme for a low-power solar home system (SHS).

- choice of flooded or sealed lead-acid batteries.
- protection against reverse polarity connection of PV modules or batteries.
- automatic selection between boost, float, and equalisation charging regimes, depending on the estimated state-of-charge (SOC) of the battery bank.
- protection against battery overcharging and deep discharging, excessive load currents, and accidental short-circuits.
- prevention of reverse current at night.
- display of such parameters as battery voltage and/or estimated SOC, PV and load currents, and warning of impending load disconnection.



Figure 5.9 This MPPT controller can control a 12 or 24V system with PV array power up to 500W, and MPP voltages up to 100V. With dimensions 19 x 15 x 7 cm, it weighs 900g (Steca Elektronik GmbH).

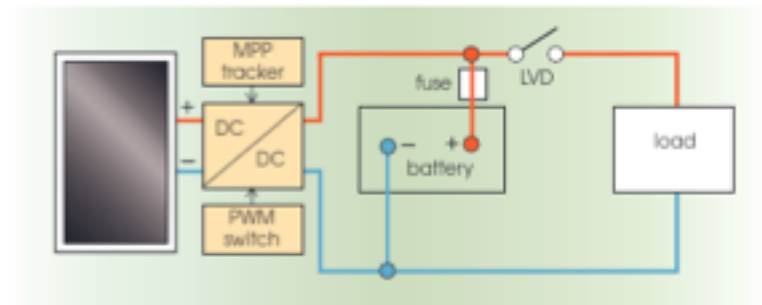


Figure 5.10 Extracting the most from a PV array: the MPPT charge controller.

Inverters

AC offers flexibility to use “normal” household devices

Grid connected inverters must match frequency and phase to match the grid

Off-grid is self-commutated

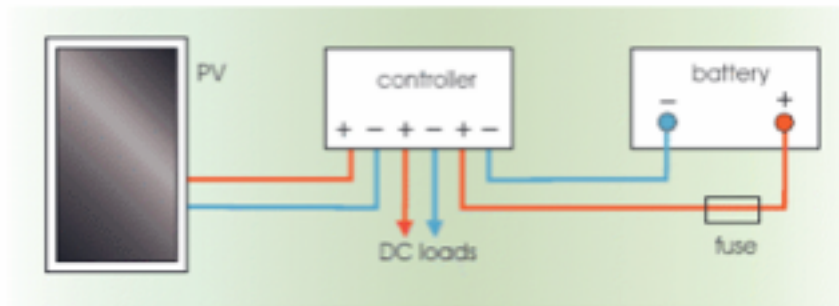


Figure 5.5 A simple scheme for a low-power solar home system (SHS).

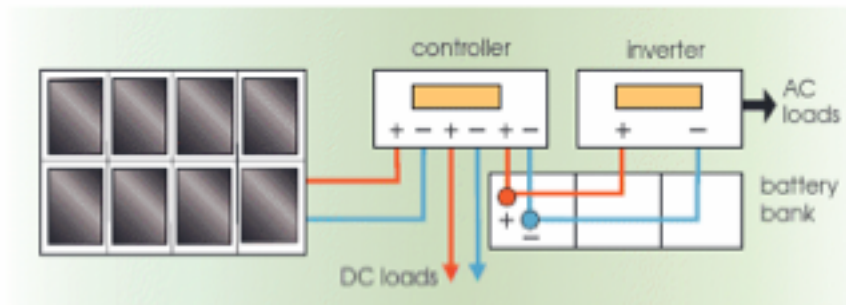


Figure 5.11 Typical connections for a mid-range stand-alone system.

- The PV is an array rather than a single module.
- A battery bank replaces a single battery, giving more storage capacity.
- The charge controller has an electronic display (or a set of coloured LEDs) indicating parameters such as battery voltage, SOC, PV current and load current.
- The inverter, connected directly to the battery bank, also indicates its operating conditions.

Inverters



Figure 5.12 This family of inverters covers the power range 200W to 2kW (continuous), with system voltages of 12, 24, and 48V (Steca Elektronik GmbH).

- A power rating sufficient for all loads that may be connected simultaneously.
- Accurate control of output voltage and frequency, with a waveform close to sinusoidal (low harmonic distortion), making the AC supply suitable for a wide range of appliances designed to run off a conventional electricity grid.
- High efficiency at low loads, and low standby power draw (possibly with automatic shut-down when all loads are turned off), to avoid unnecessary drain on batteries.
- Ability to absorb or supply reactive power in the case of reactive loads.
- Tolerance of short-term overloads, particularly caused by motor start-up.

Inverters

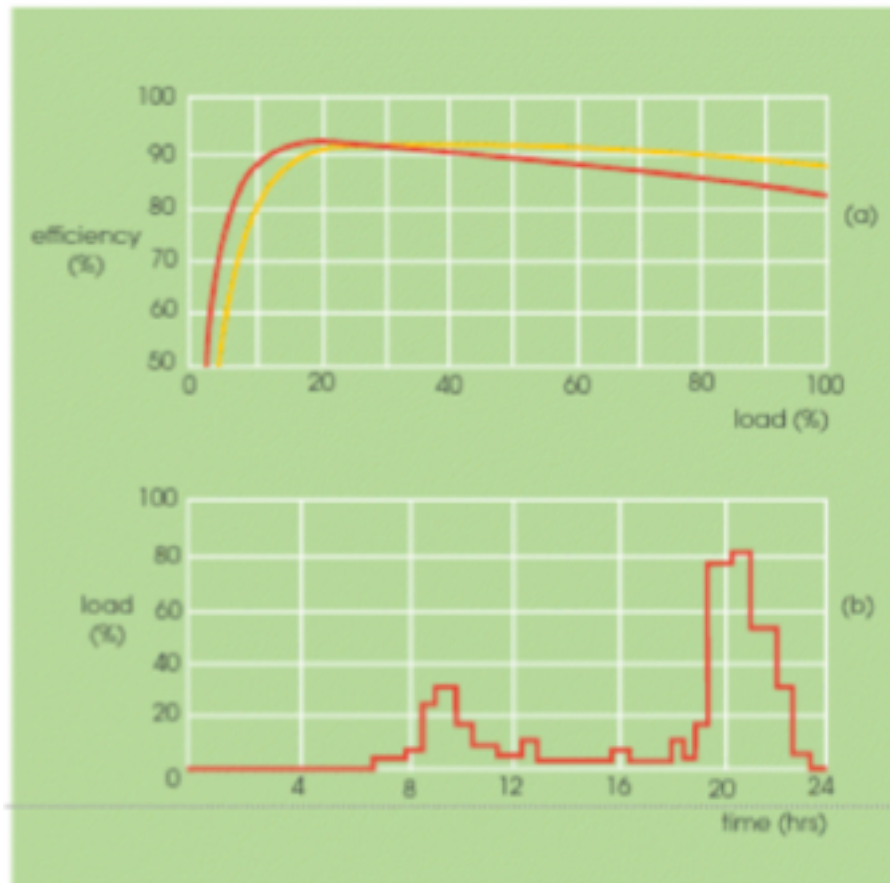


Figure 5.13 (a) Efficiency curves for two types of inverter; (b) a daily load profile for a solar home.

High Inverter Efficiency means
smaller battery bank and PV array

Red = low frequency transformer
Yellow = high frequency transformer

Hybrid Systems



Figure 5.1 Remote and independent: a stand-alone system for a farmhouse.

Diesel-PV Hybrid System

- It may be too expensive, in terms of the PV array and battery store, to provide a sufficiently reliable service with photovoltaics, especially where solar insolation is highly seasonal. For example, does it make economic sense to install a PV system that can cope with occasional high load demands in winter when sunlight is in short supply? A hybrid system with a back-up diesel generator may be a better option.
- Diesel engines are very inefficient when lightly loaded, giving poor fuel economy. Low running temperatures and incomplete combustion tend to produce carbon deposits on cylinder walls (glazing), reducing service lifetimes. It is advisable to run engines above 70–80% of full rated output whenever possible. But a lone diesel generator that can cope with occasional peak demands is likely to run at low output much of the time. Better to turn it off and use PV and the battery bank when electricity demand is low. The diesel can boost charge the batteries if necessary, at a high charging rate.
- In addition to rising fuel costs, unpleasant fumes, and the noise of diesel engines, it may be difficult to obtain reliable fuel supplies and engine maintenance services in remote locations. PV needs no fuel and, provided the battery bank is looked after properly, should be low-maintenance.
- If an existing diesel installation needs upgrading, the addition of PV may be a good solution. Being essentially modular, PV may be added in small stages, raising system power capacity in line with increasing demand.

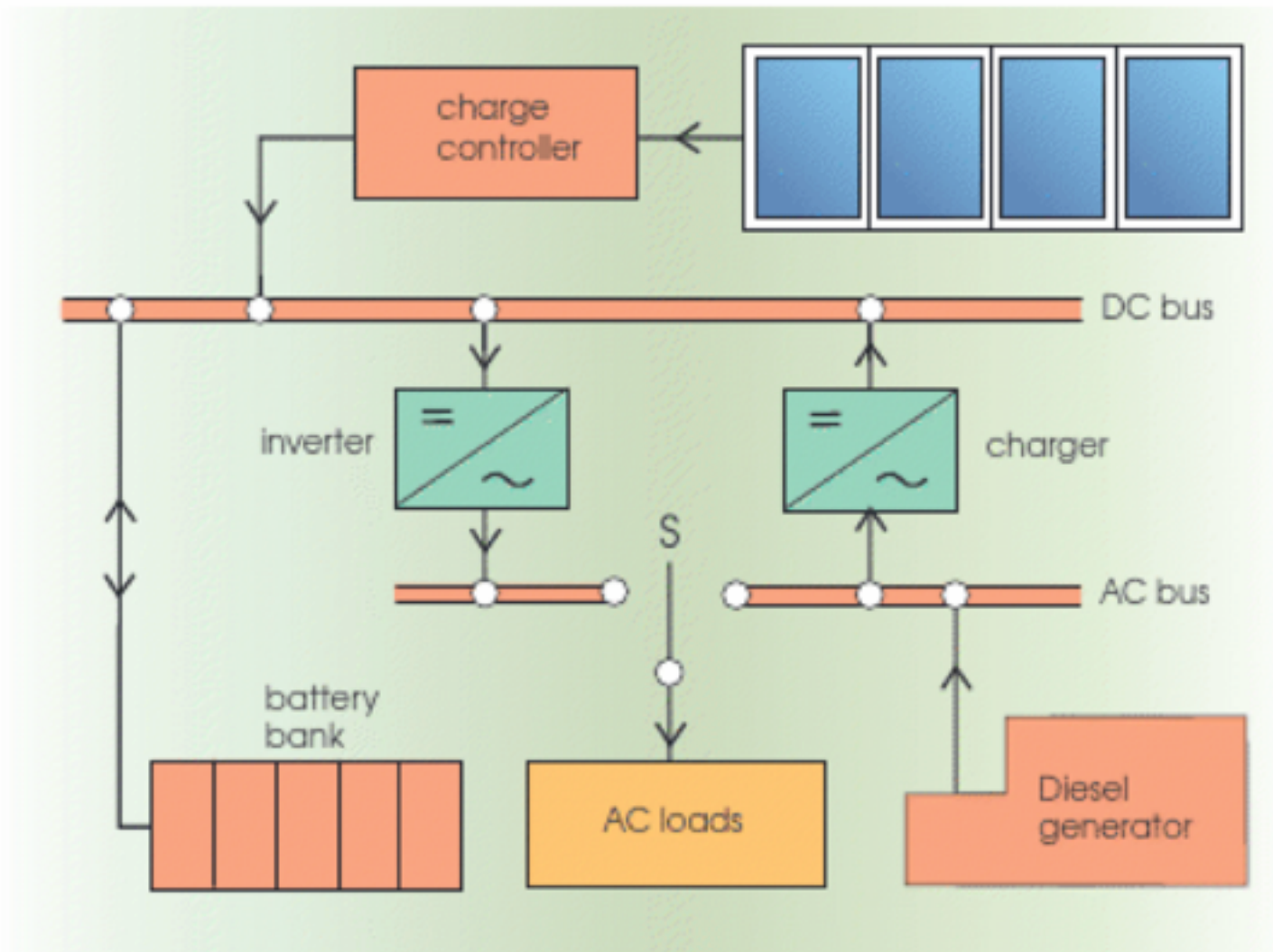


Figure 5.14 A PV–diesel hybrid system.

System Sizing

Sizing problem is the most difficult of system design

Estimate the total amount of electricity required on an average day.

Appliance		Power (W)	No.	Average hrs/day	Average Wh/day
Light		11	8	3	260
TV		60	1	4	240
Computer		60	1	3	180
Refrigerator		80	1	24 (on-off)	500
Kettle		1000	1	0.2	200
Microwave Oven		700	1	0.4	280
Food Mixer		400	1	0.15	60
Washing Machine		800	1	0.6	480
				Total	2200

Figure 5.15 Appliances and energy requirements for a stand-alone system.

– in this case 2200 Wh (2.2 kWh) per day. This is the amount of electrical energy to be supplied by the PV system and is fairly typical for a solar home system (SHS) that includes a good range of modern appliances (by contrast, simple SHSs in developing countries based on a single PV module and a battery often provide just 200–300 Wh/day). In this case the homeowners wish to use standard AC appliances, so an inverter must be included in the system.

System Sizing

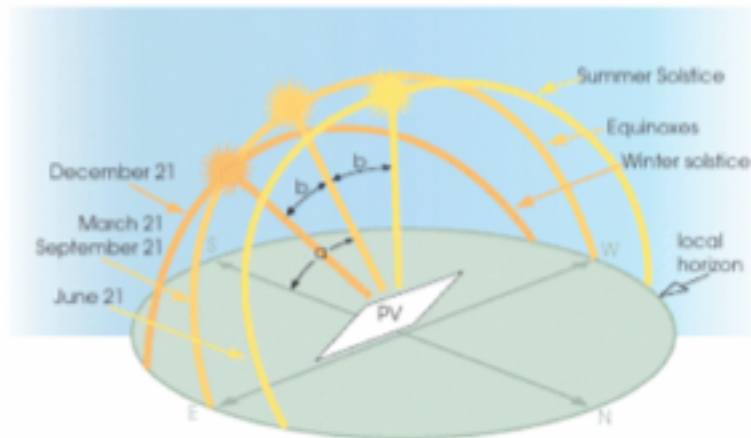


Figure 3.8 Solar trajectories.

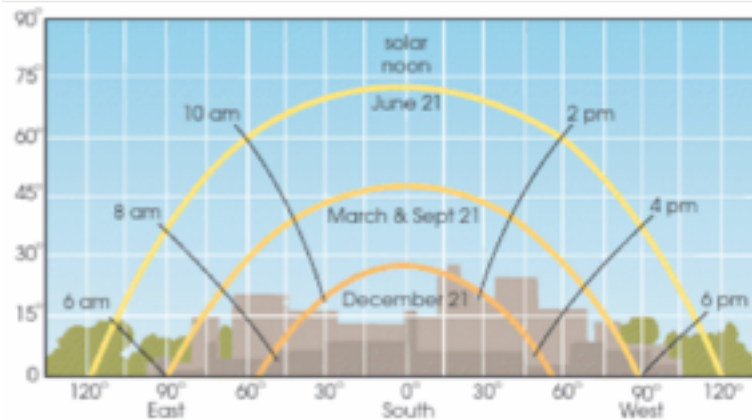


Figure 3.9 Shading effects.

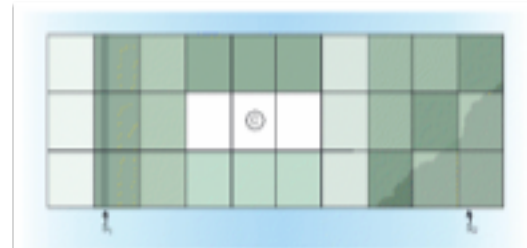


Figure 3.10 Arranging module strings to reduce the effects of shading.

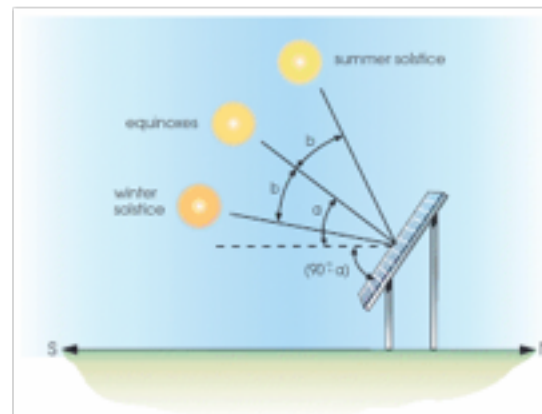
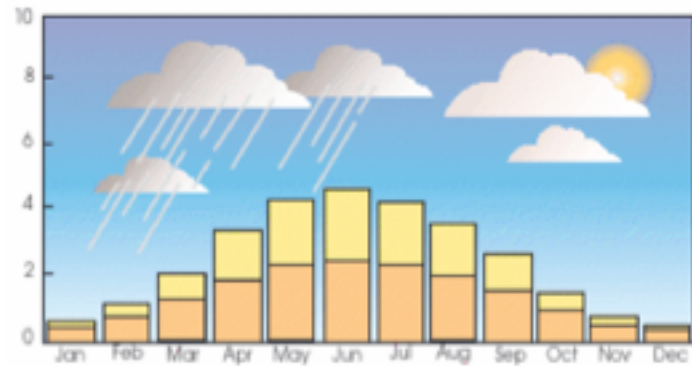
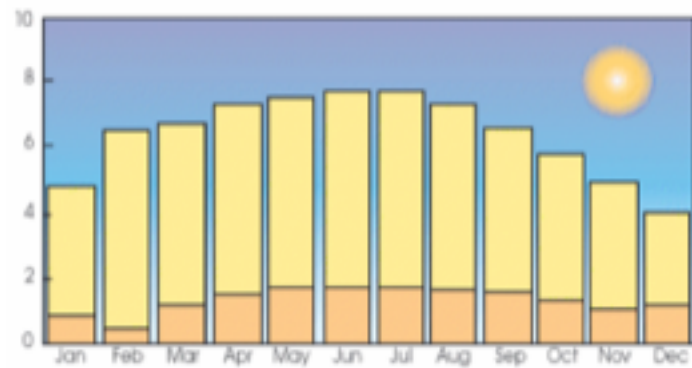


Figure 3.11 Aligning a PV array.

System Sizing

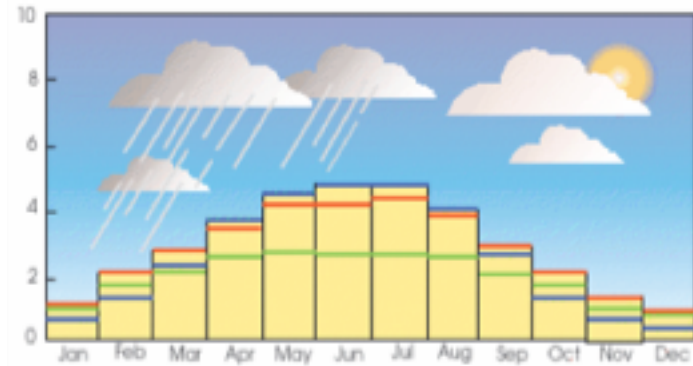


(a)

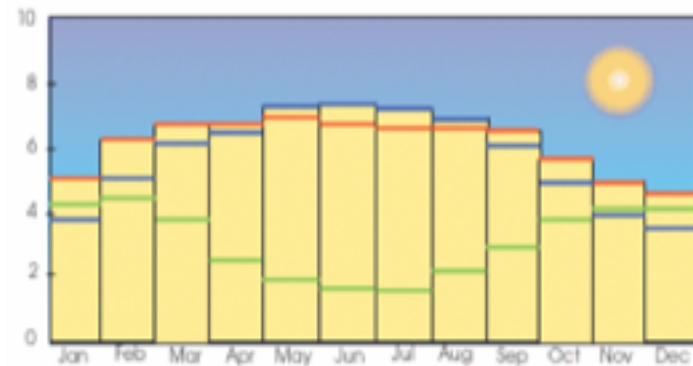


(b)

Figure 3.12 Average daily solar radiation in kWh/m^2 on a horizontal surface: in (a) London or Amsterdam; (b) in the Sahara Desert.



(a)



(b)

Figure 3.13 Daily solar radiation in kWh/m^2 on south-facing inclined PV arrays in: (a) London; (b) the Sahara Desert. In each case three values of tilt are illustrated: 0° (blue), the latitude angle (red), and 90° (green).

System Sizing

of *peak sun hours* for estimating an array's annual output. This involves compressing the total radiation (direct plus diffuse) received throughout the year into an equivalent duration of standard 'bright sunshine' (1 kW/m^2). The same concept may be used for daily radiation. For example, if an inclined array receives an average insolation of 3 kWh/m^2 per day in April, this is considered equivalent to 3 peak sun hours; so an array rated at (say) 2 kW_p is predicted to yield $3 \times 2 = 6 \text{ kWh/day}$. Although it is an approxima-

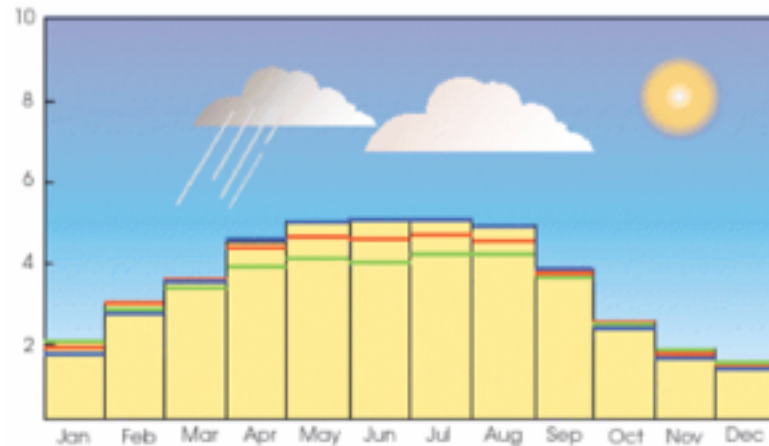


Figure 5.16 Daily solar radiation in kWh/m^2 on south-facing inclined PV arrays for a location at latitude 48°N in southern Germany. Three values of array tilt are illustrated: 33° (blue); 48° (red); and 63° (green).

At this stage the system designer must surely discuss alternatives with the homeowners. For example they might agree to restrict their demand for 2.2 kWh/day to the months March to September, covering the main holiday period, in return for a smaller PV system at lower cost. Over this 7-month period the 33° tilt angle is a good choice. The 'worst' month is now taken as March, for which the average daily radiation is 3.5 kWh/m^2 . This figure can be used for sizing the array. The homeowners will have to make do with considerably less electricity over the winter months, unless the total is boosted by an alternative energy source. Or perhaps they will agree to forgo use of the refrigerator, microwave oven and washing machine, and cut down on the drinking of coffee! Unlike the 'professional' PV systems mentioned in the previous section, a 'leisure' installation should offer plenty of opportunities for energy saving, trading convenience and reliability against cost.

System Sizing

Using the peak sun hours concept we may express the average daily amount of electricity available for running the home's appliances, E_D as:

$$E_D = P_{PV} S_p \eta \quad (5.1)$$

Where P_{PV} is the rated peak power of the PV array, S_p is the number of peak sun hours per day in the month of interest, and η is the overall system efficiency (discussed below). Therefore the peak power of the array is given by:

$$P_{PV} = E_D / S_p \eta \quad (5.2)$$

In the case of the holiday home, $E_D = 2.2 \text{ kWh/day}$, $S_p = 3.5 \text{ h}$ in March, and we will assume a system efficiency of 60% ($\eta = 0.6$), so that:

$$P_{PV} = 2.2 / (3.5 \times 0.6) = 1.05 \text{ kW}_p \quad (5.3)$$

We therefore predict that a PV array rated at just over 1 kW_p will supply the daily load requirement of 2.2 kWh during the months March to September.

System Sizing

- *PV modules (0.85).* Power output is less than the rated value in standard 'bright sunshine' (1 kW/m^2), due to such factors as raised cell operating temperatures, dust or dirt on the modules, and ageing. Also, modules are not generally operated at or close to their maximum power point (unless a controller with MPP tracking is used).
- *Battery bank (0.85).* The charge retrieved from the battery bank is substantially less than that put into it (see Section 5.2.1).
- *Charge controller, blocking diodes, and cables (0.92).* There are small losses in all these items.
- *Inverter (0.9).* This is a typical figure for a high-quality inverter, bearing in mind that it must sometimes work at low output power levels (see Section 5.2.3).

System Sizing

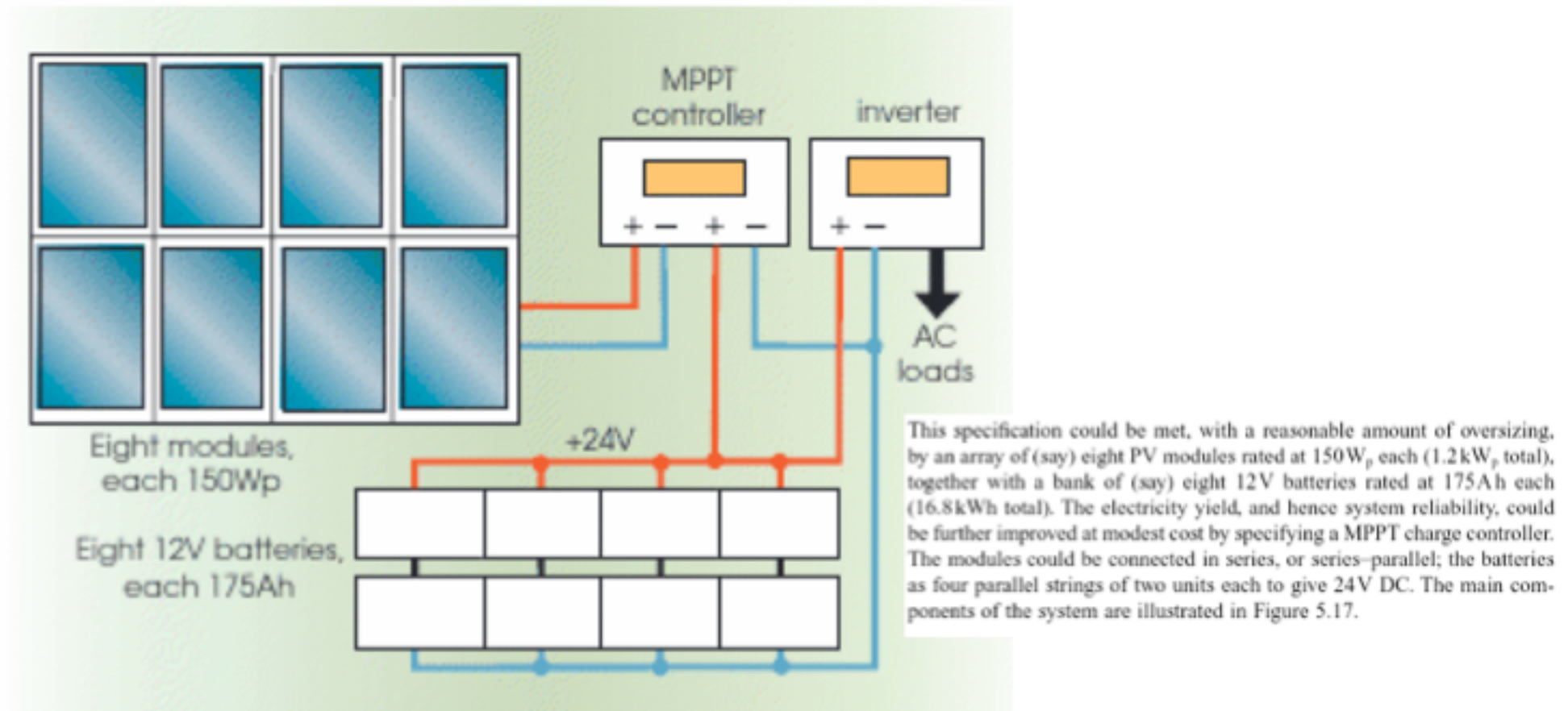


Figure 5.17 A suitable system for the holiday home.



Figure 5.27 PV for a village water supply in Niger (

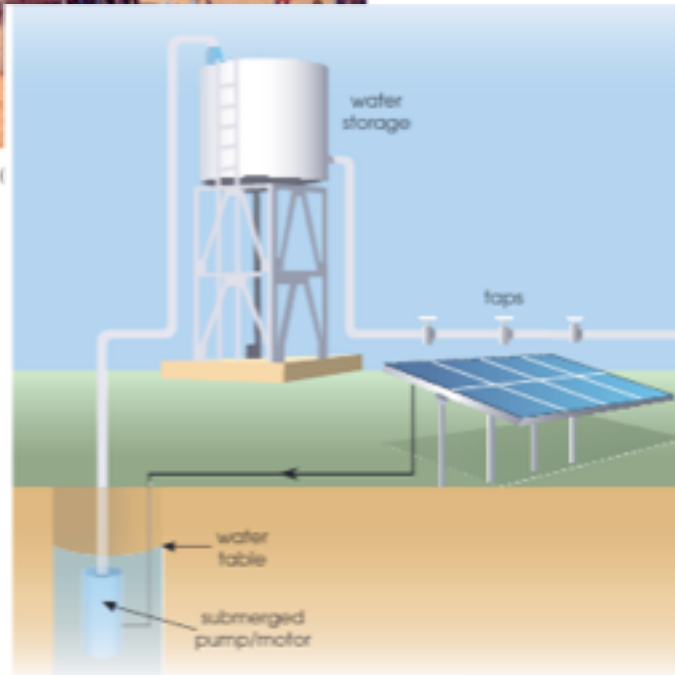


Figure 5.26 A system for village water supply.

- *Type of pump.* Of the many types of pump on the market, *centrifugal* designs are widely used to raise water against pumping heads up to about 25m (the height difference between the water table and tank's input pipe). Multi-stage versions can cope with higher heads. A centrifugal pump has an impeller that throws water against its outer casing at high speed, the kinetic energy then being converted to a pressure head by an expanding output pipe. Centrifugal pumps are compact, robust, and well-suited to PV applications, but they are not normally self-priming and must therefore be kept submerged. This makes them suitable for pump/motors positioned below the water table. Alternative *displacement* or *volumetric* pumps including various self-priming types are more suitable for lower flow rates from very deep wells or boreholes.
- *Type of motor.* DC motors are generally more efficient than AC ones, but more expensive. AC motors are very rugged and need little or no maintenance, so are suitable for submersion at the bottom of a well; but inverters are needed to convert PV electricity to AC, adding to the capital cost. Among DC motors the *permanent-magnet* type is often preferred; but all conventional designs use carbon brushes that must be periodically adjusted or replaced, making submersion awkward. Modern *brushless* DC motors overcome this difficulty, at a cost.
- *Matching the motor and PV array.* Ideally, the PV array should be operated close to its maximum power point (MPP) in all sunlight conditions. Unfortunately the resistive load offered by most motors does not allow this to happen, so a MPP tracking controller based on a DC to DC converter may be inserted to improve matching and increase efficiency.

Solar System for Clinic in Village 20 km from Haramaya

Photographs of The Site

Geransa-Darraba health post About 7 km from Haramaya University Has three rooms No tree shade Electric line installation is completed	
Geransa-Darraba health post Inside the room, no bulb	GD-Health Post-1 
Geransa-Darraba Primary School Directors office Two class room Possible to place the panel on this block About 10 km from Haramaya University	GD-Health Post-2 
	GD-School-1 



Solar System for Clinic in Village 20 km from Haramaya



Figure 8. *a) UC and HU undergraduate students design a mount for solar panels on a health clinic in Ethiopia. b) Installation of solar panels at the Qeransa-Darraba health post about 7 km from Haramaya University. c) UC and HU students with local children near the health clinic.*

Haramaya University/High School (Concordia Humana)



**Storage Tank and
Distribution (X)**

Well and Solar Pump

Haramaya University/High School (Concordia Humana)



Solar Panels



Well and Solar Pump



Haramaya University/High School (Concordia Humana)



Distribution at School



Distribution for Village of 2,000



***Small Business Manufacturing Solar Street Lights for Villages:
Outdoor lighting for safety improvement in a rural
Ethiopian village.***

- Safety at night can be enhanced by lighting, especially in rural villages
- Low cost solar lighting is simple to manufacture in Ethiopia
- Demonstration of manufacturing at Dire Dawa University
- Demonstration of usefulness of solar lighting at small village near Haramaya
- Improved design by DDU/DDIT
- Commercialization?

***Outdoor lighting for safety improvement in a rural
Ethiopian village.***



***Outdoor lighting for safety improvement in a rural
Ethiopian village.***



Figure 3. Alfredo Moser and his solar light invention in Brazil.
(www.bbc.com/news/magazine-23536914)



Outdoor lighting for safety improvement in a rural Ethiopian village.



Figure 1. Solar lanterns in use in the Philippines (www.youtube.com/watch?v=0PSsyufpZ2Q).

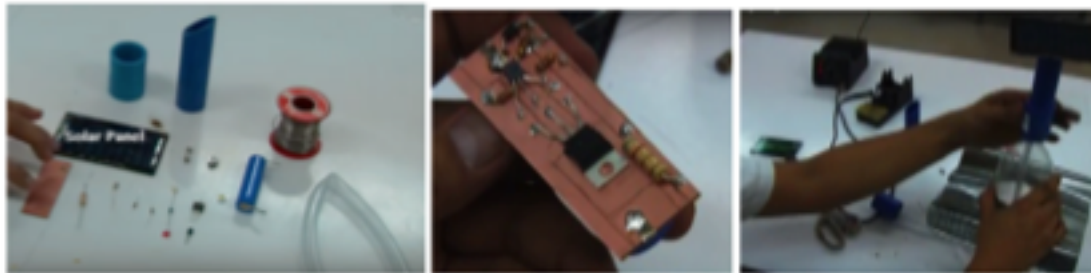


Figure 2. Assembly of a solar lantern using simple components available in country. (www.youtube.com/watch?v=bAPNtEFzrcA)

***Outdoor lighting for safety improvement in a rural
Ethiopian village.***

Number of People Impacted by Project:

Ethiopians:

Primary School Students: 600-650

Primary School Instructors: 4

Villagers: 100

Regional impact of demonstration

of simple solar technology ~many 10,000s

College students at Dire Dawa University participating

30 actively involved total impact 300

Faculty at Dire Dawa University, 50

Haramaya University, 4

Addis Ababa University 10

Outdoor lighting for safety improvement in a rural Ethiopian village.

Estimated Budget for Materials:

In country purchases:

80 Bags of Concrete	\$3 per bag	\$240	
~2 Bags per pole			
40 PVC Pipes 4' x 10"	\$20	\$800	
30 PVC T & U joints	\$10	\$400	
Solder		\$50	
Subtotal for Installation:		\$1490	Per unit cost ~\$37

Purchases in US:

40 Blank PCBs	\$25 (Amazon.com)		
40 LED Bulbs	\$15 (Ebay.com)		
40 Solar Panels	\$130 (Alibaba.com)		
40 Batteries	\$250 (BatterySpace.com)		
Wire etc.	\$100 (TBD)		
Subtotal for Lanterns:		\$520	Per unit cost ~\$13

Grand Total:	\$2,010	Per unit cost ~\$50
---------------------	----------------	----------------------------





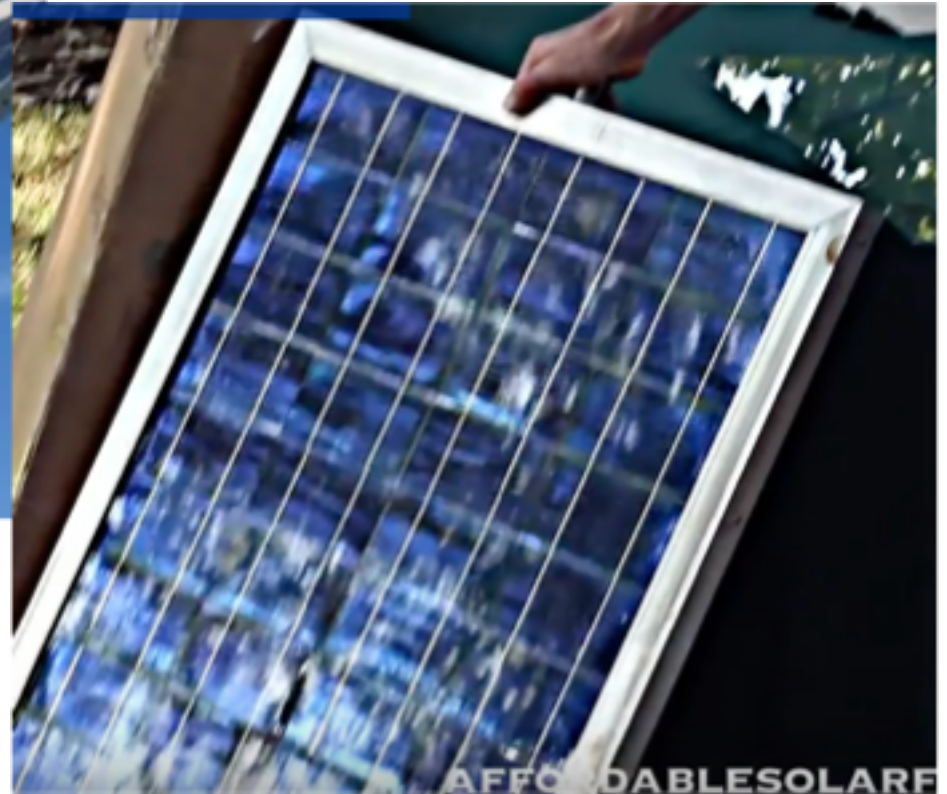
50 Solar Street Lights Installed in Village in 2015
Improved Design Installed in 2016 by DDIT Students and Faculty
(Commercialization was not followed through to date)



How to Assemble a Solar Panel

MATERIALS NEEDED

1. SOLAR FRAME W/GLASS
2. SOLAR CELLS (UNTABBED)
3. TABBING WIRE
4. BUS WIRE
5. DIODE
6. SYLGARD 184
7. FLUX
8. TERMINAL BLOCK (2 TERMINAL)
9. #12 STRANDED WIRE
10. 100% SILICONE CAULK
11. TEDLAR BACKING (IF DESIRED)



AFFORDABLESOLAR

How to Assemble a Solar Panel



Construct an Aluminum Frame



Seal a Piece of Glass with Silicon Sealant to the Frame

How to Assemble a Solar Panel



Fix the Glass with Braces



Tap the Cells

How to Assemble a Solar Panel



Layout the Tabbed cells

Solder the Cells

How to Assemble a Solar Panel



Connect the Cells in Parallel/Series
To Achieve the Desired Voltage
Using Bus Wires



Seal with Silicon Sealant

How to Assemble a Solar Panel

This seems easy

Could we make a company assembling Solar Panels in Ethiopia?

**POWER ETHIOPIA
BUSINESS PLAN**

Prepared by:

*Dr. Greg Beaucage
Professor of Chemical
and Materials Engineering
University of Cincinnati
Cincinnati, Ohio 45221, USA*

*Mr. Berhanu Mengistu
Lecturer of Physics
Haramaya University
Department of Physics
Haramaya, Ethiopia*

*Dr. Fekadu Lemessa
Academic Vice President
Dire Dawa University
Dire Dawa, Ethiopia*

Power Ethiopia

- Photovoltaics are missing in Ethiopia
 - high import tariffs
 - no financing
 - architectural adaption
 - no technical support
 - aversion to new technology
 - no sales team
- Solve these issues using University Resources
 - manufacture (assemble) PV panels
 - train technologists/business people
 - profit for faculty and students
- HU/DDU area is unique for this opportunity



© Power Ethiopia Photovoltaics Company 2014



a)



b)

Figure 1. a) Dire Dawa and Haramaya are located at the midpoint between the port of Djibouti and the population center of Addis Ababa. Dire Dawa is the second largest population center in Ethiopia. The region has some of the highest solar irradiance on earth with a population of 95 million and 90 million in a rural setting 70 million far from grid power. b) The two sites offer accessibility to the Ethiopian market of 95 million people and to the port of Djibouti on the Red Sea with shipping connections to Asia and the Mediterranean Sea through the Suez Canal.



Figure 2 a) Campus of Dire Dawa University. b) Proposed site for PV assembly plant at the new Institute of Technology on the Haramaya University campus.

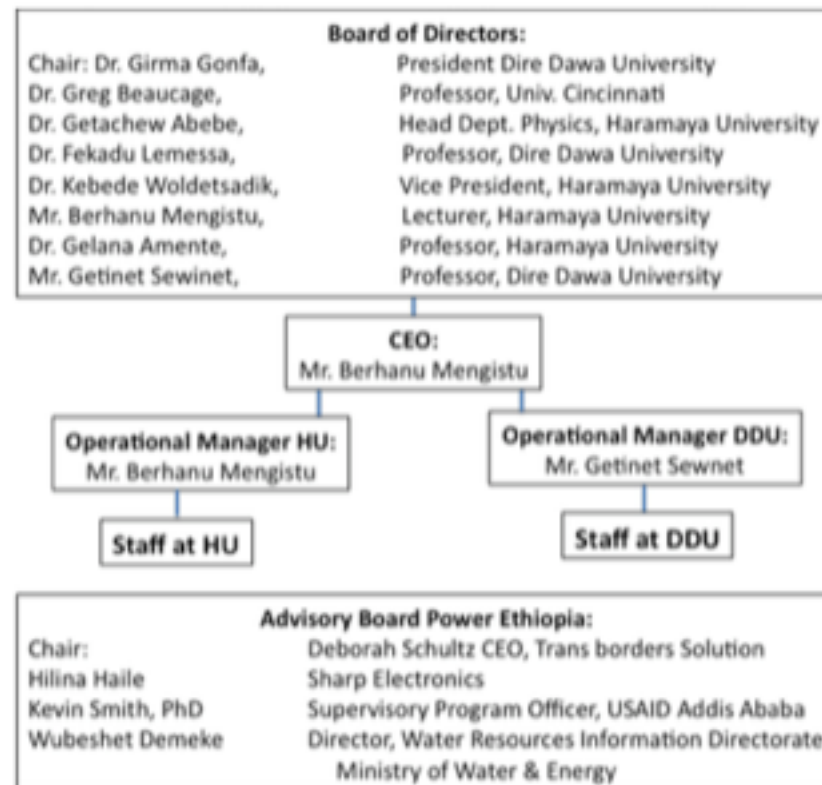


Figure 3. Management structure for *Power Ethiopia*.

Table 2. Funding Requirements (1000s of USD) for Power Ethiopia, five-year plan.

Expense	2014 (3/14 to 12/14)	2015	2016	2017	2018	2019	2020	Total
Facilities	10	12	12	24	24	24	24	130
Utilities	2	2.4	2.4	4.8	4.8	4.8	4.8	26
Operating Expenses:	2	2.4	2.4	4.8	4.8	4.8	4.8	26
Materials for Manufacture	339	362.4	319.2	460.8	506	557	613	3157.4
Transportation	1	1.2	1.2	2.4	2.4	2.4	2.4	13
Staff	4	4.8	4.8	9.6	9.6	9.6	9.6	52
Management	5	6	6	12	12	12	12	65
R&D	5	6	7	7	7	7	6	45
Shipping	20	24	24	48	53	58	62	289
Incidental Expenses	3	3	3	4	5	5	5	28
Marketing/ Sales/ Training	3	4	4	4	4	4	4	27
Total Costs	394	428.2	386	581.4	632.6	688.6	747.6	3858.4
Facilities/ Trans./ Util. Paid by HU	(13)	(15.6)	(15.6)	(15.6)	(15.6)	(15.6)	(15.6)	(106.6)
Facilities/ Trans./ Util. Paid by DDU	-	-	-	(15.6)	(15.6)	(15.6)	(15.6)	(62.4)
Outstanding Expenses	381	412.6	370.4	550.2	601.4	657.4	716.4	3,689.4
Sales	542	650.4	650.4	1,300.8	1,430	1,570	1,720	7863.6
Profit+Taxes	161	237.8	280	750.6	828.6	912.6	1,003.6	4,174.2
Est. Taxes 30% of Profit	37.2	54.9	64.6	173.2	191.2	210.6	231.6	963.3
Est. Profit	123.8	182.9	215.4	577.4	637.4	702	772	3,210.9
Income After Taxes	504.8	595.5	585.8	1,127.6	1,238.8	1,359.4	1,488.4	6,900.3

7.Funding Requirements

Table 2 indicates the funding expenses for the first 7 years of operation. The first three years are based on 100 150W panels being produced per month (see Table 1). This level of production is increased in 2017 by addition of a facility at DDU and expansion of the rate of production at the existing facilities in 2017 to 2020. Sales based on 542 USD per 150W panel in 2014. This cost decreases with materials cost reduction as sales increase from 339 USD in 2014; 302 USD in 2015; 266 USD in 2016; 192 USD in 2017 and afterwards.

Table 2. Cash input necessary for the first eight years of operation.

Year	Expenses	Cash on Hand from Previous Year (Previous Year's Income After Taxes Plus Excess Cash)	Excess Cash (Cash Needed)	Investment
2014	381	0	(381)	381
2015	412.6	504.8	92.2	
2016	370.4	687.7	317.3	
2017	550.2	903.1	352.9	
2018	601.4	1,480.5	879.1	
2019	657.4	2,117.9	1,460.5	
2020	716.4	2,819.9	2,103.5	
2021	716.4	3,591.9	2,875.5	

Assessment of Power Ethiopia

Ethiopians (and others) are risk adverse (they have their reasons)

Ethiopian university leaders are too busy to undertake serious management of an outside project

Need competent (trustworthy) people to run a moderate size business

There are investors available in Ethiopia for this project

There are investors in the US interested in this project

There are international corporate investors interested in this project

In the end the first step could not be achieved, incorporation of the group since cross institutional agreements and associations were weak

There was too much risk for the university administrators and too little direct/personal gain

A smaller scale project(s) aligned with the University/Education Ministry master plan is needed

How do PVs work?

Conductivity and Semi-Conductors

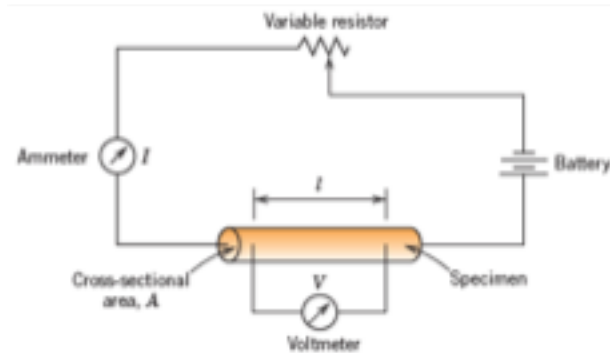


Figure 18.1 Schematic representation of the apparatus used to measure electrical resistivity.

$$V = IR$$

$$\rho = \frac{RA}{l}$$

$$\sigma = \frac{1}{\rho}$$

J = current density = I/A

$$J = \sigma \mathcal{E}$$

\mathcal{E} = Electric field intensity = V/l

where l is the distance between two points

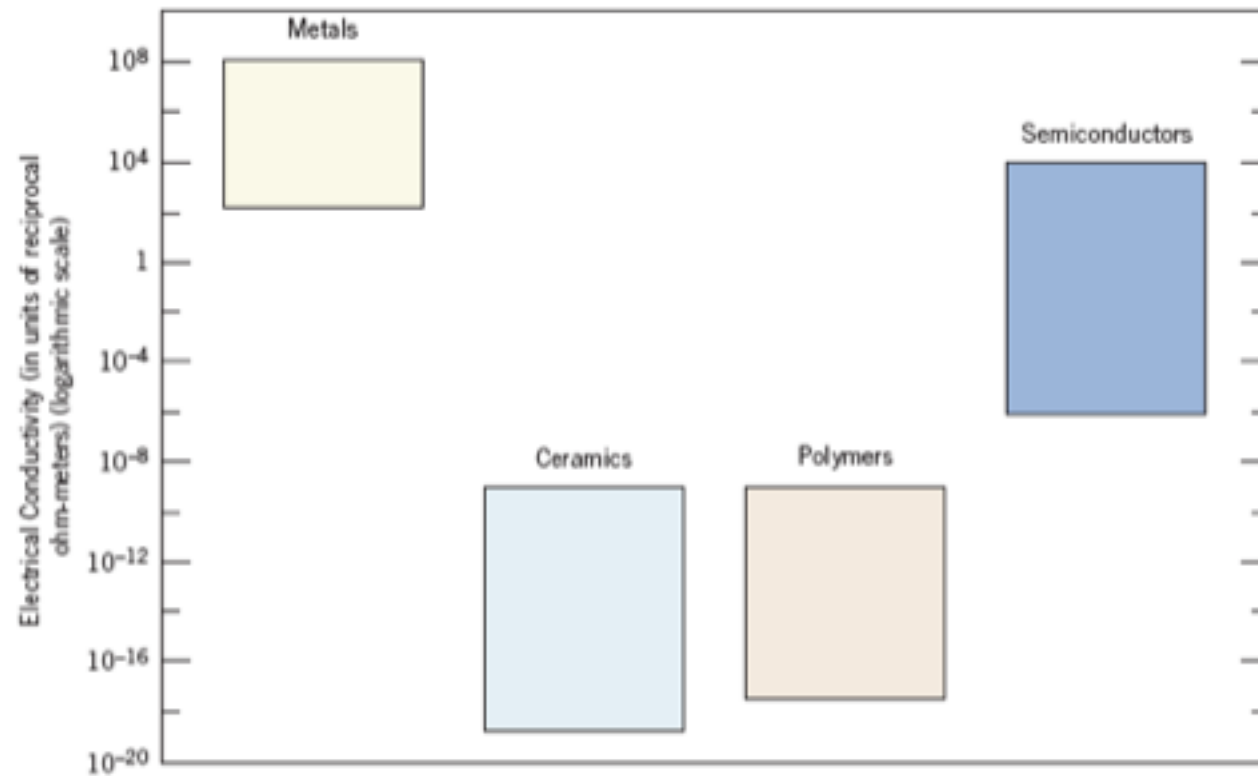
conductors, semiconductors, and insulators.

Metals:

Semiconductors:

Many Polymers and Glasses

Figure 1.7
Bar-chart of room-temperature electrical conductivity ranges for metals, ceramics, polymers, and semiconducting materials.



Electrical Conduction (motion of electrons)
Ionic Conduction (motion of ions)

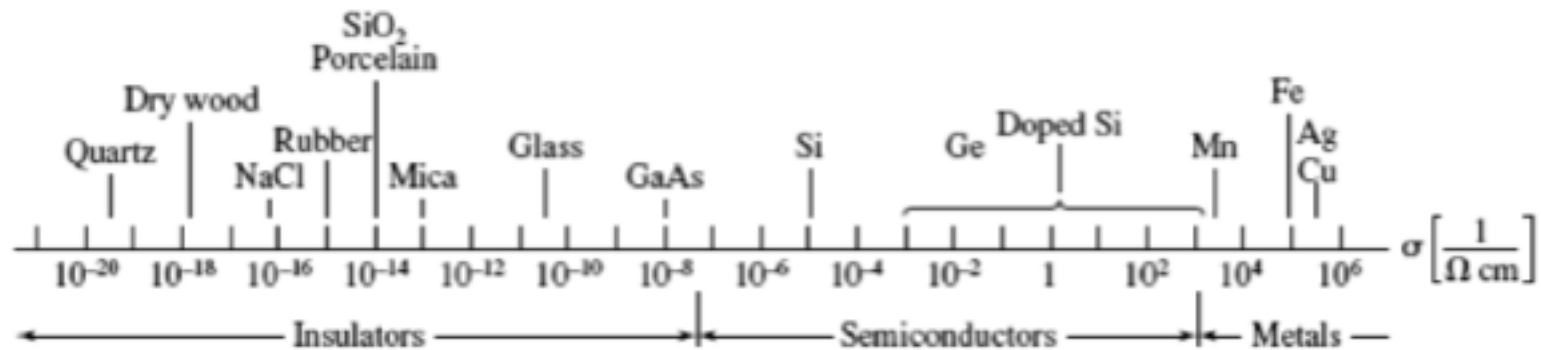


FIGURE 11.1. Room-temperature conductivity of various materials. (Superconductors, having conductivities of many orders of magnitude larger than copper, near 0 K, are not shown. The conductivity of semiconductors varies substantially with temperature and purity.) It is customary in engineering to use the centimeter as the unit of length rather than the meter. We follow this practice. The reciprocal of the ohm (Ω) is defined to be 1 siemens (S); see Appendix II. For conducting polymers, refer to Figure 11.20.

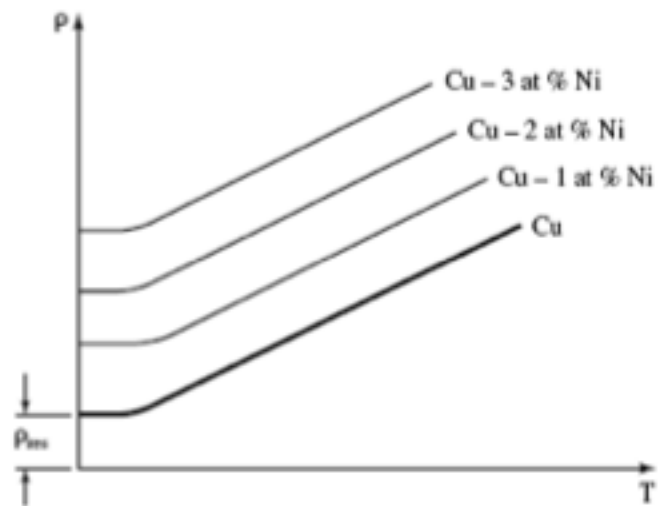


FIGURE 11.3. Schematic representation of the temperature dependence of the resistivity of copper and various copper-nickel alloys. ρ_{res} is the residual resistivity.

$$\rho_2 = \rho_1[1 + \alpha(T_2 - T_1)], \quad (11.7)$$

FIGURE 11.4. Schematic representation of an electron path through a conductor (containing vacancies, impurity atoms, and a grain boundary) under the influence of an electric field. This classical description does not completely describe the resistance in materials.



Free Electron Model

Drude Model (kinetic theory of gasses)

$$m \frac{dv}{dt} + \gamma v = e \cdot \mathcal{E}$$

$$\sigma = \frac{N_f \cdot e^2 \cdot \tau}{m},$$

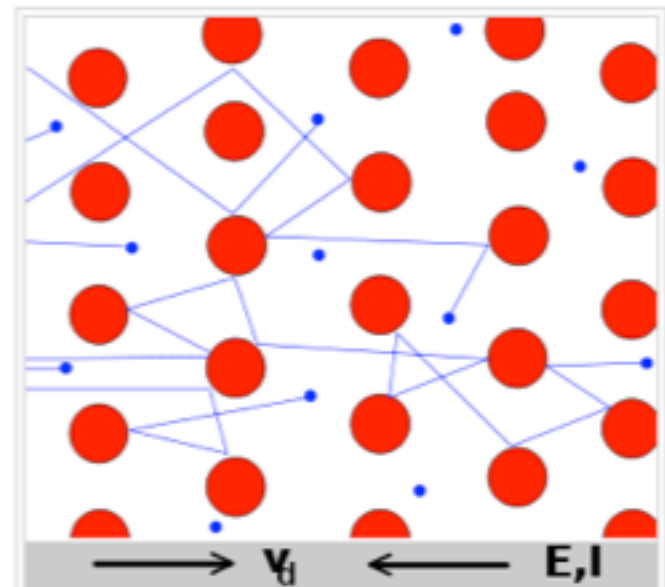
τ = time between collisions

$$\tau = m/\gamma$$

$$\sigma(\omega) = \frac{\sigma_0}{1 + i\omega\tau}, \quad \text{For AC}$$

Drude-Sommerfeld Model

Include quantum mechanics
(wave nature of electron)



Drude Model electrons (shown here in blue) constantly bounce between heavier, stationary crystal ions (shown in red).

4 Quantum Numbers: Size, Shape, Spatial Orientation, Magnetically Determined Energy State

Principle Quantum Number = n = Distance from Nucleus (Bohr number)

K, L, M, N or 1, 2, 3, 4

Second quantum number = l = Shape

s, p, d, f

n restricts the number of these

Third quantum number = m_l = magnetically distinguishable energy states

Fourth quantum number = m_s = spin moment $+1/2$ or $-1/2$ = up or down orientation

Table 2.1 The Number of Available Electron States in Some of the Electron Shells and Subshells

Principal Quantum Number n	Shell Designation	Subshells	Number of States	Number of Electrons	
				Per Subshell	Per Shell
1	K	s	1	2	2
2	L	s	1	2	8
		p	3	6	
3	M	s	1	2	18
		p	3	6	
		d	5	10	
		s	1	2	
4	N	p	3	6	32
		d	5	10	
		f	7	14	
		s	1	2	

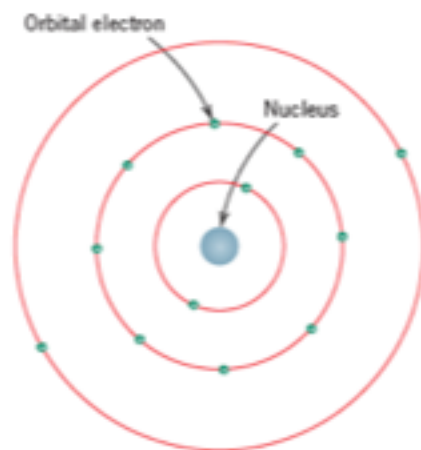


Figure 2.1 Schematic representation of the Bohr atom.

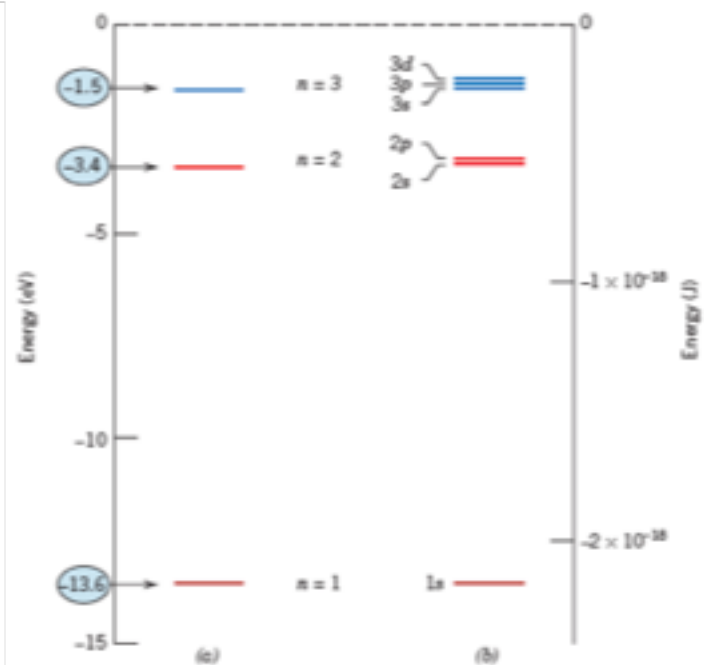


Figure 2.2 (a) The first three electron energy states for the Bohr hydrogen atom (b) Electron energy states for the first three shells of the wave-mechanical hydrogen atom. (Adapted from W. G. Moffatt, G. W. Pearsall, and J. Wulff, *The Structure and Properties of Materials*, Vol. I, Structure, p. 10. Copyright © 1964 by John Wiley & Sons, New York. Reprinted by permission of John Wiley & Sons, Inc.)

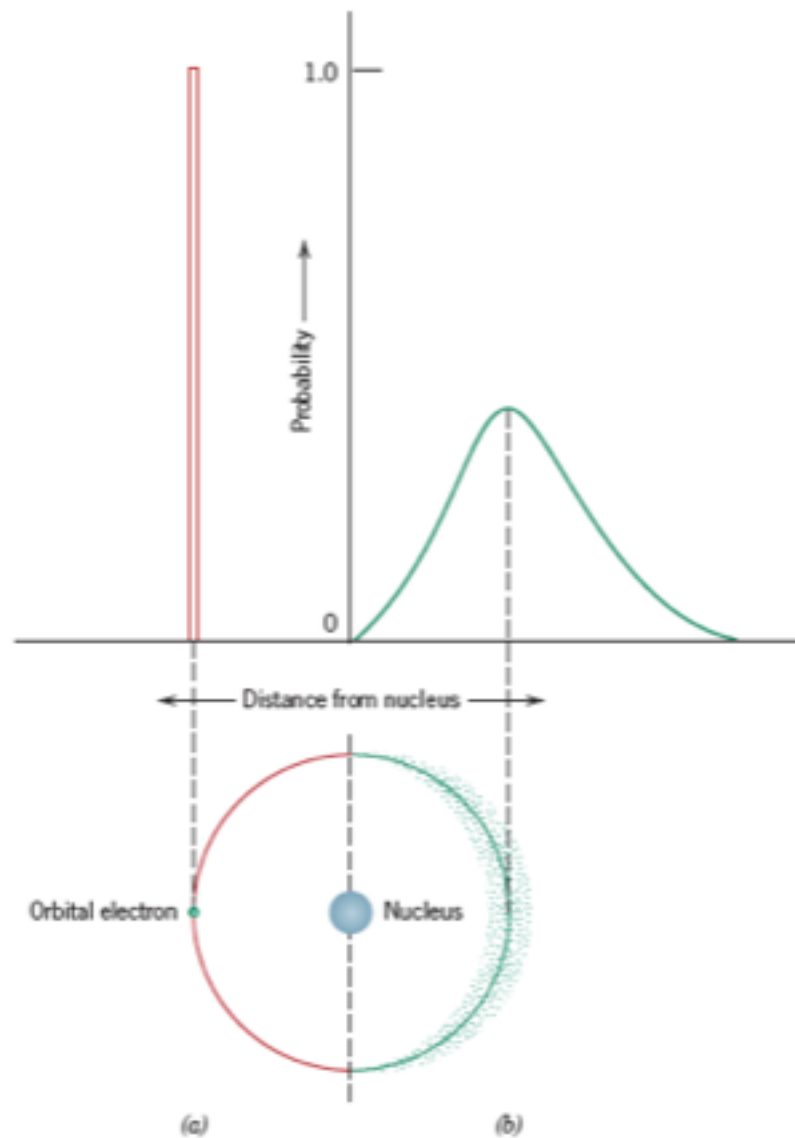


Figure 2.3 Comparison of the (a) Bohr and (b) wave-mechanical atom models in terms of electron distribution. (Adapted from Z. D. Jastrzebski, *The Nature and Properties of Engineering Materials*, 3rd edition, p. 4. Copyright © 1987 by John Wiley & Sons, New York. Reprinted by permission of John Wiley & Sons, Inc.)

Primary quantum numbers distinguished by energy

Different primary quantum number states can have overlapping energy levels.

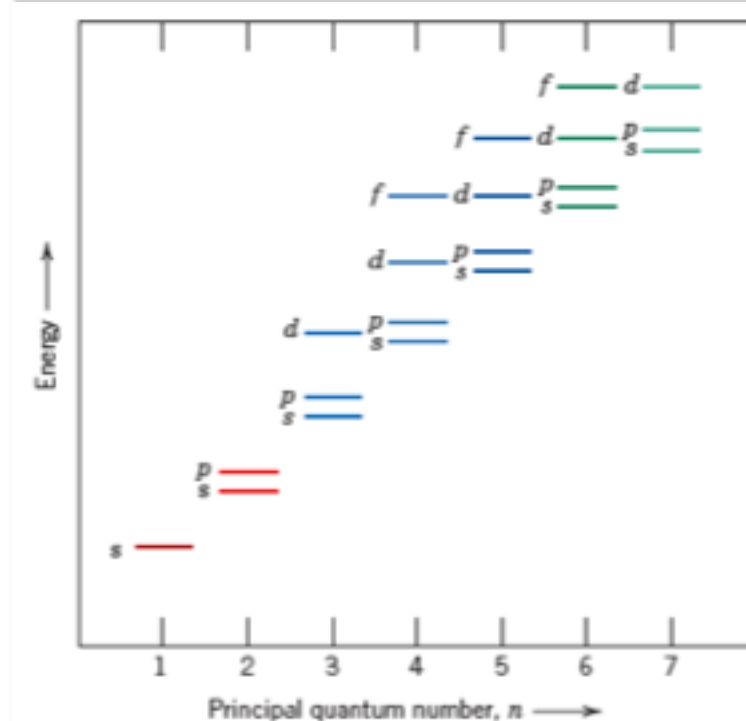


Figure 2.4 Schematic representation of the relative energies of the electrons for the various shells and subshells. (From K. M. Ralls, T. H. Courtney, and J. Wulff, *Introduction to Materials Science and Engineering*, p. 22. Copyright © 1976 by John Wiley & Sons, New York. Reprinted by permission of John Wiley & Sons, Inc.)

for each individual atom there exist discrete energy levels that may be occupied by electrons, arranged into shells and subshells. Shells are designated by integers (1, 2, 3, etc.), and subshells by letters (*s*, *p*, *d*, and *f*). For each of *s*, *p*, *d*, and *f* subshells, there exist, respectively, one, three, five, and seven states. The electrons in most atoms fill only the states having the lowest energies, two electrons of opposite spin per state, in accordance with the Pauli exclusion principle. The electron configuration of an isolated atom represents the arrangement of the electrons within the allowed states.

Density of States $Z(E)$

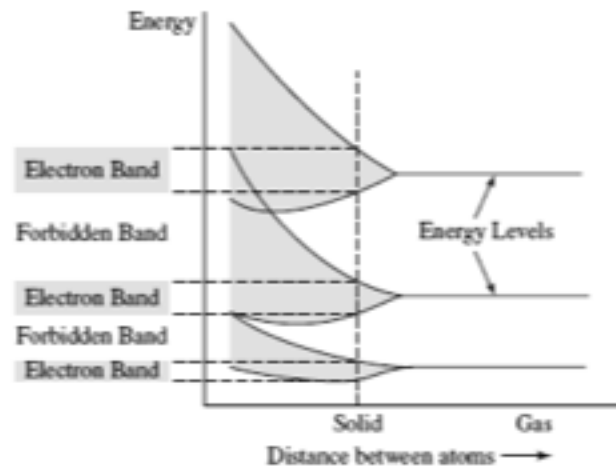
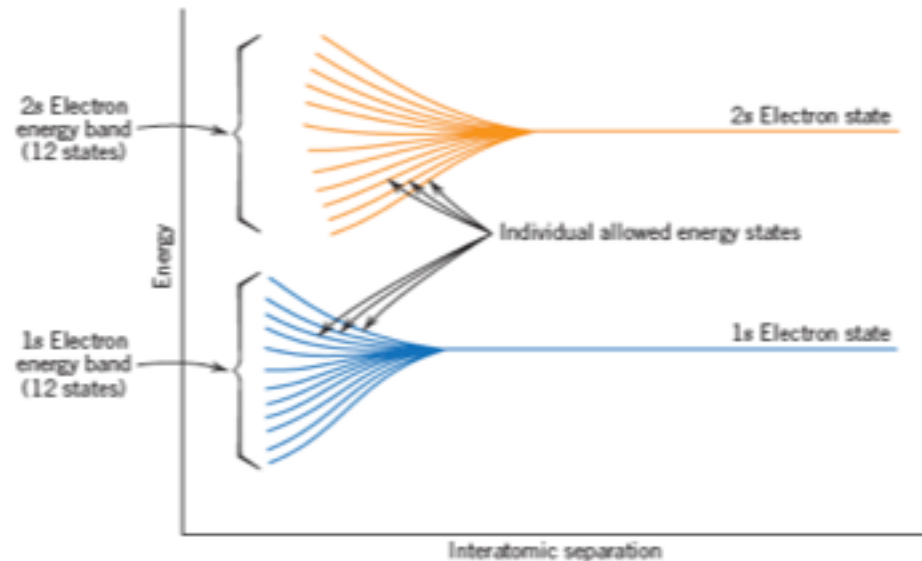


FIGURE 11.5. Schematic representation of energy levels (as for isolated atoms) and widening of these levels into energy bands with decreasing distance between atoms. Energy bands for a specific case are shown at the left of the diagram.

Figure 18.2
Schematic plot of electron energy versus interatomic separation for an aggregate of 12 atoms ($N = 12$). Upon close approach, each of the 1s and 2s atomic states splits to form an electron energy band consisting of 12 states.



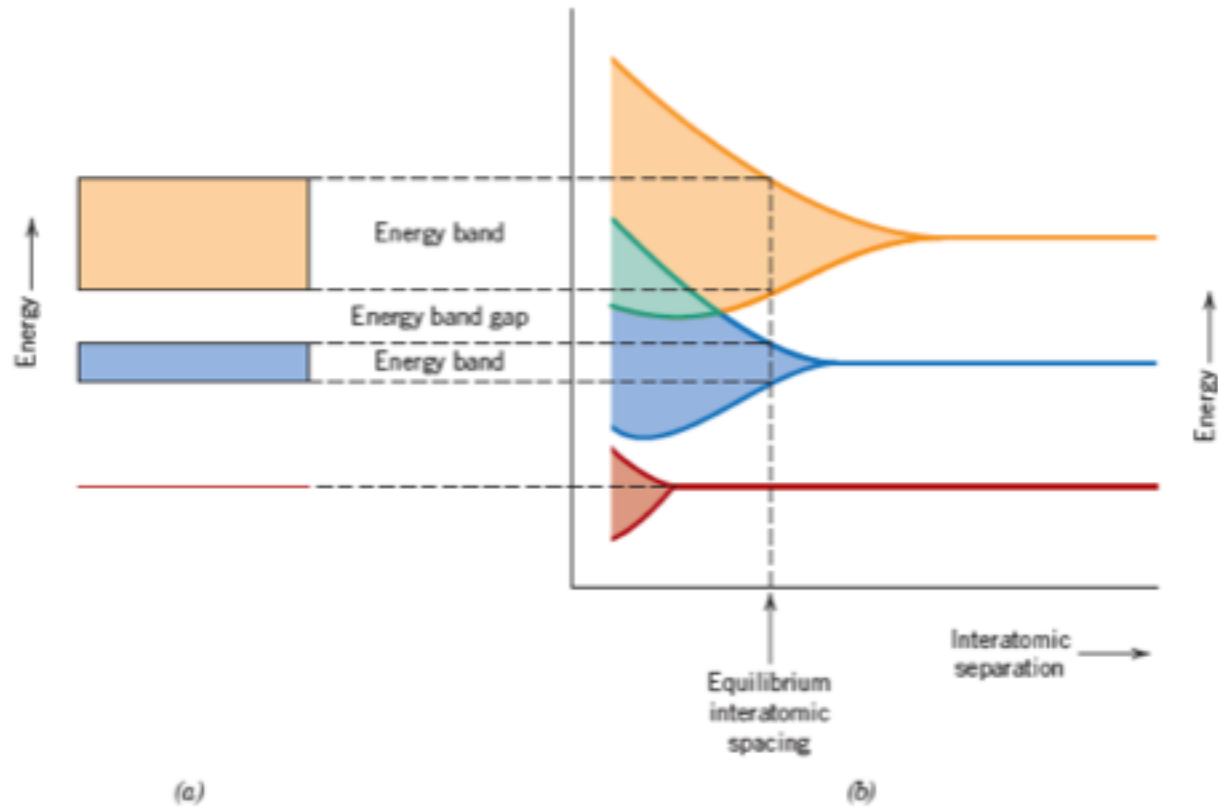


Figure 18.3 (a) The conventional representation of the electron energy band structure for a solid material at the equilibrium interatomic separation. (b) Electron energy versus interatomic separation for an aggregate of atoms, illustrating how the energy band structure at the equilibrium separation in (a) is generated. (From Z. D. Jastrzebski, *The Nature and Properties of Engineering Materials*, 3rd edition. Copyright © 1987 by John Wiley & Sons, Inc. Reprinted by permission of John Wiley & Sons, Inc.)

The number of states within each band will equal the total of all states contributed by the N atoms. For example, an s band will consist of N states, and a p band of $3N$ states. With regard to occupancy, each energy state may accommodate two electrons, which must have oppositely directed spins. Furthermore, bands will contain the electrons that resided in the corresponding levels of the isolated atoms; for example, a $4s$ energy band in the solid will contain those isolated atom's $4s$ electrons. Of course, there will be empty bands and, possibly, bands that are only partially filled.

The electrical properties of a solid material are a consequence of its electron band structure—that is, the arrangement of the outermost electron bands and the way in which they are filled with electrons.

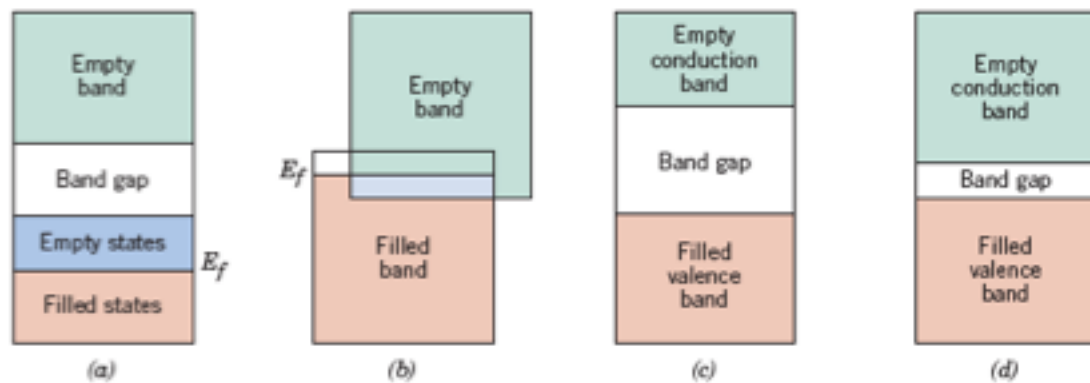


Figure 18.4 The various possible electron band structures in solids at 0 K. (a) The electron band structure found in metals such as copper, in which there are available electron states above and adjacent to filled states, in the same band. (b) The electron band structure of metals such as magnesium, wherein there is an overlap of filled and empty outer bands. (c) The electron band structure characteristic of insulators; the filled valence band is separated from the empty conduction band by a relatively large band gap (>2 eV). (d) The electron band structure found in the semiconductors, which is the same as for insulators except that the band gap is relatively narrow (<2 eV).

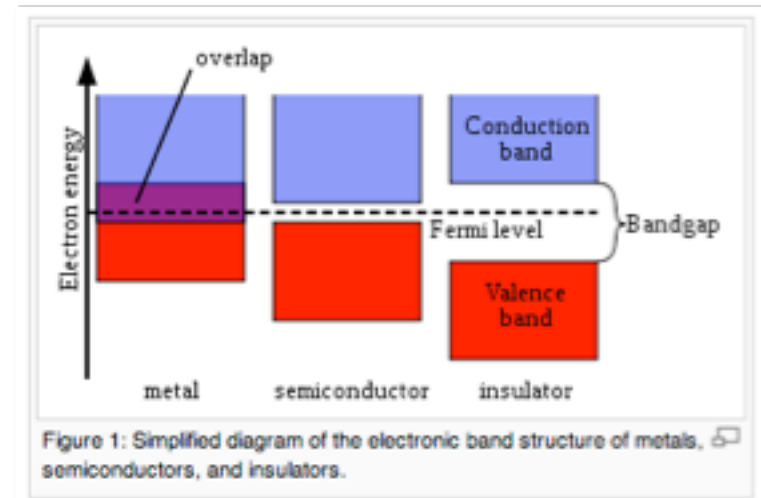


Figure 1: Simplified diagram of the electronic band structure of metals, semiconductors, and insulators.

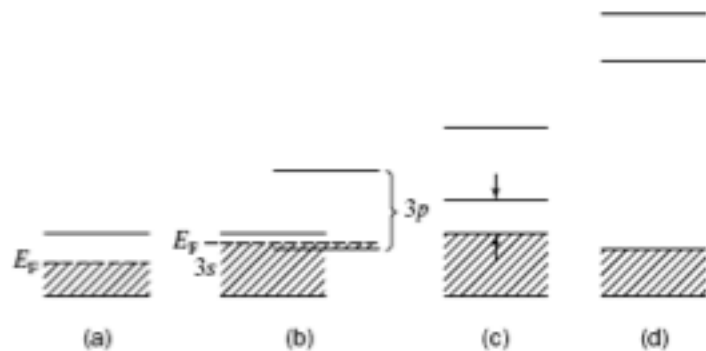


FIGURE 11.6. Simplified representation for energy bands for (a) monovalent metals, (b) bivalent metals, (c) semiconductors, and (d) insulators. For a description of the nomenclature, see Appendix I.

$$\text{Fermi Energy} = E_F$$

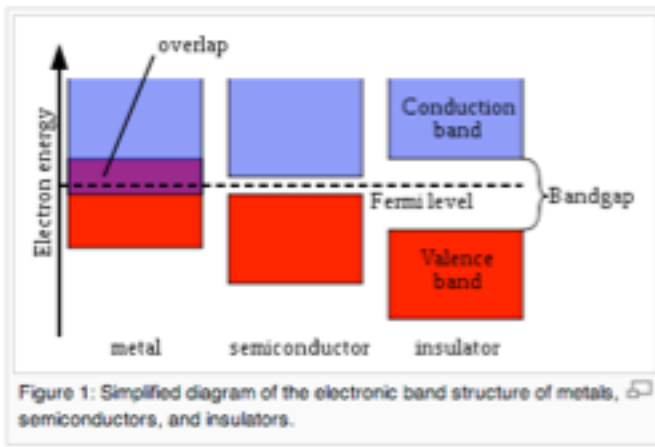
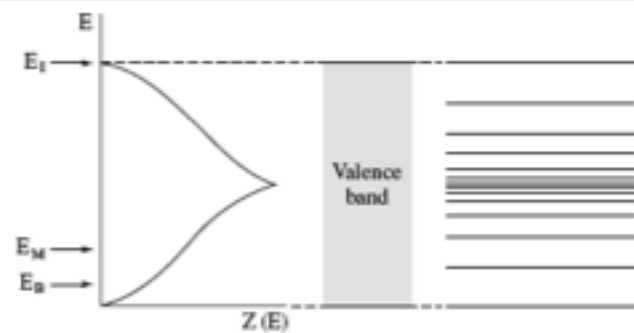


FIGURE 11.7. Schematic representation of the density of electron states $Z(E)$ within an electron energy band. The density of states is essentially identical to the population density $N(E)$ for energies below the Fermi energy, E_F (i.e., for that energy level up to which a band is filled with electrons). Examples of highest electron energies for a monovalent metal (E_M), for a bivalent metal (E_B), and for an insulator (E_I) are indicated.

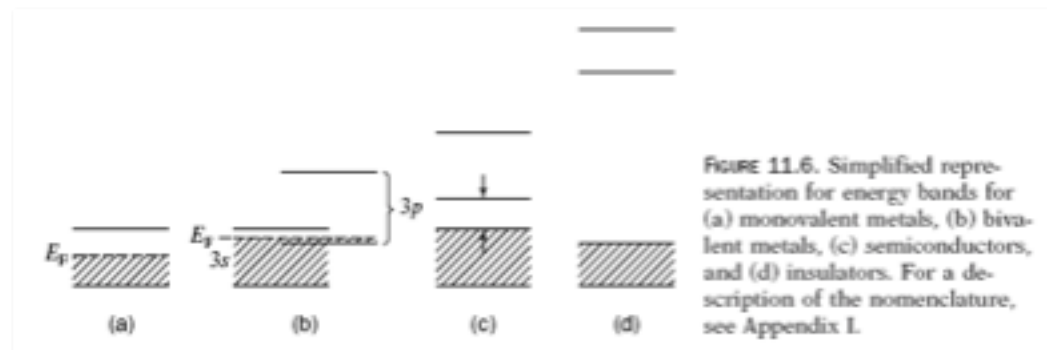


$$\sigma = \frac{1}{3} e^2 v_F^2 \tau N(E_F)$$

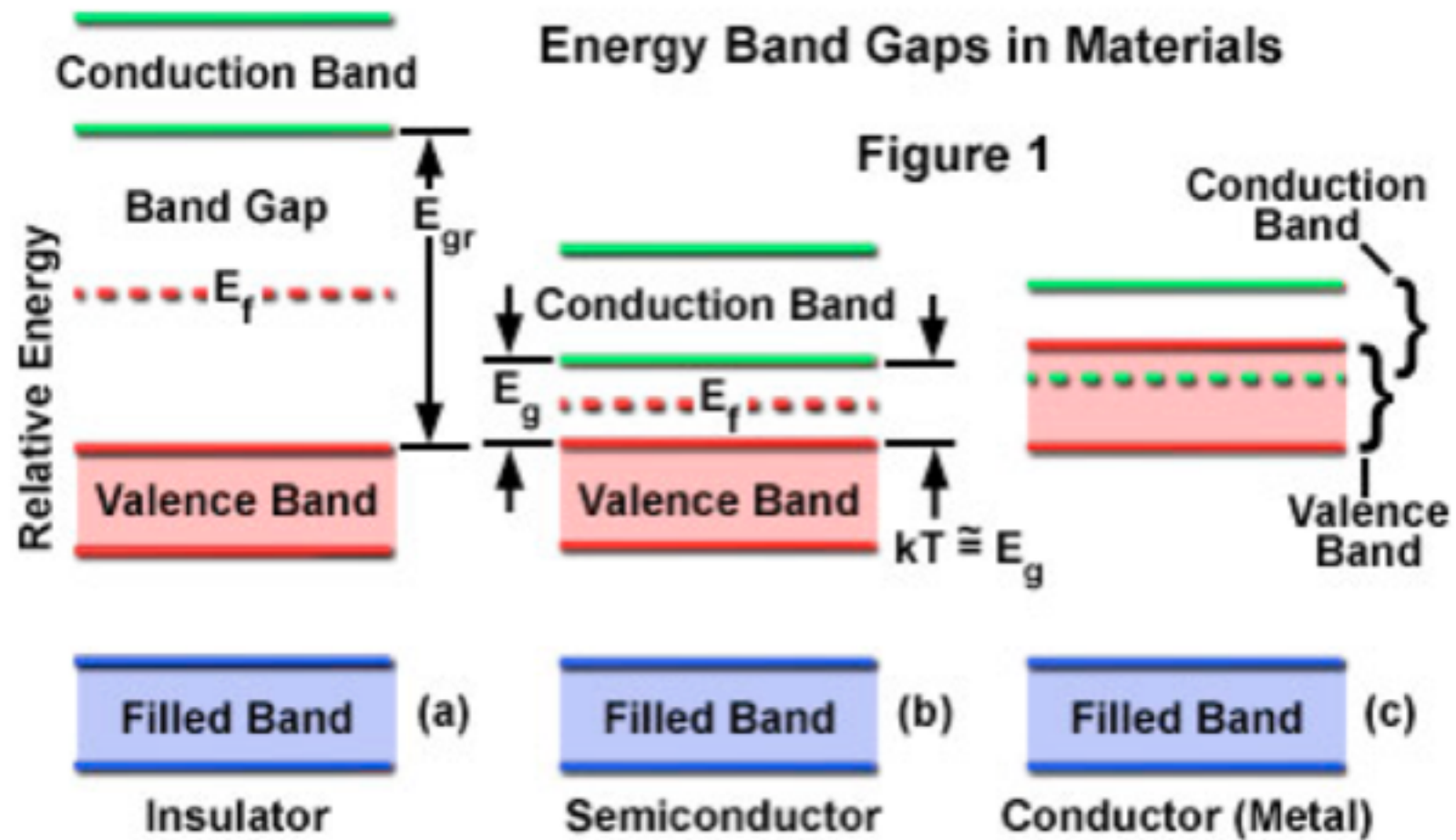
Quantum Mechanics Model
Fermi drift velocity v_F

$$\sigma = \frac{N_f \cdot e^2 \cdot \tau}{m},$$

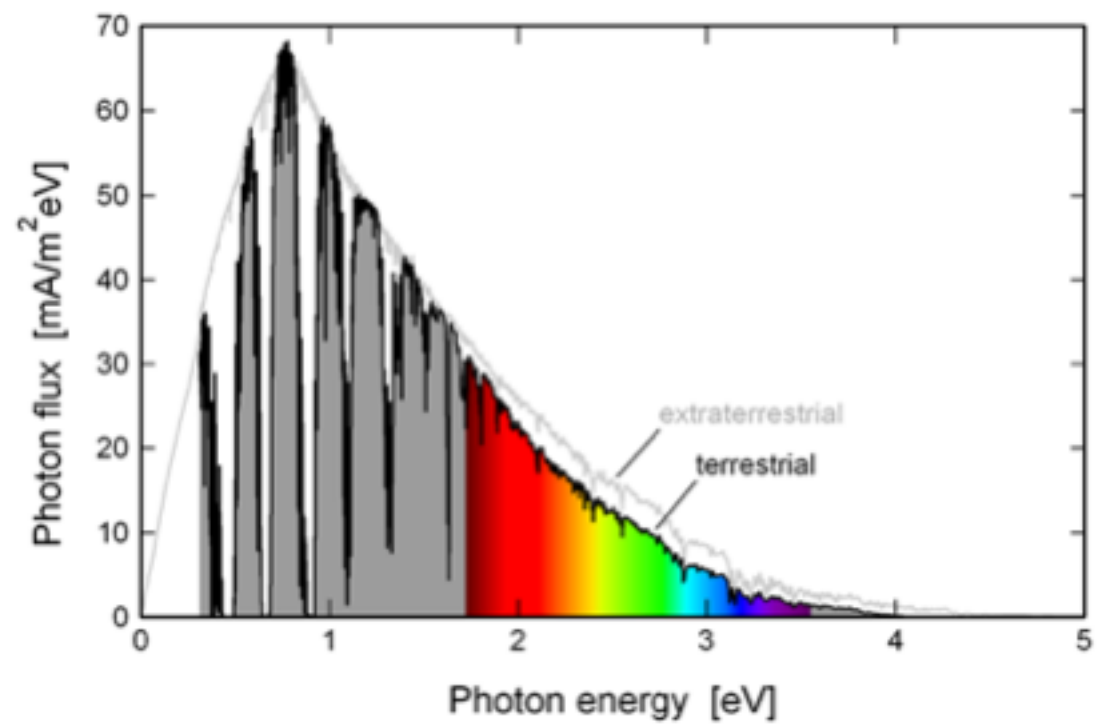
Drude Model

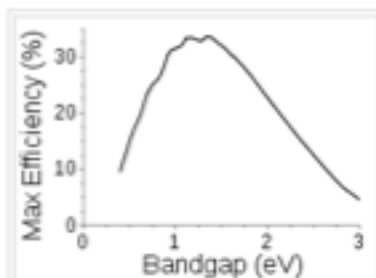


Fermi Energy = E_F



Description of the electronic bands in solids[8].



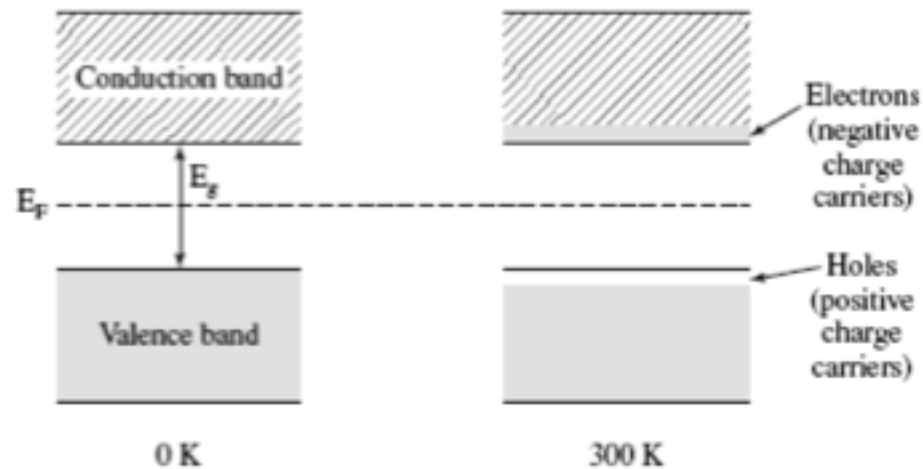


The [Shockley–Queisser limit](#) gives the maximum possible efficiency of a single junction solar cell under un-concentrated sunlight, as a function of the semiconductor bandgap. If the bandgap is too high, most daylight photons cannot be absorbed; if it is too low, then most photons have much more energy than necessary to excite electrons across the bandgap, and the rest is wasted. The semiconductors commonly used in commercial solar cells have bandgaps near the peak of this curve, for example silicon (1.1eV) or [CdTe](#) (1.5eV). The Shockley–Queisser limit can be exceeded by [tandem solar cells](#), concentrating sunlight onto the cell, and other methods.

Material	Symbol	Band gap (eV) @ 302K	Reference
Silicon	Si	1.11	[6]
Selenium	Se	1.74	
Germanium	Ge	0.67	[6]
Silicon carbide	SiC	2.86	[6]
Aluminium phosphide	AlP	2.45	[6]
Aluminium arsenide	AlAs	2.16	[6]
Aluminium antimonide	AlSb	1.6	[6]
Aluminium nitride	AlN	6.3	
Diamond	C	5.5	
Gallium(III) phosphide	GaP	2.26	[6]
Gallium(III) arsenide	GaAs	1.43	[6]
Gallium(III) nitride	GaN	3.4	[6]
Gallium(II) sulfide	GaS	2.5	
Gallium antimonide	GaSb	0.7	[6]
Indium antimonide	InSb	0.17	[6]
Indium(III) nitride	InN	0.7	[7]
Indium(III) phosphide	InP	1.35	[6]
Indium(III) arsenide	InAs	0.36	[6]
Zinc oxide	ZnO	3.37	
Zinc sulfide	ZnS	3.6	[6]
Zinc selenide	ZnSe	2.7	[6]
Zinc telluride	ZnTe	2.25	[6]
Cadmium sulfide	CdS	2.42	[6]
Cadmium selenide	CdSe	1.73	[6]
Cadmium telluride	CdTe	1.49	[6]
Lead(II) sulfide	PbS	0.37	[6]
Lead(II) selenide	PbSe	0.27	[6]
Lead(II) telluride	PbTe	0.29	[6]
Copper(II) oxide	CuO	1.2	[8]
Copper(I) oxide	Cu ₂ O	2.1	[10]
Iron disilicide	β-FeSi ₂	0.87	[11]

Semiconductors

FIGURE 11.11. Simplified band diagrams for an intrinsic semiconductor such as pure silicon at two different temperatures. The dark shading symbolizes electrons.



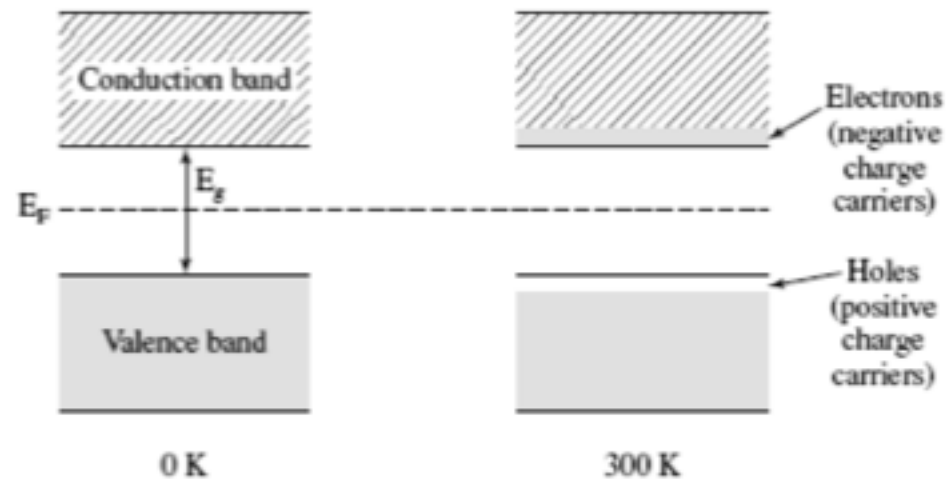
$$N_e = 4.84 \times 10^{15} T^{3/2} \exp \left[-\left(\frac{E_g}{2k_B T} \right) \right],$$

Number of Electrons in the Conduction Band

$$\sigma = N_e \cdot \mu \cdot e,$$

Semiconductors

FIGURE 11.11. Simplified band diagrams for an intrinsic semiconductor such as pure silicon at two different temperatures. The dark shading symbolizes electrons.

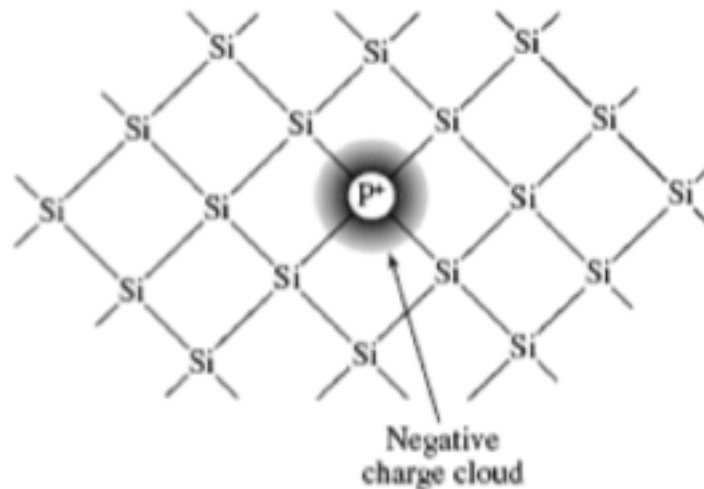


$$\sigma = N_e \mu_e e + N_h \mu_h e,$$

Holes left in the valence band are positive charge carriers
Intrinsic Conduction in an Intrinsic Semiconductor

Group→ ↓Period	1	2	3	4	5	6	7	8	9	10	11	12	13	14	15	16	17	18
1	1 H																	2 He
2	3 Li	4 Be											5 B	6 C	7 N	8 O	9 F	10 Ne
3	11 Na	12 Mg											13 Al	14 Si	15 P	16 S	17 Cl	18 Ar
4	19 K	20 Ca	21 Sc	22 Ti	23 V	24 Cr	25 Mn	26 Fe	27 Co	28 Ni	29 Cu	30 Zn	31 Ga	32 Ge	33 As	34 Se	35 Br	36 Kr
5	37 Rb	38 Sr	39 Y	40 Zr	41 Nb	42 Mo	43 Tc	44 Ru	45 Rh	46 Pd	47 Ag	48 Cd	49 In	50 Sn	51 Sb	52 Te	53 I	54 Xe
6	55 Cs	56 Ba	57 La	* 72 Hf	73 Ta	74 W	75 Re	76 Os	77 Ir	78 Pt	79 Au	80 Hg	81 Tl	82 Pb	83 Bi	84 Po	85 At	86 Rn
7	87 Fr	88 Ra	89 Ac	** 104 Rf	105 Db	106 Sg	107 Bh	108 Hs	109 Mt	110 Ds	111 Rg	112 Cn	113 Nh	114 Fl	115 Mc	116 Lv	117 Ts	118 Og
				* 58 Ce	59 Pr	60 Nd	61 Pm	62 Sm	63 Eu	64 Gd	65 Tb	66 Dy	67 Ho	68 Er	69 Tm	70 Yb	71 Lu	
				** 90 Th	91 Pa	92 U	93 Np	94 Pu	95 Am	96 Cm	97 Bk	98 Cf	99 Es	100 Fm	101 Md	102 No	103 Lr	

n-Type Semiconductors



0.0001 % P

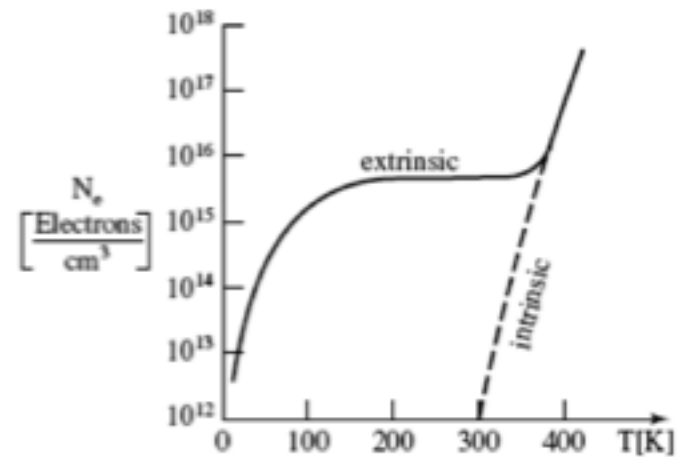
FIGURE 11.12. Two-dimensional representation of a silicon lattice in which a phosphorous atom substitutes a regular lattice atom, and thus introduces a negative charge cloud about the phosphorous atom. Each electron pair between two silicon atoms constitutes a covalent bond [see Chapter 3, particularly Figure 3.4(a)].

Silicon has 4 valence electrons, Group V elements have 5

For Phosphorous the binding energy for the donor electron is
0.045 eV (small/weakly bound)

n-Type Semiconductors

FIGURE 11.13. Schematic representation of the number of electrons per cubic centimeter in the conduction band as a function of temperature for extrinsic semiconductors, assuming low doping.



Extra conducting electrons contributed by P

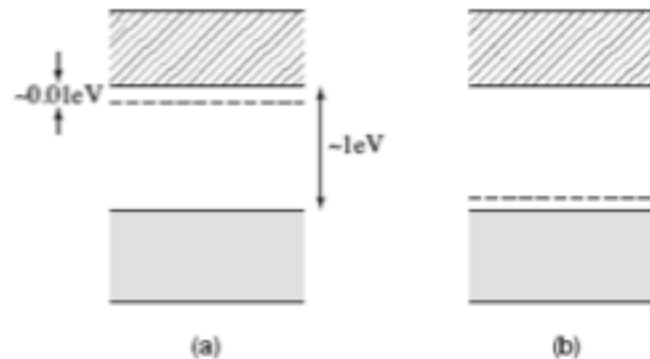


FIGURE 11.14. (a) Donor and (b) acceptor levels in extrinsic semiconductors.

p-Type Semiconductors

Group III impurities (B, Al, Ga, In) are deficient in one electron

Acceptor Impurities

Positive Charge Carriers (Holes) in the valence band

$$\sigma = N_{de} e \mu_e,$$

At room temperature only the majority carriers need be considered
(intrinsic effects are ignored)

H 1																	He 2						
																		III	IV	V	VI		
Li 3	Be 4													B 5	C 6	N 7	O 8	F 9	Ne 10				
Na 11	Mg 12													II	Al 13	Si 14	P 15	S 16	Cl 17	Ar 18			
K 19	Ca 20	Sc 21	Ti 22	V 23	Cr 24	Mn 25	Fe 26	Co 27	Ni 28	Cu 29	Zn 30	Ga 31	Ge 32	As 33	Se 34	Br 35	Kr 36						
Rb 37	Sr 38	Y 39	Zr 40	Nb 41	Mo 42	Tc 43	Ru 44	Rh 45	Pd 46	Ag 47	Cd 48	In 49	Sn 50	Sb 51	Te 52	I 53	Xe 54						
Cs 55	Ba 56	Lu 71	Hf 72	Ta 73	W 74	Re 75	Os 76	Ir 77	Pt 78	Au 79	Hg 80	Tl 81	Pb 82	Bi 83	Po 84	At 85	Rn 86						
Fr 87	Ra 88	Lr 103	Db 104	Jl 105	Rf 106	Bh 107	Hn 108	Mt 109															

Compound Semiconductors

III & V

GaAs

II & VI

ZnO

ZnS

ZnSe

CdTe

For LED's
Solar Cells

La 57	Ce 58	Pr 59	Nd 60	Pm 61	Sm 62	Eu 63	Gd 64	Tb 65	Dy 66	Ho 67	Er 68	Tm 69	Yb 70
Ac 89	Th 90	Pa 91	U 92	Np 93	Pu 94	Am 95	Cm 96	Bk 97	Cf 98	Es 99	Fm 100	Md 101	No 102

Hall Effect

Are the Charge Carriers Positive or Negative?

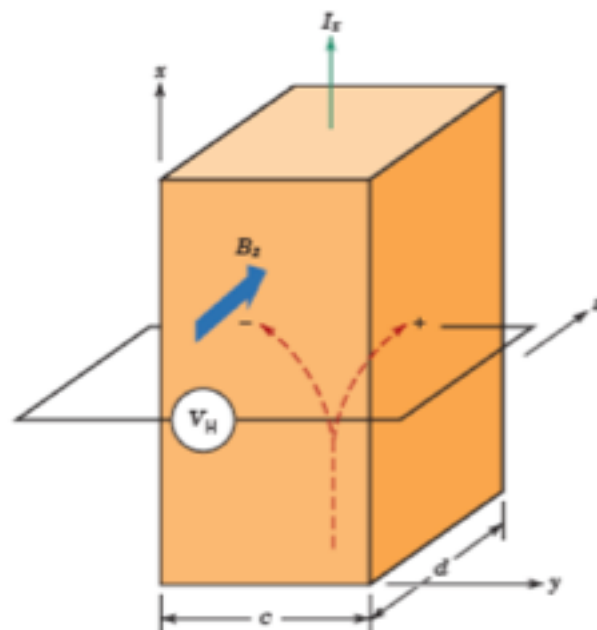


Figure 18.20 Schematic demonstration of the Hall effect. Positive and/or negative charge carriers that are part of the I_x current are deflected by the magnetic field B_z and give rise to the Hall voltage, V_H .

$$V_H = \frac{R_H I_x B_z}{d}$$

$$R_H = \frac{1}{n|e|}$$

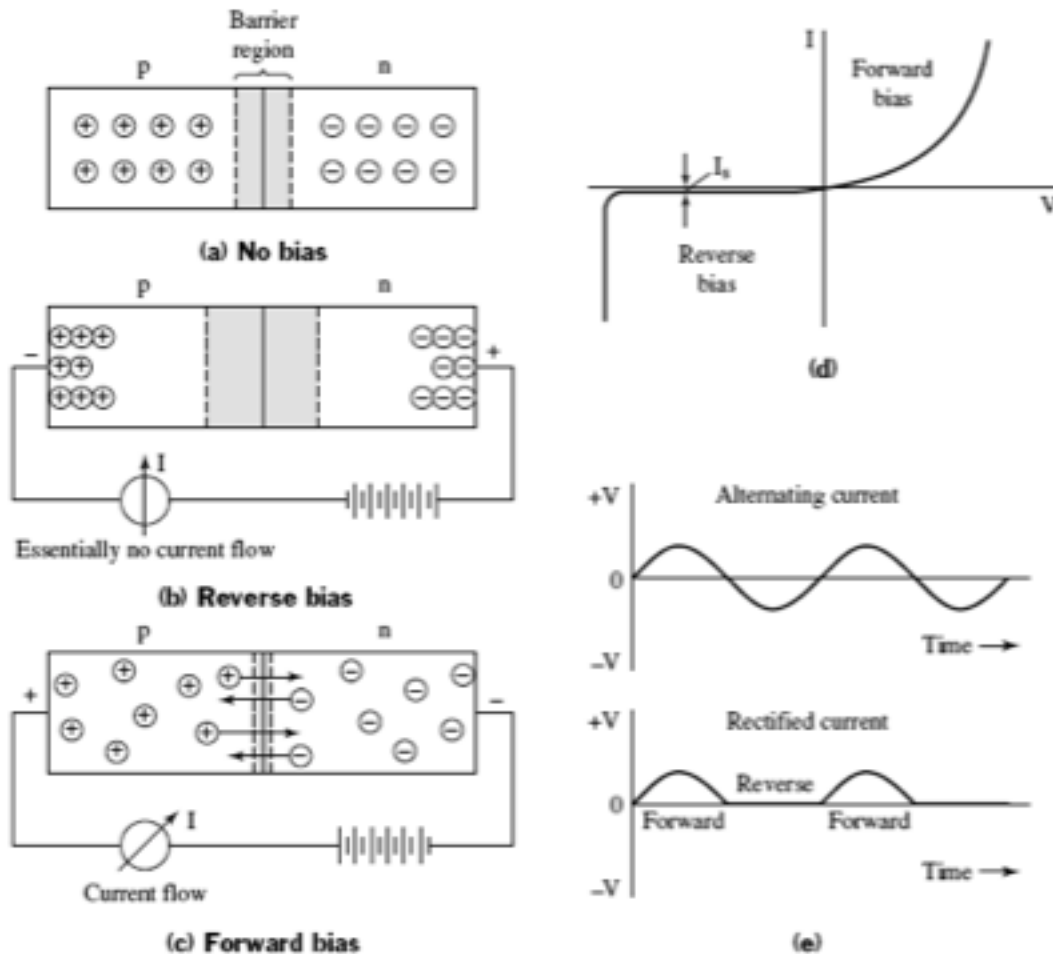
Metals Negative

$$\mu_e = \frac{\sigma}{n|e|}$$

$$\mu_e = |R_H| \sigma$$

R_H = Hall Coefficient

Rectifier or Diode



$$I = I_s \left[\exp\left(\frac{eV}{k_B T}\right) - 1 \right],$$

FIGURE 11.15. Schematic representation of (a) an unbiased p-n junction, (b) a p-n junction in reverse bias, (c) a p-n junction in forward bias, (d) current-voltage characteristics of a p-n rectifier, and (e) voltage versus time curves.

Rectifier or Diode

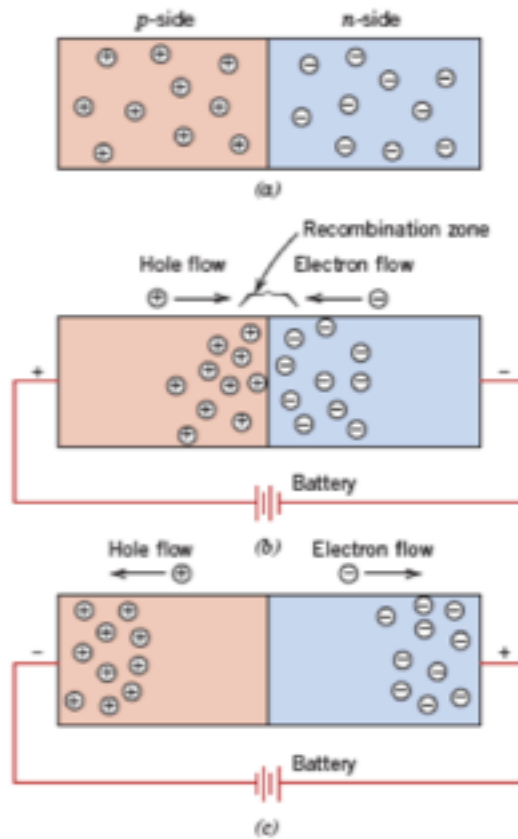


Figure 18.21 For a p - n rectifying junction, representations of electron and hole distributions for (a) no electrical potential, (b) forward bias, and (c) reverse bias.

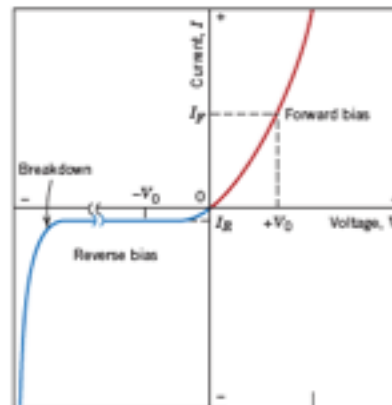


Figure 18.22 The current-voltage characteristics of a p - n junction for forward and reverse biases. The phenomenon of breakdown is also shown.

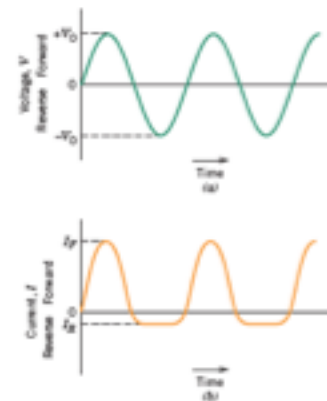


Figure 18.23 (a) Voltage versus time for the input to a p - n rectifying junction. (b) Current versus time, showing rectification of voltage in (a) by a p - n rectifying junction having the voltage-current characteristics shown in Figure 18.22.

Rectifier or Diode

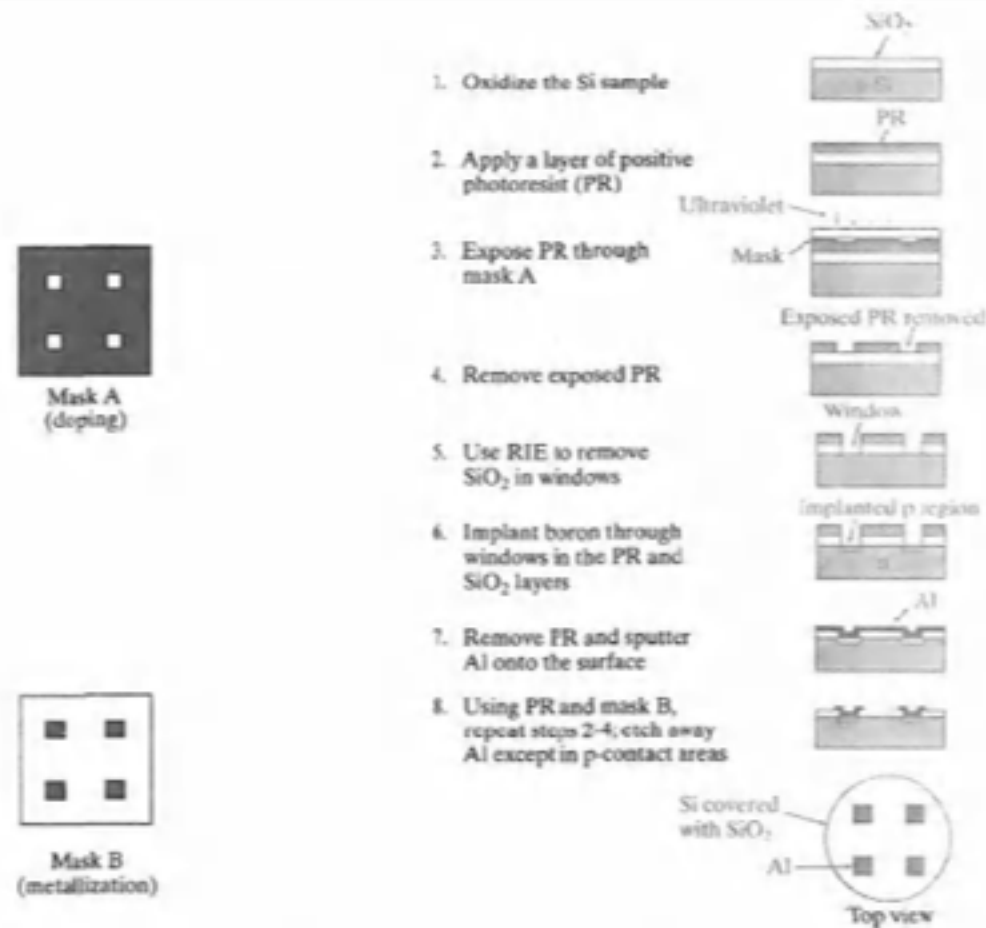


Figure 5-10

Simplified description of steps in the fabrication of p-n junctions. For simplicity, only four diodes per wafer are shown, and the relative thicknesses of the oxide, PR, and the Al layers are exaggerated.

Rectifier or Diode

On contact a potential is setup between p and n materials due to flow of electrons from n to p and holes from p to n

This barrier potential opposes flow of electrons. If electrons are added to the p side the potential barrier drops (Forward Bias).

If electrons are added to n the potential barrier increases (Reverse Bias).

So current can only flow from p to n under normal circumstances.

A slight time lag occurs due to motion of minority carriers in a p-n junction and there is energy loss due to this motion.

Rectifier or Diode

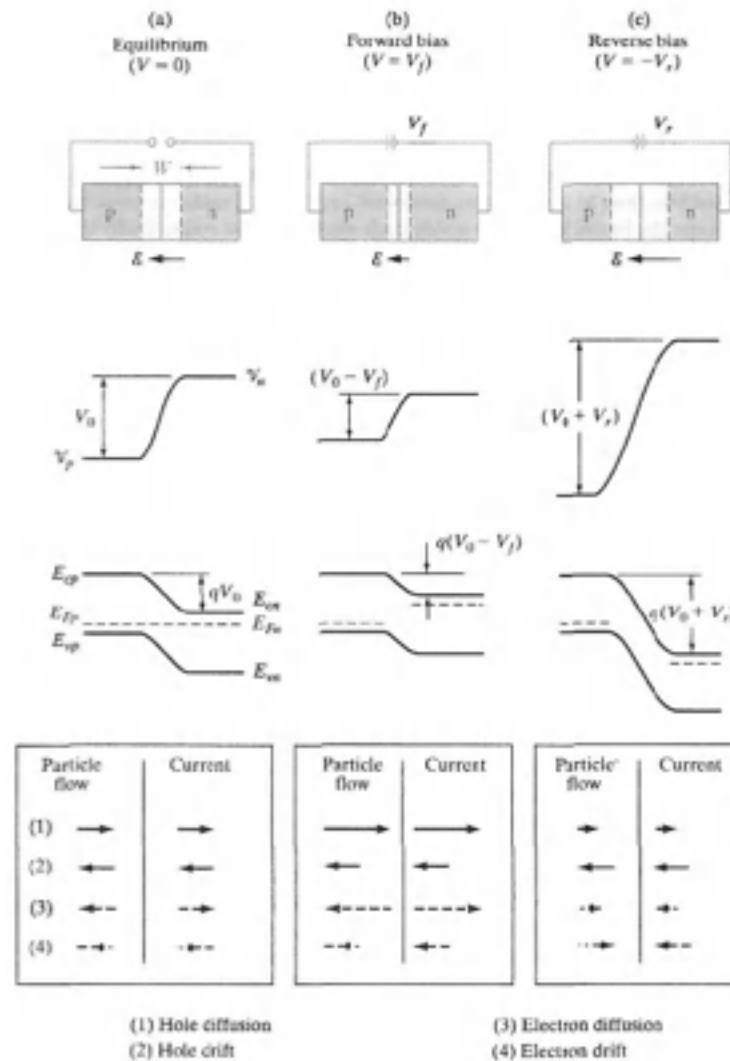
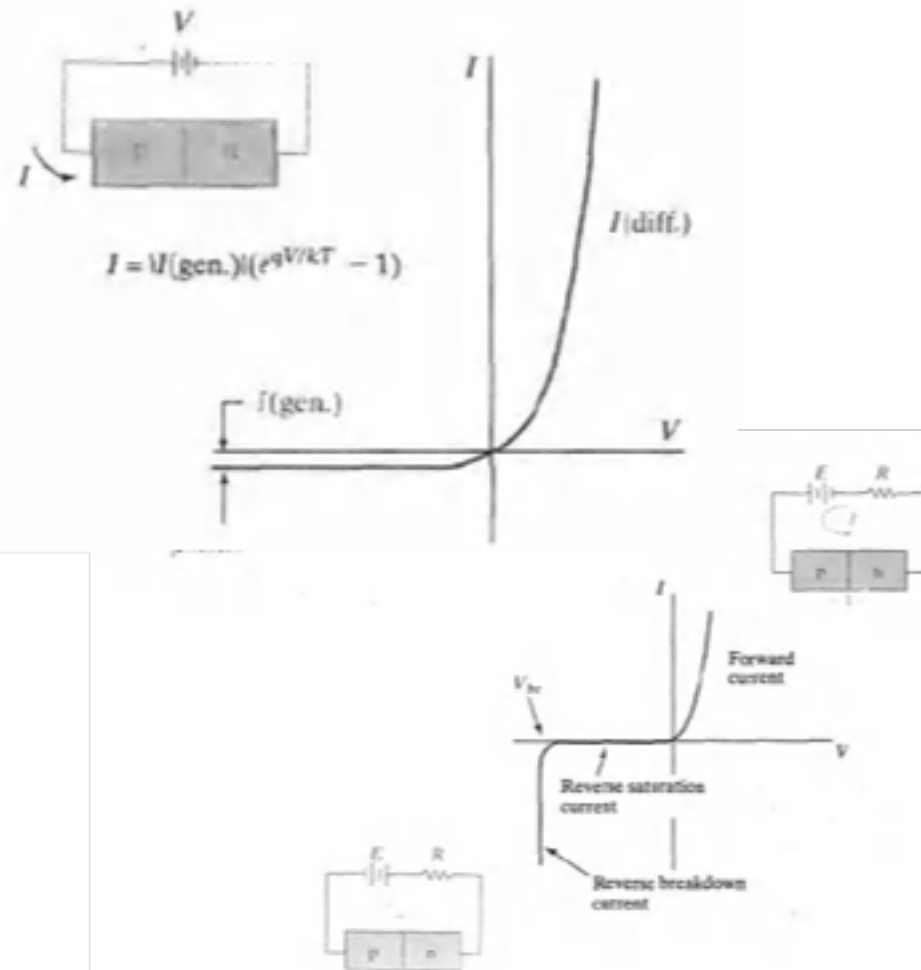


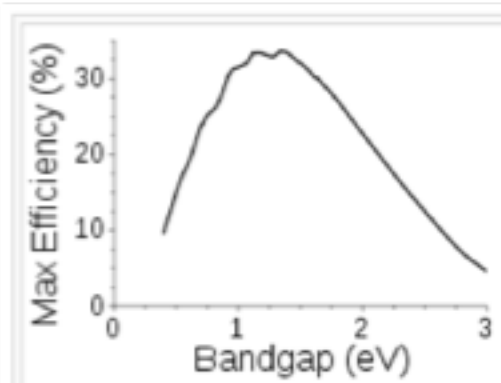
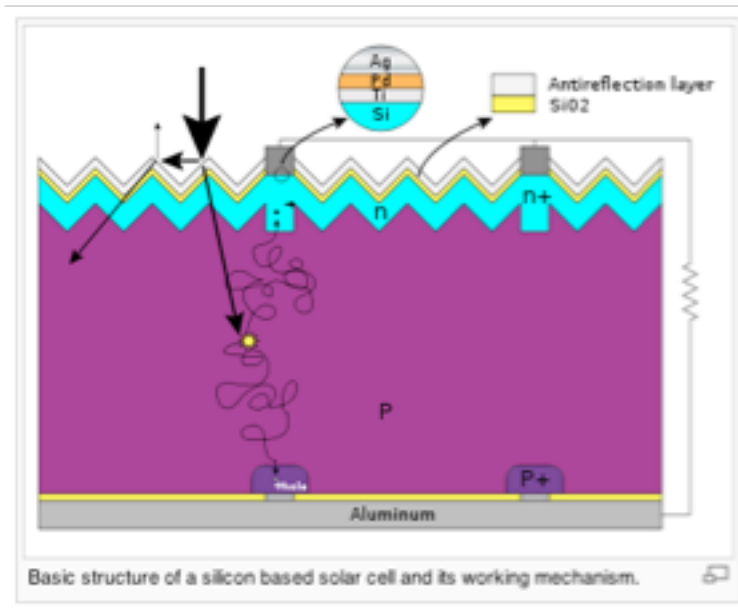
Figure 5-13
Effects of a bias at a p-n junction; transition region width and electric field, electrostatic potential, energy band diagram, and particle flow and current directions within W for (a) equilibrium, (b) forward bias, and (c) reverse bias.

Rectifier or Diode

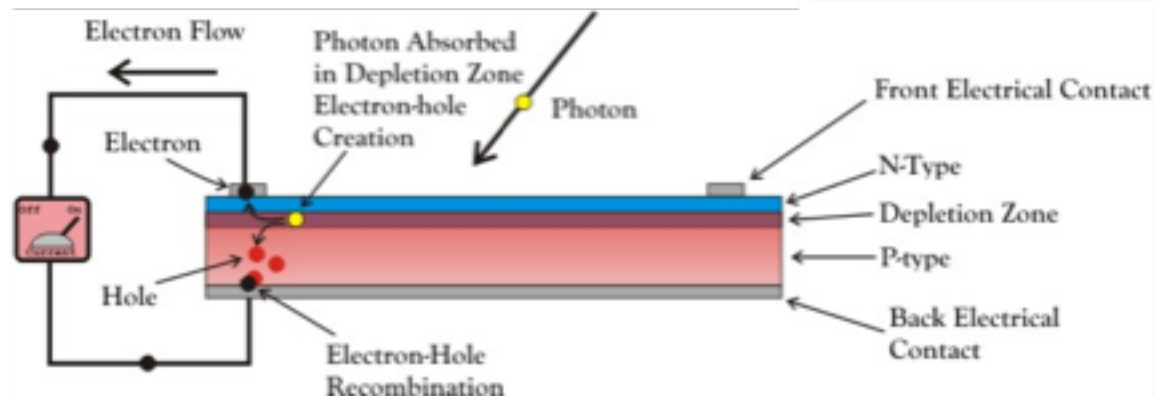
Figure 5-14
I-V characteristic
of a p-n junction.



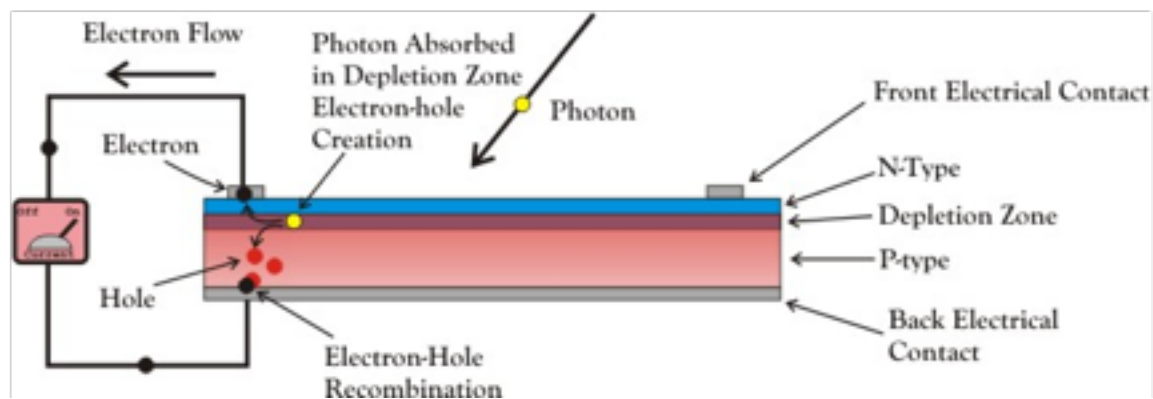
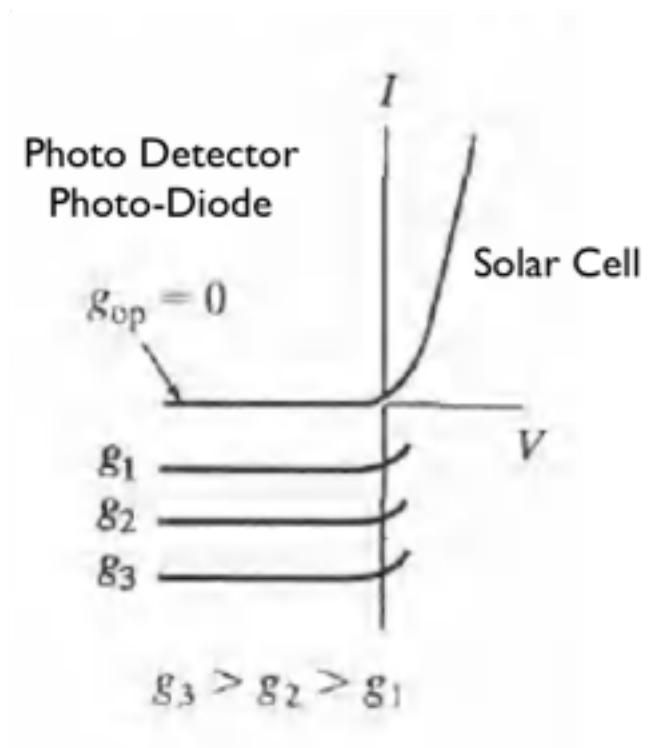
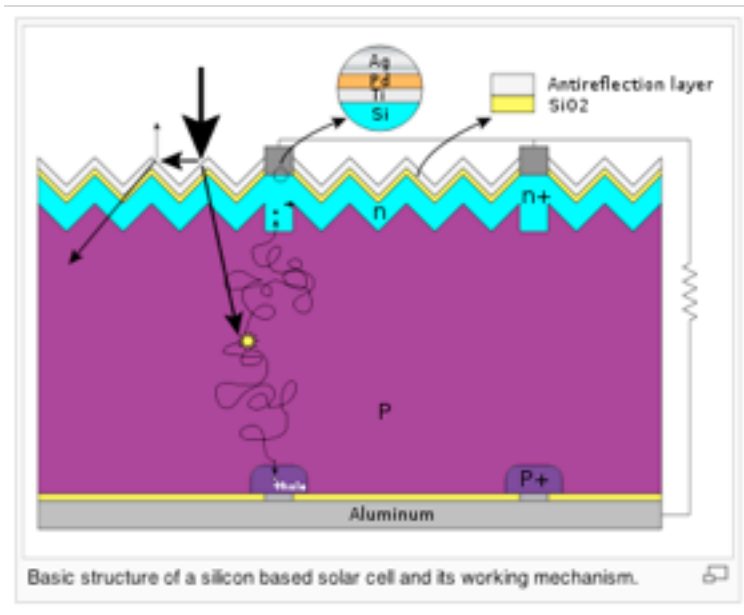
Solar Cell



The [Shockley-Queisser limit](#) for the theoretical maximum efficiency of a solar cell. Semiconductors with [band gap](#) between 1 and 1.5eV have the greatest potential to form an efficient cell. (The efficiency "limit" shown here can be exceeded by [multijunction solar cells](#).)



Solar Cell



Solar Cell

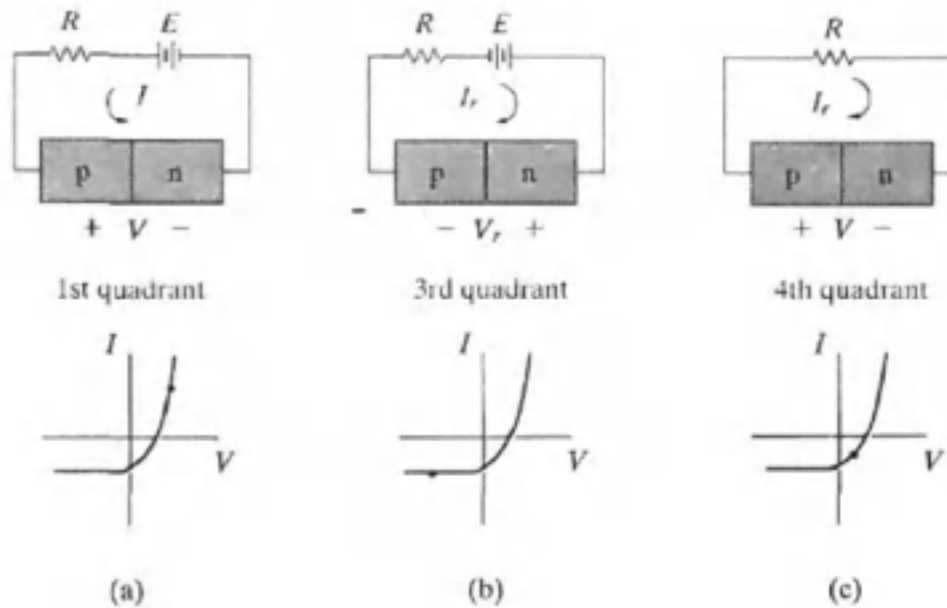
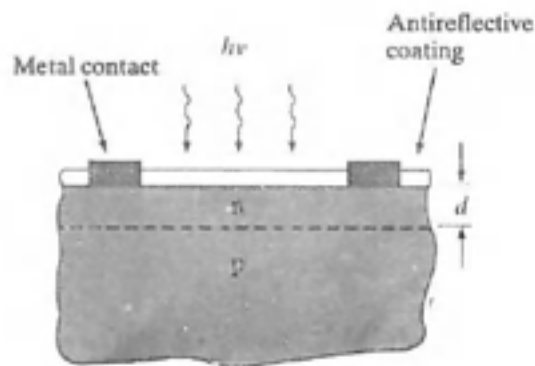
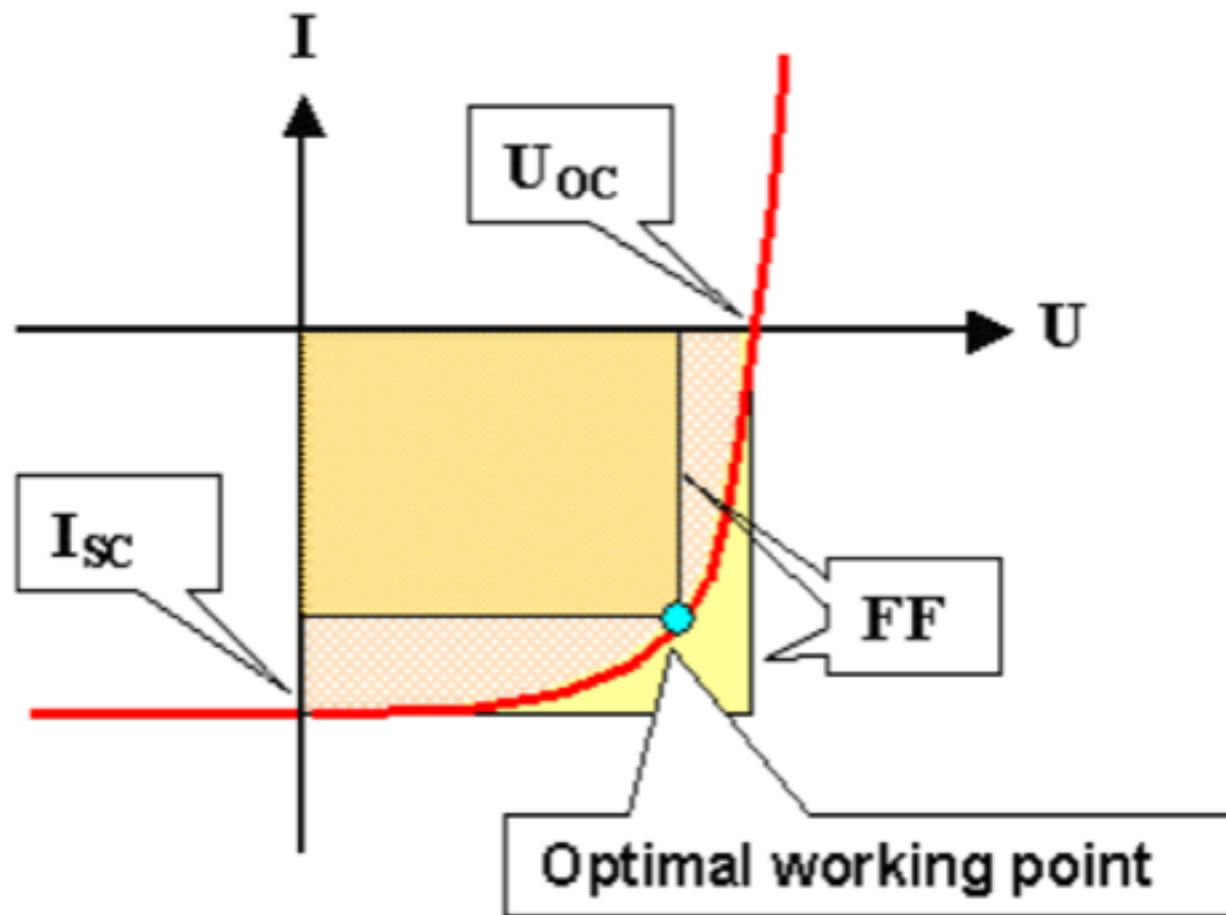


Figure 8-3
Operation of an illuminated junction in the various quadrants of its I - V characteristic; in (a) and (b), power is delivered to the device by the external circuit; in (c) the device delivers power to the load.



Solar Cell



Transistor

Three terminal device in which current through two terminals is controlled by a small current or voltage through the third terminal

Transistors are used for Amplification and Switching

Transistor is a control device

Bipolar Junction Transistor

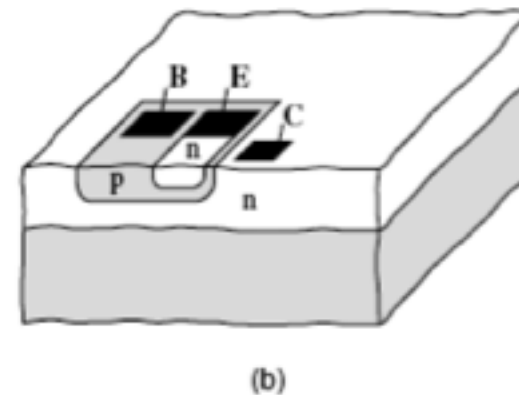
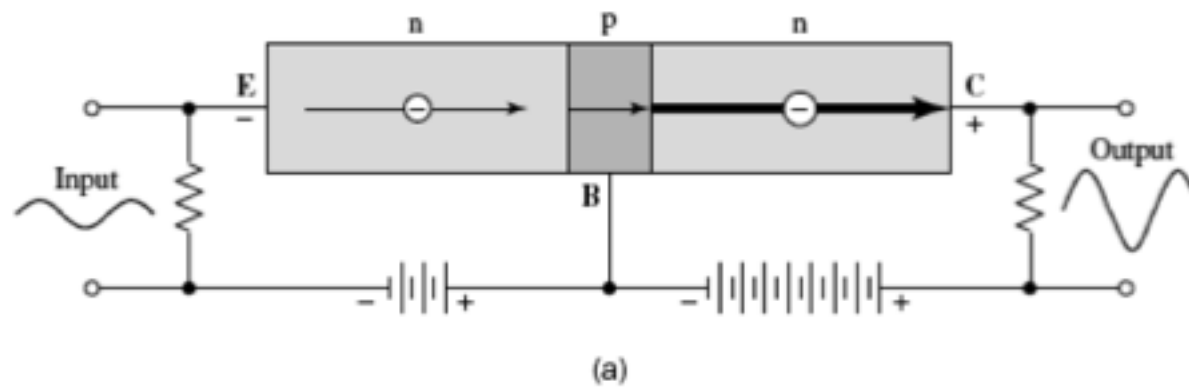


FIGURE 11.16. (a) Biasing of an n-p-n bipolar transistor. (b) Schematic representation of an n-p-n bipolar transistor. The dark areas are the contact pads.

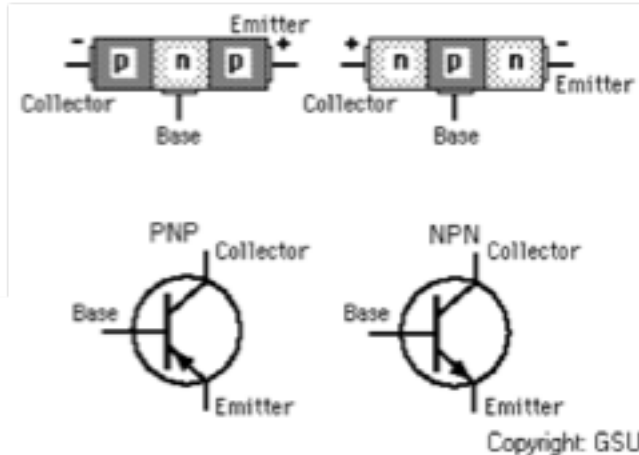
Emitter (E) Base (B) Collector (C)

Bipolar Junction Transistor

Acts like a valve. You have a gate controlled by a small voltage
That controls a large current.
It can act as an amplifier or as a switch.



Assorted discrete transistors.
Packages in order from top to bottom:
TO-3, TO-18, TO-18, SOT-23



Copyright: GSU

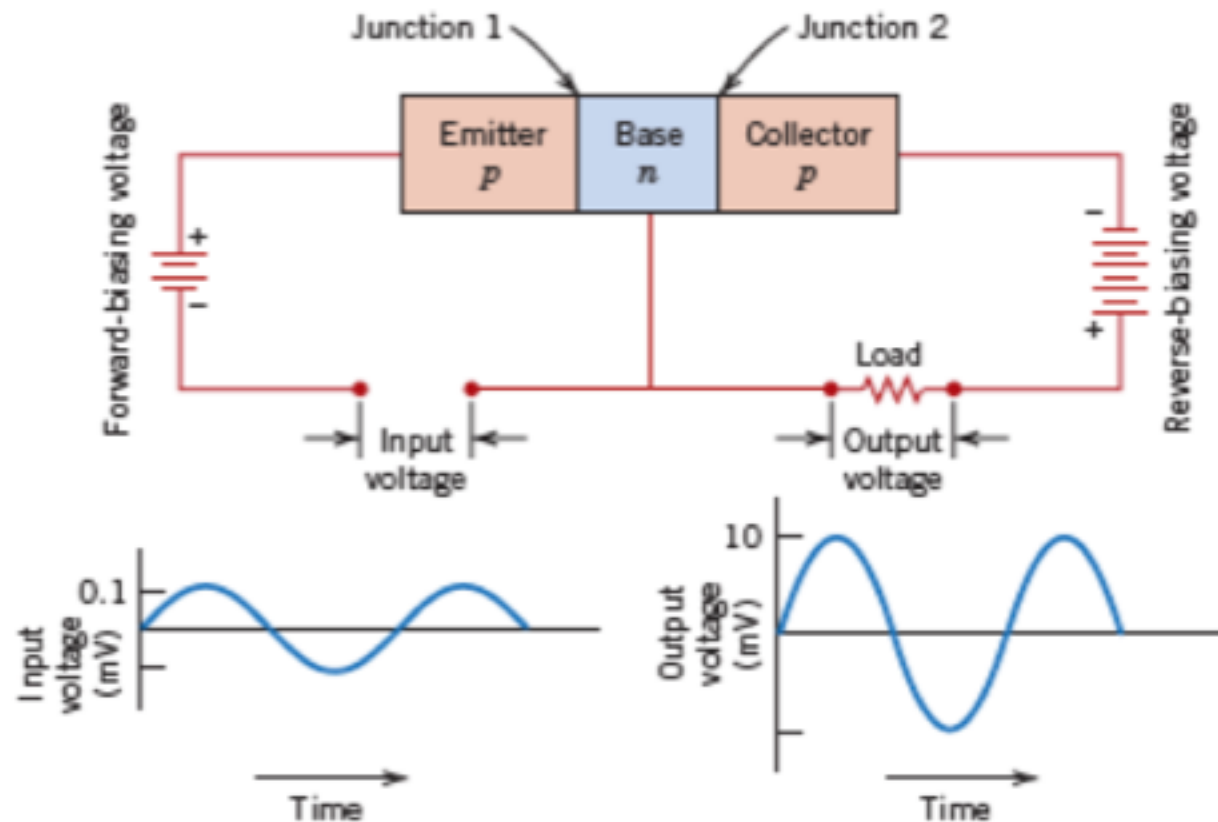
	PNP		NPN	
<i>Number of holes in base control flow</i>	Emitter more positive than the Base Base more positive than Collector		Base more positive than the Emitter Collector more positive than Base	<i>Number of electrons in base control flow</i>

Bipolar Junction Transistor

Figure 18.24

Schematic diagram of a $p-n-p$ junction transistor and its associated circuitry, including input and output voltage-time characteristics showing voltage amplification.

(Adapted from A. G. Guy, *Essentials of Materials Science*, McGraw-Hill Book Company, New York, 1976.)



Summary:

- Development needs are tied to energy
- Solar energy is highly applicable in Ethiopia and is under utilized
- Several examples of solar installations in Haramaya were given
- a business plan for solar panel assembly was shown
- Some details of the physics of silicon PV were given

Send an e-mail to snabeaucage@gmail.com. I will send the homework assignment to you.

In the subject line put “**Technology for Development**”

Send your completed homework to the same address with the subject “**HW1 Technology for Development**”

Homework 1 Development Technology
December 17, 2018

Viability of a simple solar light manufactured in Ethiopia

There are many online sources for the design of a solar light. For example <https://www.youtube.com/watch?v=8earltsP35w>

Compare this design with existing products such as the following NGO:

<https://www.indiegogo.com/projects/unite-to-light-solar-usb-charger-led-light#/>

which will be offered for \$15 in the developing world and is manufactured in China.

Or the \$50 Panasonic solar lantern for the developing world

<https://news.panasonic.com/global/stories/2013/24710.html>

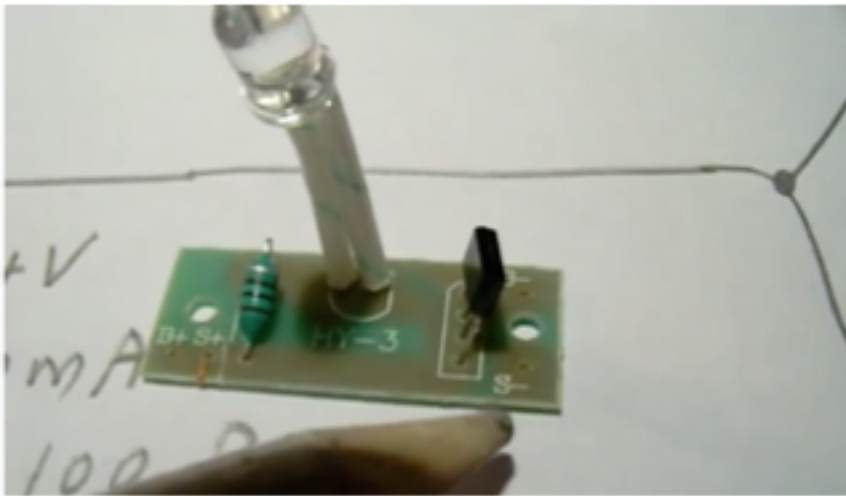
Try to find the approximate cost of the design given on the first webpage by searching at Mouser.com

<https://www.mouser.co.uk>

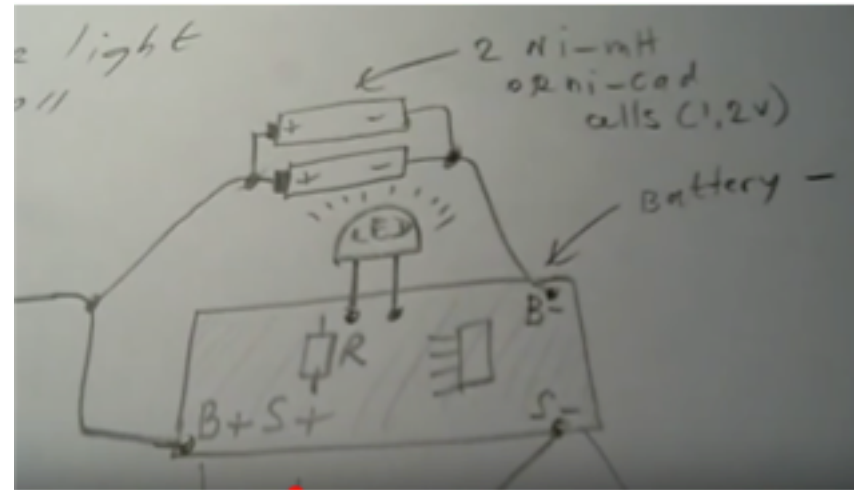
Consider the logistics of setting up manufacturing, marketing and distribution for an Ethiopian solar light/cell phone charger system and give a crude assessment of the viability of manufacturing these devices in Ethiopia for the Ethiopian market.

You answer should be less than one page.

<https://www.youtube.com/watch?v=8earltsP35w>



Resistor and Transistor
LED



Transistor switches to solar charge when sun hits solar panel.
Resistor reduces the voltage from solar panel $V = IR$ to run the LED

When powered charge battery
Use Battery to power LED, could have a switch
Use Battery to charge cell phone

<https://www.indiegogo.com/projects/unite-to-light-solar-usb-charger-led-light#/>



<https://news.panasonic.com/global/stories/2013/24710.html>



Six ways of usage: it can be used as a portable lamp, put on a table or hung in the room.

<https://www.mouser.com>

Contact Mouser (London) +44 (0) 1494-427500 | Feedback

Change Location USD

MOUSER ELECTRONICS

Products Manufacturers More ▾ Order History Log In Register

All ▾ Part No. / Keyword ☐ In Stock ☐ RoHS

PRODUCT FINDER

NEWEST PRODUCTS

- Circuit Protection
- Connectors
- Electromechanical
- Embedded Solutions
- Enclosures
- Engineering Tools
- Industrial Automation
- LED Lighting
- Memory & Data Storage
- Opto-electronics
- Passive Components
- Power
- Semiconductors
- Sensors
- Test & Measurement
- Thermal Management
- Tools & Supplies
- Wire & Cable

[View All](#)

FREE SHIPPING*
on orders over £33

2-3 Day Delivery

[New Shipping](#)

*Some restrictions apply. [Learn more >](#)

AS4006 SAE AEROSPACE STANDARD ACCREDITED

NEWEST PRODUCTS 1 - 4 of 40 | [View More](#)

 Neural Compute Stick 2	 MKR MEM Shield Adds 2MB of flash memory	 i.MX RT Crossover Processors	 X-Lok Mini IP68 Waterproof Connectors
-----------------------------------	---	---	--

December 18 1.5 hours (Batteries)

Questions

Lead acid batteries

Deep cycle batteries

Flow batteries

Nickel iron battery

Lithium ion battery

Battery assembly business plan

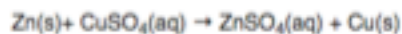
Sensors business plan

Questions

Oxidation/Reduction Metal Displacement Reaction

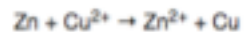
Metal displacement [\[edit \]](#)

In this type of reaction, a metal atom in a compound (or in a solution) is replaced by an atom of another metal. For example, **copper** is deposited when **zinc** metal is placed in a **copper(II) sulfate** solution:



In the above reaction, zinc metal displaces the copper(II) ion from copper sulfate solution and thus liberates free copper metal.

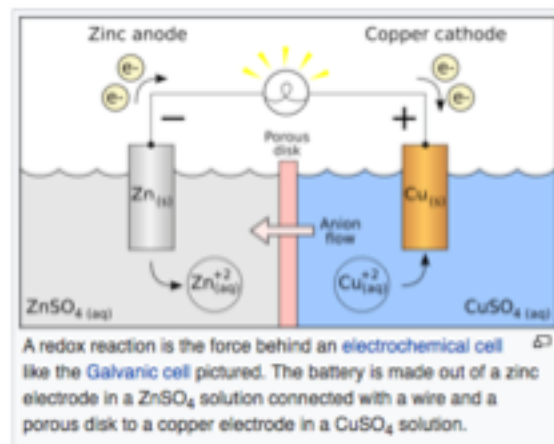
The ionic equation for this reaction is:



As two **half-reactions**, it is seen that the zinc is oxidized:

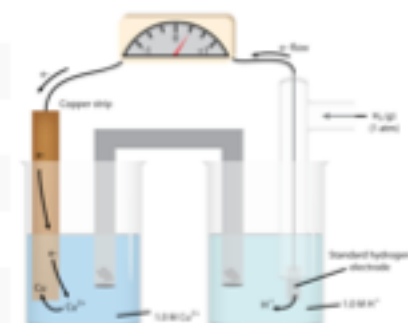
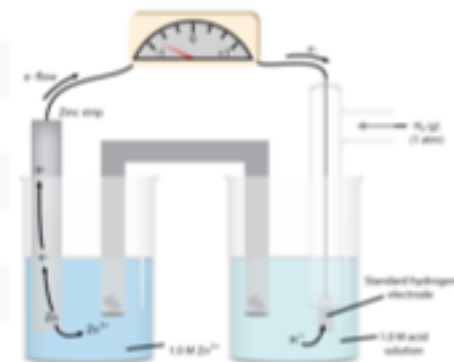


And the copper is reduced:



1.10 Volts for each cell

Activity Series of Metals (in Order of Reactivity)		
Element	Oxidation Half Reaction	
Lithium	$\text{Li(s)} \rightarrow \text{Li}^+(\text{aq}) + \text{e}^-$	Most active or most easily oxidized
Potassium	$\text{K(s)} \rightarrow \text{K}^+(\text{aq}) + \text{e}^-$	
Barium	$\text{Ba(s)} \rightarrow \text{Ba}^{2+}(\text{aq}) + 2\text{e}^-$	
Calcium	$\text{Ca(s)} \rightarrow \text{Ca}^{2+}(\text{aq}) + 2\text{e}^-$	
Sodium	$\text{Na(s)} \rightarrow \text{Na}^+(\text{aq}) + \text{e}^-$	
Magnesium	$\text{Mg(s)} \rightarrow \text{Mg}^{2+}(\text{aq}) + 2\text{e}^-$	
Aluminum	$\text{Al(s)} \rightarrow \text{Al}^{3+}(\text{aq}) + 3\text{e}^-$	
Zinc	$\text{Zn(s)} \rightarrow \text{Zn}^{2+}(\text{aq}) + 2\text{e}^-$	← -0.76 V
Iron	$\text{Fe(s)} \rightarrow \text{Fe}^{2+}(\text{aq}) + 2\text{e}^-$	
Nickel	$\text{Ni(s)} \rightarrow \text{Ni}^{2+}(\text{aq}) + 2\text{e}^-$	
Tin	$\text{Sn(s)} \rightarrow \text{Sn}^{2+}(\text{aq}) + 2\text{e}^-$	
Lead	$\text{Pb(s)} \rightarrow \text{Pb}^{2+}(\text{aq}) + 2\text{e}^-$	
Hydrogen	$\text{H}_2(\text{g}) \rightarrow 2\text{H}^+(\text{aq}) + 2\text{e}^-$	
Copper	$\text{Cu(s)} \rightarrow \text{Cu}^{2+}(\text{aq}) + 2\text{e}^-$	← 0.34 V
Mercury	$\text{Hg(l)} \rightarrow \text{Hg}^{2+}(\text{aq}) + 2\text{e}^-$	
Silver	$\text{Ag(s)} \rightarrow \text{Ag}^+(\text{aq}) + \text{e}^-$	
Platinum	$\text{Pt(s)} \rightarrow \text{Pt}^{2+}(\text{aq}) + 2\text{e}^-$	
Gold	$\text{Au(s)} \rightarrow \text{Au}^{3+}(\text{aq}) + 3\text{e}^-$	Least active or most difficult to oxidize

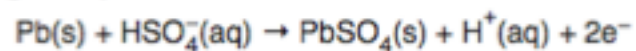


$$E_{\text{cell}}^{\circ} = 0.34 \text{ V (copper)} - (-0.76 \text{ V zinc}) = 1.10 \text{ volts for the cell}$$

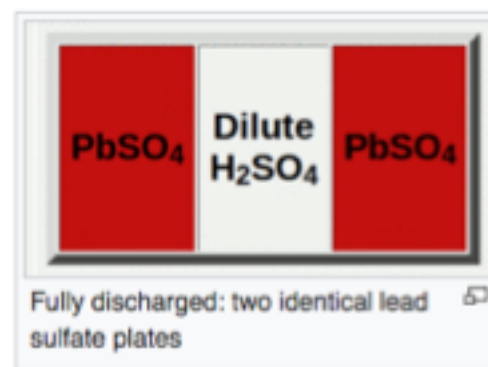
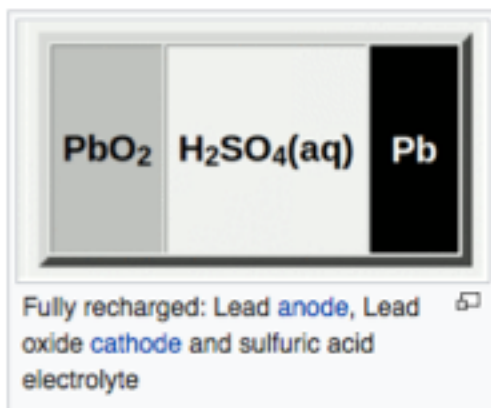
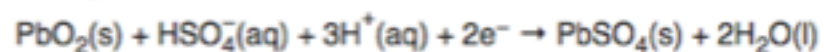
Standard Reduction Potentials at 25°C	
Half Reaction	E ⁰ (V)
$F_2 + 2e^- \rightarrow 2F^-$	+2.87
$PO_4^{3-} + 4H^+ + 5e^- \rightarrow PO_4^{3-} + 2H_2O$	+1.70
$MnO_4^- + 8H^+ + 5e^- \rightarrow Mn^{2+} + 4H_2O$	+1.51
$Au^{3+} + 3e^- \rightarrow Au$	+1.50
$O_2 + 2e^- \rightarrow 2O^{2-}$	+1.36
$Cr_2O_7^{2-} + 14H^+ + 6e^- \rightarrow 2Cr^{3+} + 7H_2O$	+1.33
$O_2 + 4H^+ + 4e^- \rightarrow 2H_2O$	+1.23
$Br_2 + 2e^- \rightarrow 2Br^-$	+1.07
$NO_3^- + 4H^+ + 3e^- \rightarrow NO + 2H_2O$	+0.96
$2Hg^{2+} + 2e^- \rightarrow Hg_2^{2+}$	+0.92
$Hg^{2+} + 2e^- \rightarrow Hg$	+0.85
$Ag^+ + e^- \rightarrow Ag$	+0.80
$Fe^{3+} + e^- \rightarrow Fe^{2+}$	+0.77
$I_2 + 2e^- \rightarrow 2I^-$	+0.53
$Cu^+ + e^- \rightarrow Cu$	+0.52
$O_2 + 2H_2O + 4e^- \rightarrow 4OH^-$	+0.40
$Cu^{2+} + 2e^- \rightarrow Cu$	+0.34
$Sn^{4+} + 2e^- \rightarrow Sn^{2+}$	+0.13
$2H^+ + 2e^- \rightarrow H_2$	0.00
$Pb^{2+} + 2e^- \rightarrow Pb$	-0.13
$Sn^{2+} + 2e^- \rightarrow Sn$	-0.14
$Ni^{2+} + 2e^- \rightarrow Ni$	-0.25
$Co^{2+} + 2e^- \rightarrow Co$	-0.28
$PbSO_4 + 2e^- \rightarrow Pb + SO_4^{2-}$	-0.35
$Ce^{3+} + 2e^- \rightarrow Ce$	-0.40
$Fe^{2+} + 2e^- \rightarrow Fe$	-0.44
$Cl_2 + 2e^- \rightarrow 2Cl^-$	-0.74
$Zn^{2+} + 2e^- \rightarrow Zn$	-0.76
$2H_2O + 2e^- \rightarrow H_2 + 2OH^-$	-0.83
$Mn^{2+} + 2e^- \rightarrow Mn$	-1.18
$Al^{3+} + 3e^- \rightarrow Al$	-1.66
$Be^{2+} + 2e^- \rightarrow Be$	-1.70
$Mg^{2+} + 2e^- \rightarrow Mg$	-2.37
$Na^+ + e^- \rightarrow Na$	-2.71
$Ca^{2+} + 2e^- \rightarrow Ca$	-2.87
$Sr^{2+} + 2e^- \rightarrow Sr$	-2.89
$Ba^{2+} + 2e^- \rightarrow Ba$	-2.90
$Rb^+ + e^- \rightarrow Rb$	-2.92
$K^+ + e^- \rightarrow K$	-2.92
$Cs^+ + e^- \rightarrow Cs$	-2.92
$Li^+ + e^- \rightarrow Li$	-3.05

Deep Cycle Lead Acid Battery Manufacture

Negative plate reaction



Positive plate reaction

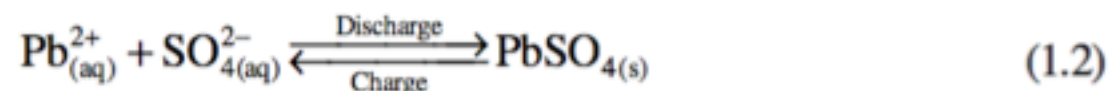
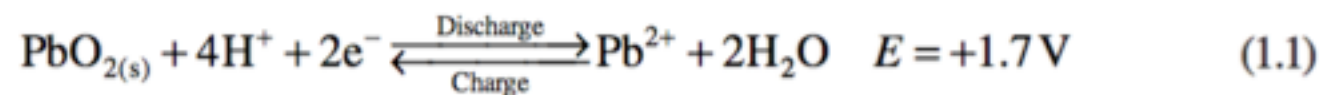


The total reaction can be written as



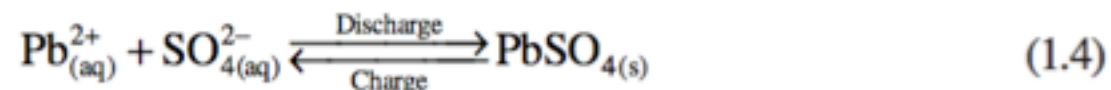
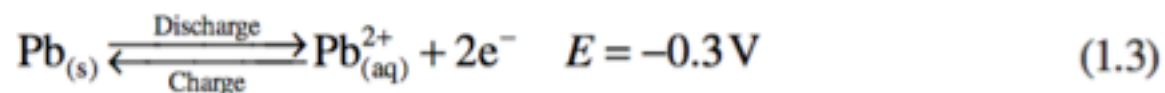
[Lead Acid Battery Technologies \(eBook at UC\)](#)

Reduction

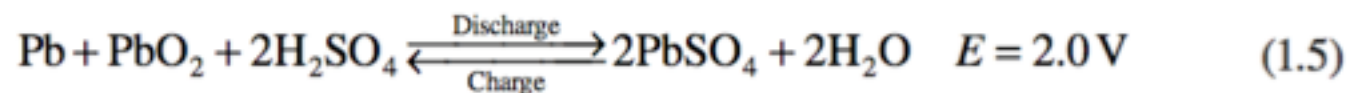


Negative electrode (cathode):

Oxidation



Overall reaction:



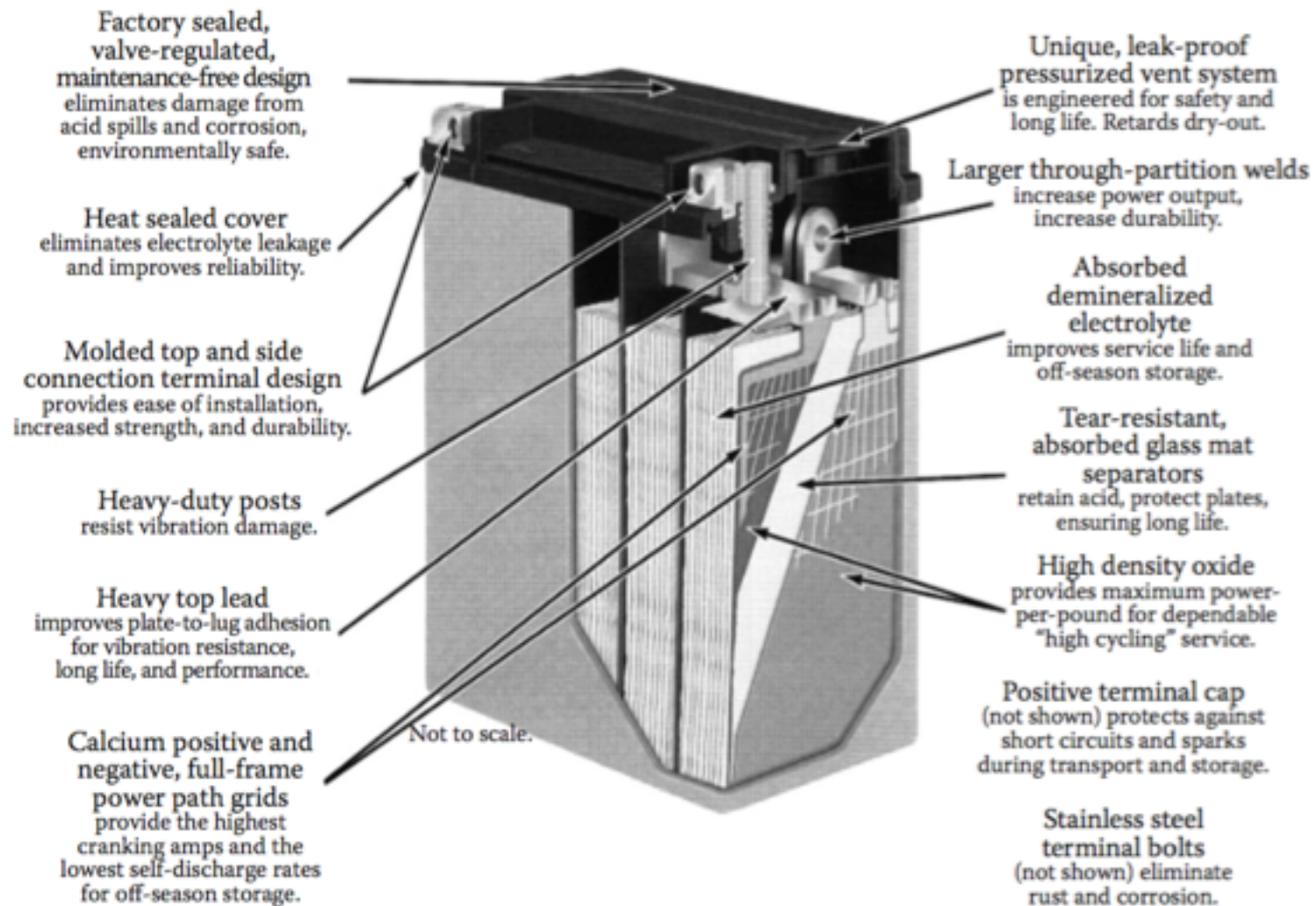


FIGURE 1.1 Cut-away of lead-acid battery. (From East Penn Manufacturing Co.)

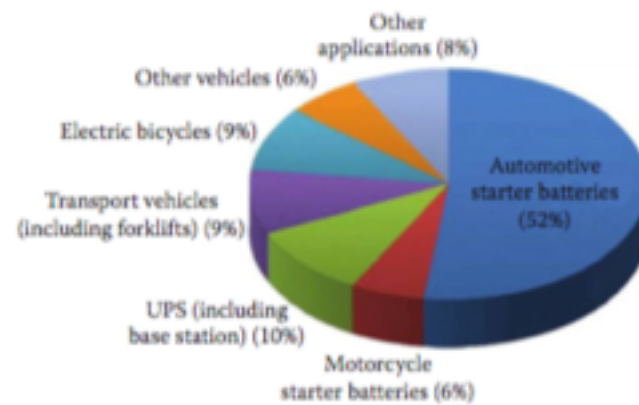


FIGURE 10.1 Lead-acid battery market application category ratio. (Available at <http://www.systems-sunlight.com/blog/global-lead-acid-battery-market-development-status>.)

10.2 LEAD BATTERIES IN APPLICATIONS

10.2.1 TYPES OF LEAD-ACID BATTERIES

The many different types of lead-acid batteries on the market are used for various applications. The major types of lead-acid batteries can be described as follows [3]:

1. *Valve-regulated lead-acid (VRLA) batteries.* Also called *sealed lead-acid (SLA) batteries*, the VRLA batteries can prevent electrolyte evaporation loss, spillage, and gassing, which leads to a prolonged maintenance-free life span. The top of the battery has a capped vent that is used for the escape of gas. It also has some pressure valves that can open only under extreme conditions. This type of battery uses a specially designed electrolyte to reduce the release of gases such as oxygen and hydrogen generated by the side reactions that occur during charging. A recombinant system with a catalyst inside the battery is needed to facilitate the combination reaction between hydrogen and oxygen to recombine into water. This type of battery is normally safer than other types because the acid electrolyte spoilage is eliminated. This type of battery is used mainly in automobiles.
2. *Absorbed glass mat (AGM) batteries.* Also known as *absorptive glass microfiber (AGMF) batteries*, this type of battery belongs to the class of VRLA batteries, but it has a boron silicate fiber glass mat that acts as a separator between the electrodes, which can absorb the free electrolyte in much the same way a sponge absorbs water. This separator can promote recombination of the hydrogen and oxygen produced during the charging process. The fiber glass mat can absorb and immobilize the acid in the mat as a form of liquid rather than a gel form, therefore, there is no gel electrolyte in this type of battery. Furthermore, in the presence of such a mat separator, the acid electrolyte is more readily available to the plates, allowing for faster reactions between the acid and the plate material, resulting in higher charge-discharge rates as well as deep cycling. In addition, because the electrolyte is kept inside the mat separator, the battery is more robust and able to withstand severe shock and vibration without leakage even if the case is cracked. To realize this, the fiber glass mat separator is normally 95% saturated with sulfuric acid with excess electrolyte. For this reason, AGM batteries are also sometimes called “starved electrolyte” or “dry” batteries.
3. *Gel batteries.* This type of battery also belongs to the class of VRLA batteries. The acid electrolyte is in the form of a gel, however, rather than mobile liquid, which promotes oxygen recombination. In addition, batteries that use a gel as the electrolyte are more robust.

4. *Starting, lighting, and ignition (SLI) batteries.* SLI batteries are specially designed for automobile starting-lighting-ignition applications. The design does not allow the battery to be discharged below 50% depth of discharge (DOD) because discharging below these levels could damage the plates and shorten battery life. In general, automotive batteries are always fully charged before starting the car. After starting the vehicle, the lost charge, typically 2% to 5% of the charge, is immediately replaced by the alternator and the battery returns to the fully charged state.
5. *Deep-cycle batteries.* Deep-cycle batteries are designed to be completely discharged before recharging. This is required by applications such as marine applications, golf carts, forklifts, and electric vehicles, where the batteries could be deeply cycled. In this deep-cycling process, excessive heat is produced, which can warp the plates. Therefore, thicker and stronger or solid plate grids are normally used for deep-cycle applications.

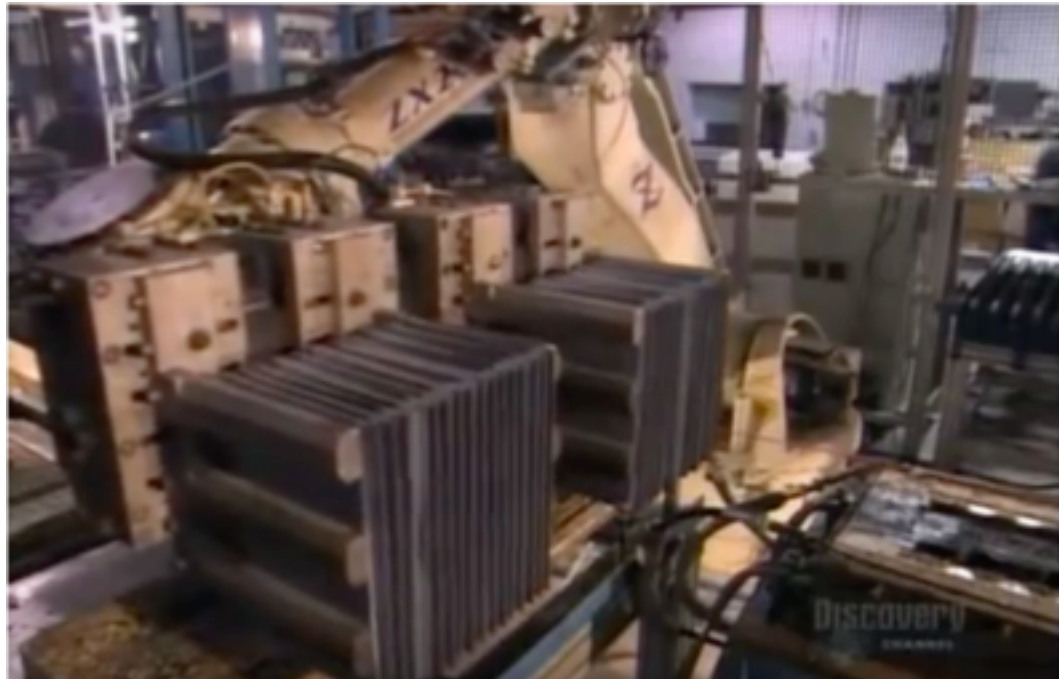
Gelled electrolytes [\[edit \]](#)

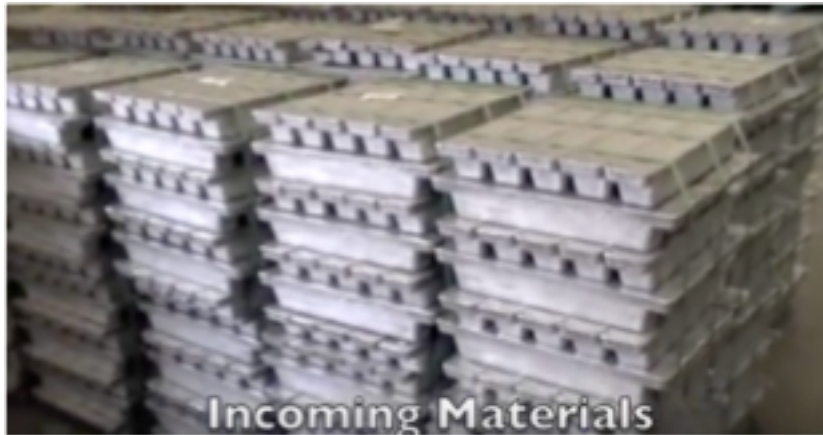
Main article: VRLA battery § Gel_battery

During the 1970s, researchers developed the sealed version or "gel battery", which mixes a silica gelling agent into the electrolyte (silica-gel based lead-acid batteries used in portable radios from early 1930s were not fully sealed). This converts the formerly liquid interior of the cells into a semi-stiff paste, providing many of the same advantages of the AGM. Such designs are even less susceptible to evaporation and are often used in situations where little or no periodic maintenance is possible. Gel cells also have lower freezing and higher boiling points than the liquid electrolytes used in conventional wet cells and AGMs, which makes them suitable for use in extreme conditions.

The only downside to the gel design is that the gel prevents rapid motion of the ions in the electrolyte, which reduces carrier mobility and thus surge current capability. For this reason, gel cells are most commonly found in energy storage applications like off-grid systems.

Deep Cycle Battery Manufacture in the Developed World

















<https://www.youtube.com/watch?v=MOTFBDLziHI>

[Battery Manufacture in Nepal Part 1](#)

[Battery Manufacture in Nepal Part 2](#)



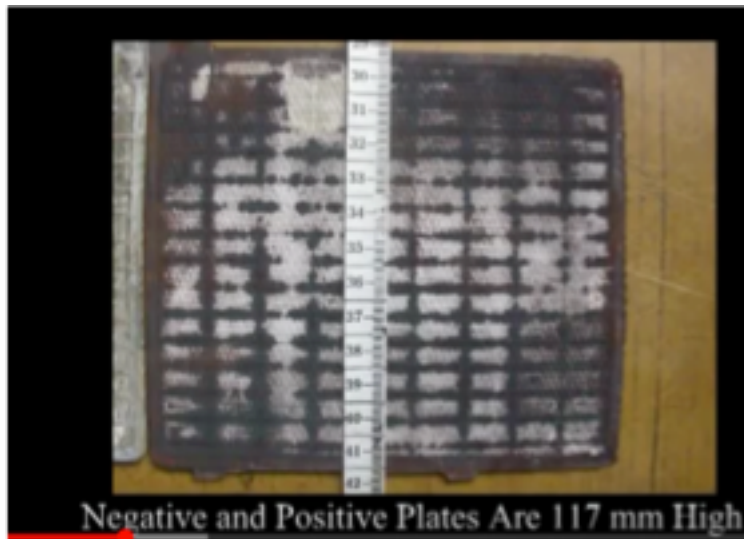
manufacturing of local batteries in Nepal has been stimulated by the enormous amounts of installed lead-acid batteries, as part of the last decades nation wide installed Solar PV Systems in the remote and fragile high altitude communities of Nepal's Himalayas. Uncountable batteries have not provided the expected energy storage capacity and



Battery Plates Are Flat, Rectangular Components



Support Structure Called A Grid. Plates Are Either







4 Negative Cells Soldered Together



Positive Battery Cells



Cleaning The Soldering Iron







Such As: Polyethylene, Polyvinyl Chloride.



Separators Divide The Positive and Negative Plates



Than The Area Of The Plates To Prevent Material









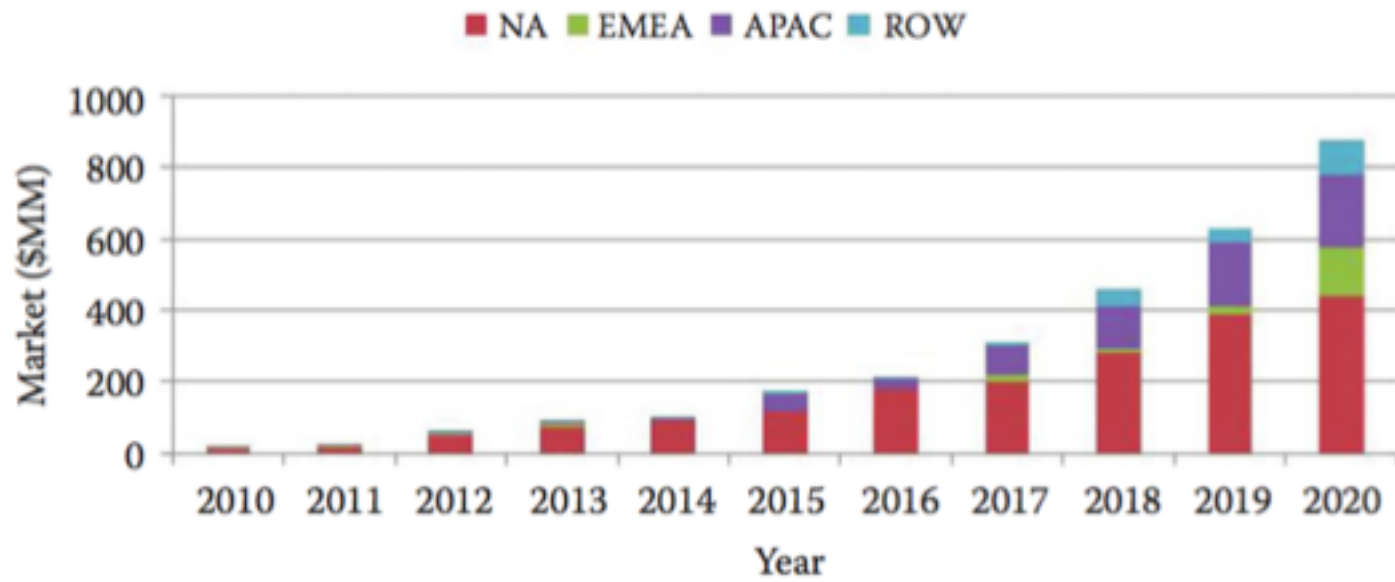


FIGURE 1.7 Emerging grid battery market projection.

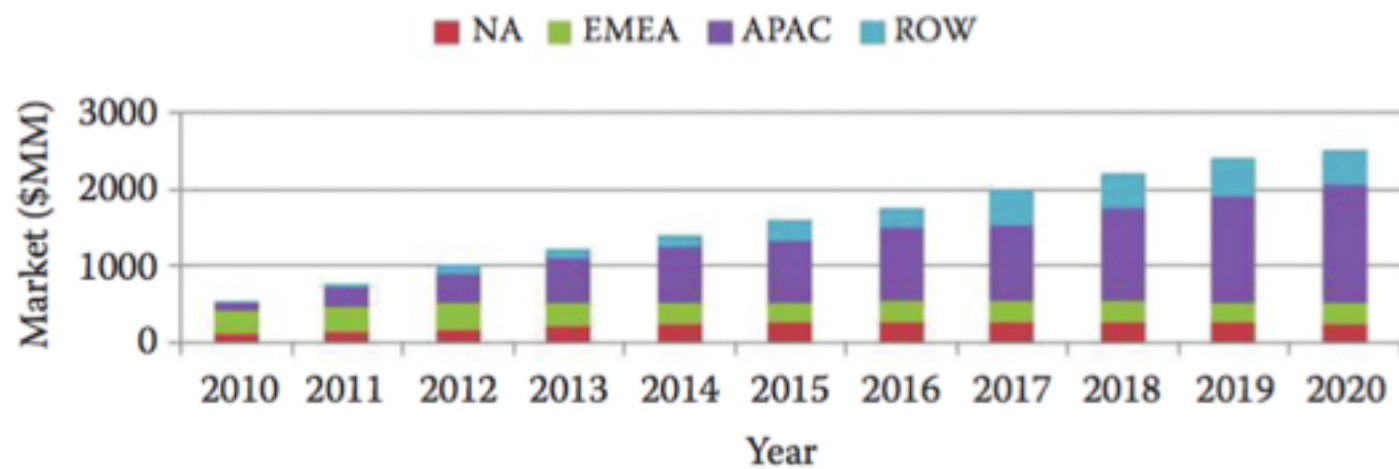
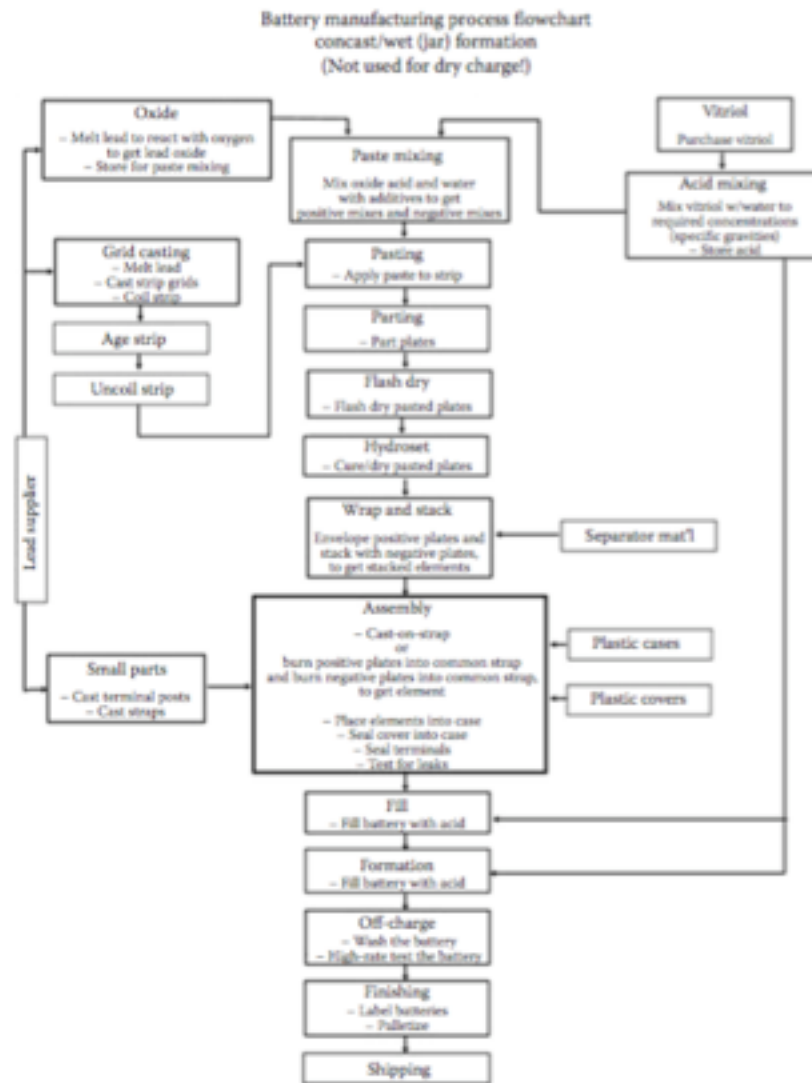


FIGURE 1.8 Distributed renewable battery market projection.



Vitriol = Sulfate

FIGURE 1.23 Battery assembly process. (From <http://www.docstoc.com>.)



FIGURE 7.1 Battery manufacturing process. (From International Thermal Systems. Available at <http://internationalthermalsystems.com/batterymanufacturing>.)

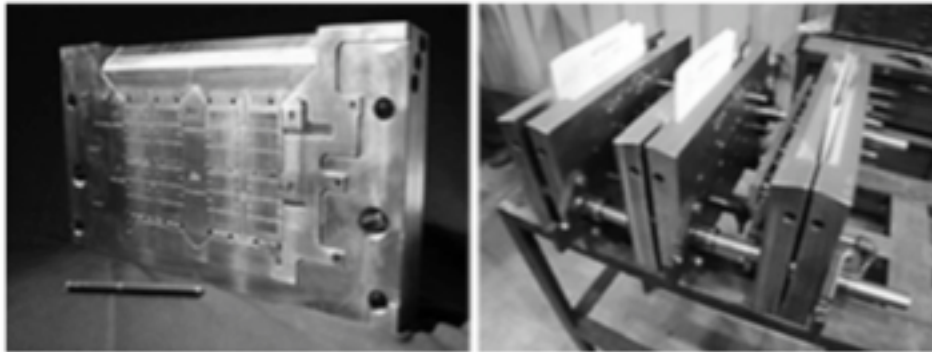


FIGURE 7.2 Battery grid casting mold (book mold). (From Wirtz Manufacturing. Available at <http://www.wirtzusa.com>.)



FIGURE 7.3 Book mold grid caster. (From Wirtz Manufacturing. Available at <http://www.wirtzusa.com>.)

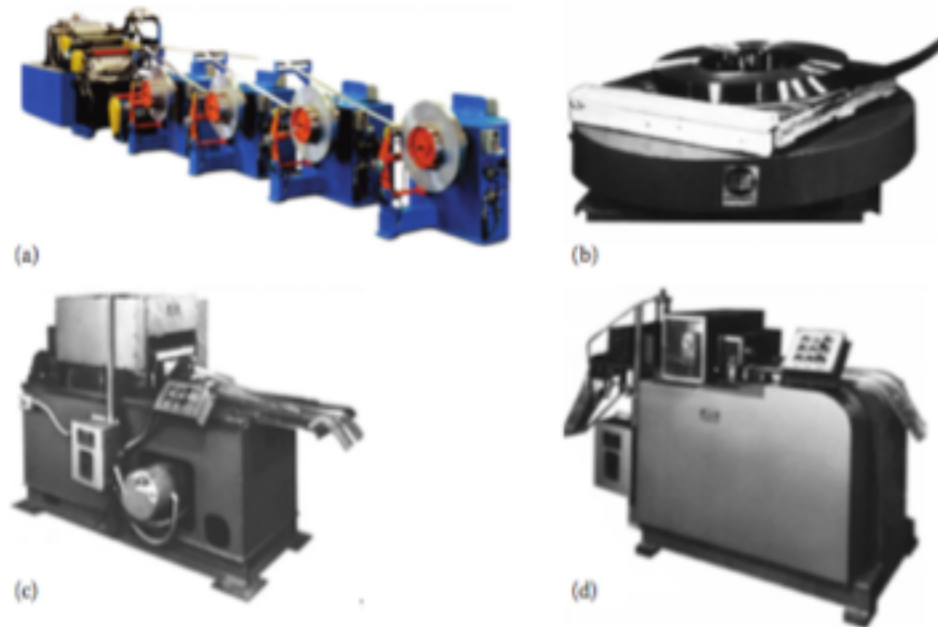


FIGURE 7.4 Strip expansion process equipment. (a) Lead-alloy strip caster: Multialloy caster produces fully edge-trimmed lead alloy strips; (b) Coil feeder: This machine feeds the coiled lead from the horizontal position; (c) Expander: Using a die, the expander produces controlled expansion, which results in the grid's diamond pattern and height; (d) Shaper: The shaper forms the lugs and accurately sizes the grid for height and thickness. A positive feed mechanism aligns and positions the expanded strip and a punch-and-die knocks out clean, reclaimable lead from the unexpanded center portion of the strip. (From MAC Engineering. Available at <http://www.mac-eng.com>; Battery Technology Solutions Inc. Available at <http://www.batechsol.com>.)



FIGURE 7.6 Continuous grid caster. (From Wirtz Manufacturing. Available at <http://www.wirtzusa.com>.)

7.2 LEAD OXIDE PRODUCTION

Lead oxide is the main component of the active material for both positive and negative electrodes. Lead oxide is made by oxidizing lead using either the Barton pot process or the Ball mill process.

7.2.1 BARTON POT PROCESS

The Barton pot process (also called the Barton-like process) is a process that melts lead ingots and feeds them into a vessel or pot. The molten lead is rapidly stirred and atomized into very small droplets via a rotating paddle in proximity to the bottom of the vessel. The droplets of molten lead are then oxidized by oxygen in the air to produce an oxide coating around the droplet. Figure 7.7 shows a flowchart for the Barton pot process.

The lead oxidation process is exothermic and the generated heat is essential for sustaining a continuous reaction as more lead is introduced. The process temperature is critical for determining the degree of oxidation and crystal morphology of the lead oxide. The Barton pot process typically produces a product containing lead oxide with 15% to 30% free lead, which exists as the core of the lead oxide spherically shaped particles. Figure 7.8 shows a Barton pot.

7.2.2 BALL MILL PROCESS

In the Ball mill process, as shown in Figure 7.9, lead pieces are fed into a rotating mill and the attrition of the lead pieces produces fine metallic lead flakes. The friction of lead flakes tumbling against each other inside the mill chamber creates sufficient heat to oxidize the lead flakes' surfaces. The degree of lead oxidation is impacted by the airflow through the system. The airflow also moves the lead oxide particles to be collected in a baghouse. The product of the Ball mill process contains 15% to 30% free lead in the shape of a flattened platelet core surrounded by an oxide coating. Figure 7.10 shows a Ball mill [3,5].

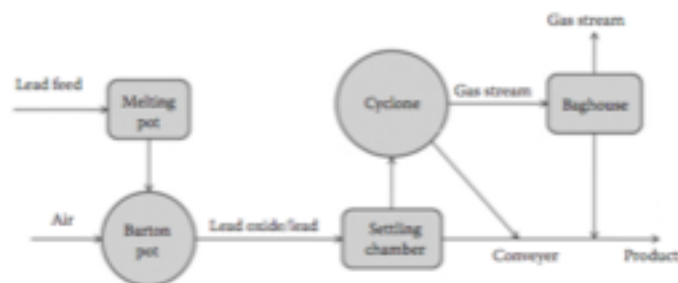


FIGURE 7.7 Flowchart of the Barton pot process.



FIGURE 7.8 Barton pot. (From Wirtz Manufacturing. Available at <http://www.wirtzusa.com/>.)



FIGURE 7.9 Flowchart of Ball mill process.



FIGURE 7.10 Ball mill. (From MAC Engineering. Available at <http://www.mac-eng.com/>; Leader Tech United. Available at <http://www.ltucompany.com/>.)

TABLE 7.1
Lead Oxide Characteristics of the Products of the Barton Pot and Ball Mill Processes

Characteristic	Barton Pot	Ball Mill
Particle size	3–4 mm in diameter	2–3 mm in diameter
Stability/reactivity in air	Stable	High reactivity in air
Oxide crystal structures (wt%)	5–30% β -PbO, remaining balance α -PbO	100% α -PbO
Acid adsorption (mg H ₂ SO ₄ /g oxide)	160–200	240
Surface area (m ² /g)	0.7	2.0–3.0
Free lead content (wt%)	18–28	25–35
Paste mixing characteristics	Softer paste	Stiffer paste
Paste curing	Average curing rate	Faster curing rate
Battery performance	Better battery life, low capacity	Good capacity, shorter life
Deep-cycle ability	Usually good	Sometimes good
Process control	More difficult	Easier
Production rate (kg/h)	300–900	1000
Operating costs	Low operating and maintenance costs	Higher operating and maintenance costs
Facility requirement	Smaller footprint	Bigger footprint
Energy consumption (kWh/ton)	Up to 100	100–300

Table 7.1 lists the lead oxide characteristics produced by the Barton pot and Ball mill processes.

7.3.1 BATCH PASTE MIXER

Conventional mechanical mixers are batch type. The major types of mechanical mixers are the pony mixer, the muller, or the vertical muller (Figure 7.11). The batch paste mixer contains three major components: the paste tank, mixing system, and cooling system.

1. *Paste tank.* The paste tank is a closed cylindrical steel tank. The upper part of the tank has inspection doors and hoses for cooling air inlet and outlet. There are also pipes for the inlet of acid and water. The sides of the tank have two discharging doors that are used to dump the final prepared paste into the cone feeder.
2. *Mixing system.* The mixing system contains rotating paddles, which provide a complete mixing action of the various components (lead, acid, water, and additives/expanders) to obtain a uniform and easily pasted paste.



FIGURE 7.11 Vertical muller mixer. (From MAC Engineering. Available at <http://www.mac-eng.com>.)

3. *Cooling system.* In the mixing cycle, cooling is essential because heat is generated by the exothermic reaction between H_2SO_4 and lead oxide. Failure to maintain proper paste temperature causes hardening of the paste before it can be used. The temperature of the paste needs to be controlled, and this is often achieved by either cooling the mixer or evaporating the extra volume of water in the paste mixture. It is important to maintain the mixing temperature to ensure a good-quality paste results. Often, two types of cooling systems are used in the paste mixing system. The first cooling system, an air-conditioning (AC) system, uses a fan blowing over the paste surface for cooling. The second cooling system uses circulating water that runs through the bottom and surrounding area of the tank to maintain the desired temperature/cooling. The peak temperature limit for the pasting cycle is 60°C , whereas the final paste or dumping paste temperature should be less than 50°C .

The paste viscosity will rise in the beginning of paste mixing, but then gradually decreases. The ratio of lead oxide, water, and sulfuric acid varies depending on the type of battery applications. For example, plates for SLI application are generally made at a low $\text{PbO}:\text{H}_2\text{SO}_4$ ratio, whereas plates for deep-cycle applications are made at a high $\text{PbO}:\text{H}_2\text{SO}_4$ ratio. On the other hand, the amount of sulfuric acid affects the plate density because the more acid used, the lower the plate density. Paste density is measured by using a cup with a hemispherical cavity and by the measurement of paste consistency (viscosity) with a penetrometer.



FIGURE 7.12 Continuous paste mixer. (From Battery Technology Solutions Inc. Available at <http://www.batechsol.com>.)



FIGURE 7.13 Continuous belt paster. (From Wirtz Manufacturing. Available at <http://www.wirtzusa.com>.)

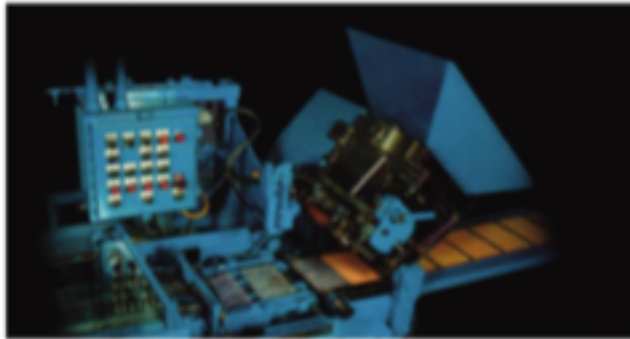


FIGURE 7.14 Continuous orifice pasteur. (From Wirtz Manufacturing. Available at <http://www.wirtzusa.com>.)

1.7.2 DEEP-CYCLE AND TRACTION BATTERIES

Deep-cycle batteries require good cycle life, high energy density, and low cost. The cycle life of a deep-cycle battery is usually longer than that of an SLI battery. The longer cycle life is achieved in the following manner:

1. Use thick plates with high paste density.
2. Cure the plates with a high-temperature and high-humidity profile.
3. Employ a low-specific-gravity electrolyte for formation.

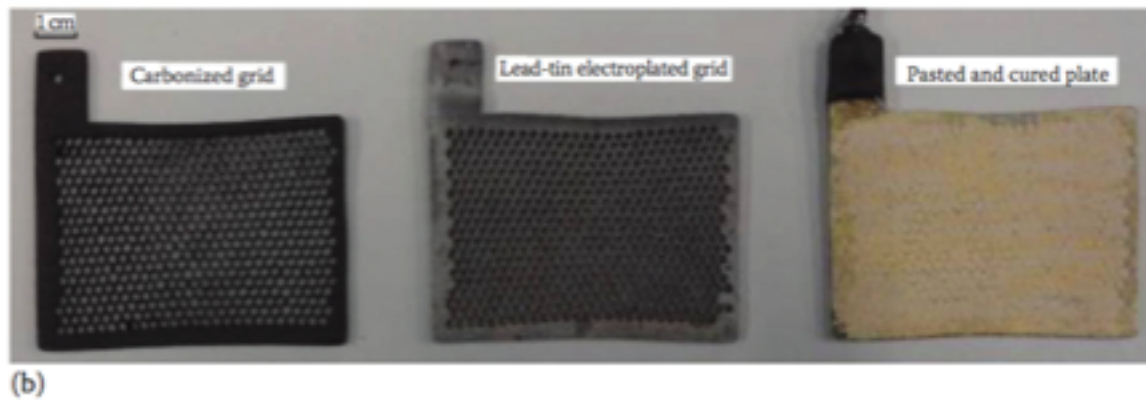
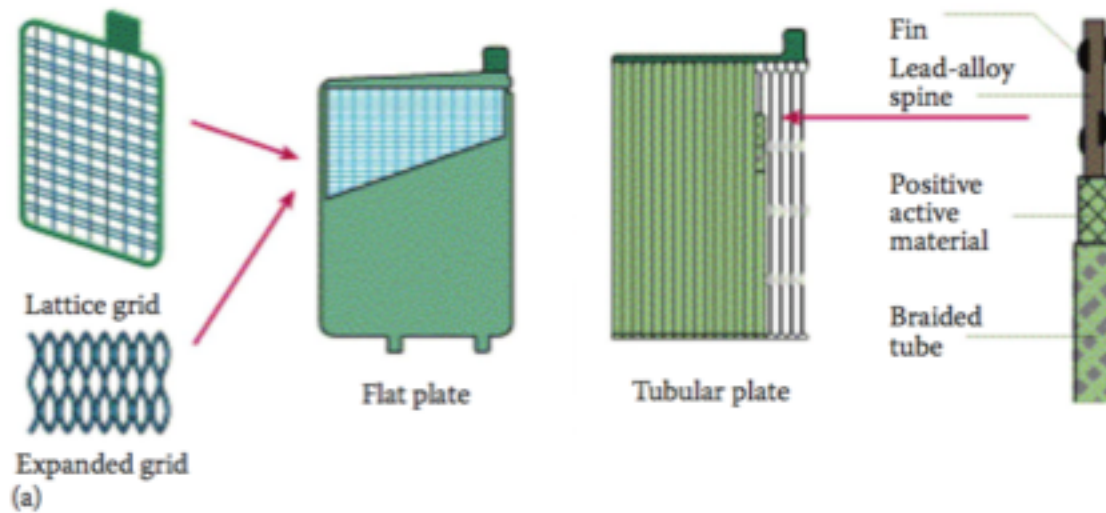


FIGURE 3.1 Lead-acid battery electrode structures: (a) flat and tubular plates; (b) pasted flat electrode, in which the two grids on the left are made of carbon and lead, respectively. After the grid is pasted and cured, the electrode is formed as shown at right. ([a] From <http://www.checkthatcar.com/carfaq2.asp>. [b] From A. Kirchev et al., *J. Power Sources*, 196(20), 8773–8788, 2011.)

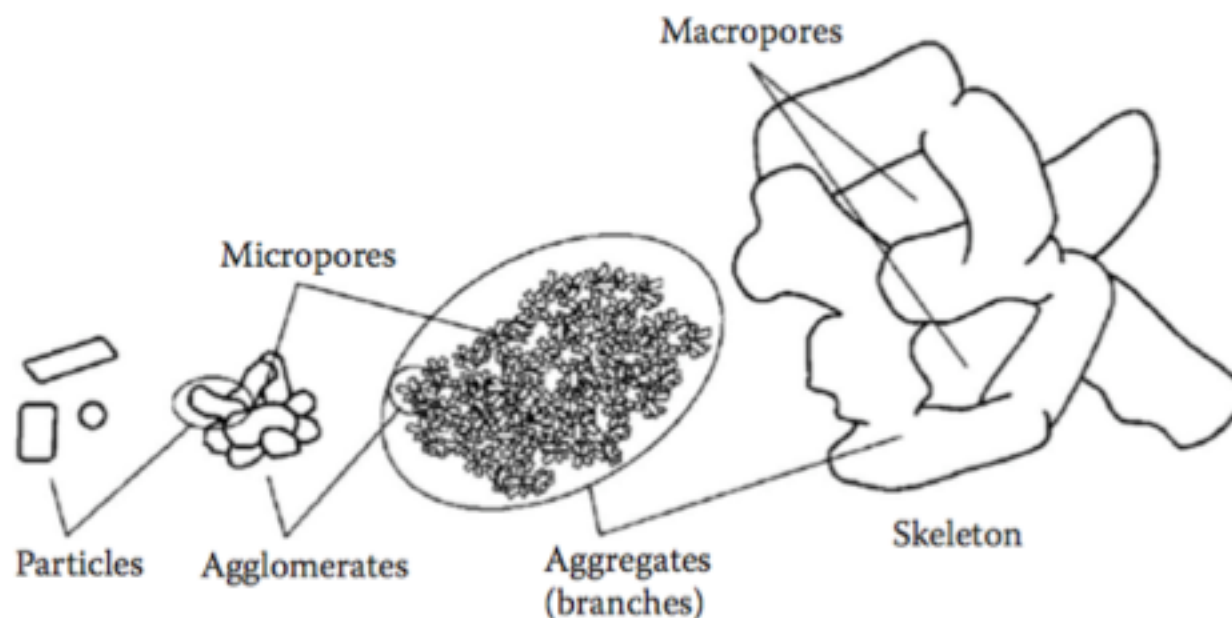


FIGURE 3.3 Structure of the lead dioxide active mass. (From D. Pavlov, and E. Bashtavelova, *J. Electrochem. Soc.*, 131, 1468, 1984; D. Pavlov, and E. Bashtavelova, *J. Electrochem. Soc.*, 133, 241, 1986; D. Pavlov et al., "Structure of the Lead-Acid Battery Active Masses," in *Proc. Int. Symp. Advances in Lead-Acid Batteries*, Vol. 84-14, p. 16, Electrochemical Society, Pennington, NJ, 1984.)

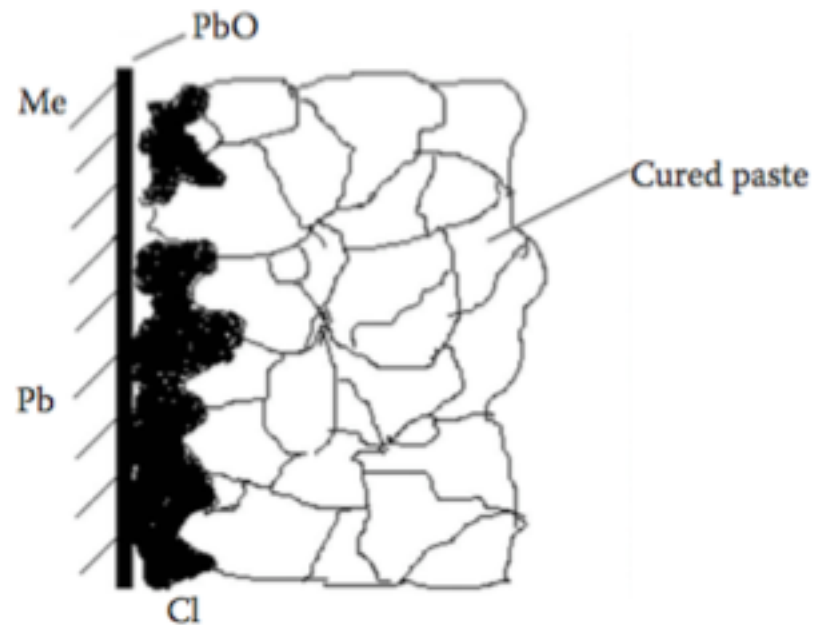


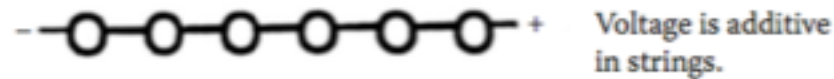
FIGURE 3.4 Scheme of the grid/PAM interface where a corrosion layer is formed during the curing process. (From M. Dimitrov, and D. Pavlov, *J. Power Sources*, 93, 234, 2001.)

4.7.2 DEEP-CYCLE BATTERIES

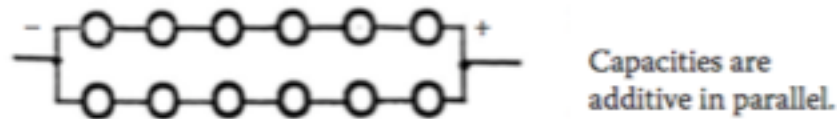
In deep-cycle batteries, two general trends have been observed. First, AGM batteries have found growth opportunities because they demonstrate low or no water loss, have the ability to prevent acid stratification, positively support the positive active material, and prevent shedding. In these same applications, a high resistance to heat, the ability to prevent soft shorts, and lower costs are normally associated with flooded battery designs and the separators utilized. Obviously, the best designed battery would combine all of the aforementioned attributes and the separator appears to be one of the primary paths to realize these goals. As with all design modifications, desired properties need to be prioritized for each individual application because trade-offs are likely between attribute performances and component costs. At the same time, other avenues will be pursued to modify the lead-acid chemistry or other electrochemical systems.

Consider a 12 V/10 Ah battery. How can we build it?

Series string: Six 2 V/10 Ah cells in series.



Parallel strings: Two 2 V/5 Ah 6-cell strings in parallel.



Parallel matrix: Five 2 V/2 Ah 6-cell strings in parallel with cross-matrixing.

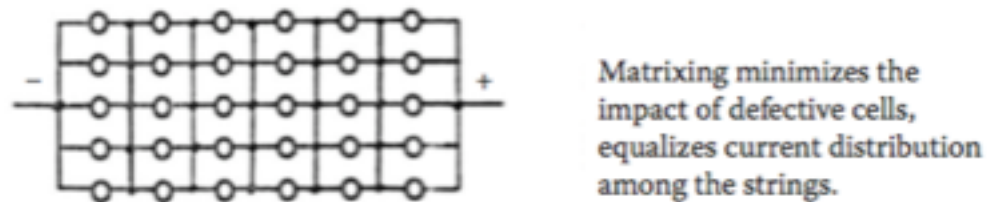


FIGURE 10.3 Battery configurations for charging. (From R. F. Nelson, *Lecture Course on VRLA*, Beijing, China, 2003.)

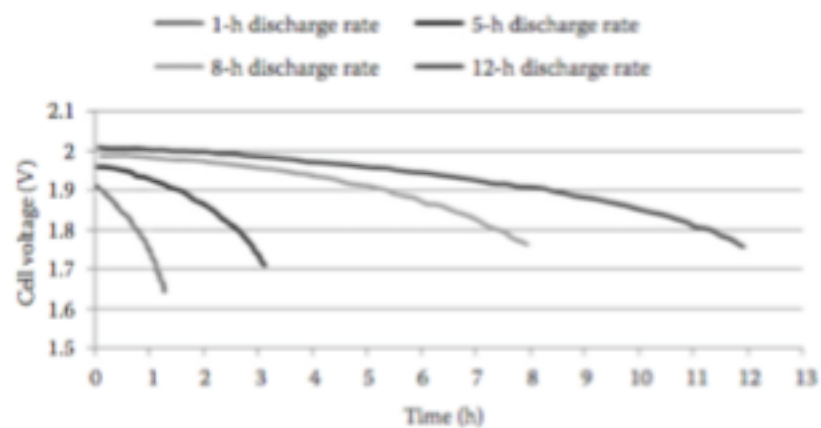


FIGURE 1.10 Discharge voltage curves for a 12-V SLI battery for different discharge currents at 25°C. (*Lead-Acid Battery, Electrochemical Technologies for Energy Storage and Conversion*, Chapter 4. 2012. Copyright Wiley-VCH Verlag GmbH & Co. KGaA. Reproduced with permission.)

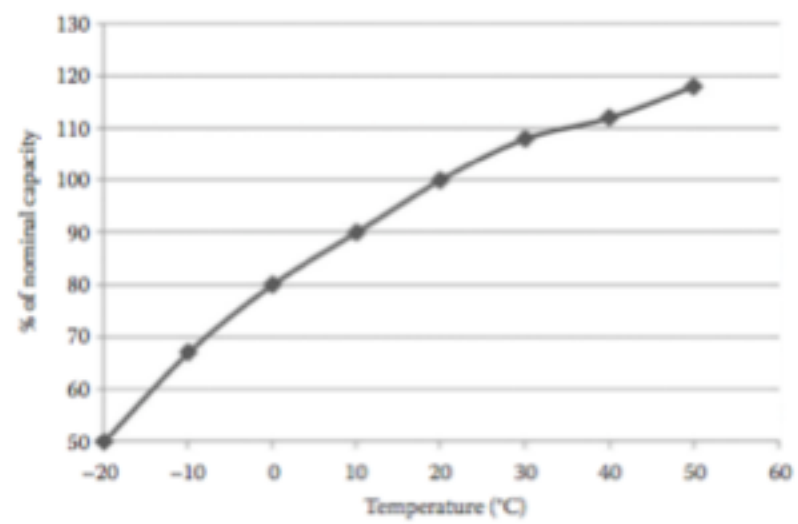
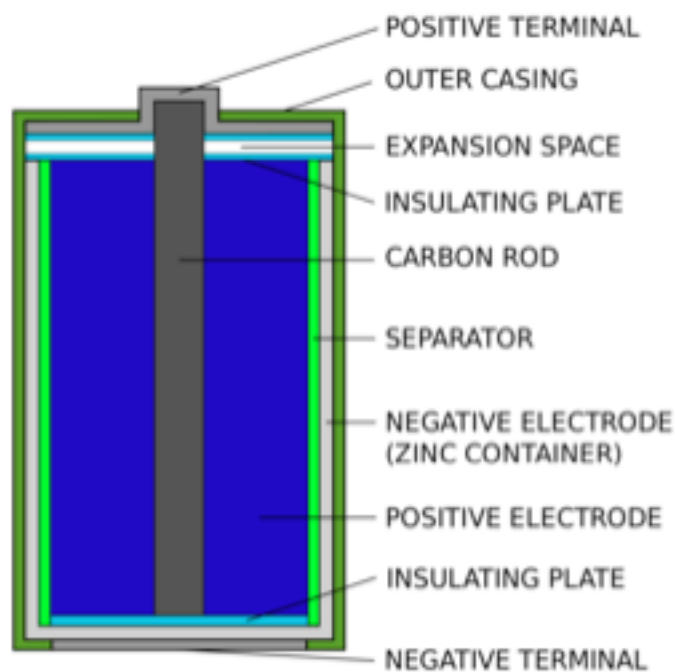


FIGURE 1.13 Capacity (10-h discharge rate) versus temperature.

Dry Cells

Many common batteries, such as those used in a flashlight or remote control, are voltaic dry cells. These batteries are called *dry cells* because the electrolyte is a paste. They are relatively inexpensive, but do not last a long time and are not rechargeable.



Alkaline Dry Cell

A zinc-carbon dry cell.

In the zinc-carbon dry cell, the anode is a zinc container, while the cathode is a carbon rod through the center of the cell. The paste is made of manganese(IV) oxide (MnO_2), ammonium chloride (NH_4Cl), and zinc chloride (ZnCl_2) in water. The half-reactions for this dry cell are:

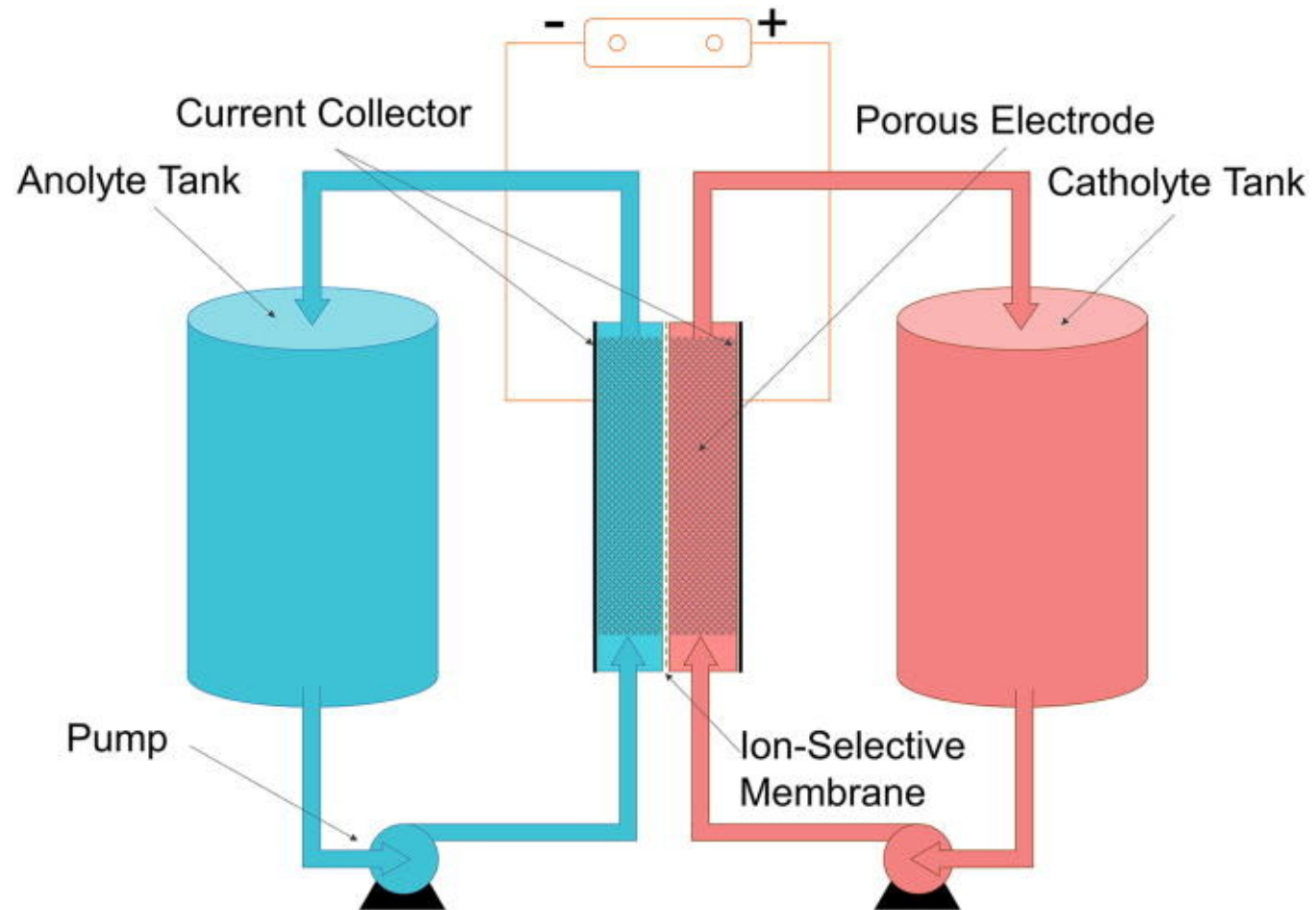


The paste prevents the contents of the dry cell from freely mixing, so a salt bridge is not needed. The carbon rod is a conductor only and does not undergo reduction. The voltage produced by a fresh dry cell is 1.5 V, but decreases during use.

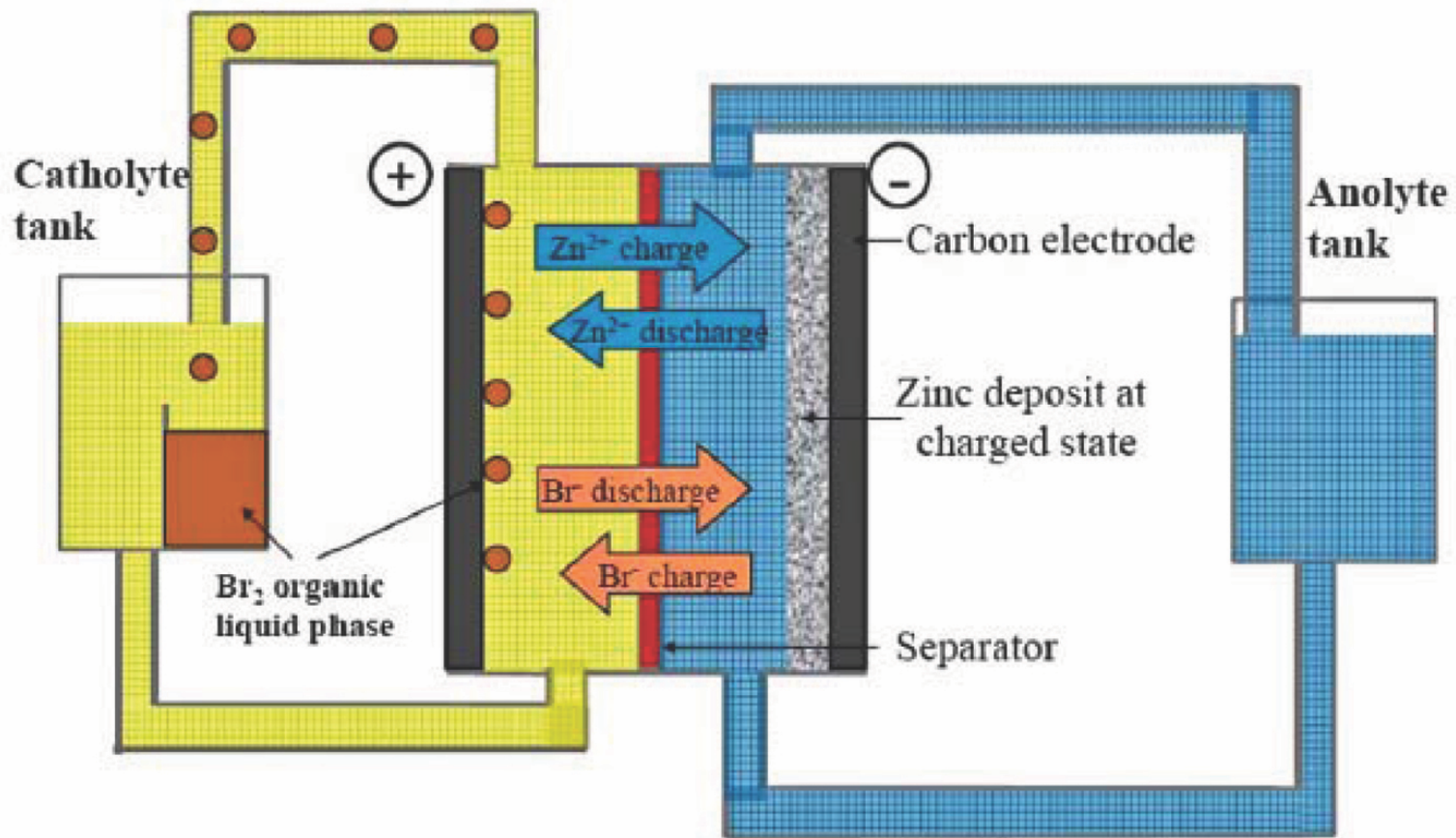
An alkaline battery is a variation on the zinc-carbon dry cell. The alkaline battery has no carbon rod and uses a paste of zinc metal and potassium hydroxide instead of a solid metal anode. The cathode half-reaction is the same, but the anode half-reaction is different.



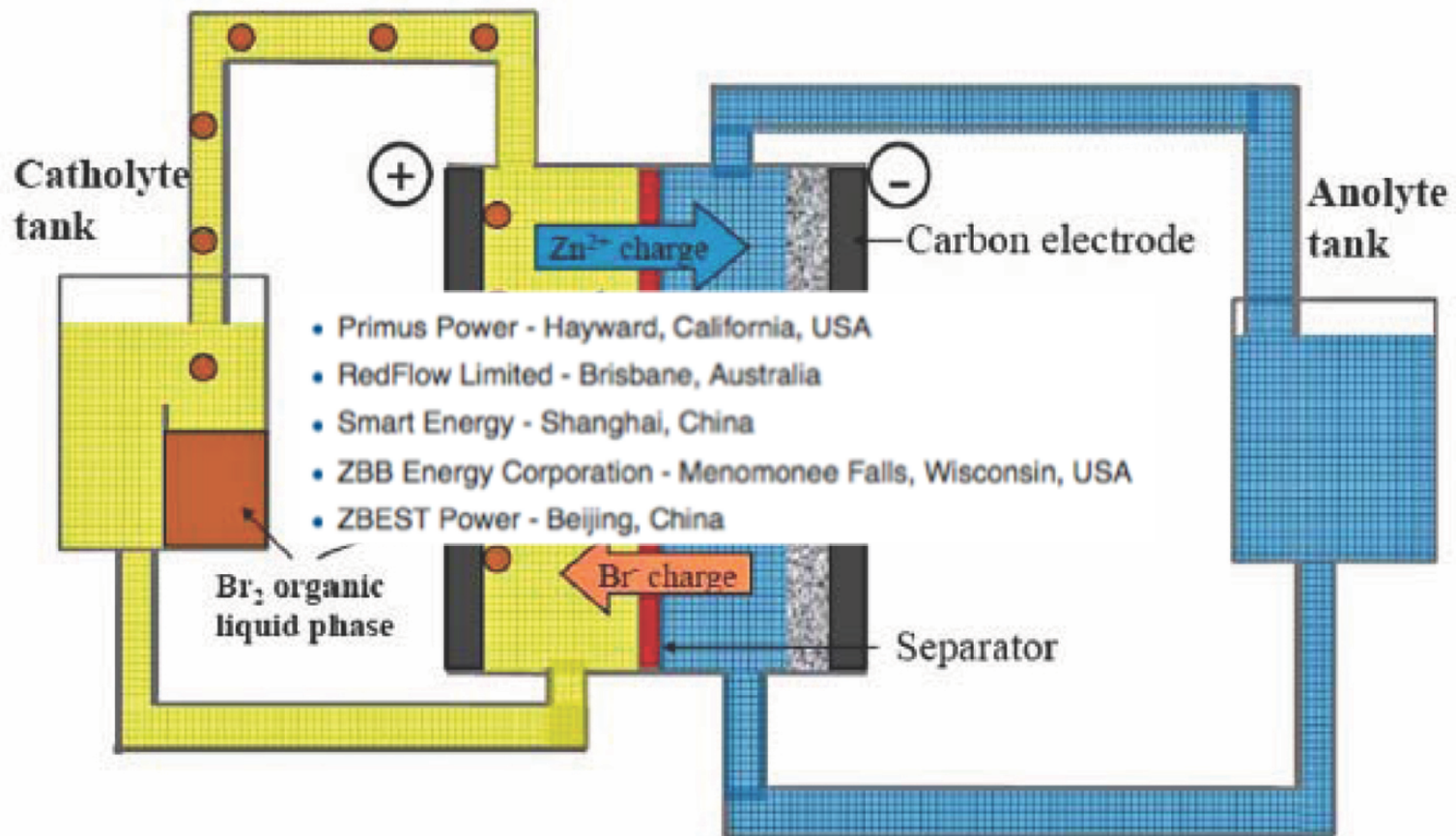
Flow Cells (Flow Batteries)



Zinc Bromide Flow Cell

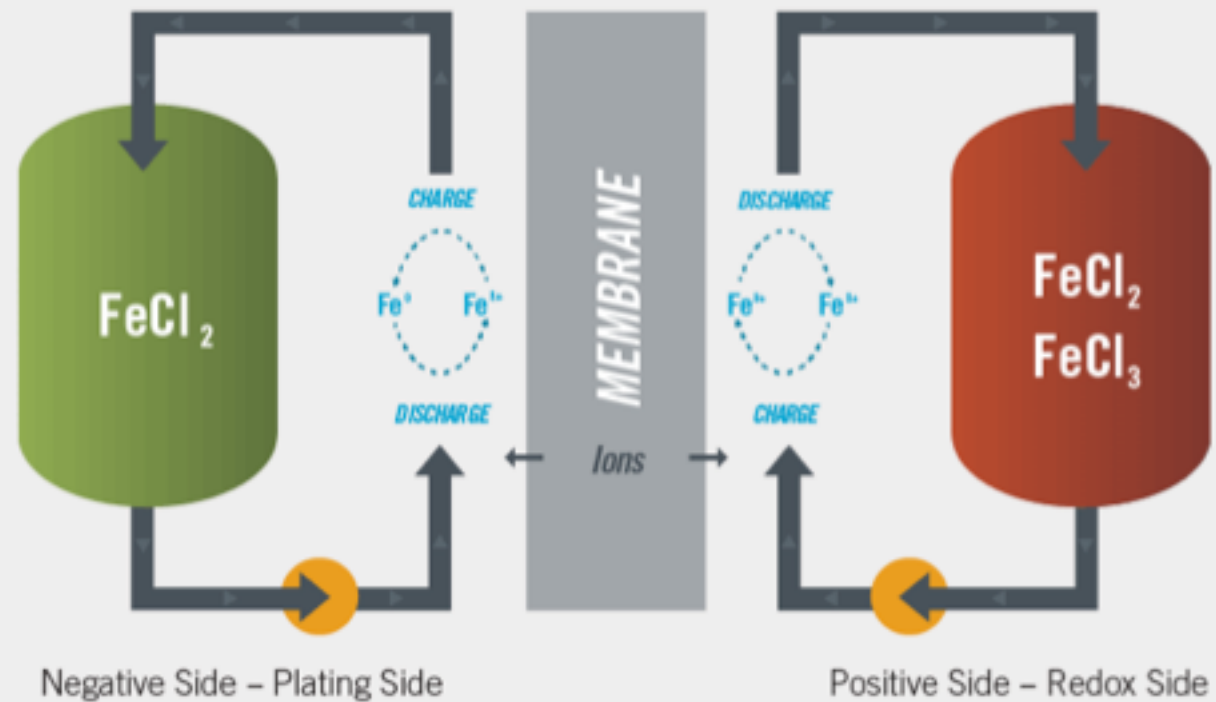


Zinc Bromide Flow Cell

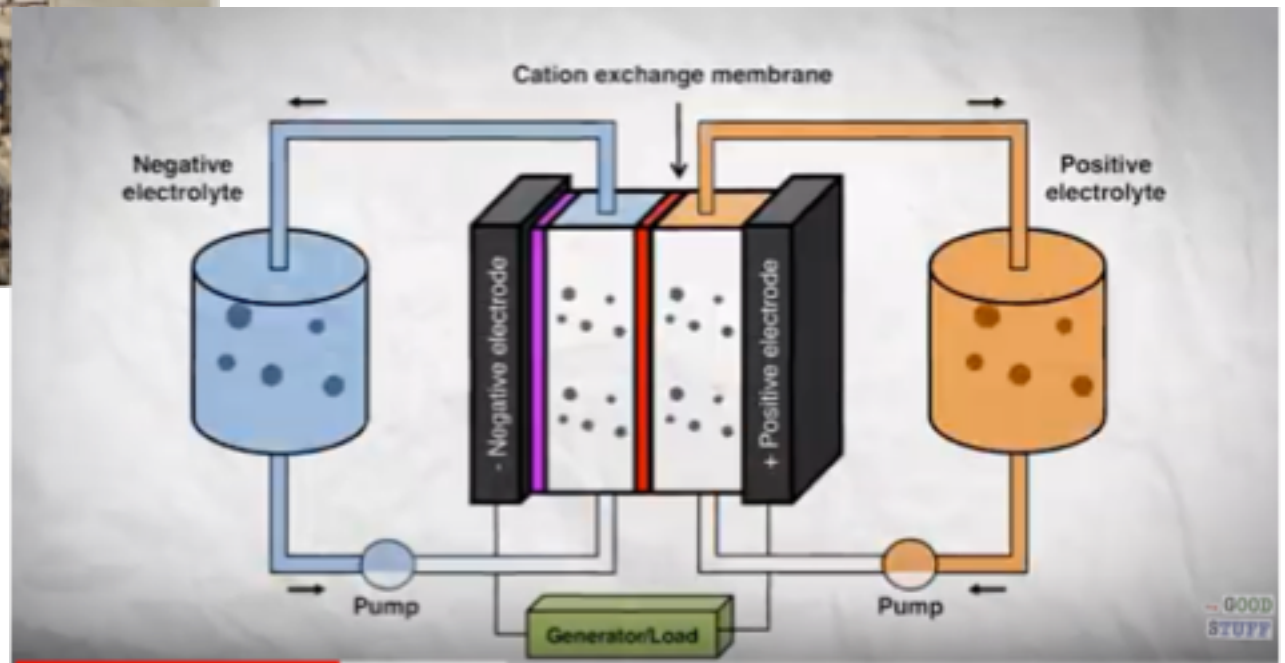


Iron Water Flow Cell

How It Works: A Simple Transfer of Electrons Changed Everything



Iron Water Flow Cell



<https://www.youtube.com/watch?v=Hmtl8Wat7rY>

Iron Water Flow Cell



<https://www.youtube.com/watch?v=Hmtl8Wat7rY>

Iron Water Flow Cell



<https://www.youtube.com/watch?v=Hmtl8Wat7rY>

ARTICLE

Received 20 Oct 2014 | Accepted 16 Jan 2015 | Published 24 Feb 2015

OPEN

Ambipolar zinc-polyiodide electrolyte for a high-energy density aqueous redox flow battery

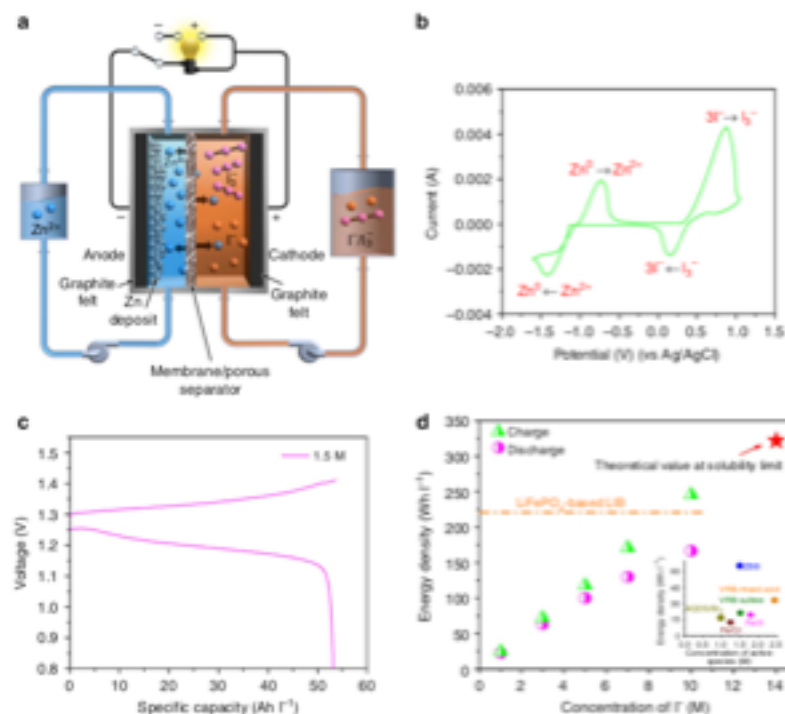
Bin Li¹, Zhen Nie², M. Vijayakumar², Guohong Li¹, Jun Liu¹, Vincent Sprenkle² & Wei Wang¹PNL
Zinc Polyiodide
Cell

Figure 1 | Zn-I RFB and its electrochemical performance. (a) Schematic representation of the proposed ZIB system. (b) CV of 0.085M ZnI₂ on a glassy carbon electrode at the scan rate of 50 mV s⁻¹. (c) Typical charge-discharge curves at 1.5M ZnI₂ at a current density of 20 mA cm⁻². (d) The charge and discharge energy densities as a function of the concentration of I⁻. The inset lists concentration versus energy density of several current aqueous RFB chemistries for comparison³⁴⁻⁸.

Table 1 | ZIB performance as a function of ZnI₂ concentration.

ZnI ₂ (M)	CE (%)	VE (%)	EE (%)	OCV (V)	Avg. charge voltage (V)	Avg. discharge voltage (V)
0.5	99.5	91.3	90.9	1.430	1.399	1.265
1.5	99.3	88.7	88.2	1.330	1.343	1.185
2.5	99.0	85.7	84.8	1.285	1.321	1.132
3.5	99.2	76.6	76.0	1.270	1.342	1.066
5.0	96.3	70.4	67.8	1.220	1.330	0.960

CE, coulombic efficiency; EE, energy efficiency; OCV, open-circuit voltage; VE, voltage efficiency.

ARTICLE

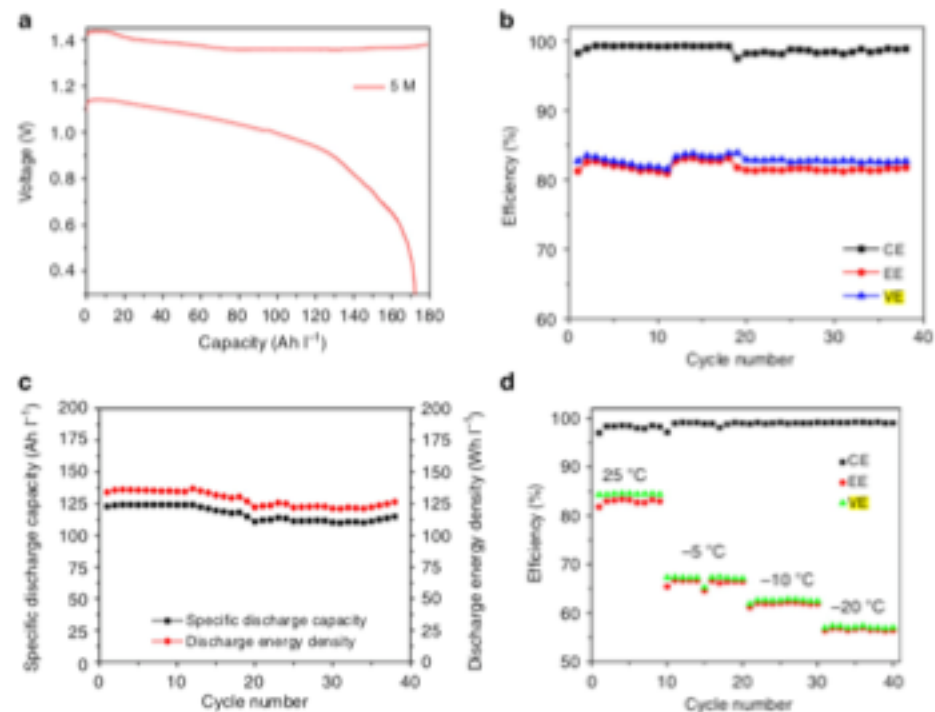
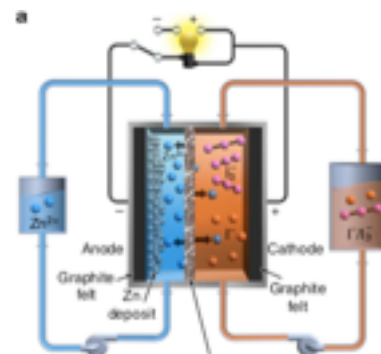
Received 20 Oct 2014 | Accepted 16 Jan 2015 | Published 24 Feb 2015

OPEN

Ambipolar zinc-polyiodide electrolyte for a high-energy density aqueous redox flow battery

Bin Li¹, Zhen Nie², M. Vijayakumar², Guohong Li¹, Jun Liu¹, Vincent Spiculis² & Wei Wang¹

PNL Zinc Polyiodide Cell

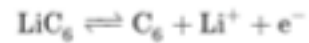


Lithium Ion Battery

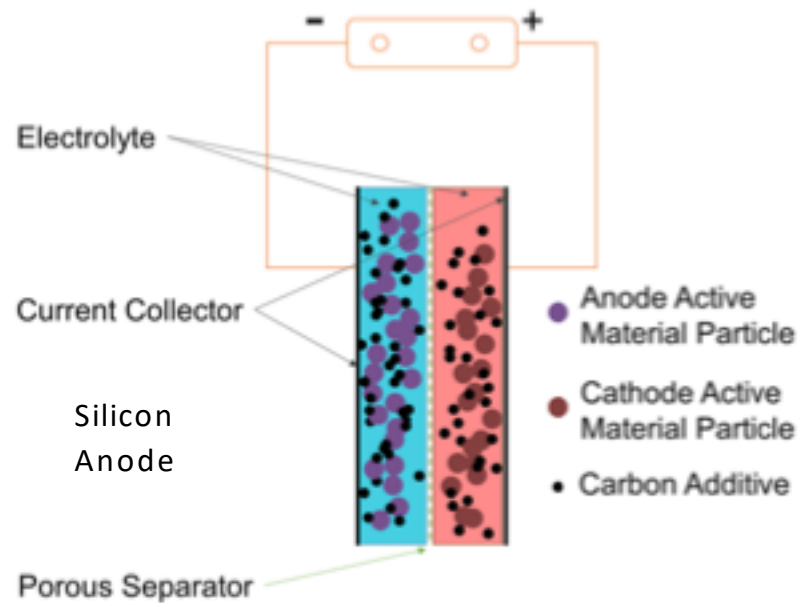
The positive electrode (cathode) [half-reaction](#) in the lithium-doped cobalt oxide substrate is:^{[90][91]}



The negative electrode (anode) [half-reaction](#) for the graphite is:



The full reaction (left to right: discharging, right to left: charging) being:



Lithium
Cobalt Oxide
Cathode

Sizing up a battery – basic parameters and calculations

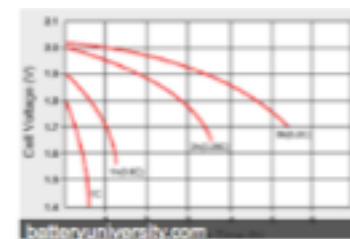
Voltage (V), Current (A)

Parallel and series circuits

Capacity, energy (Ah, Wh)

C-rate (C)

A C-rate is a measure of the rate at which a battery is discharged relative to its maximum capacity. A 1C rate means that the discharge current will discharge the entire battery in 1 hour. For a battery with a capacity of 100 Amp-hrs, this equates to a discharge current of **100 Amps**.



Sizing up a battery – voltage, current, power



Electrical Engineering parameter	Chemical Engineering equivalent parameter
Voltage (V)	Fluid pressure (kPa, psi)
Current (A)	Flowrate (m ³ /s)
Electrical power (W)	Mechanical, or pump power (W)

$$\text{Voltage} * \text{Current} = \text{Power}$$

$$\text{Pressure} * \text{Flowrate} = \text{Power}$$

Sizing up a battery – parallel and series circuits

In series circuit (S), output voltage increases,
current stays the same

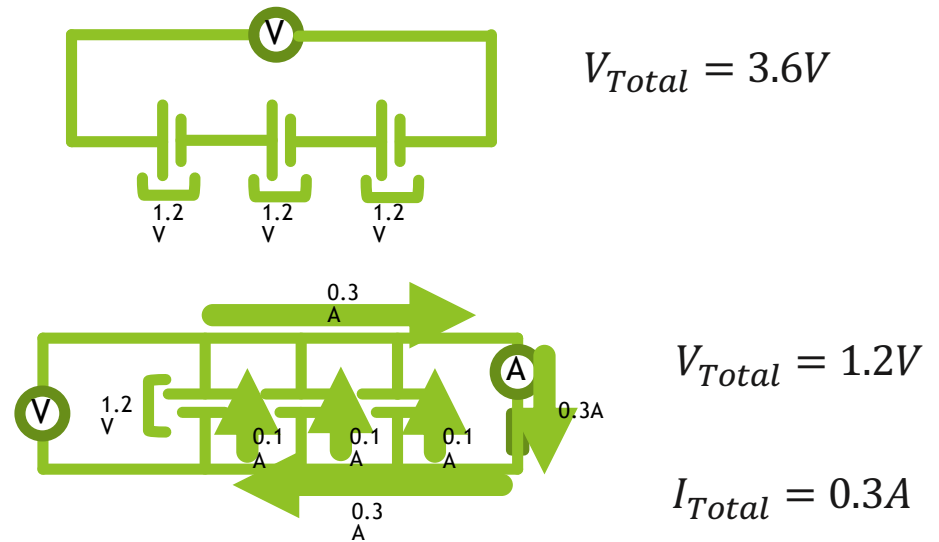
In parallel circuit (P), output current increases,
voltage stays the same

Batteries have maximum safe operating voltage
(and current)

Approx. 4V for Li-ion

1.2 - 1.5V for NiMH

Increase voltage and current by connecting in P
and S



Sizing up a battery - capacity

I = Current, in amperes

C = Charge, in coulombs

t = time, in seconds

Capacity, measured in amp-hours
(Ah)

$$I = \frac{C}{t}$$

$$\text{Capacity} = I * t$$

$$\text{Capacity} = \frac{C}{t} * t$$

$$\text{Capacity} = C$$

1 Ah capacity can supply a current of 1 A for 1 hour

Sizing up a battery - energy

Capacity (Ah)

Voltage (V)

Power (W)

Energy content (Wh)

$$P = \frac{E}{t}$$

$$E = P * t \quad \text{Voltage} * \text{Current} = \text{Power}$$

$$E = V * \underbrace{I * t}_{\text{Capacity}}$$

Hence, *energy content = capacity x voltage*

Units of energy content in a battery given in watt-hours

Sizing up a battery – C-rate

Rate of charging/discharging of a battery

Quoted as multiple of capacity of battery

For example: taking a 3 Ah battery

C-rate	Current (A)
1C	3
0.5C	1.5
0.1C	0.3
0.01C	0.03

Problem 1 – Boiling the kettle

2 kW kettle

Takes approx. 45 sec to boil 1 cup of tea

$$2 \frac{kJ}{s} * 45 s = 90 kJ$$

or 25 Wh

Problem 2 - charging your phone

3000 mAh capacity (Samsung Galaxy S8)

Charger capable of 3A

Charging time (nominated 0% to 100%) approx. 1 hour (1C)

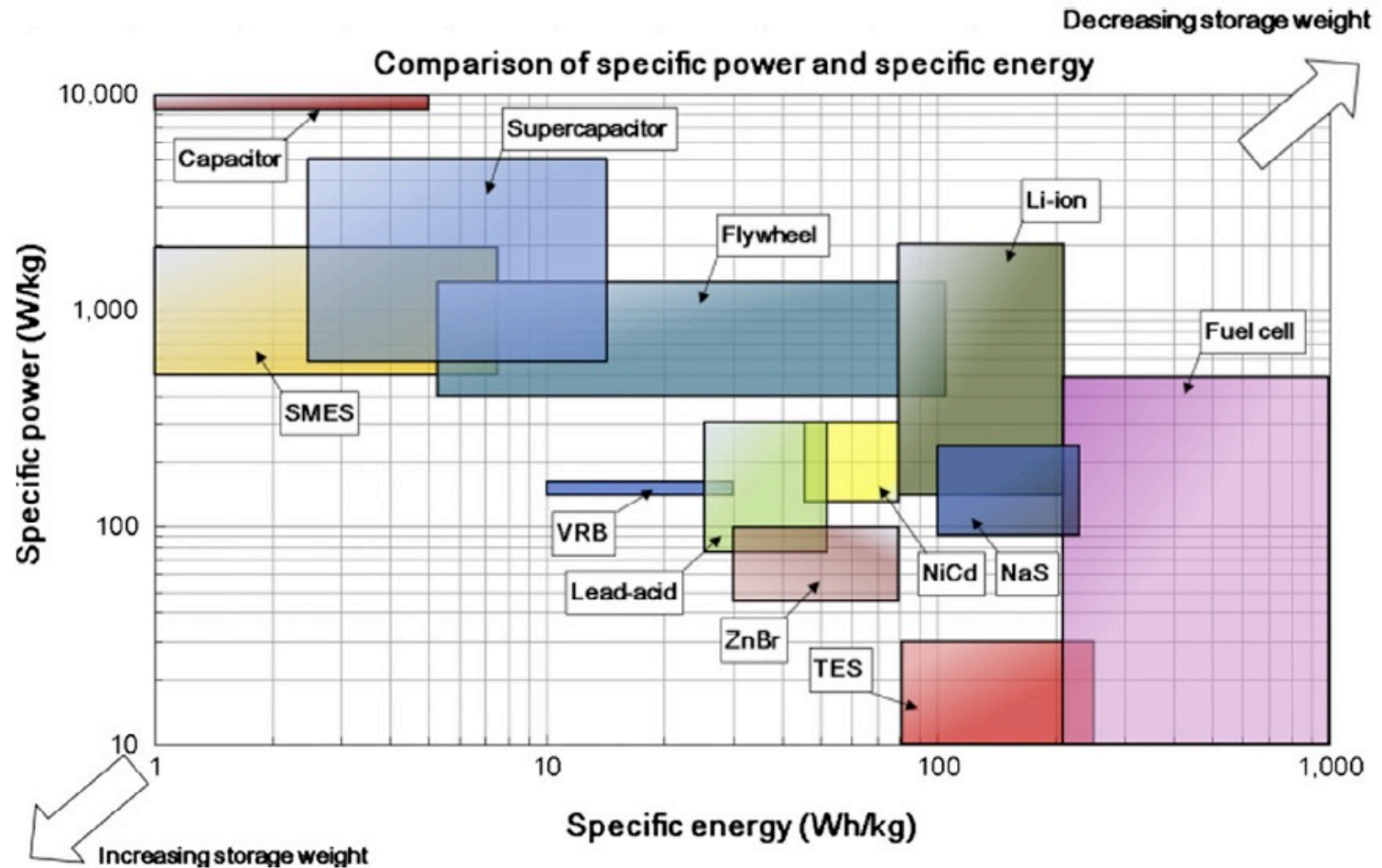
Voltage: 5V

Energy consumed = $3A * 5V * 4000s$

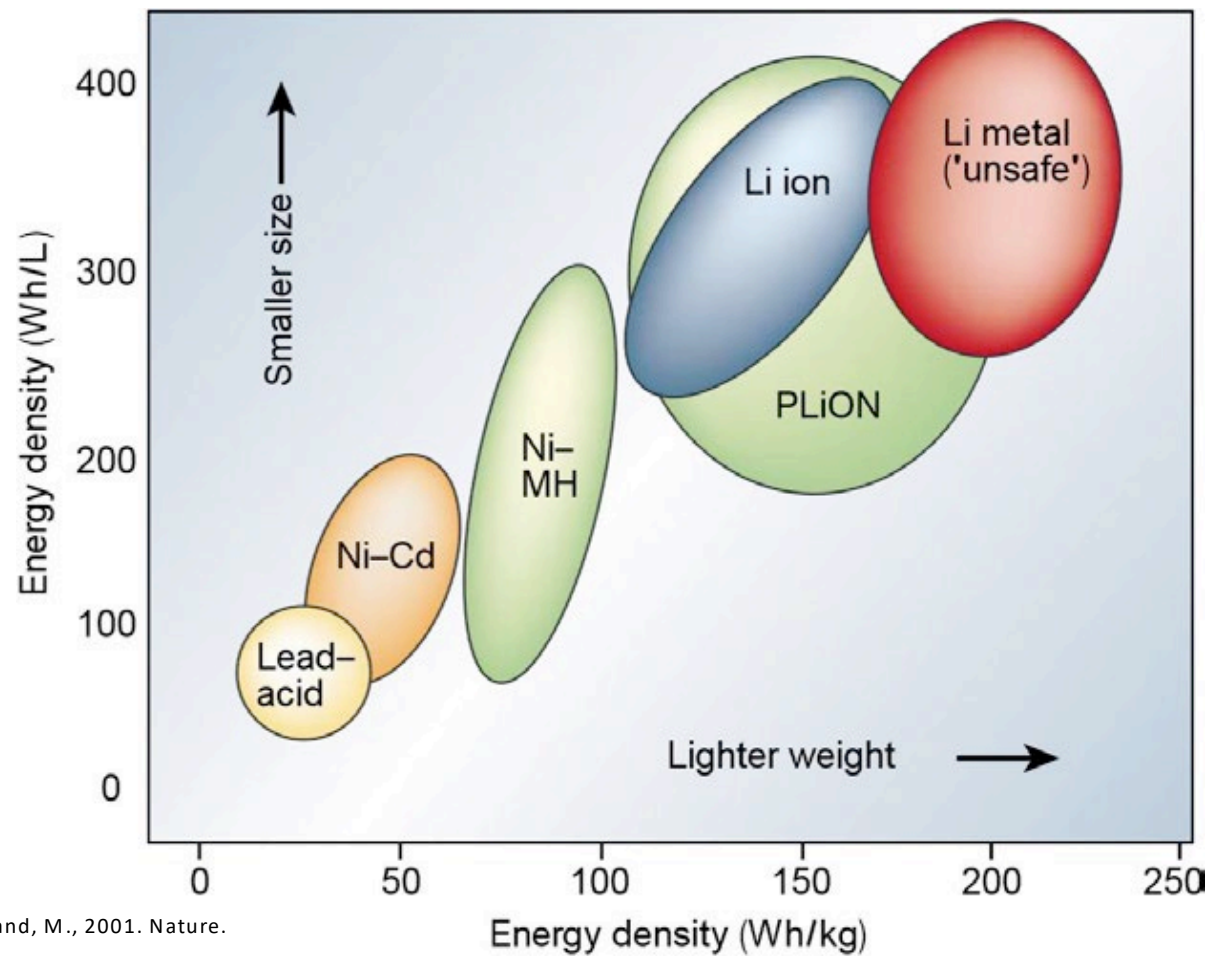
60 kJ or 16 Wh



Comparing energy storage techniques



Comparing batteries



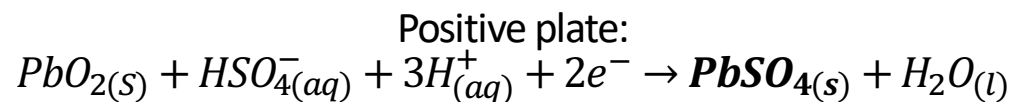
Tarascon, J.-M., Armand, M., 2001. Nature.

Lead acid

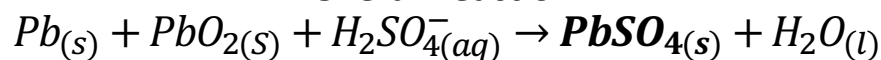
Negative plate:



Positive plate:



Overall reaction:



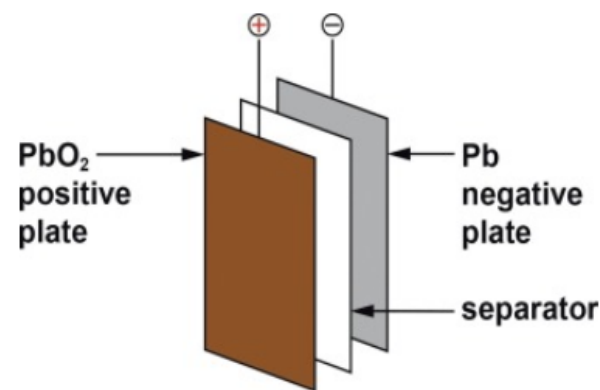
Battery voltage roughly 2V

Overcharging can cause water splitting

Measure state of charge by

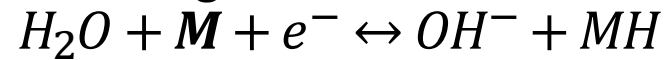
Measuring voltage,

Gravimetric measurement of electrolyte



Nickel metal hydride

Negative electrode:



Positive electrode:



Hydrogen ion shuttling back and forth

Nominal voltage of 1.2V



Lithium ion battery

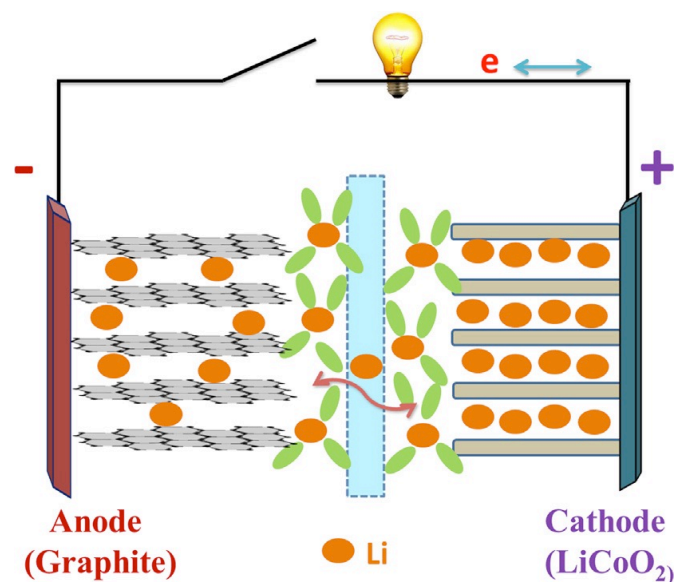
Intercalation reactions occur

Lithium-ions move into material lattices

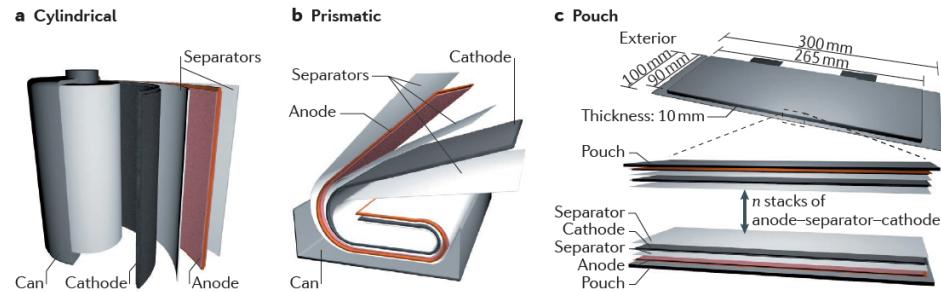
Lithium ions shuttle back and forth

Graphite stores lithium when fully charged

Cathode accepts lithium during discharge



Cell configurations



Cylindrical cells are most efficient

Can be wound with high tension

Commonly made into 18650

AA batteries are 14500, not usually lithium ion

Lithium ion battery calculations

What is the minimum amount of lithium in your smartphone?

Smartphone battery capacity around 2500 mAh (2.5 Ah)

9000 C (coulombs)

$5.61798 \times 10^{22}\text{ electrons}$

$5.61798 \times 10^{22}\text{ Lithium ions}$

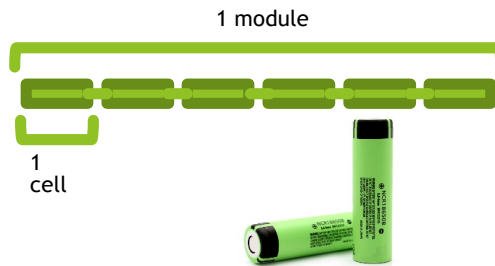
0.093 moles of Li

$0.6475\text{ g of Lithium}$

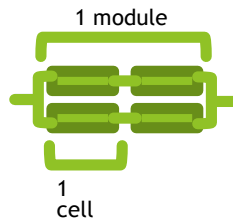
0.6475g of lithium metal was required to make the battery, but no longer in elemental form in the battery.

Lithium ion batteries for EVs

Tesla Model S 85
85 kWh battery pack
18650 cell type
6 cells per module, 16
modules
74 in parallel
7104 cells total
360V

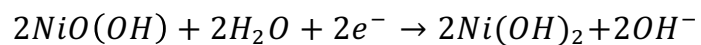
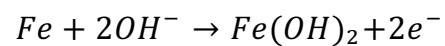


Nissan Leaf
24 kWh battery
Pouch-cell type
4 cells per module, 48
modules
32.5 Ah per cell
192 pouch cells total

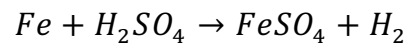


Nickel Iron battery

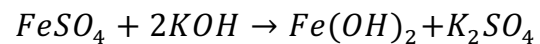
Discharge reactions:



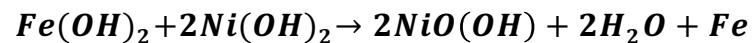
Start with iron, dissolve in sulfuric acid:



Precipitate by dissolving in a strong base:



Overall charging reaction:



Capacitors, supercapacitors

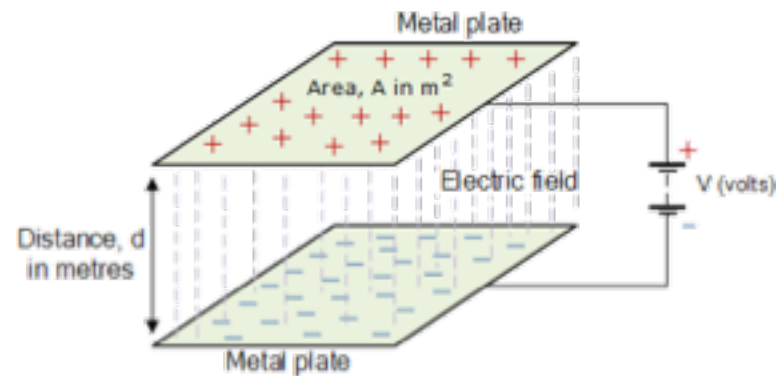
Store charge in an electric field

Charge stored is directly related to:

Distance between plates

Surface area of plates

Permittivity of dielectric



Capacitors, supercapacitors

Ceramic capacitors

Small capacitance

Used in electronic circuits for smoothing

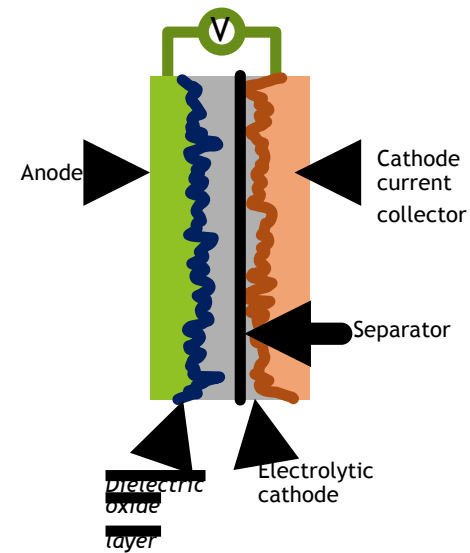
Electrolytic capacitors

Makes use of an electrolyte (solid or liquid)

High capacitance

Oxide layer on metal is the dielectric

Asymmetric



Capacitors, supercapacitors – EDLC

Electrochemical double-layer capacitor

Charge separation

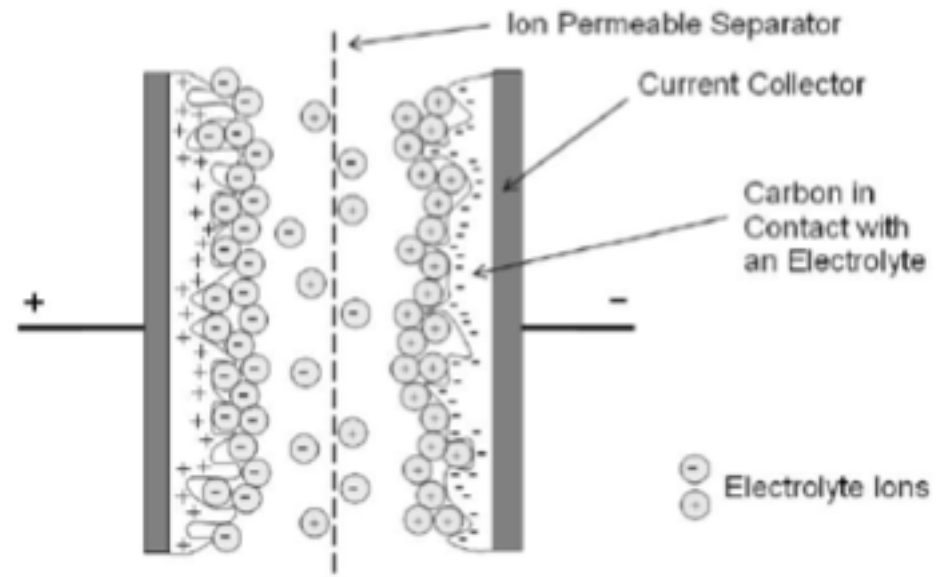
No electrochemical reaction

Chemical reactions can be introduced

Called pseudocapacitance

Transition metal oxide electrode material

Conducting polymers



Simple symmetric EDLC construction

Components:

Electrodes

Electrolyte

Current collectors

Separator

Preparation:

Electrode usually in powder form, need to be made into an ink

Electrolyte – salt solution that won't evolve gas, and similar ionic radius

Current collector – low resistance metal strip

Separator – prevents short circuit between electrodes

Batteries vs supercapacitors

Batteries	Supercapacitors
Relatively slower rate of charge/discharge	Quick rate of charge/discharge
Higher energy density	Lower energy density
Energy stored in chemical reactions	Electrostatic charge is stored, no chemical reactions
Lower durability (cycles to failure) approx. 1000 cycles	Higher durability, approx. 100,000 cycles

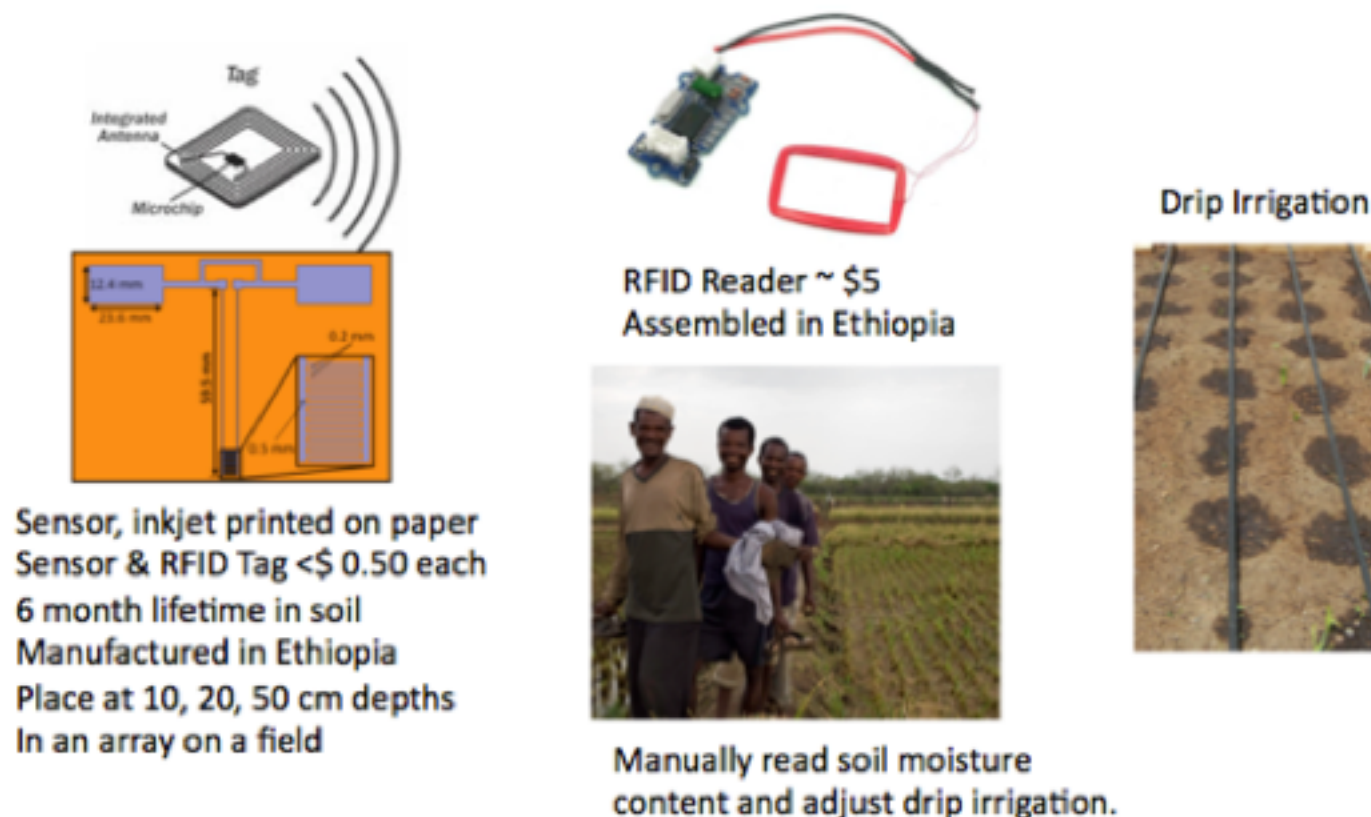


Figure 1. Sketch of printed soil moisture sensor concept. The sensor and RFID tag can be screen or inkjet printed on paper in Ethiopia. These would be buried at variable depths through a field to monitor soil moisture with a hand held RFID reader, assembled in Ethiopia. The system could be automated or manually read to control a drip irrigation system. The Hararghe Catholic Secretariat near Dire Dawa already installs drip irrigation systems in the Oromo/Somali Region. (Sensor drawing from Kim S, Le T, Tentzeris MM, Harrabi A, Collado A, Georgiadis A (2014).)

Printed Soil Moisture Sensors for Drip Irrigation

- Uses printable conductive ink
- Doped titania nanoparticles
- RFID interrogation
- Moisture affects impedance
- Can be used for chemical detection (CO)

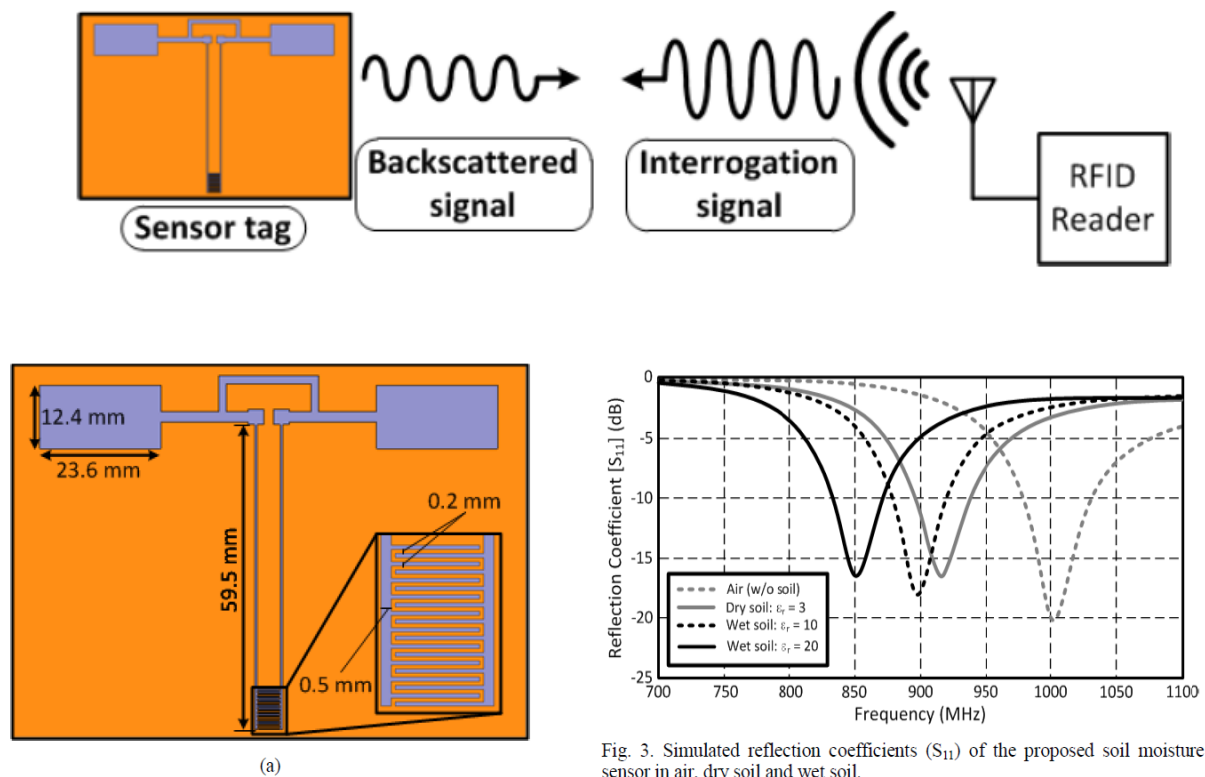
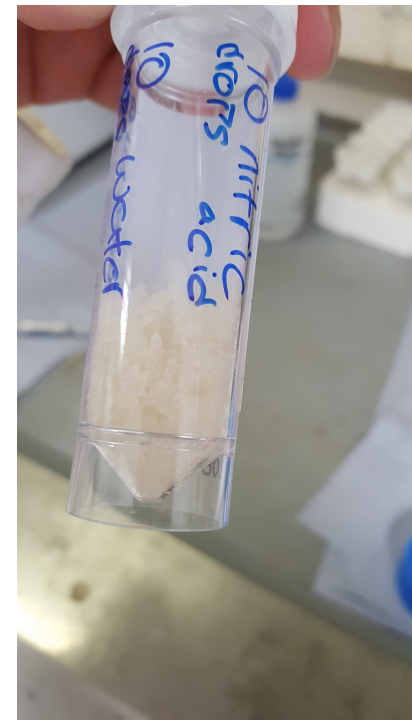


Fig. 3. Simulated reflection coefficients (S_{11}) of the proposed soil moisture sensor in air, dry soil and wet soil.

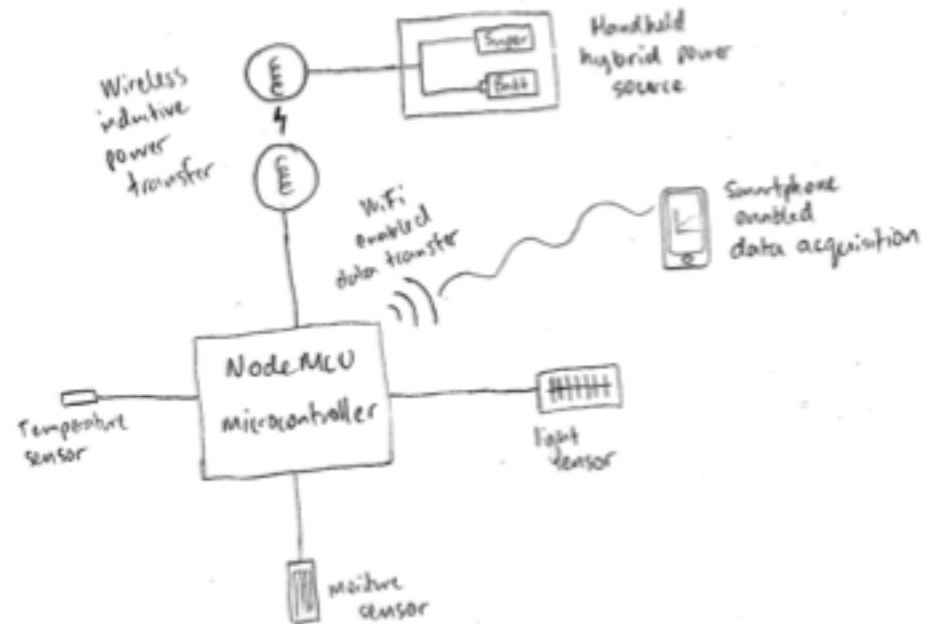
Niobium-doped titania nanoparticles

- Chemical synthesis
- Reagents:
 - Titanium chloride
 - Niobium ethoxide
 - Tert-butyl alcohol
- Challenging to produce printable consistency
- Requires screen printer
- Alternative to titania is silver nanoparticles



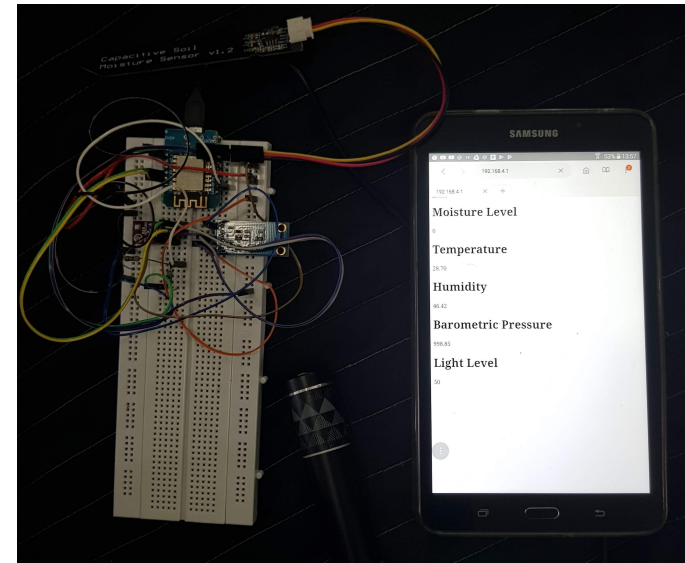
Electronic sensor

- Electronic sensor platform system
- 5V system
- Controlled by microcontroller
- Inductive power transfer
- Data sent wirelessly to smartphone
- Can charge using solar panel
- Can be modified to accept power from supercapacitors
- Costs roughly \$5
- (cost does not include smartphone)



Electronic sensor

- Capacitive sensor
- Additional Sensors included, but not necessary
 - Temperature
 - Humidity
 - Light
- Expandable (NodeMCU microcontroller has many digital I/O pins)
- Soil conductivity measurement?



Field test

- Tested in field
 - Initial reading taken
 - Reading increased when water added
 - Reading decreased as soil dried (10 mins)



ETHIOPIA SENSORS ELECTRONICS COMPANY

BUSINESS PLAN

ESEC has three goals:

- 1) Manufacture of moisture sensors targeting initially foreign development funding for drip irrigation systems and later the larger Ethiopian agricultural market.
- 2) Training of a new generation of entrepreneurial technologists and businessmen who will expand the market for sensors and battery technology in Ethiopia, as well as support indigenously manufactured and locally installed equipment. Market expansion will take advantage of expertise and centers at *TUOS* and *UC*.
- 3) Enhance the economic situation for faculty and administrators at Ethiopian universities through an Ethiopian adaptation of the US/UK university-based start-up incubator model.

<p>Strengths</p> <ul style="list-style-type: none"> • The proposed sensor design is efficient, sustainable, cheap and easily constructible • Availability of trained human power with technical expertise • Associated Universities management have a strong commitment and initiation to the implementation of the project and are pioneers in irrigation regulation 	<p>Weaknesses</p> <ul style="list-style-type: none"> • Need for full characterisation and scale up production of sensors • Need for RFID devices for measurement read • Need for i
<p>Opportunities</p> <ul style="list-style-type: none"> • Promising market in the rural area of the region • Development of the sensor technology to suit other applications • Possibility of sensor being produced from locally sourced starting materials in the near future • Sensor could also be exported to other African countries • Provision of Temporary Taxes relief by the government to import inputs to the solar panel production plant 	<p>Threats</p> <ul style="list-style-type: none"> • Delay at maritime transit and shortage of foreign currencies • Lack of basic knowledge and trust of the customers in purchasing the product manufactured locally

December 19 1.5 hours (Non-PV Solar)

Questions

Solar desalinisation/Solar disinfection

Solar hot water

Solar boiler for electricity

Solar chimney

Solar cooling

Solar cooking

Solar charcoal processing

Solar redox hydrogen processes

Biogas

Algae for food

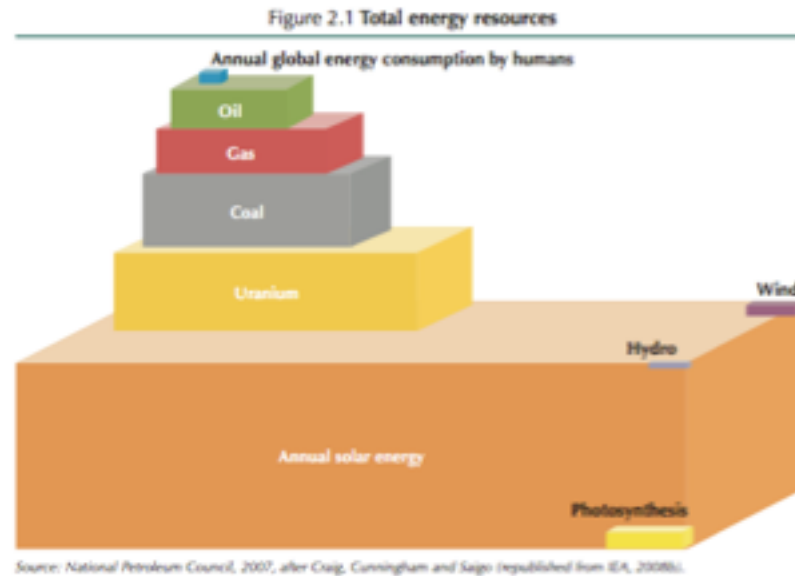
Oil from algae

Summary of the potential for technical business opportunities
to solve development problems

Questions

Non-Photovoltaic Solar Energy Harvesting

Solar Chimney
Solar Greenhouse
Biomass
Solar Heat
Passive Solar
Solar Water Heater
Solar Oven
Desalination
Solar Towers
ZnO Redox Reaction
Biomass/syngas
Solar Thermolysis
Solar Electricity & Electrolysis
Algae Tower



Key point

Solar energy is the largest energy resource on Earth – and is inexhaustible.

Solar Desalination/Water Purification

[Solar Still Video](http://www.youtube.com/watch?v=GrPRnaS449w) (http://www.youtube.com/watch?v=GrPRnaS449w)



Solar Desalination/Water Purification

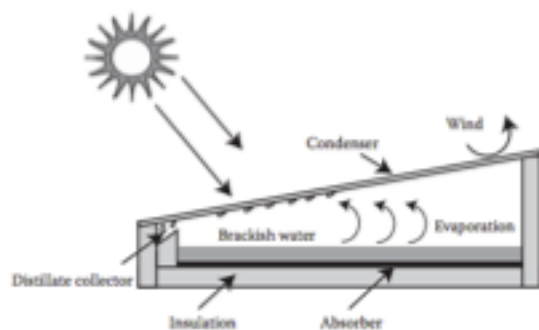


FIGURE 4.26 Basic operation of a solar still.

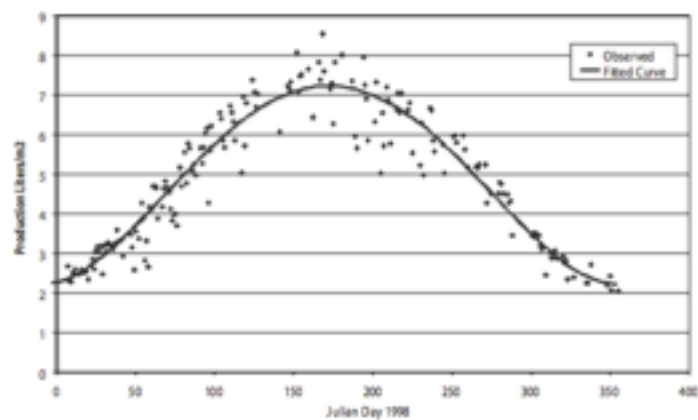


FIGURE 4.27 Measured basin solar still annual performance in Las Cruces, New Mexico, on a square-meter basis (Zachritz, 2000).

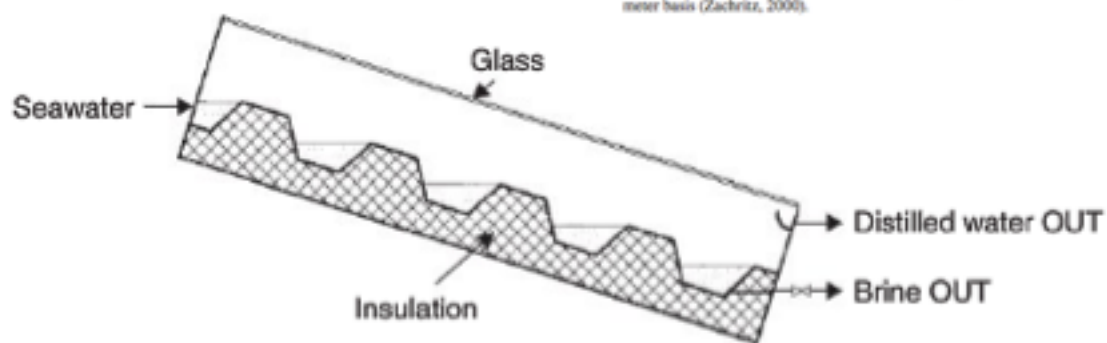


FIGURE 8.3 Schematic of a cascaded solar still.

Solar Desalination/Water Purification

TABLE 4.7
Sandia National Laboratories Still-Water Quality Test Results (Zirzow, SAND92-0100)

Sample type	13% Salinity feedwater	Distilled water (13% case)	16% Salinity feedwater	Distilled water (16% case)
Calcium (total)	340	1.5	371	<0.10
Iron (total)	0.27	<0.05	0.48	<0.06
Magnesium (total)	2.1	2.1	<0.005	<0.005
Manganese (total)	0.04	<0.02	0.07	<0.02
Ammonia as N	<0.1	0.1	<0.1	<0.1
Chloride	19,000	<1.0	25,000	2.6
Fixed solids	32,000	<1.0	41,000	31
Nitrate as NO ₃	34	0.1	26	<0.1
Nitrate as NO ₂	0.013	<0.01	0.02	<0.01
TDS	36,000	<1.0	48,000	<1.0
Volatiles and organics	4,200	<1.0	6,000	13

TABLE 4.6
Microbial Test Results for Solar Stills

Sample	Volume tested ml	Total organisms per liter
Supply	50	16,000
Distillate	1,000	4
<i>E. coli</i> seed		2,900,000,000
Distillate	750	11 (No <i>E. coli</i>)
<i>E. coli</i> seed	—	7,500,000,000
Distillate	1,000	18 (No <i>E. coli</i>)
Supply	10	24,000
Distillate	1,000	13
Supply	1	12,000
Distillate	1,000	6

Source: New Mexico State University, 1992.



FIGURE 4.28 SolAqua solar still village array under test at Sandia National Laboratories.

Solar Desalination/Water Purification



Figure 7-2 Demonstration solar still.

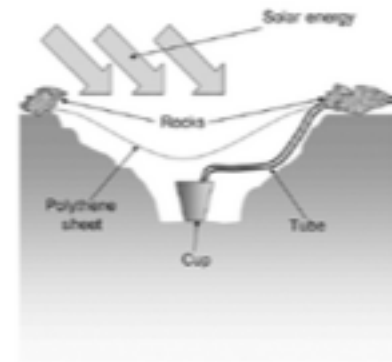


Figure 7-4 Diagram of a pit solar still.



Figure 7-5 A solar still in operation. Image courtesy © U.S. Department of Agriculture—Agricultural Research Service.

Solar Desalination/Water Purification

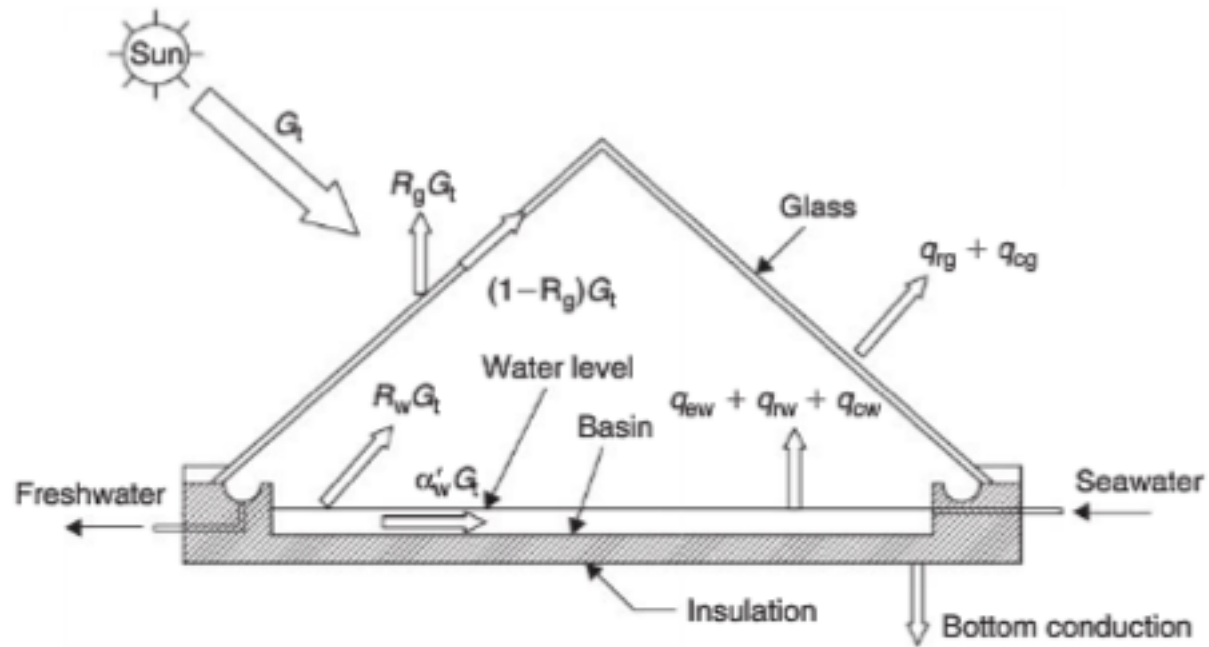


FIGURE 8.1 Schematic of a solar still.

Solar Desalination/Water Purification

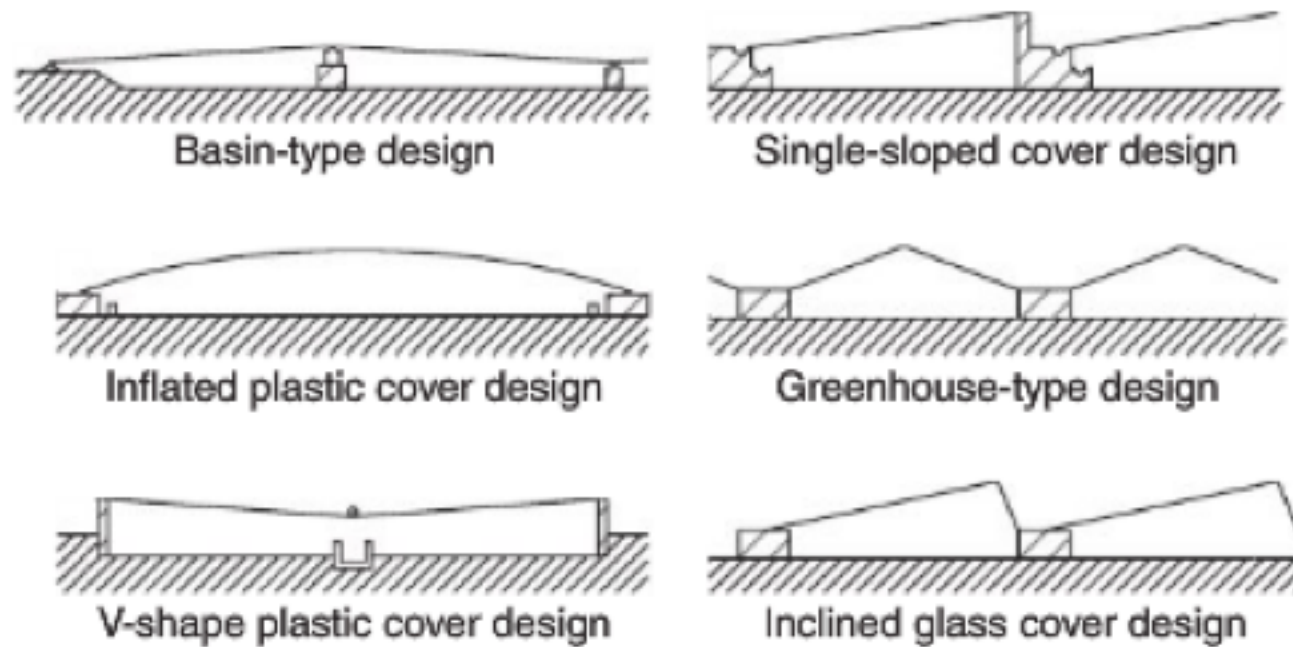


FIGURE 8.2 Common designs of solar stills.

Solar Desalination/Water Purification

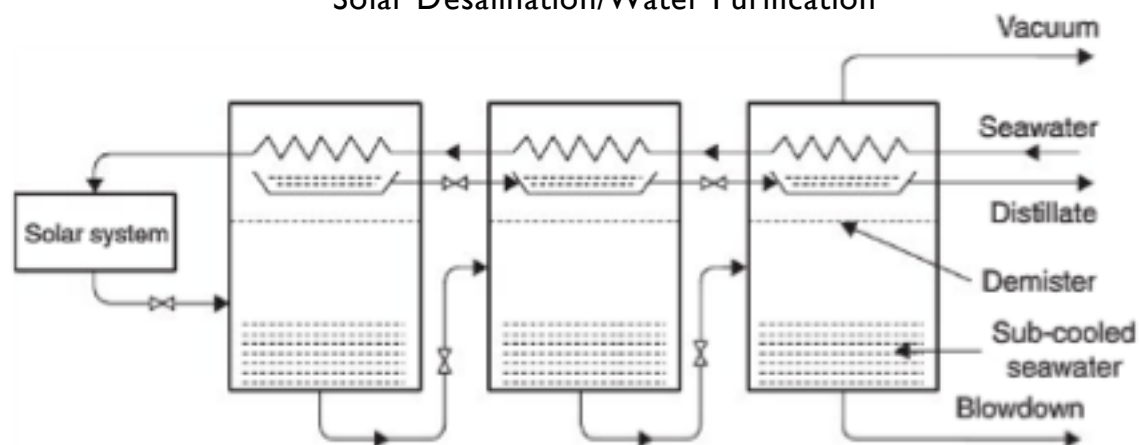


FIGURE 8.4 Principle of operation of the multi-stage flash (MSF) system.

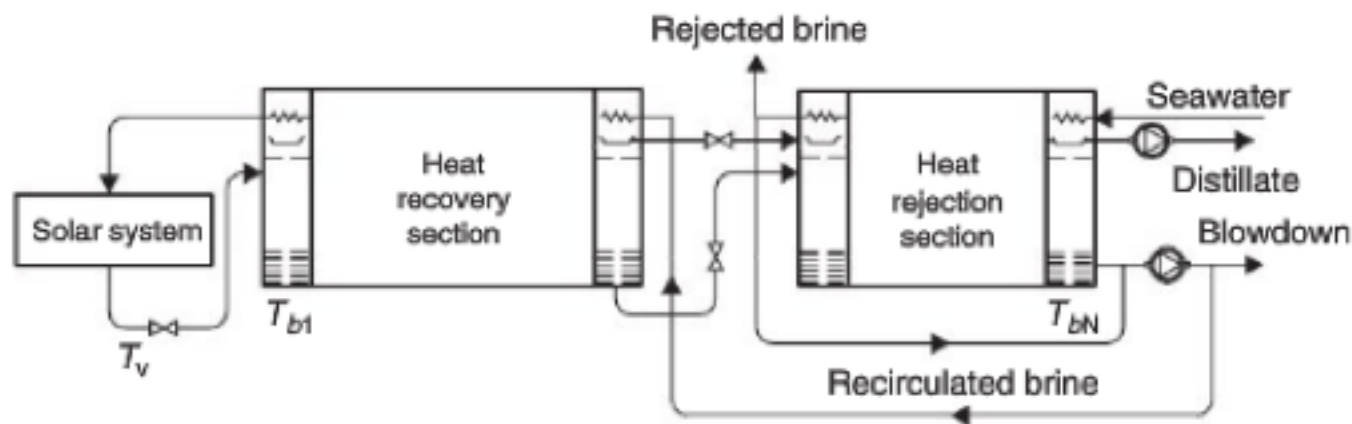


FIGURE 8.5 A multi-stage flash (MSF) process plant.

Solar Desalination/Water Purification

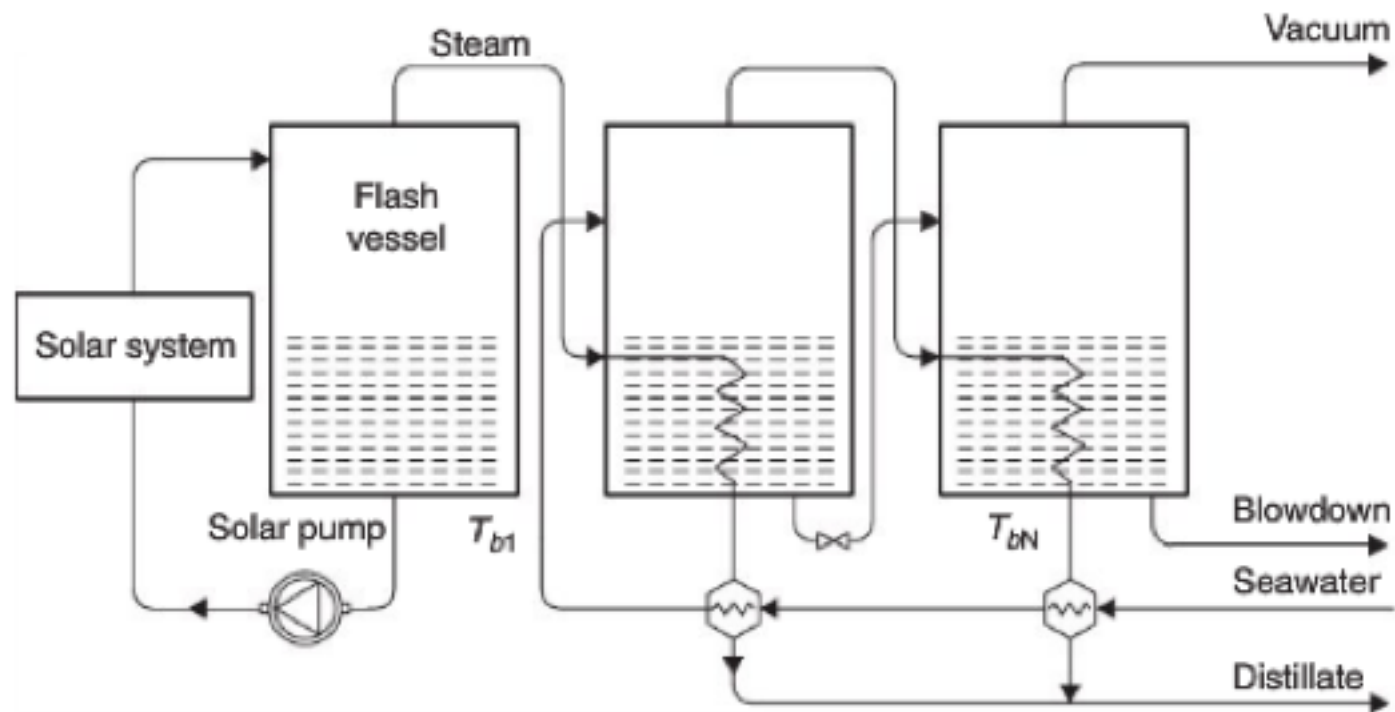


FIGURE 8.6 Principle of operation of a multiple-effect boiling (MEB) system.

Solar Desalination/Water Purification

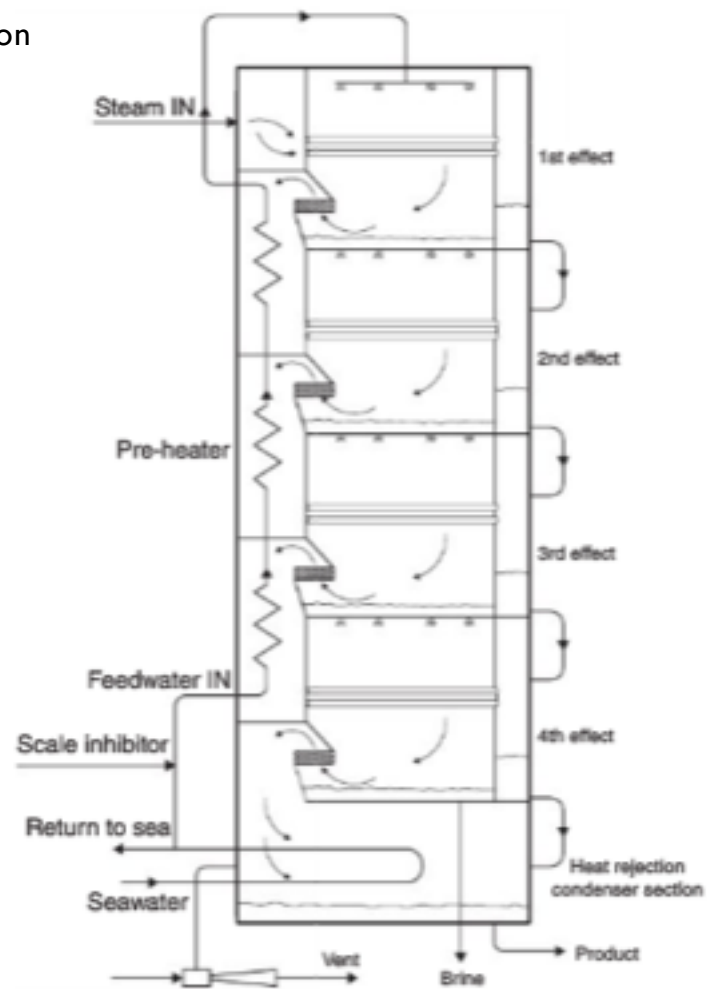
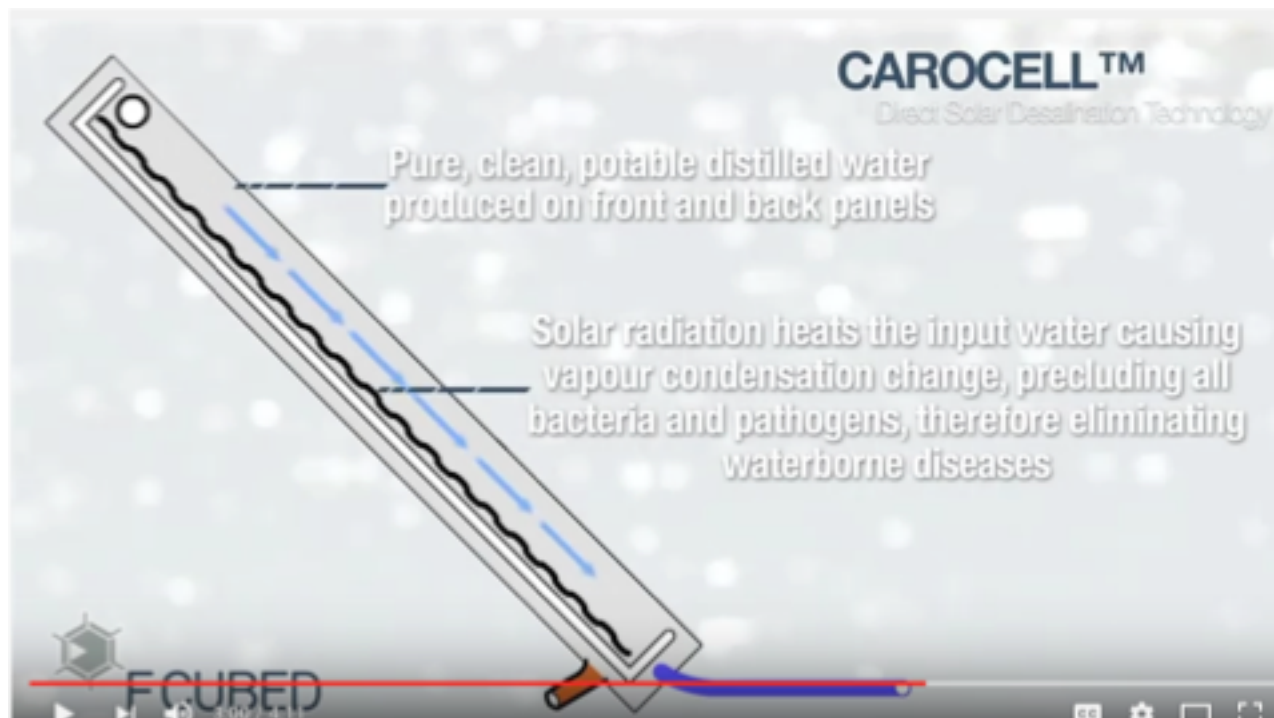


FIGURE 8.8 Schematic of the MES evaporator.

[Carocell Australia](#)



King Abdullah's Desalinization Plant



Seawater Greenhouse

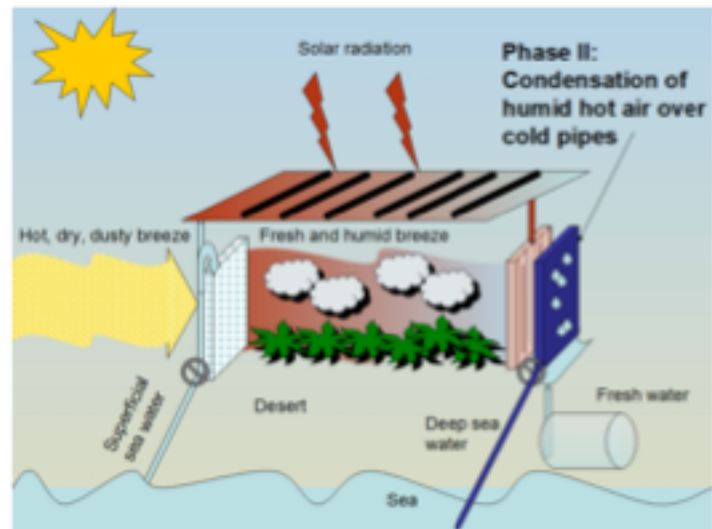
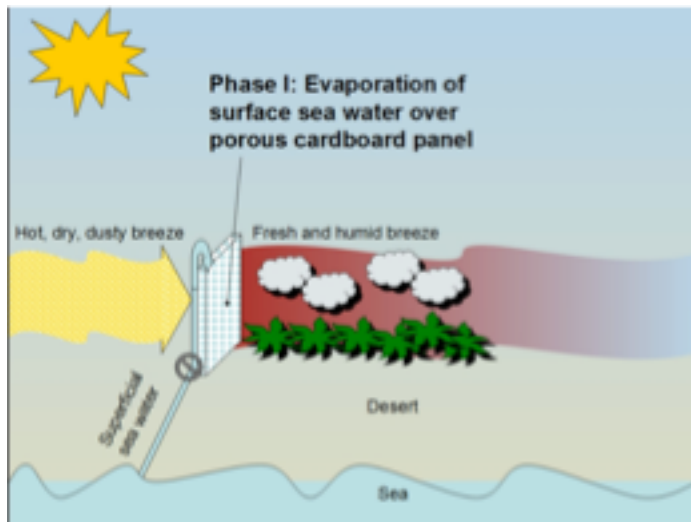


Figure 3. The surrounding area from the front of the greenhouse



Figure 4. Two years into operation from the back of the greenhouse

Seawatergreenhouse.com

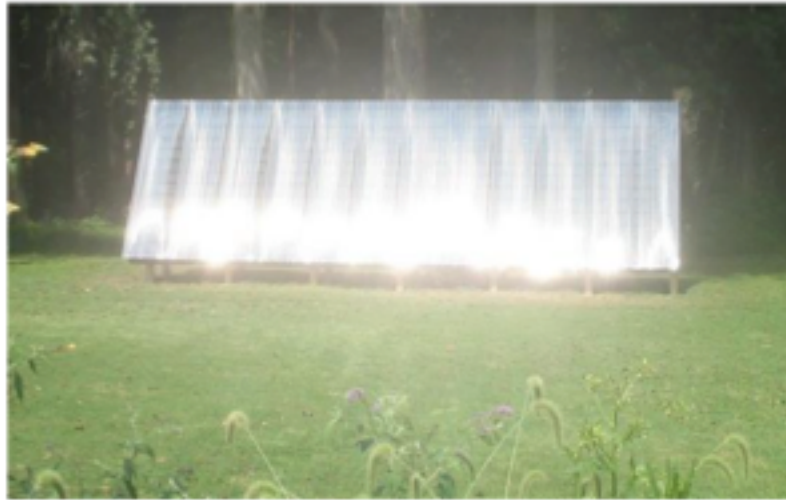
A restorative approach to agriculture



Solar Heat Collectors

[Do it yourself webpage](http://www.n3fjp.com/solar/construction101/construction101.htm)

<http://www.n3fjp.com/solar/construction101/construction101.htm>



- Direct or open loop systems, in which potable water is heated directly in the collector.
- Indirect or closed loop systems, in which potable water is heated indirectly by a heat transfer fluid that is heated in the collector and passes through a heat exchanger to transfer its heat to the domestic or service water.

- Natural (or passive) systems.
- Forced circulation (or active) systems.

Table 5.1 Solar Water Heating Systems

Passive systems	Active systems
Thermosiphon (direct and indirect)	Direct circulation (or open loop active) systems
Integrated collector storage	Indirect circulation (or closed loop active) systems, internal and external heat exchanger
	Air systems
	Heat pump systems
	Pool heating systems

Passive Systems

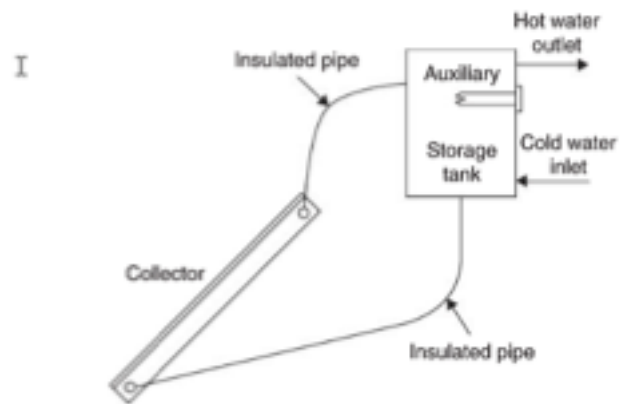
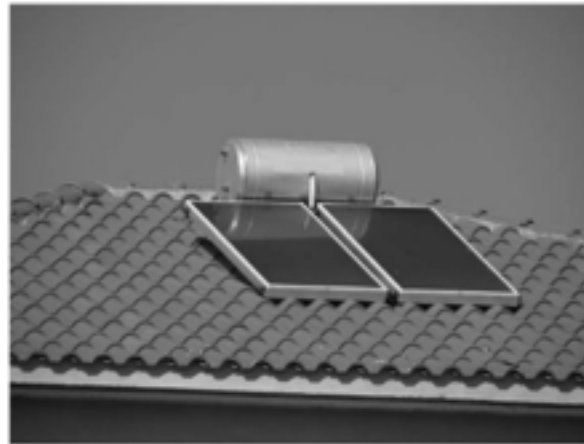


FIGURE 5.1 Schematic diagram of a thermosiphon solar water heater.



(a)



(b)

FIGURE 5.2 Thermosiphon system configurations. (a) Flat-plate collector configuration. (b) Evacuated tube collector configuration.

Solar Heat Collectors

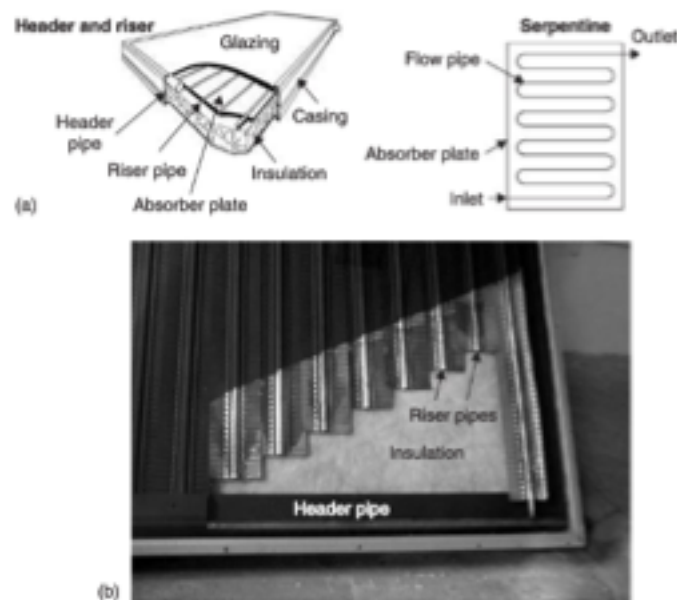


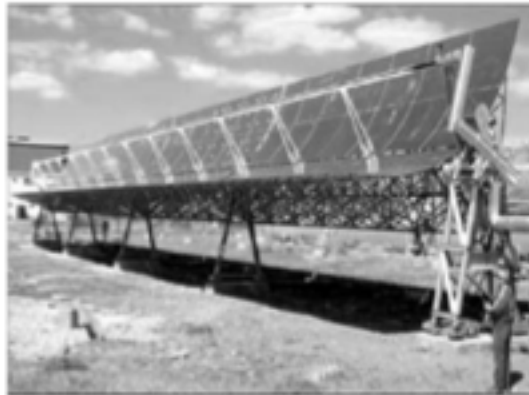
FIGURE 3.1 Typical flat-plate collector. (a) Pictorial view of a flat-plate collector. (b) Photograph of a cut header and riser flat-plate collector.

Table 3.1 Solar Energy Collectors

Motion	Collector type	Absorber type	Concentration ratio	Indicative temperature range (°C)
Stationary	Flat-plate collector (FPC)	Flat	1	30–80
	Evacuated tube collector (ETC)	Flat	1	50–200
	Compound parabolic collector (CPC)	Tubular	1–5	60–240
5–15			60–300	
Single-axis tracking	Linear Fresnel reflector (LFR)	Tubular	10–40	60–250
	Cylindrical trough collector (CTC)	Tubular	15–50	60–300
	Parabolic trough collector (PTC)	Tubular	10–85	60–400
Two-axis tracking	Parabolic dish reflector (PDR)	Point	600–2000	100–1500
	Heliostat field collector (HFC)	Point	300–1500	150–2000

Note: Concentration ratio is defined as the aperture area divided by the receiver/absorber area of the collector.

Solar Heat Collectors



(a)



(b)

FIGURE 3.14 Photos of actual parabolic trough collectors. (a) The EuroTrough (from www.sbp.de/en/html/projects/detail.html?id=1043). (b) An Industrial Solar Technology collector.



FIGURE 3.13 Schematic of a parabolic trough collector.

Solar Heat Collectors

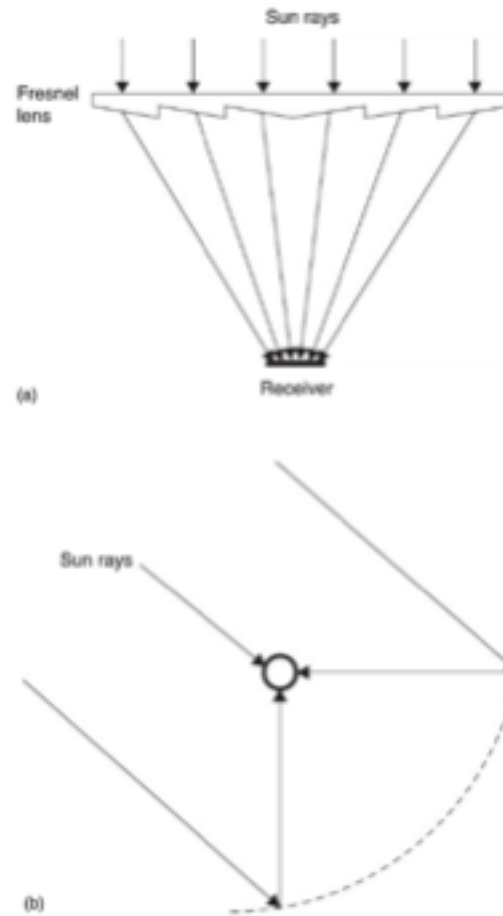


FIGURE 3.17 Fresnel collectors. (a) Fresnel lens collector (FLC). (b) Linear Fresnel-type parabolic trough collector.

Solar Heat Collectors

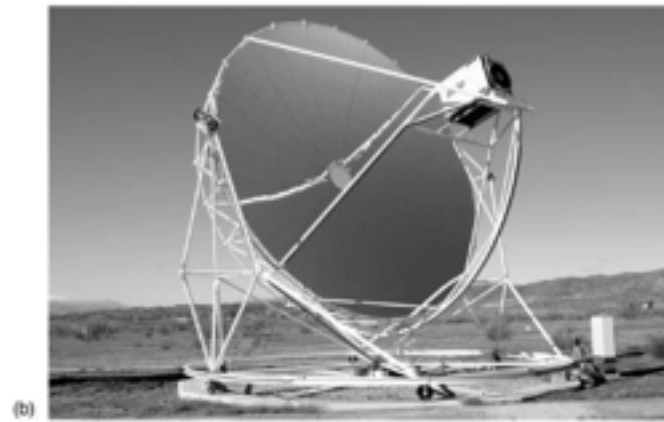
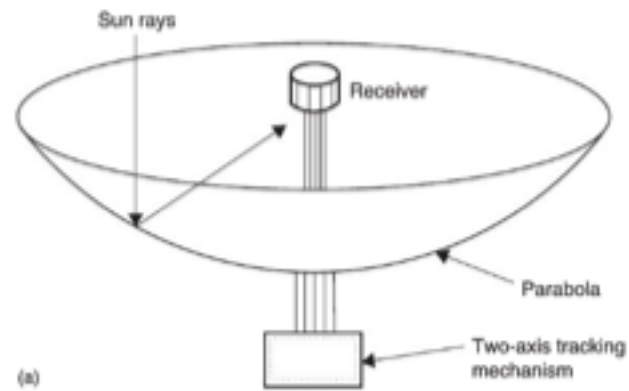


FIGURE 3.20 Parabolic dish collector. (a) Schematic diagram. (b) Photo of a Eurodish collector (from www.psa.es/webeng/instalaciones/discos.html).

Solar Heat Collectors



FIGURE 10.8 Photograph of a dish concentrator with Stirling engine (source: www.energylan.sandia.gov/sunlab/pdfs/dishen.pdf).



FIGURE 10.7 Heliostat detail of the Solar Two plant (source: www.energylan.sandia.gov/sunlab/overview.htm).

[Eurodish Solar Stirling Engine](https://www.youtube.com/watch?v=wfdW0qyToBg) (<https://www.youtube.com/watch?v=wfdW0qyToBg>)

[Sterling Engine Wiki](http://en.wikipedia.org/wiki/Stirling_engine) (http://en.wikipedia.org/wiki/Stirling_engine)

[Sterling Engine Water Pump \(Large\)](http://www.youtube.com/watch?v=CEBuzq5ilqk)
(<http://www.youtube.com/watch?v=CEBuzq5ilqk>)

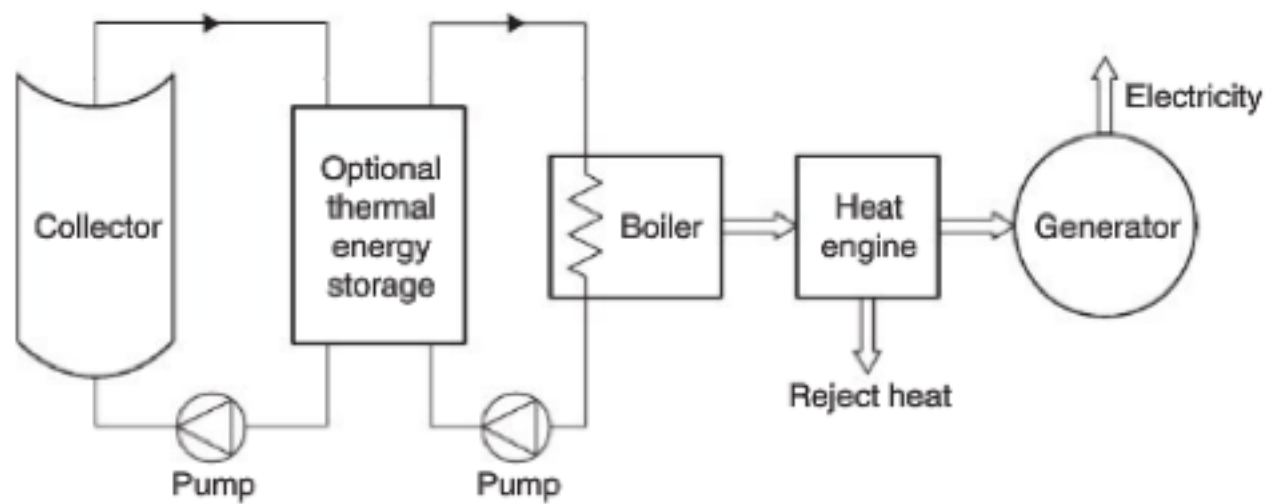


FIGURE 10.1 Schematic diagram of a solar-thermal energy conversion system.

Solar Heat Collectors



FIGURE 3.22 Detail of a heliostat.

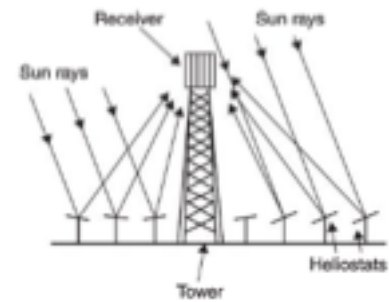


FIGURE 3.21 Schematic of central receiver system.

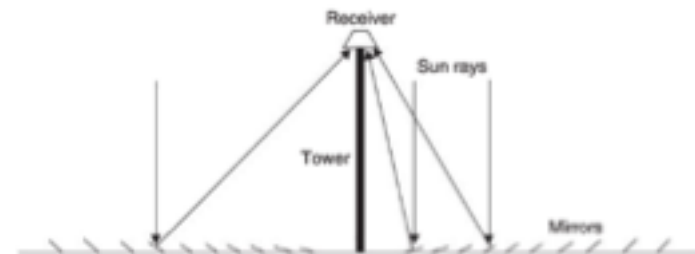


FIGURE 3.18 Schematic diagram of a downward-facing receiver illuminated from an LFR field.

Solar Heat Collectors

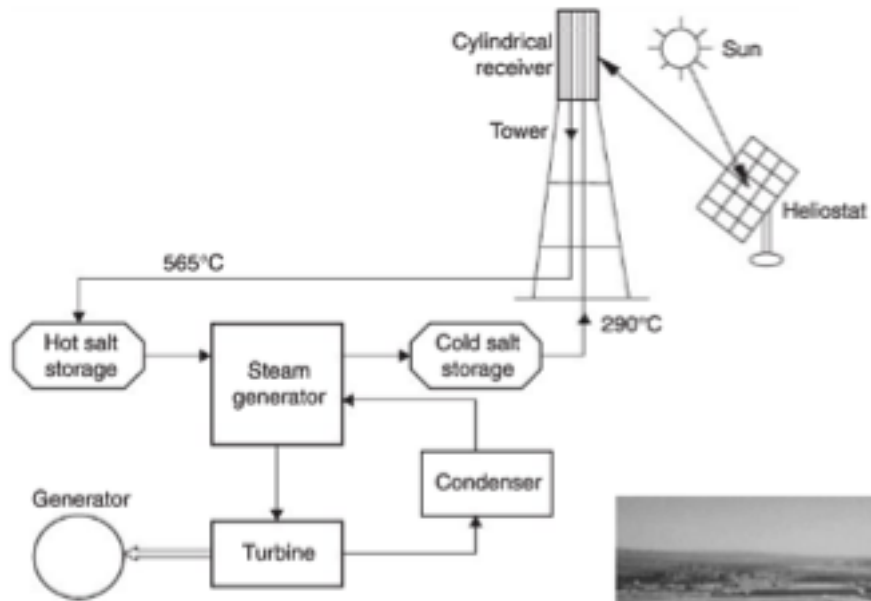


FIGURE 10.5 Schematic of the Solar Two plant.



FIGURE 10.6 Photograph of the Solar Two central receiver plant (source: www.energy.lanl.sandia.gov/sunlab/Snapshot/STFUTURE.HTM).

Solar Heat Collectors

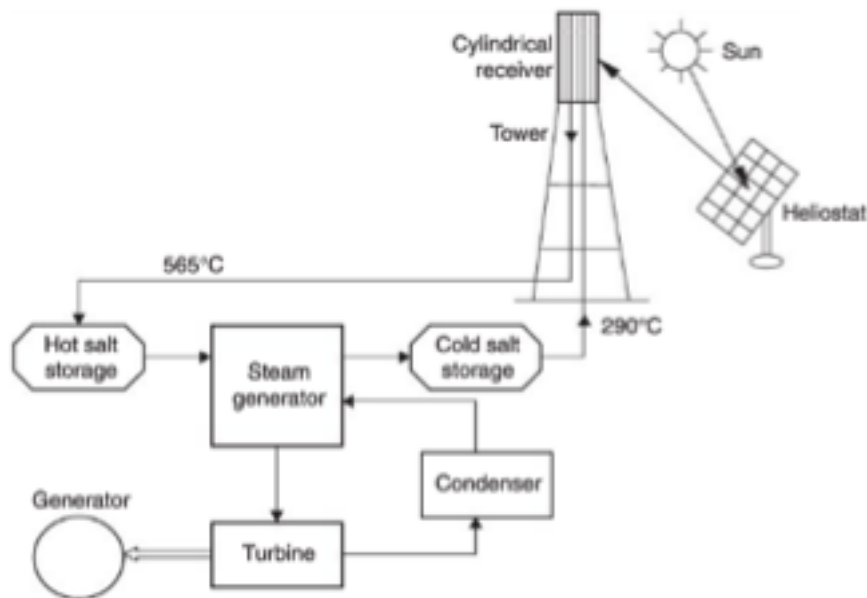


FIGURE 10.5 Schematic of the Solar Two plant.

Solar Tres (Gemasolar)

How it works

<http://www.youtube.com/watch?v=GhV2LT8KvgA>

<https://www.youtube.com/watch?v=5nd7fGMXciA>

Gemasolar	
	
	
Location of Gemasolar	
Country	Spain
Location	Fuentes de Andalucía, Sevilla
Coordinates	 37°33'29.11"N 5°19'44.6"W
Status	Operational
Commission date	May 2011
Owner(s)	Torresol Energy
Solar farm	
Type	CSP
CSP technology	Solar power tower
Heliostats	2,650
Power generation	
Installed capacity	19.9 MW
Annual generation	110 GWh

Photo 3.1 **The Gemasolar power tower near Sevilla (Spain)**



Source: Torresol Energy.

Key point

Molten-salts solar towers can generate electricity round the clock.

[Aoraa Solar Ethiopia](#)

<http://www.alternative-energy-news.info/tulip-solar-ethiopia/>



[Aoraa Solar .com](#)

<https://sustainability.asu.edu/research/project/aora-solar-tulip/>

Table 10.1 Performance Characteristics of Various CSP Technologies

Technology	Capacity range (MW)	Concentration	Peak solar efficiency (%)	Solar-electric efficiency (%)	Land use (m ² /MWh-a)
Parabolic trough	10–200	70–80	21	10–15	6–8
Fresnel reflector	10–200	25–100	20	9–11	4–6
Power tower	10–150	300–1000	20	8–10	8–12
Dish-Stirling	0.01–0.4	1000–3000	29	16–18	8–12

[Images for dish stirling](#) - Report images



Solar Chimney's

Enviromission (Australia)

http://www.enviromission.com.au/EVM/content/about_companyprofile.html



Solar Chimney Spain (Madrid)

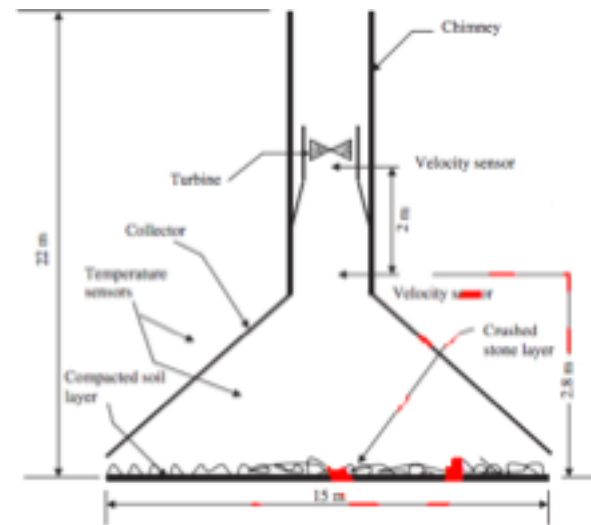
<http://www.youtube.com/watch?v=XCGVTYtEFk>



Solar Chimney's



Gaborone, Botswana



Hot Water Systems

This webpage goes through types of solar water heaters

<http://www.alternative-energy-tutorials.com/solar-hot-water/evacuated-tube-collector.html>

Hot Water Systems

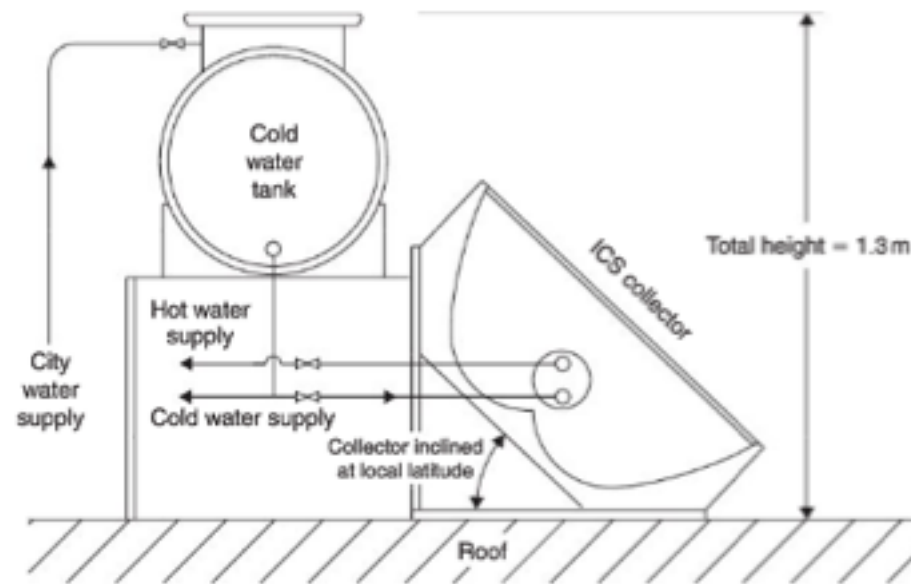
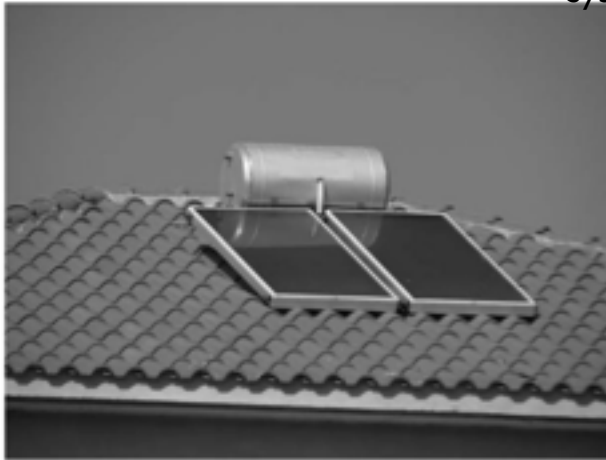


FIGURE 5.8 The complete solar ICS hot water system.

Hot Water Systems



(a)



(b)

FIGURE 5.2 Thermosiphon system configurations. (a) Flat-plate collector configuration. (b) Evacuated tube collector configuration.

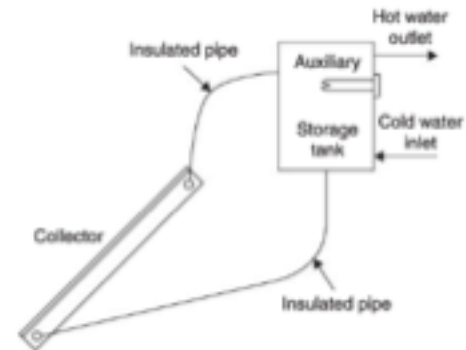


FIGURE 5.1 Schematic diagram of a thermosiphon solar water heater.

Hot Water Systems

Direct vs Indirect Systems

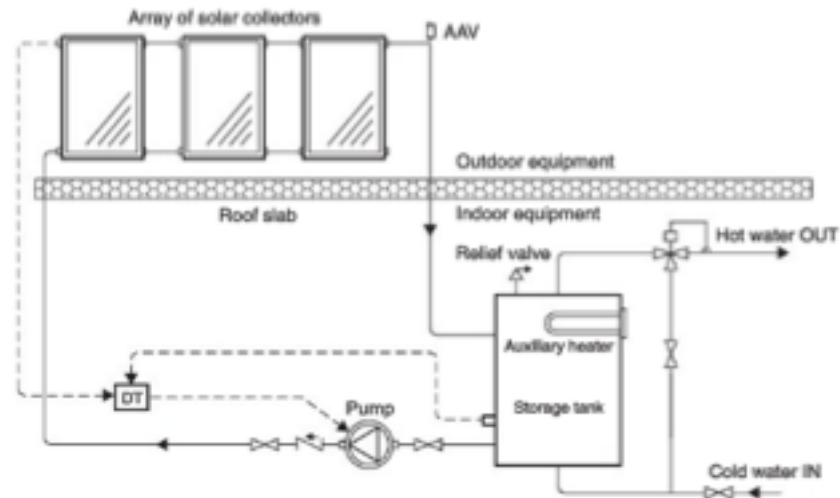


FIGURE 5.9 Direct circulation system.

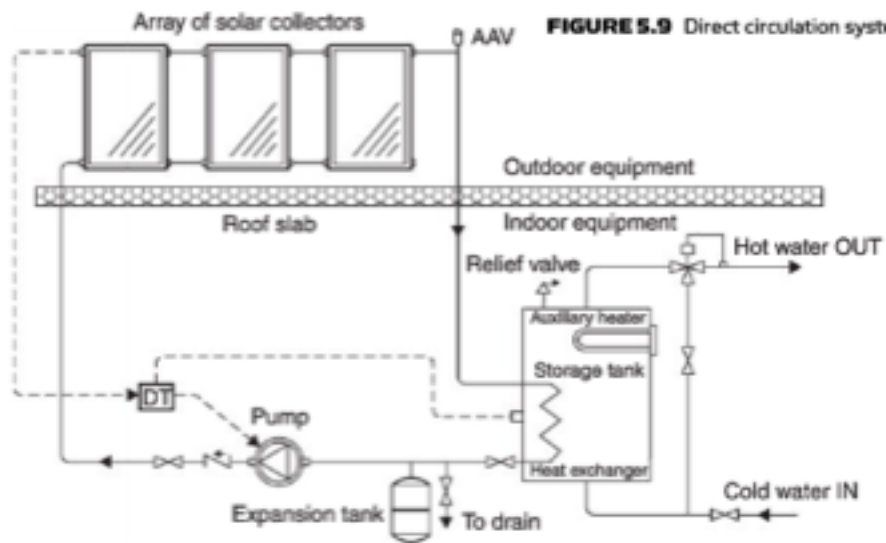


FIGURE 5.11 Indirect water heating system.



Figure 4-7 A home-made clip fin collector.

that faces away from the sun. We need to try to eliminate thermal bridges as far as we possibly can.

Aluminum clip fins are one of the easiest ways of assembling a solar collector quickly, as they essentially clip onto a matrix of copper pipe.

Another way of constructing a solar collector is to use an old radiator painted black inside an insulated box—crude but effective! (Figure 4-9). This system contains more water, and as a result has a slower response time. This is because it takes more time to heat up the thermal mass of the radiator.

Warning

One of the problems that solar collectors suffer from is freezing in the winter. When temperatures drop too low, the water in the pipes of the collectors expands—this runs the risk of severely damaging the collectors.



Figure 4-8 Aluminum clip fins.



Figure 4-9 A recycled radiator collector.

Hot Water Systems

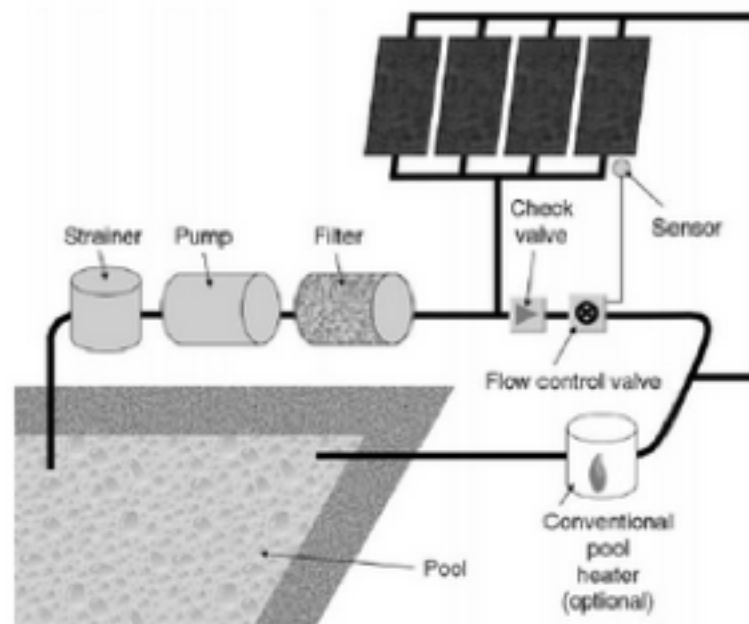


Figure 4-10 *Solar pool heating.*

Tip

Enerpool is a free program that can be used to simulate your swimming pool being heated with solar collectors. By inputting information such as your location, and how the pool is covered. The program can predict what temperature your pool will be at, at any given time!

www.powernet.com/enerpool.html

Hot Air Heating Systems

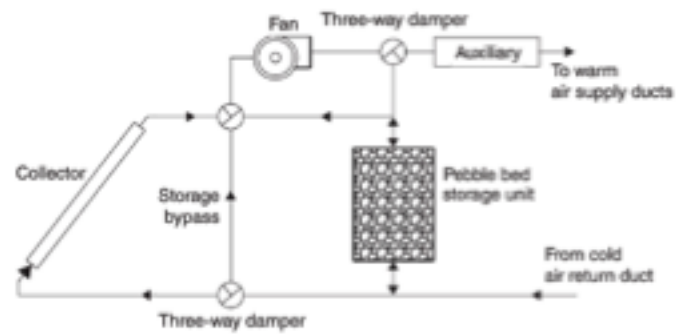


FIGURE 6.11 Schematic of basic hot air system.

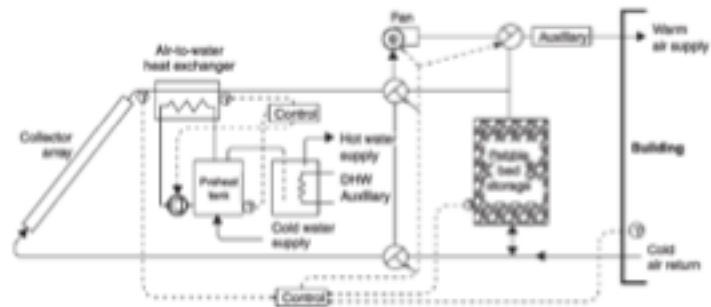


FIGURE 6.12 Detailed schematic of a solar air heating system.

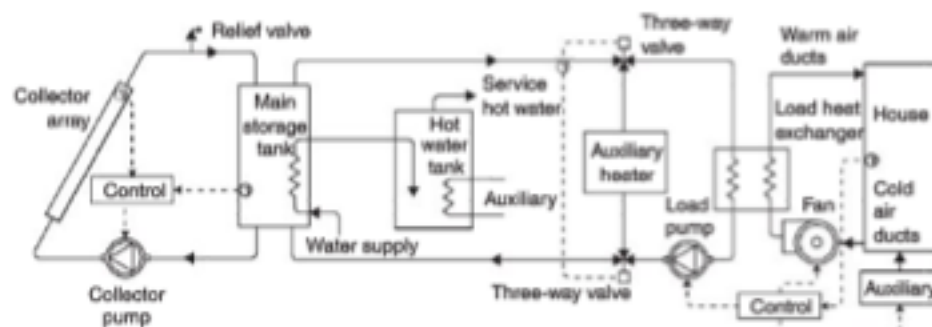


FIGURE 6.13 Schematic diagram of a solar space heating and hot water system.

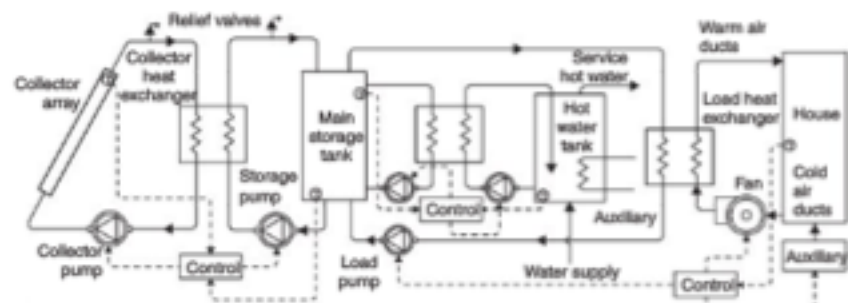


FIGURE 6.14 Detailed schematic diagram of a solar space heating and hot water system with antifreeze solution.

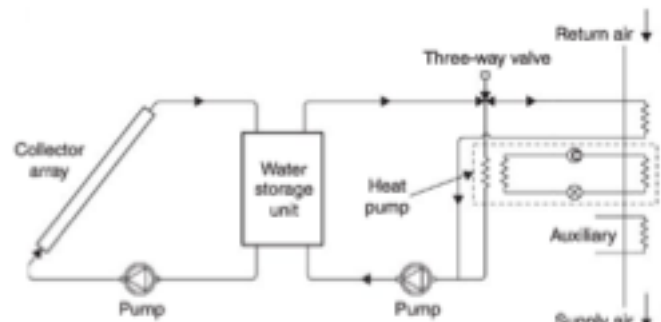


FIGURE 6.16 Schematic diagram of a domestic water-to-air heat pump system (series arrangement).

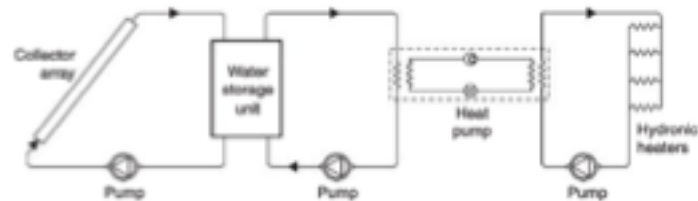


FIGURE 6.17 Schematic diagram of a domestic water-to-water heat pump system (parallel arrangement).

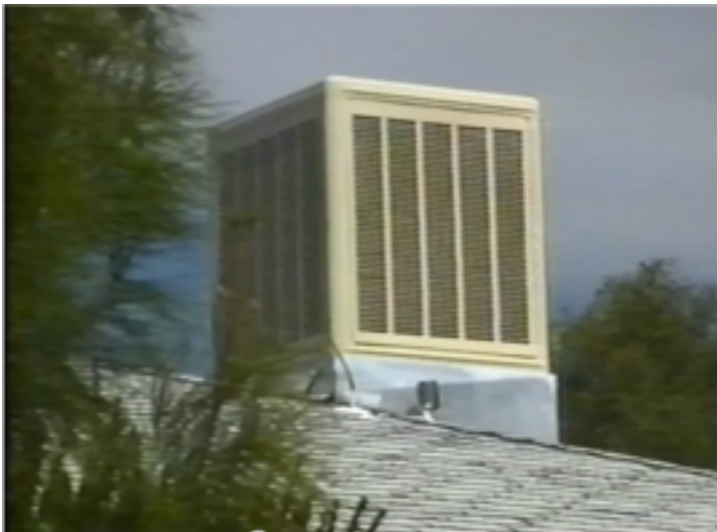
Industrial Solar Water Heating Mek'elle Ethiopia

http://www.solarthermalworld.org/sites/gstec/files/Kahsay_ISES%20Kassel.pdf

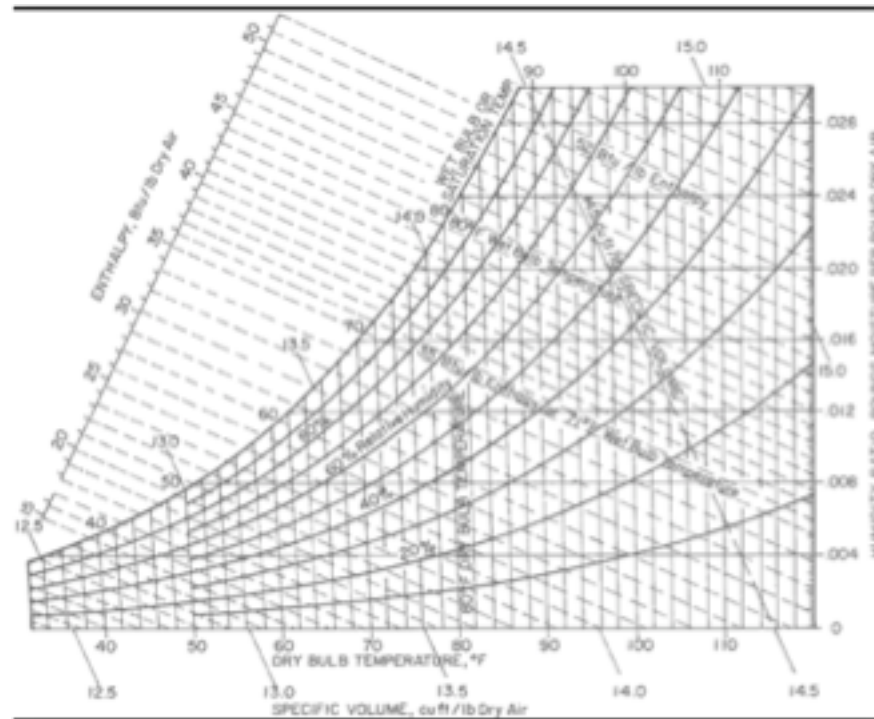
No.	Factory	Process	Working Temperature (°C)	Consumption (m³/day)	Current Source of Energy
1.	Sheba Tannery	Skin Tanning	35	18.4	Furnace oil for a steam boiler
		Skin Re-tanning	50	66.6	
		Hide Tanning	40	29.3	
		Hide Re-tanning	65	27.0	
2.	Maichew Particleboard	Glue preparation	40	6.0	Furnace oil, fire wood
		Impregnation	55	1.2	
3.	Bahirdar Textile	Pre-heater	60	36.0	Furnace oil for a steam boiler
		Washing	70	7.8	
		Chemical Preparation	80	5.2	
4.	Ashraf Edible Oil	Conditioning	85	6.0	Furnace oil for a steam boiler
		Degumming	90	5.0	
		Neutralization	90	5.0	
		Washing	70	7.7	

Solar Power Cooling

Swamp Cooler (http://www.youtube.com/watch?v=6ooAAcsbf_0)



Psychrometric Chart



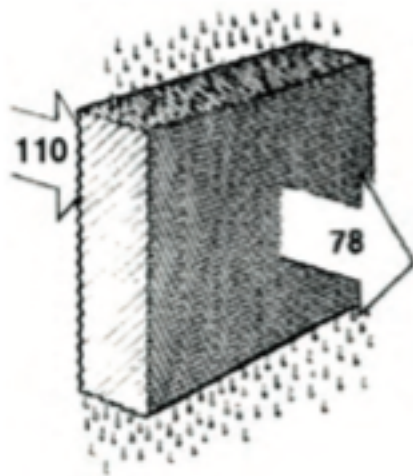


Figure 1. Direct evaporative cooling through a wetted medium. Source: www.energy.ca.gov/appliances/2003rulemaking/documents/case_studies/CASE_Evaporative_Cooler.pdf

Up to 38°F (21.1°C) of cooling can theoretically be achieved (110°F (43.3°C) – 72°F (22.2°C)) by simply

PSYCHROMETRIC CHART

Sea Level

Direct evaporative cooling process

A: Entering air properties

$T_{DB} = 110^{\circ}\text{F}$ (43.3°C)

$T_{WB} = 72^{\circ}\text{F}$ (22.2°C)

$\text{RH} = 15\%$

B: Leaving air properties

$T_{DB} = 78^{\circ}\text{F}$ (25.6°C)

$T_{WB} = 72^{\circ}\text{F}$ (22.2°C)

$\text{RH} = 75\%$

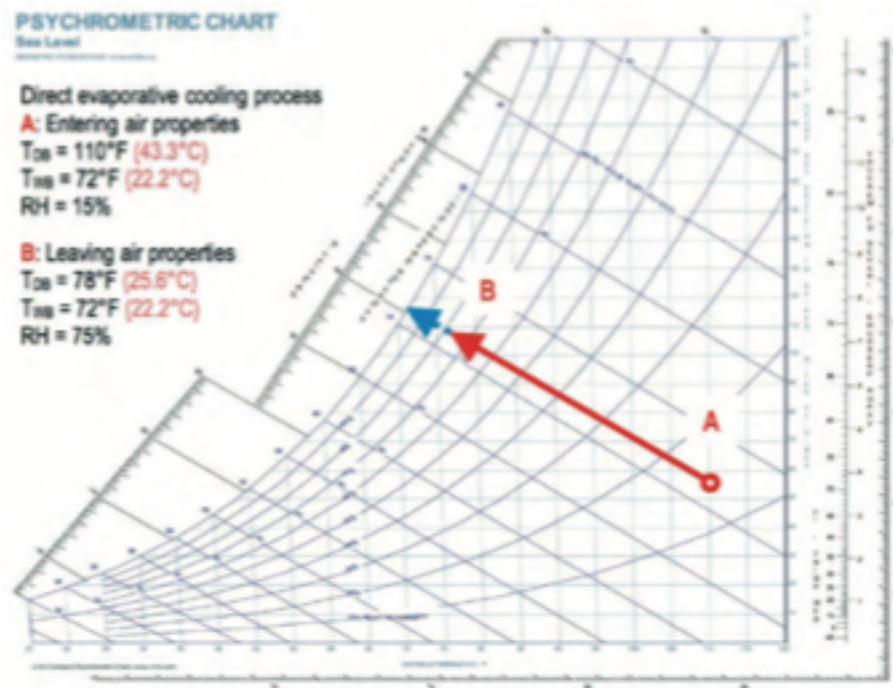


Figure 2. Direct evaporative cooling process shown psychrometrically.

Source: PsycPro software at www.Linric.com

PSYCHROMETRIC CHART

Sea Level

Potential cooling from direct evaporative cooling

A: 95°F (35°C) - 86°F (30°C) = 9°F (5°C) of cooling possible

B: 95°F (35°C) - 60°F (15.6°C) = 35°F (19.4°C) of cooling possible

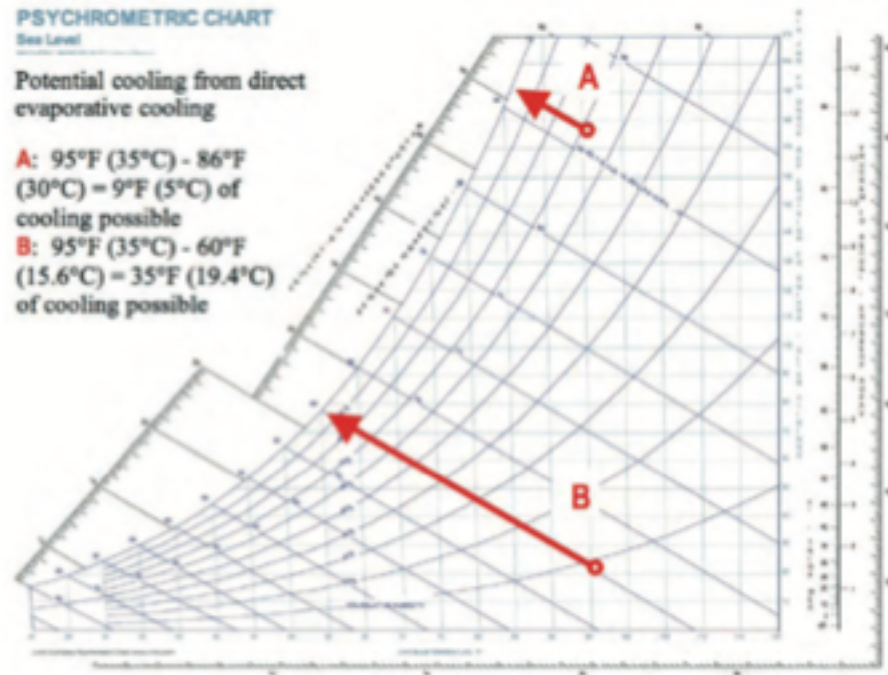


Figure 3. Comparison of the direct evaporative cooling possible when starting with T_{db} of 95°F (35°C) at 70% RH vs. at 10% RH. Source: *PsycPro* software at www.Linric.com

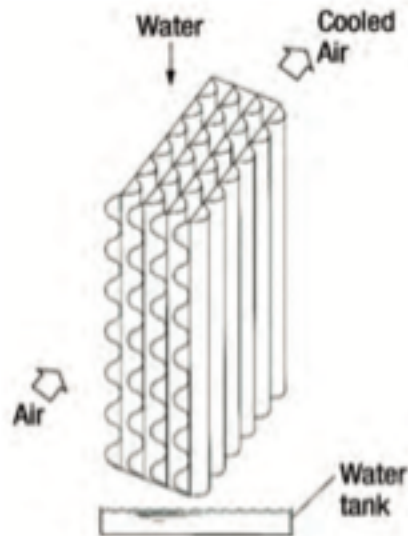


Figure 4. In an indirect evaporative cooling process, the primary airstream flows in a different channel than the secondary airstream. Source: Wang, Shan K., *Handbook of Air Conditioning and Refrigeration (2nd Edition)*, McGraw-Hill, p. 5, 2001; www.knovel.com/knovel2/Toc.jsp?BookID=568&VerticalID=0

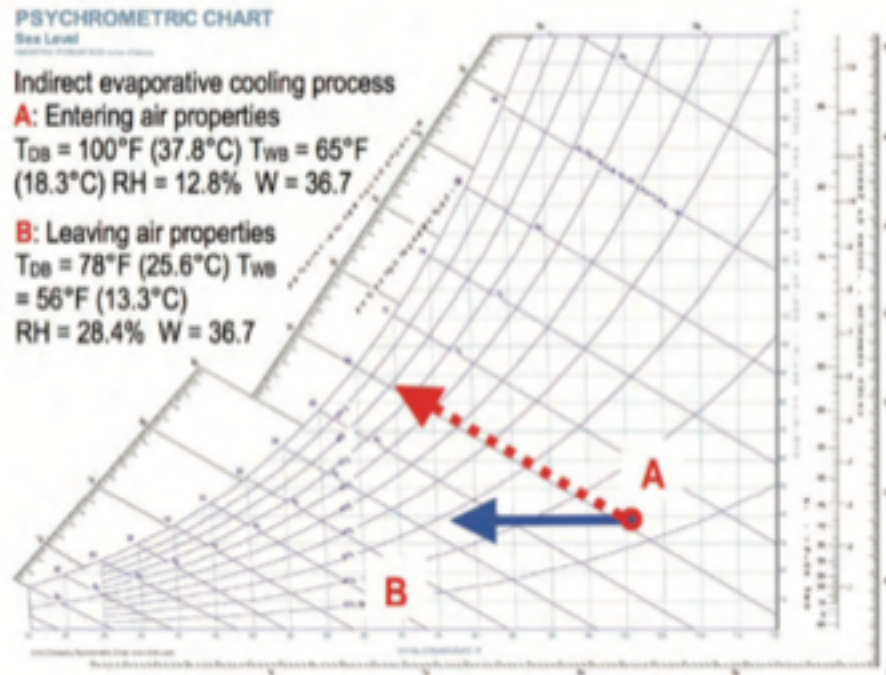


Figure 5. In the indirect evaporative cooling process, no water is shown being added to the primary airstream as it cools from A to B. Source: *PsycPro* software, www.Linric.com

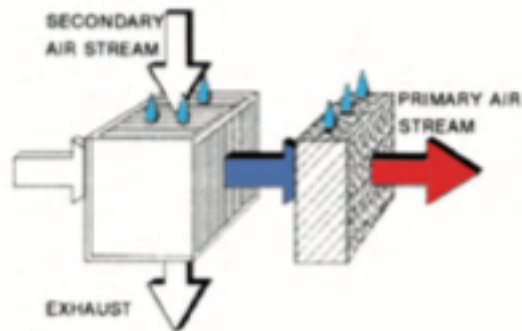


Figure 6. Two-stage indirect/direct evaporative cooling. Source: www.energy.ca.gov/appliances/2003rulemaking/documents/case_studies/CASE_Evaporative_Cooler.pdf

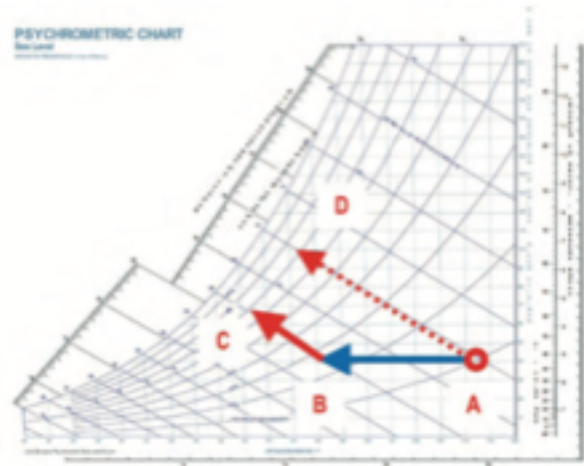


Figure 7. Two-stage indirect/direct evaporative cooling (indirect from A to B and then direct from B to C) yields a lower T_{db} than does direct-only from A to D. Source: PsychPro software at www.Linric.com

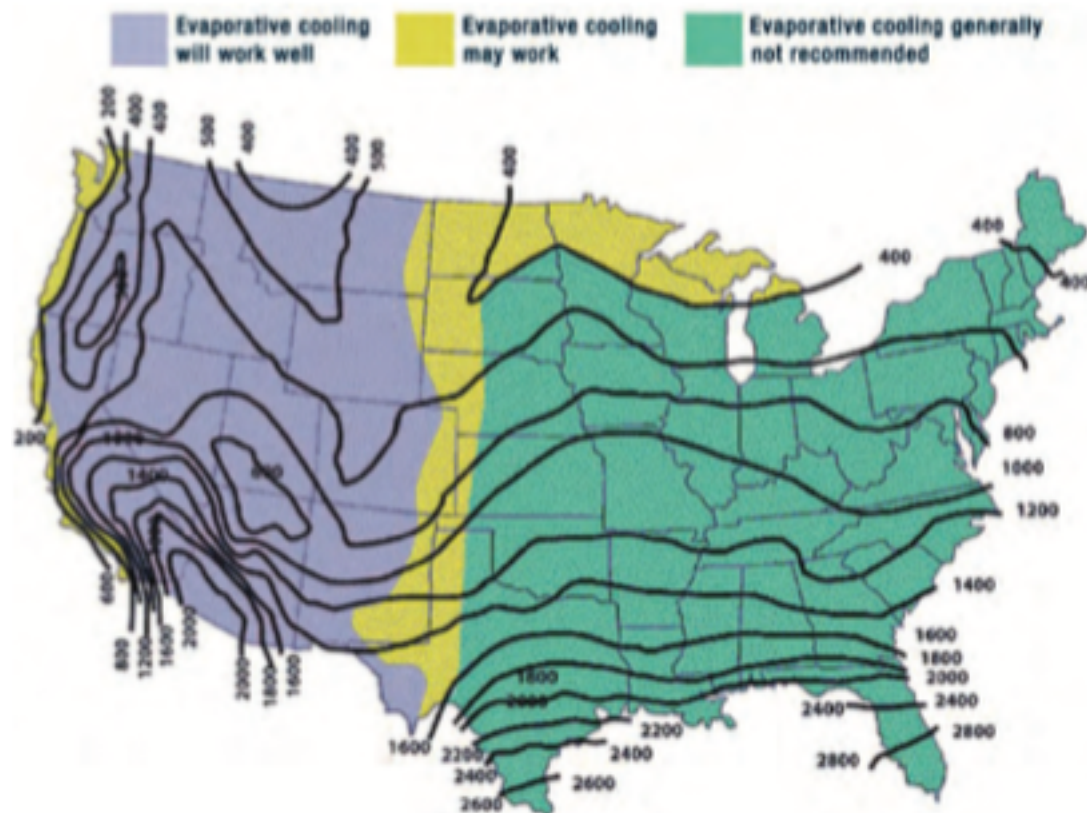
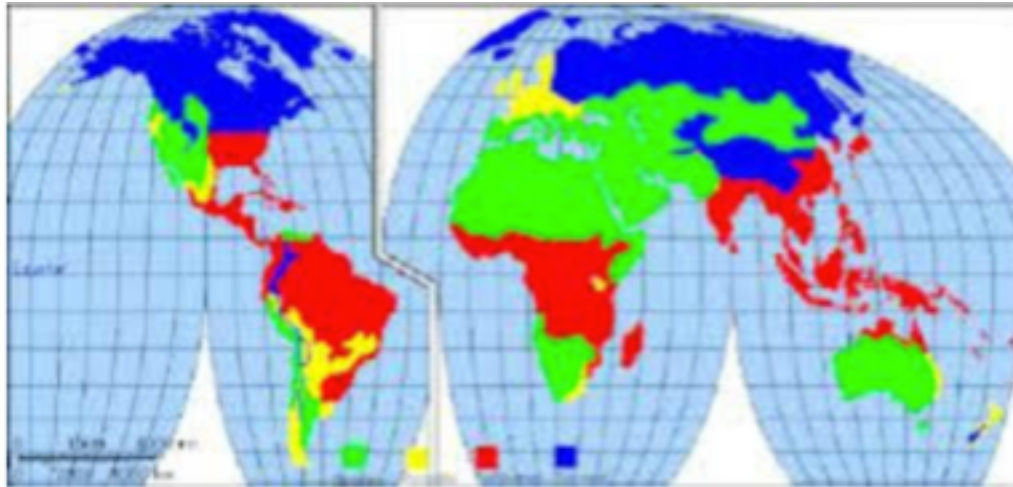
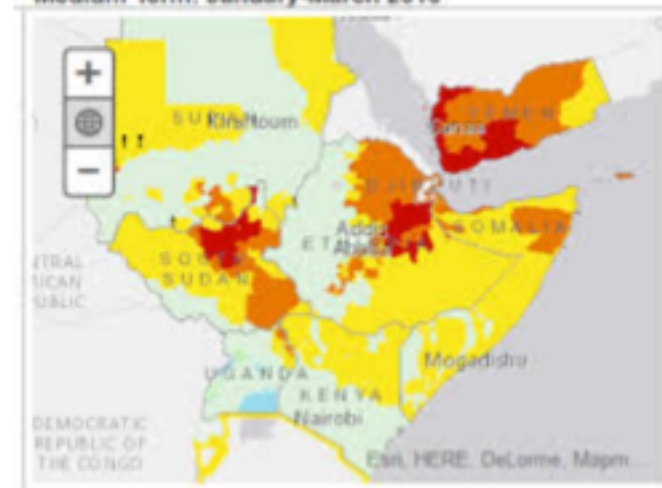


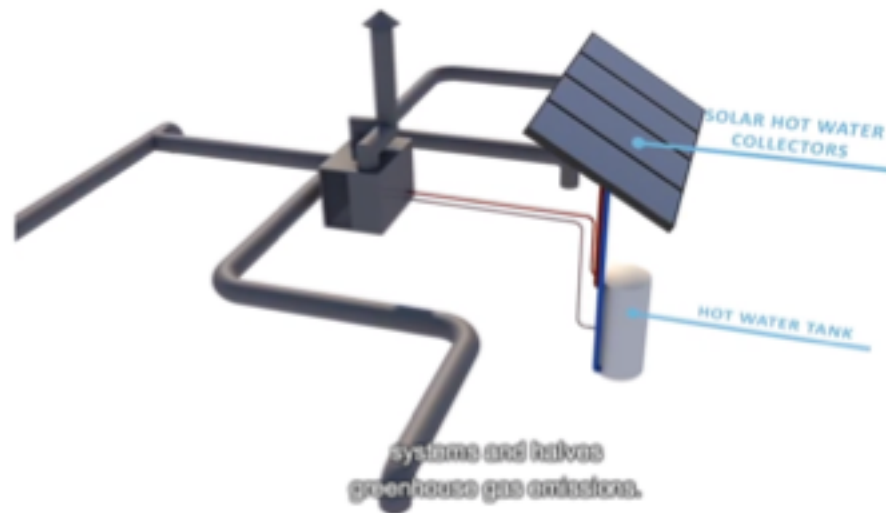
Figure 15. Map of summer cooling load hours. *Source: ARI Unitary Directory, August 1, 1992, to January 31, 1993, pp. 16-17; Air-Conditioning and Refrigeration Institute, www.energyexperts.org/ac_calc/default.asp.*



Medium Term: January-March 2016



[A simple system](http://www.youtube.com/watch?v=cz-kquRmvqk) (<http://www.youtube.com/watch?v=cz-kquRmvqk>)



<http://www.dairyreporter.com/Processing-Packaging/Sub-Saharan-milk-cooler-project-awarded-1m-grant>

Evaporative cooler to cool milk





Cooperative Extension Service

College of Agricultural and Environmental Science/Athens, Georgia 30602-4356



Poultry Housing Tips

Evaporative Cooling Pad Quality Makes a Difference

Volume 20 Number 7

June, 2008



Six-inch evaporative cooling pad systems are a vital part of a tunnel-ventilated poultry house's cooling system. When properly installed and maintained, a six-inch pad system can reduce the incoming air temperature on a hot summer day 20°F or more, dramatically reducing heat-stress-related problems. Furthermore, six-inch pad systems have virtually eliminated the need for interior fogging nozzles which has resulted in cleaner houses, increased equipment life, and reduced risk of electrical shocks due to wet thermostats. Last but not least, six-inch pad systems have eliminated the wasteful run-off associated with traditional two-inch fogging pad systems. Most people would agree that the transition of the poultry industry from fogging and fogging pad systems to six-inch evaporative cooling pad systems has proven to be very beneficial to the birds we grow as well as to growers.

Though on the surface the construction of an evaporative cooling pad looks fairly simple, there is in fact a fair amount of science and engineering that goes into their design. The paper used to construct the pads has to have just the right type and amount of resins that will not only enable the pad to last seven years or more when exposed to the elements, but also allow water to easily "wick" throughout the pad to maximize water evaporation. The "flutes" need to be just the right size and angle to produce maximum cooling of the incoming air while at the same time not causing excessive static pressure that would adversely affect the air moving capacity of the exhaust fans. Last but not least, pad surface coatings need to be formulated and applied in a way that surface rigidity is maximized, while at the same time not adversely affecting pad cooling or air flow through the pad.

The good news for poultry producers is that the vast majority of pads sold in the U.S. are of superior design and quality. The bad news is that because all pads look very similar, producers may unknowingly purchase a pad from a new manufacturer that is not of the same quality as those traditionally sold in the U.S. The following are a few things to look for when considering installing new evaporative cooling pads, that though not always conclusive, can provide some indication as to pad quality.

[BBC Article](http://www.bbc.com/future/story/20120727-when-good-milk-turns-bad)

<http://www.bbc.com/future/story/20120727-when-good-milk-turns-bad>

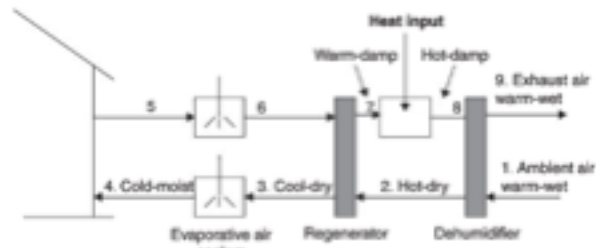


FIGURE 6.19 Schematic of a solar adsorption system.

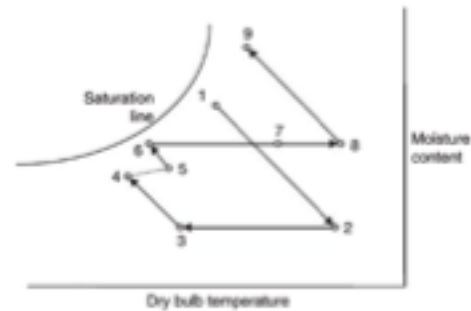


FIGURE 6.20 Psychrometric diagram of a solar adsorption process.

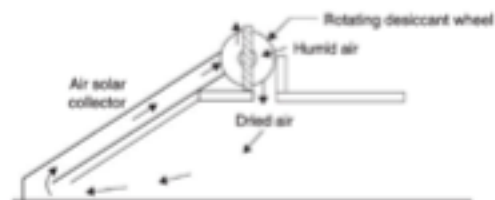


FIGURE 6.21 Solar adsorption cooling system.

**Solar Refrigeration Using
Absorption/Desorption/Evaporation**

Carbon/Solvent Systems

AN ENERGY EFFICIENT SOLAR ICE-MAKER

A Simple Solar Ice Maker

K. Senthil
Department of Mechanical Engineering, University of Hong Kong, Hong Kong.
Fax: 852-2858-5413; e-mail: k.senthil@hku.hk

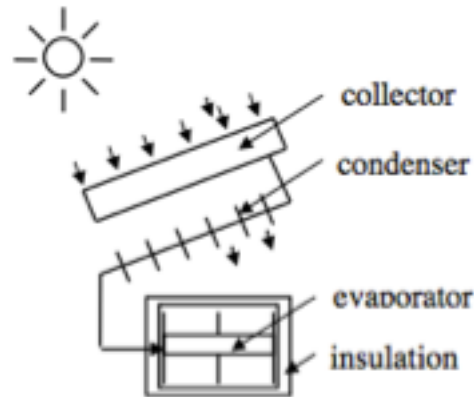


Fig.1 Schematic of a prototype adsorption refrigerator

The principle of the solid-adsorption ice-maker is explained using a P-T-X diagram as shown in Fig.2. To begin with, the adsorption bed along with the refrigerant gets heated up, and when it reaches the required desorption temperature (T_{d1}), the methanol gets desorbed. In the evening, the flat-plate collector (adsorption bed) loses its heat to the surroundings and hence the temperature of the adsorbent bed is reduced rapidly ($T_{d1} \rightarrow T_{d2}$), and the pressure in the adsorber drops to a value below evaporation pressure (P_e). Evaporation could happen if the connecting valve is open, and ice will be made in the refrigeration box.

A laboratory prototype system built is capable of producing 4 to 5 kg of ice a day and could achieve a COP of about 0.12. The total size of the ice-maker is about 1 cu m, and weighs about 50 kg. The experimental tests were carried out at various working conditions ($-10^\circ\text{C} < T_E < -5^\circ\text{C}$ – evaporation; $30^\circ\text{C} < T_C < 45^\circ\text{C}$ – condensation; $100^\circ\text{C} < T_G < 105^\circ\text{C}$ – generation). The refrigerator performance (Specific cooling power, SCP, and the amount of ice made per day) at the evaporating temperature limits ($T_E = -10^\circ\text{C}$ and $T_E = 15^\circ\text{C}$) are shown in Table 1. The performance is relatively low mainly because of the high cycle time (only one cycle a day).

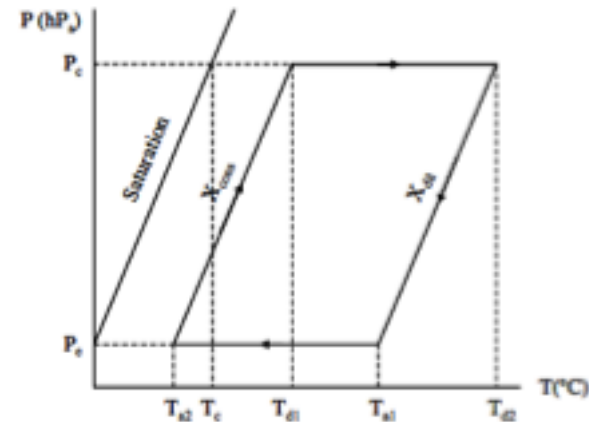


Fig. 2 Thermodynamic cycle for adsorption

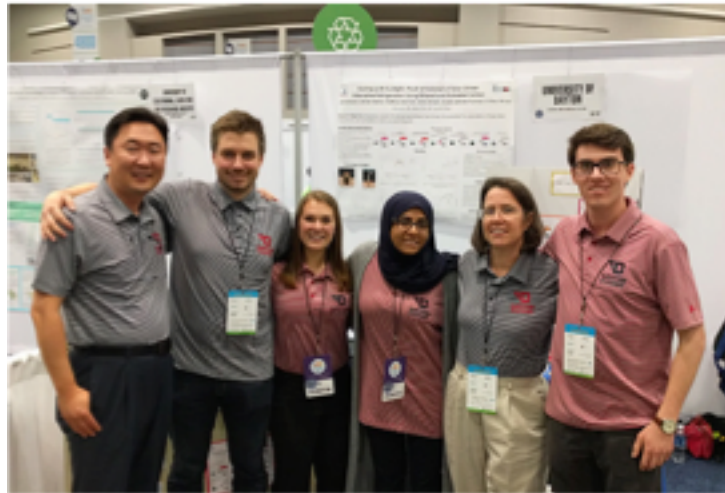
A Simple Solar Ice Maker (Anthony Tong/Amanda)



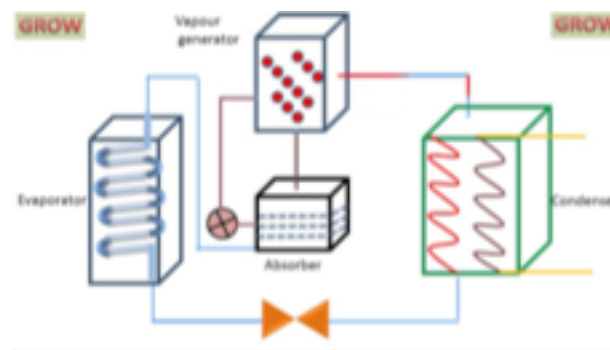
Methanol/Carbon Based
Absorption Refrigerator/Ice
Maker



Amy Ciric University of Dayton (aciric1@udayton.edu)



Ethanol/Carbon Based
Absorption Refrigerator



A Simple Solar Ice Maker

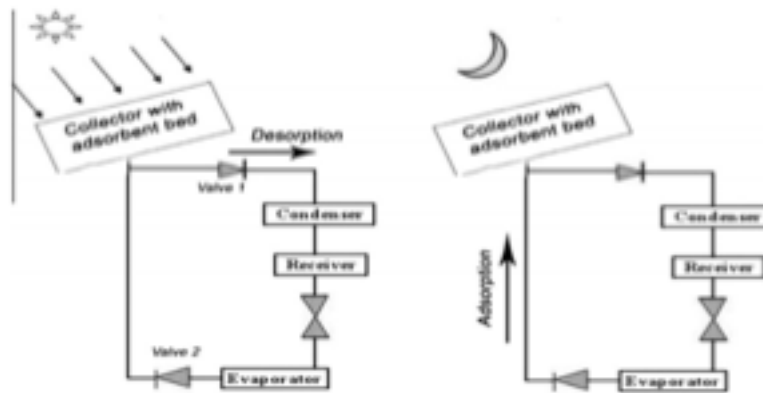


Fig. 1a. Schematic of the solar adsorption cooling system.

There is a single adsorbent bed in the intermittent solar adsorption cooling cycle. The adsorption system consists of three main parts: solar collector with adsorbent bed where activated carbon is placed, condenser and evaporator as shown in Fig. 1a. The operating cycle of the system has four processes as shown in the Clapeyron diagram in Fig. 1b. The heating process (1-2) and the desorbing process (2-3) represent half the cycle while the cooling (3-4) and adsorption (4-1) processes represent the other half. During the heating period, the adsorbent bed receives heat from solar energy that raises the temperature of the pair of

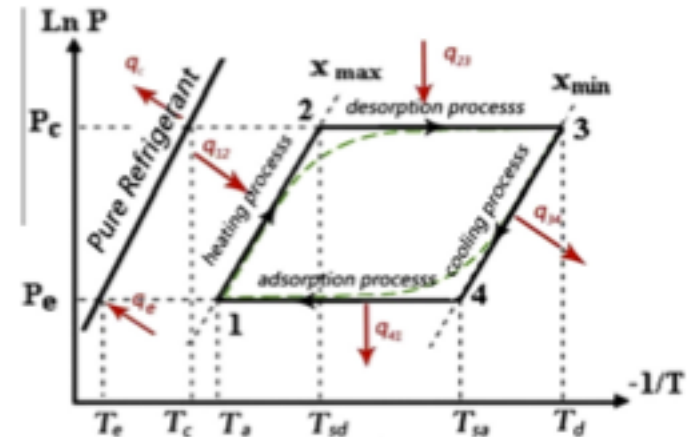


Fig. 1b. Schematic view of the adsorption process on Clapeyron diagram.

adsorbent and adsorbate as shown in Fig. 1b by line 1-2 (isosteric heating process, at constant concentration of the adsorbate = x_{max}). When the adsorbent bed pressure reaches the condenser pressure, the adsorbate vapor diffuses from the collector to the condenser and condensed there (line 2-3, desorption process at condenser pressure). So the concentration of the adsorbate in the reactor reaches the minimum value (x_{min}) at the end of this desorption process. This process is followed by cooling the generator (line 3-4, isosteric cooling process). Then, the liquid adsorbate flows from the condenser to the evaporator where it vaporizes by absorbing heat from the water to be cooled. As a result, the liquid water in evaporator becomes cold or may be converted totally or partially into ice. After that, the adsorbent adsorbs the refrigerant vapor that is coming from the evaporator (line 4-1, adsorption process at evaporator pressure). Thus, the heating and cooling processes are run at constant concentration of adsorbate while the concentration of refrigerant varies through adsorption and desorption processes.

N.A.A. Qasem, M.A.I. El-Shaarawi / Solar Energy 98 (2013) 523–542

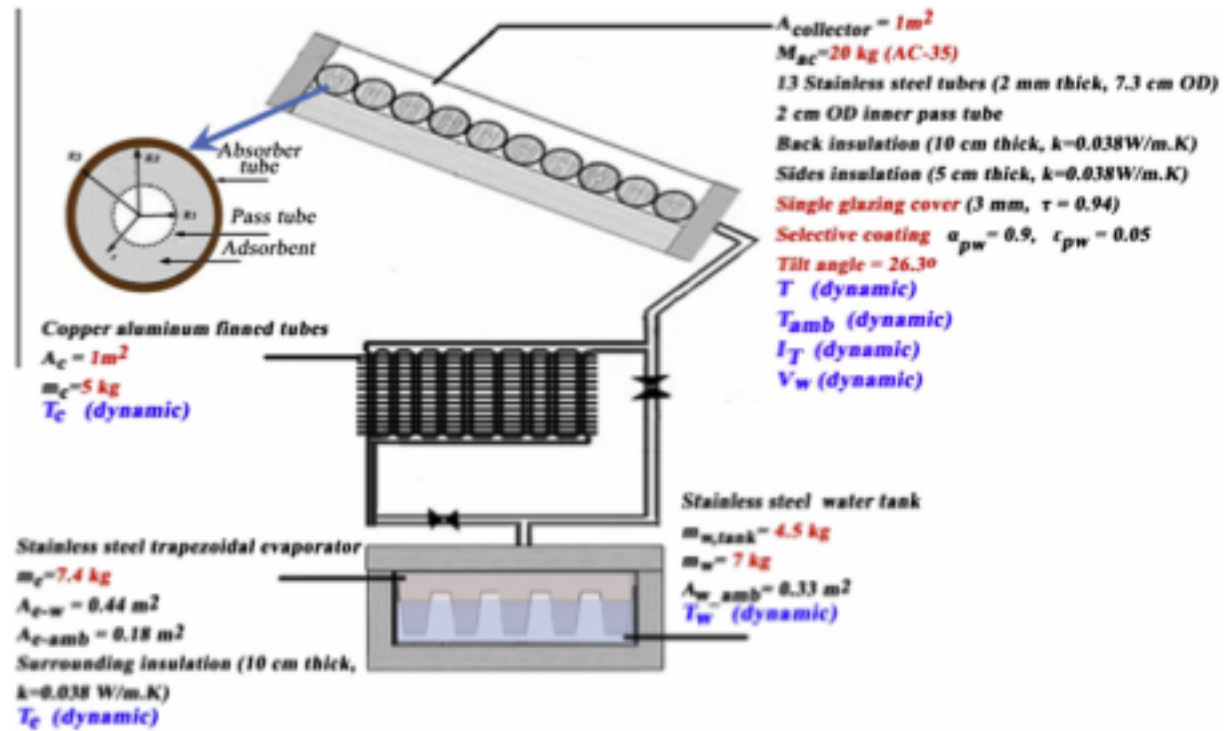


Fig. 2. Schematic details of the system.

Ammonia/Water Systems

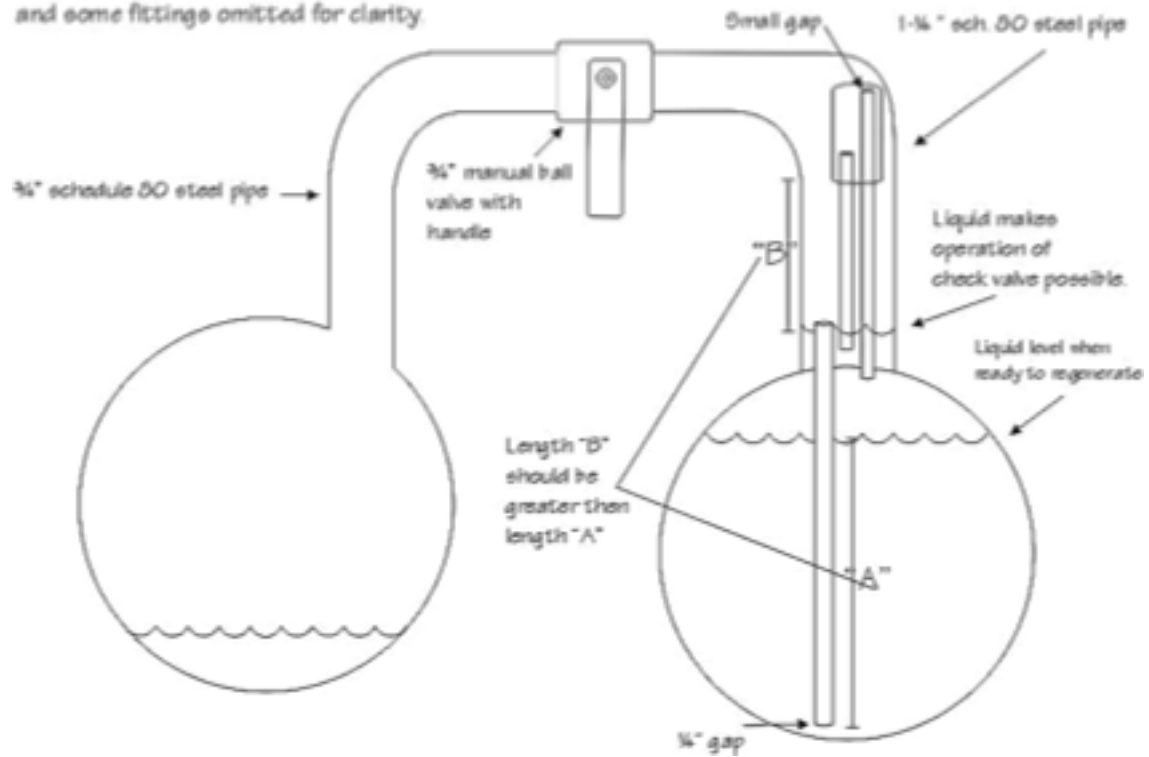
THE
CROSLEY
ICYBALL



The Crosley Radio Corporation
Cincinnati, Ohio, U. S. A.



Sketch of Larry D. Hall's homemade icyball.
 Pressure gauges, service valves, sight glasses
 and some fittings omitted for clarity.



Rural Milk Preservation with the ISAAC Solar Icemaker

Carl Erickson
Solar Ice Company
627 Ridgely Avenue
Annapolis, Maryland 21401



Figure 2. Local people helped install the solar icemakers.



Figure 3. Three units were installed in Kilifi District at Sovimwamri Dairy.



Figure 4. Three more units installed in Kwale District at Kidzo Farmer's Dairy Co-operative.

[ISAAC write-up](#)

Rural Milk Preservation with the ISAAC Solar Icemaker

Carl Erickson
Solar Ice Company
627 Ridgely Avenue
Annapolis, Maryland 21401



Figure 5. On a good solar day, the icemaker makes six blocks. Each block is 2 by 9.5 by 26 inches, weighing 8.3 kg each.



Figure 6. Milk is chilled in an ice-bath milk chiller. Each ISAAC produces enough ice to chill 100 liters per day.

Rural Milk Preservation with the ISAAC Solar Icemaker

Carl Erickson
Solar Ice Company
627 Ridgely Avenue
Annapolis, Maryland 21401



Figure 7. Farmers average 3 liters per day. Mostly they bring milk by bicycle or by foot. The two dairies are serving a total 138 farmers.



Figure 8. Milk, yogurt, and mala are sold from the dairy or distributed to the local community via bicycle.

Rural Milk Preservation with the ISAAC Solar Icemaker

Carl Erickson
Solar Ice Company
627 Ridgely Avenue
Annapolis, Maryland 21401

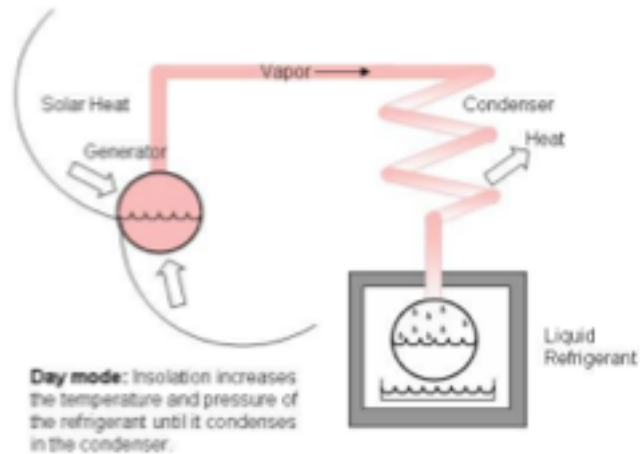


Figure 9. Day Mode Diagram

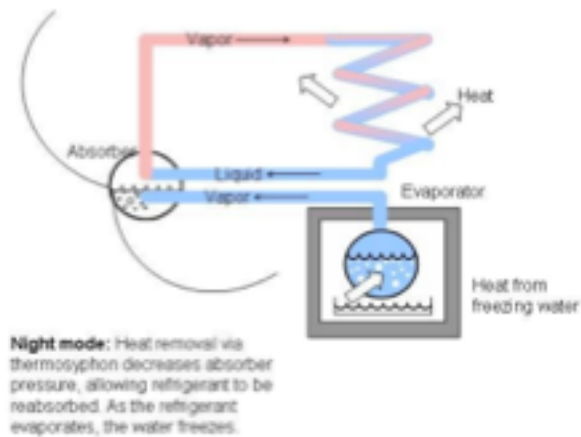


Figure 10. Night Mode Diagram.

Rural Milk Preservation with the ISAAC Solar Icemaker

Carl Erickson
Solar Ice Company
627 Ridgely Avenue
Annapolis, Maryland 21401



Figure 11. The system is operated by manual valves. Operation is routine and easy to do. The valves are operated in the morning and late afternoon. Water to be frozen is put into the evaporator in the afternoon; it is ready to be removed as ice early the next morning.

Issac Ice Maker (<http://www.energy-concepts.com>)

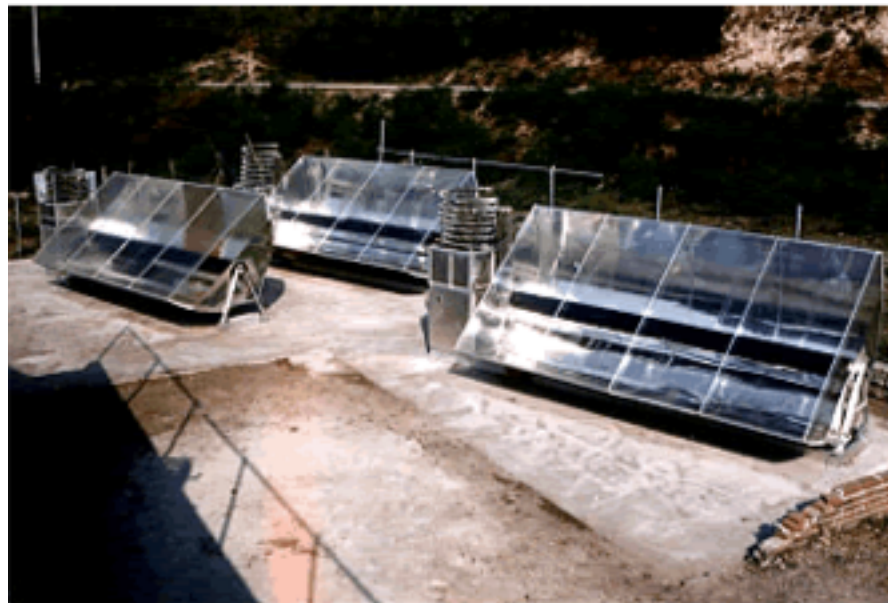
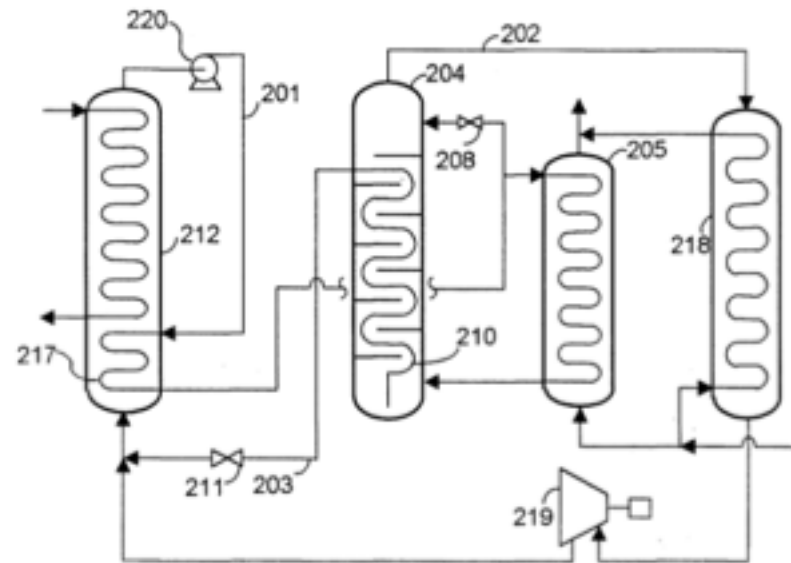
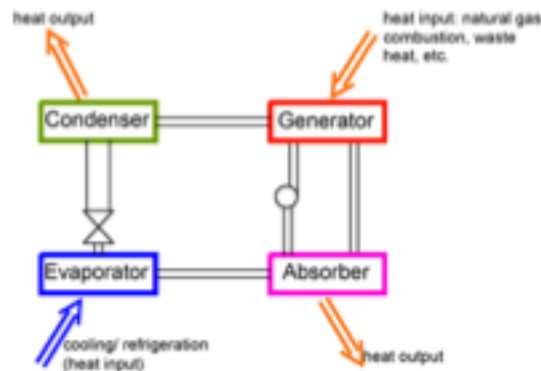


Fig.2



Referring to FIG. 2, weak absorbent solution in conduit **201** is separated into volatile component vapor of at least 95% purity in conduit **202** and strong absorbent liquid in conduit **203** by fractionating apparatus comprised of fractionating column **204** and co-current desorber **205**. Preheater **217** (an "absorption heat exchanger" (AHX) in this example) heats the solution to near saturation temperature before it is divided by divider **208** into a reflux stream for column **204** and a feed stream for desorber **205**. Desorbed mixture from desorber **205** is separated and fractionated in column **204** to bottom liquid and overhead vapor, and the bottom liquid causes additional reboil via heat exchange from GHX **210**. Distilled vapor in conduit **202** is superheated in superheater **218** and work-expanded in expander **219**. The superheating is done over the same approximate temperature range as desorption, i.e., desorber **205** and superheater **218** are heated in parallel, thus maximizing the temperature glide linearity. The expanded vapor is absorbed into the strong absorbent after pressure letdown by valve **211**, in absorber **212**, cooled both by external fluid in the colder section, and by absorbent in AHX **217**. Pump **220** completes the absorbent cycle. The low temperature glide heat can be geothermal liquid, solar heated liquid, combustion exhaust gases, etc. Thus, a simple, economical, and highly efficient absorption power cycle is realized.

<http://www.google.ch/patents/US6715290>



The basic operation of an ammonia-water absorption cycle is as follows. Heat is applied to the generator, which contains a solution of ammonia water, rich in ammonia. The heat causes high pressure ammonia vapor to desorb the solution. Heat can either be from combustion of a fuel such as clean-burning natural gas, or waste heat from engine exhaust, other industrial processes, solar heat, or any other heat source. The high pressure ammonia vapor flows to a condenser, typically cooled by outdoor air. The ammonia vapor condenses into a high pressure liquid, releasing heat which can be used for product heat, such as space heating.

The high pressure ammonia liquid goes through a restriction, to the low pressure side of the cycle. This liquid, at low pressures, boils or evaporates in the evaporator. This provides the cooling or refrigeration product. The low pressure vapor flows to the absorber, which contains a water-rich solution obtained from the generator. This solution absorbs the ammonia while releasing the heat of absorption. This heat can be used as product heat, or for internal heat recovery in other parts of the cycle, thus unloading the burner and increasing cycle efficiency. The solution in the absorber, now once again rich in ammonia, is pumped to the generator, where it is ready to repeat the cycle.

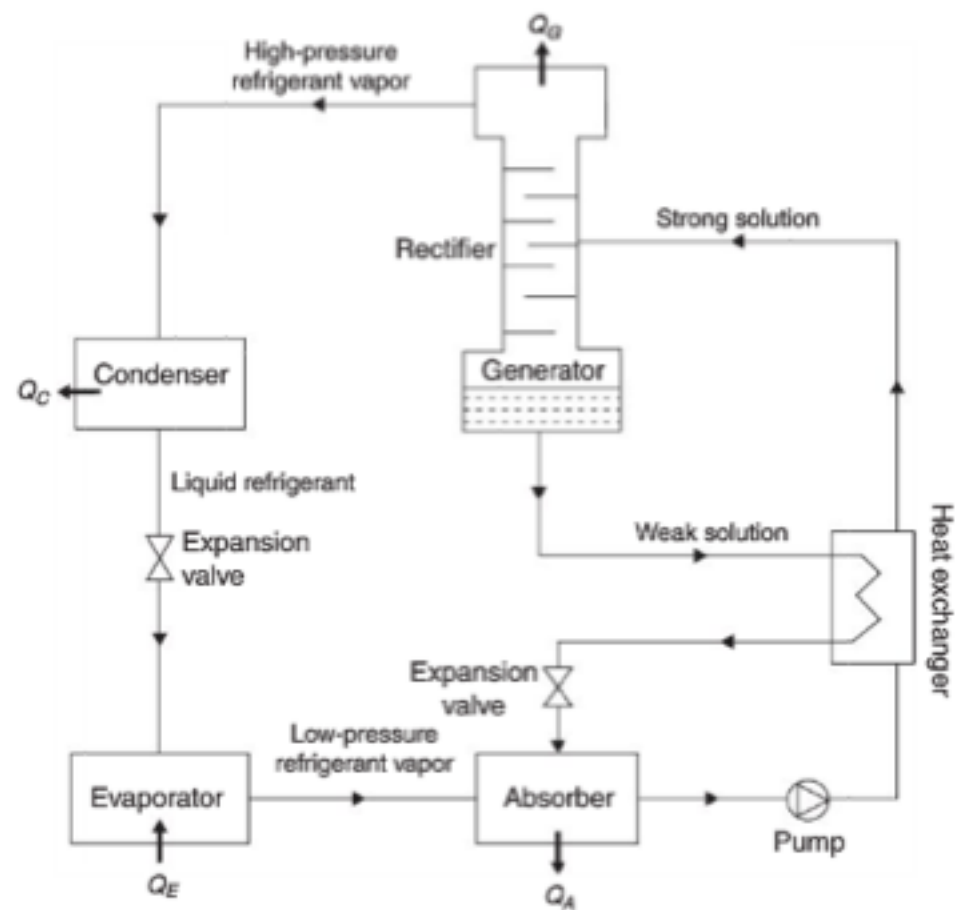


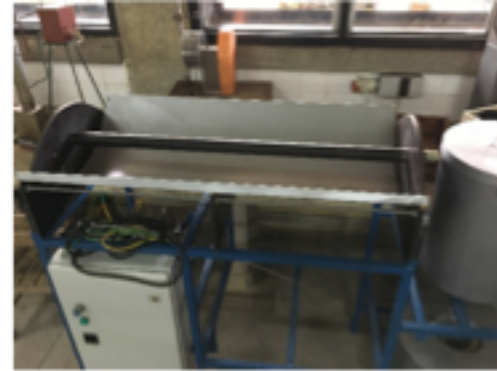
FIGURE 6.27 Schematic of the ammonia-water refrigeration system cycle.

Michael John UDSM



Cuthbert Kimambo, Provost UDSM





LiBr/Water Systems

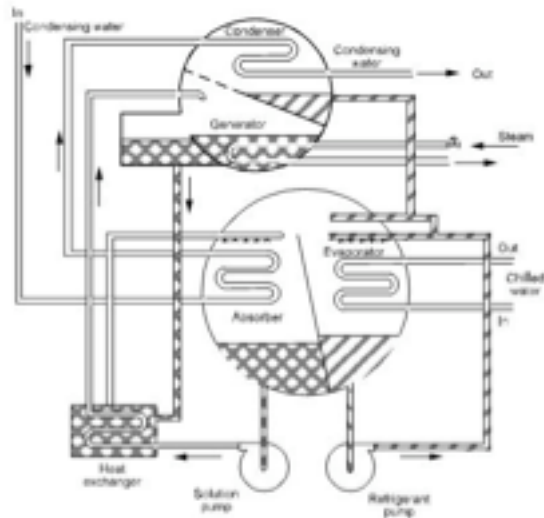


Figure 13.1 Diagram of two-shell lithium bromide cycle water chiller (ASHRAE, 1983).

1) Evaporator: Water as the refrigerant enters the evaporator at a very low pressure and temperature. Since very low pressure is maintained inside the evaporator the water exists in a partial liquid state and partial vapor state. This water refrigerant absorbs the heat from the substance to be chilled and gets fully evaporated. It then enters the absorber.

2) Absorber: A concentrated solution of lithium bromide is available in the absorber. Since water is highly soluble in lithium bromide, solution of water-lithium bromide is formed. This solution is pumped to the generator.

3) Generator: Heat is supplied to the refrigerant water and absorbent lithium bromide solution in the generator from the steam or hot water. The water becomes vaporized and moves to the condenser, where it gets cooled. As water refrigerant moves further in the refrigeration piping and through nozzles, its pressure is reduced along with the temperature. This water refrigerant then enters the evaporator where it produces the cooling effect. This cycle is repeated continuously. Lithium bromide on the other hand, leaves the generator and re-enters the absorber for absorbing water refrigerant.

As seen in the image above, the condenser water is used to cool the water refrigerant in the condenser and the water-Li Br solution in the absorber. Steam is used for heating water-Li Br solution in the generator. To change the capacity of this water-Li Br absorption refrigeration system the concentration of Li Br can be changed.

LiBr/Water
Refrigerator

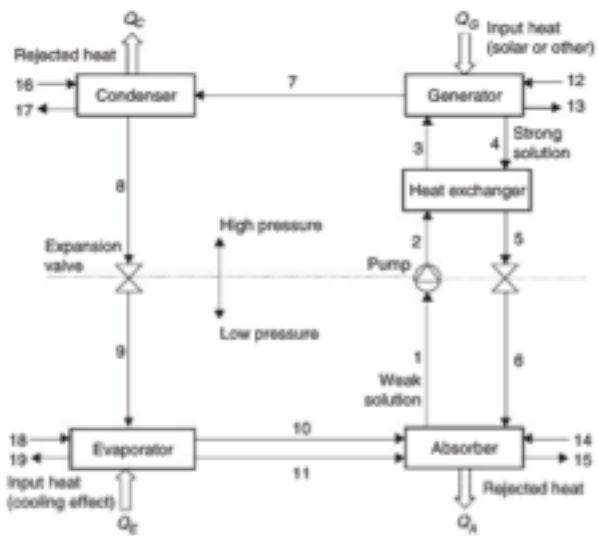


FIGURE 6.23 Schematic diagram of an absorption refrigeration system.

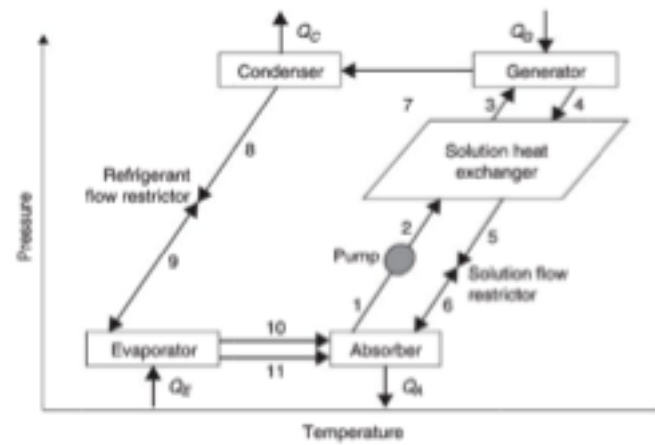


FIGURE 6.24 Pressure-temperature diagram of a single effect, LiBr-water absorption cycle.

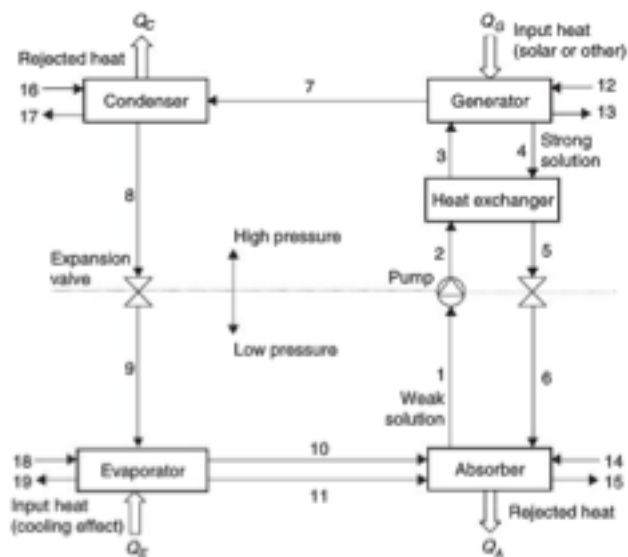


FIGURE 6.23 Schematic diagram of an absorption refrigeration system.

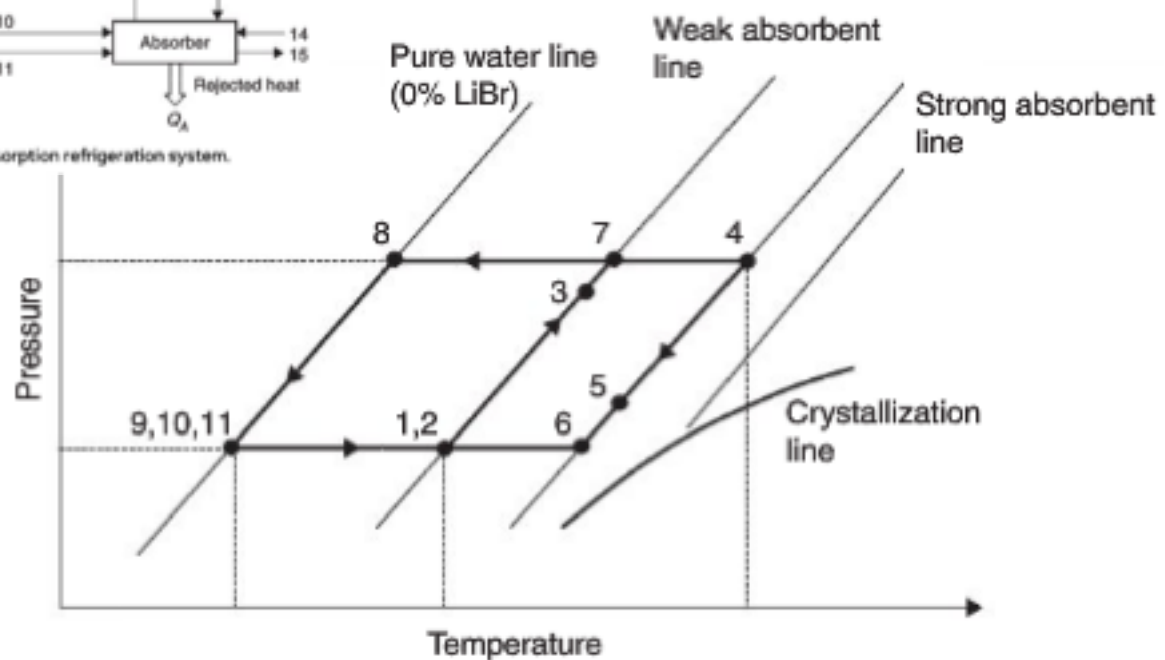
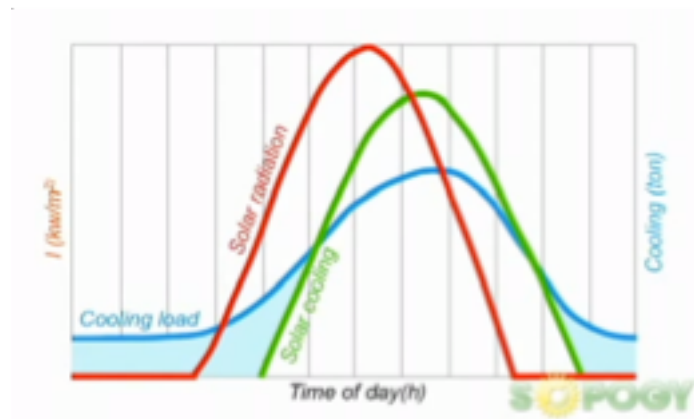
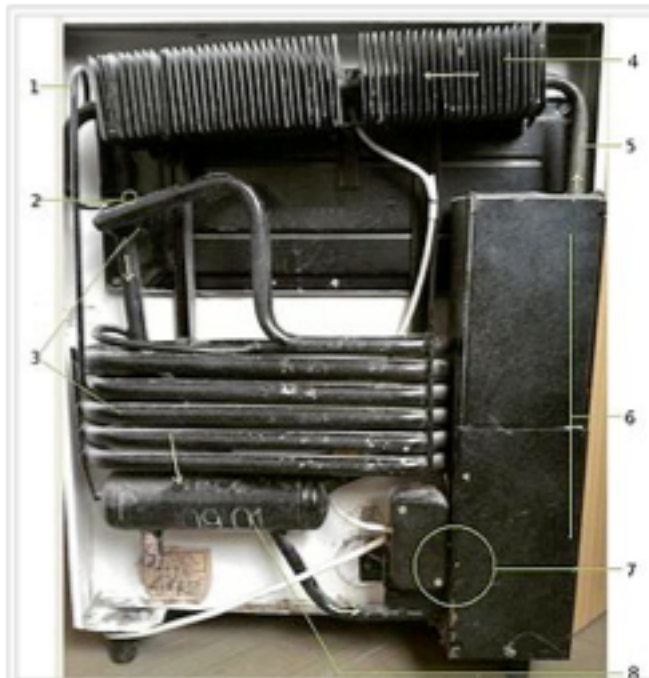


FIGURE 6.25 Duhring chart of the water–lithium bromide absorption cycle.

SOPOGY Solar Air Conditioning LiBr

http://www.youtube.com/watch?v=2usC_Bb1LSw





Labeled photo of a domestic absorption refrigerator.

1. Hydrogen enters the pipe with liquid ammonia
2. Ammonia+hydrogen enter the inner compartment of the refrigerator. Change in partial pressure causes ammonia to evaporate. Energy is being drawn from the surroundings - this causes the cooling effect. Ammonia+hydrogen return from the inner part, ammonia returns back to absorber and dissolves in water. Hydrogen is free to rise upwards
3. Ammonia gas condensation (passive cooling)
4. Hot ammonia (gas)
5. Heat insulation and separation of water from ammonia gas
6. Heat source (electric)
7. Absorber vessel (water + ammonia solution)

How it works: Absorption Refrigerator

https://youtu.be/udeSVyx6_9A

Industrial Solar Refrigerator in Tunisia

<http://www.youtube.com/watch?v=EPbjwv-7fVVI>



[Example of one of these large scale systems](http://www.youtube.com/watch?v=AtMC2MXc_n8) (http://www.youtube.com/watch?v=AtMC2MXc_n8)

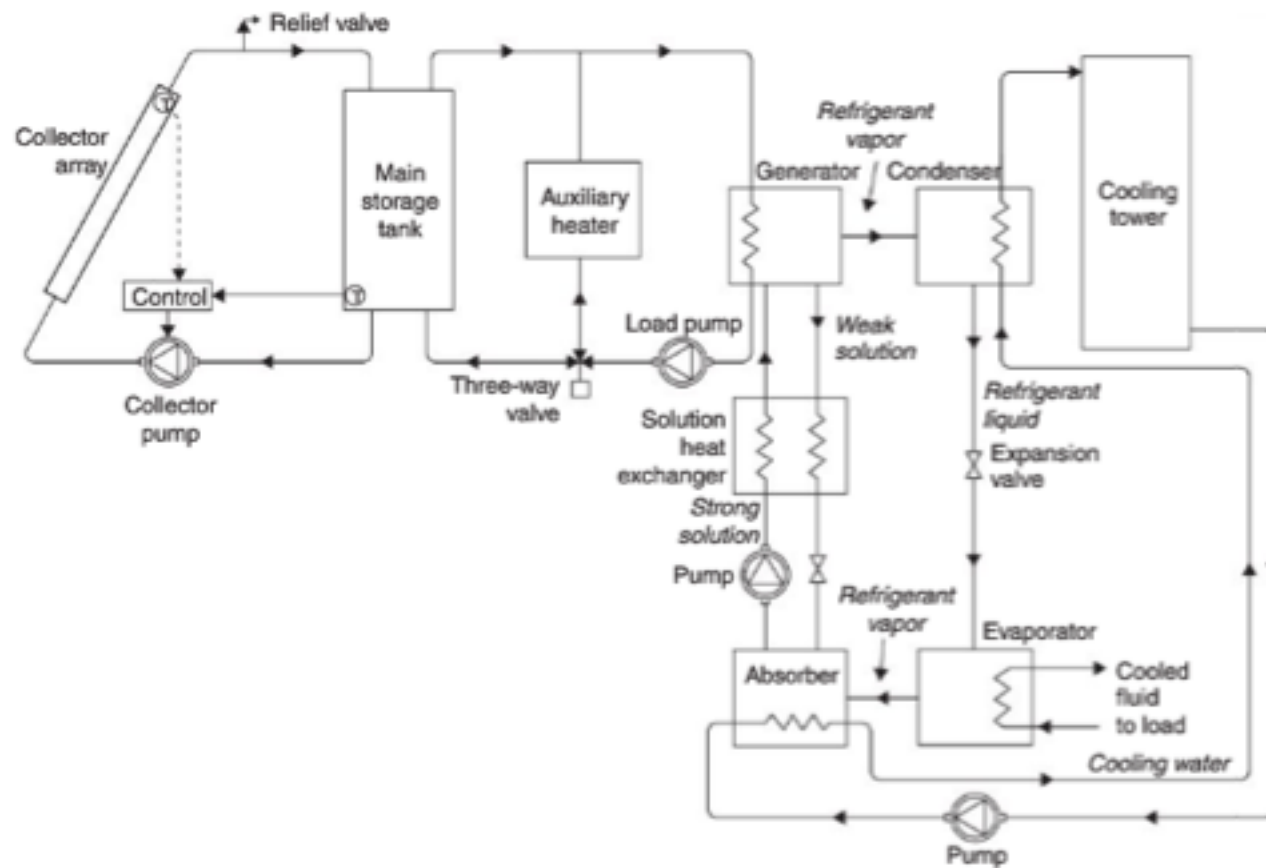
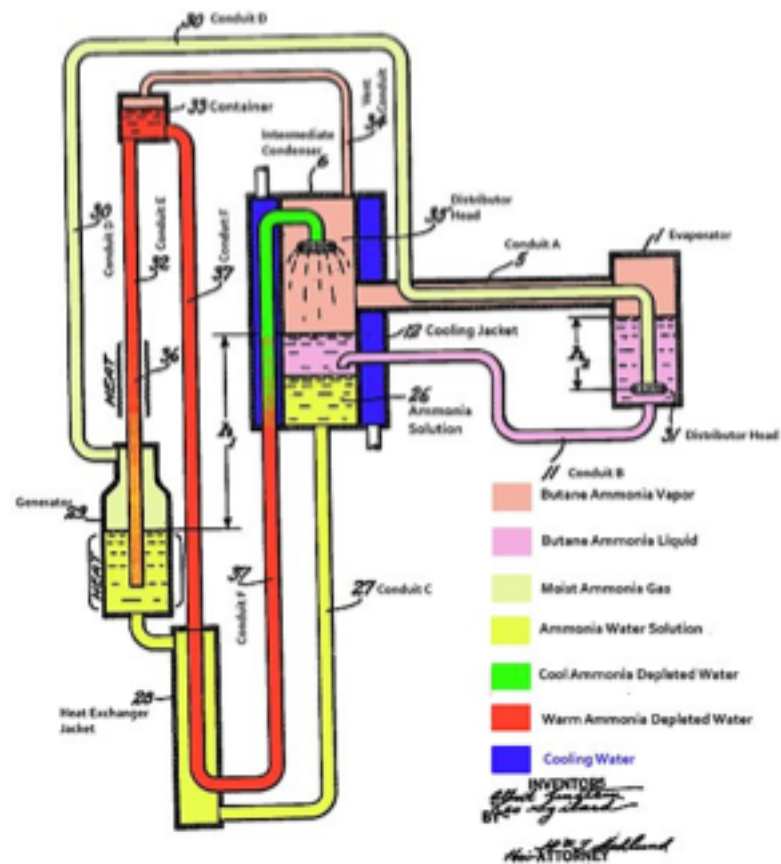


FIGURE 6.28 Schematic diagram of a solar-operated absorption refrigeration system.

Einstein Refrigerator



- You will need**
- Four sheets galvanized steel, 36 ga.
 - 3 in. black iron pipe, 21 ft length
 - 120 sq ft mirror plastic
 - 21 in. stainless steel valves
 - Evaporator tank 14 in. pipe
 - Pressure box (one if scavenged)
 - 4 ft x 8 ft sheet 1/2 in. plywood
 - six 2 x 4 timbers, 10 ft long
 - Miscellaneous 1/2 in. plumbing
 - Two 3 in. caps
 - 11 in. black iron pipe, 21 ft length
 - Four 78 in. long 1 1/2 in. angle iron supports
 - 15 lb ammonia
 - 10 lb calcium chloride
- This design is for an ice-maker which will produce about 10 lb of ice in a single cycle. It uses the evaporation and condensation of ammonia as a refrigerant. If you remember in the explanation above, I mentioned that we needed a refrigerant and an absorber for this type of cooler to work. Well, the ammonia is our refrigerant, and we use a salt—calcium chloride—as the absorber. You might have seen small gas fridges often used in caravans and RV's which can be powered by propane—these also generally use ammonia as a

Figure 5-5 The solar cooler cycle.



Figure 5-4 Solar cooler plumbing details.

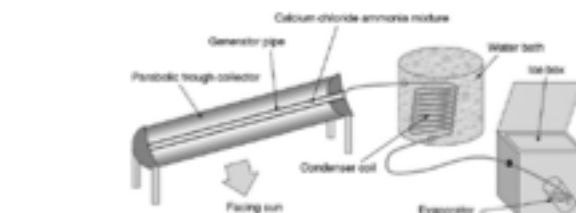


Figure 5-3 Solar cooler layout.

Warning

For the system to operate for long periods of time, the materials used should be resistant to corrosion by ammonia. Steel and stainless steel are ideal in this respect as both are immune to corrosion by ammonia. Another consideration is the pressure under which the system will have to operate.

How does the ice-maker work?

The ice-maker works on a cycle—during the daytime ammonia is evaporated from the pipe at the focal point of the parabolic mirrors. This is because the sun shines on the collector which is painted black to absorb the solar energy—this collector heats up, driving the ammonia from the salt inside.

At night, the salt cools and absorbs the ammonia, as it does this, it sucks it back through the collector. As it evaporates from the storage vessel, it takes heat with it.

http://www.ted.com/talks/adam_grosser_and_his_sustainable_fridge.html

Ted Talk on Developing World Refrigerator





Roll over image to zoom in

BestFire

BestFire Car Mini Fridge Portable Thermoelectric Cooler and Warmer Travel Refrigerator for Home ,Office, Car or Boat AC & DC, White - 12L Capacity

★★★★☆ 6 customer reviews

Price: **\$91.88** ✓prime

Your cost could be \$81.88: Qualified customers get a \$10 bonus on their first reload of \$100 or more.

In Stock.

Want it Saturday, Oct. 14? Order within **8 hrs 21 mins** and choose **Two-Day Shipping** at checkout. [Details](#)

Sold by [BestFire](#) and [Fulfilled by Amazon](#). Gift-wrap available.

- **[BestFire Advantage]** -- A built-in removable shelf for different capacity and demand, which makes this 12L fridge holds up to 4



COWIN

DC12V 68W Solar Refrigerator Freezer 7.4 Cubic. ft, Cowin Solar Powered Fridge, 150 W Solar Pannel, Double Doors, Low Voltage

Be the first to review this item | 15 answered questions

Price: \$2,198.80

Sale: \$1,998.80 & FREE Shipping

You Save: \$200.00 (9%)

Item is eligible: No interest if paid in full within 12 months with the Amazon.com Store Card.

Note: Not eligible for Amazon Prime.

In stock.

Get it as soon as Nov. 6 - 29 when you choose **Standard Shipping** at checkout.

<https://sundanzer.com/product/bfrv15/>

3-5% propylene glycol in water

Solar Powered Medical Refrigerator, 15 liters

Category: [Medical](#)

Pre-Qualified by the World Health Organization (WHO) the SunDanzor BFRV15 provides vaccine storage using solar direct-drive battery-free technology. Designed in conjunction with DDAF and PATH, the BFRV55 solves a very important problem in the vaccine cold chain by eliminating the need for batteries.

Features

- Meets WHO/PQS/E003/RF05-VP.2 standard
- Rated for Hot Zone + 43° C
- Requires no battery or charge controller
- User Independent Freeze Protection
- Complete kit in crate includes PV array, mount, wiring and grounding, user and installation manual, external digital temperature display, lock and key



\$2,495.00

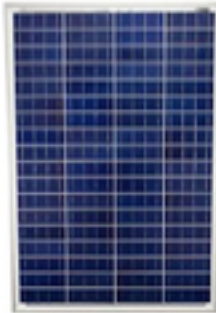
1



Add to cart

2

Amazon's Choice



100 Watts 100W Solar Panel 12V Poly Off Grid Battery Charger for RV - Mighty Max Battery brand product

by Mighty Max Battery

\$99⁹⁵ ✓prime

Get it by **Saturday, Oct 14**

More Buying Choices

\$79.96 (3 used & new offers)

★★★★★ = 41

Product Features

MLS-100WP is 12v 100 watt polycryst solar panel

4



SunDancer

Sundancer Solar-Powered Refrigerator - 8 Cubic Ft., 30in.L x 50in.W x 37in.H

★★★★☆ = 7 customer reviews

Price: **\$1,870.00** + \$159.99 shipping

Get \$40 off instantly: Pay \$1,830.00 upon approval for the Amazon.com Store Card.

Note: Not eligible for Amazon Prime.

Get it as soon as Nov. 17 - Dec. 7 if you choose Standard Shipping at checkout.

Ships from and sold by Casana Solar Industries, Ltd



FlexMax 60-Amp Solar Charge Controller OutBack Power 150V 60A FM60
by OutBack

\$453.00 (5 used & new offers)

★★★★★ = 7



Sponsored

NPP 6V 200 Amp NPS 200Ah AGM Deep Cycle Camper Golf Cart RV Boat Solar Wind Battery

\$219⁹⁹

★★★★★ = 2

Total = \$3500

Solar Cooking



Figure 6-1 A solar cooker being used in the developing world. Image courtesy Tom Sponheim.

Project II: Build a Solar Cooker

You will need

- Sheet of thin MDF
- Sheet of flexible mirror plastic
- Sheet of thin polystyrene
- Veneer panel pins

Tools

- Band saw
- Pin hammer
- Sharp knife/scalpel
- Angle marking gauge

This solar cooker is a very simple project to construct—we will be harnessing the sun's energy from a relatively wide area and concentrating it to a smaller area using mirrors (read more in Chapter 8 about this). The area which we will concentrate it into will be lined with polystyrene to keep in the heat.

Construct a box for your cooker out of MDF. I find small veneer pins to be very useful as they can be hammered neatly into the end grain of thin MDF without splitting the wood. For this application they are perfectly strong enough. When you have finished the box it should look something like Figure 6-6.

Now you need to line the box with polystyrene, this will prevent the heat from escaping. The lined box will look like Figure 6-7.

Now measure the size of the cube inside the lined polystyrene box. You should cut the mirror plastic to this size, and further line the box with it. Duck Tape is more than ideal for making good all of the joints and securing things into place.

We now need to cut the mirrored reflectors. Cut a strip of mirror plastic about two feet wide on the band saw. Now, using an angle marking gauge, mark from the long side of the mirror to the very corner of the mirror, a line which makes an angle of 67°, forming a right-angled triangle in the scrap piece of plastic. You now need to mark out a series of trapeziums along this length of mirror, where

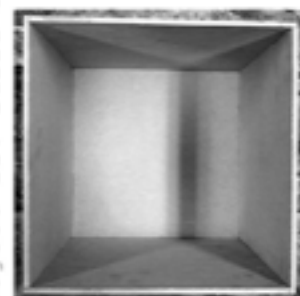


Figure 6-6 The box constructed from MDF.



Figure 6-7 The box lined with polystyrene.

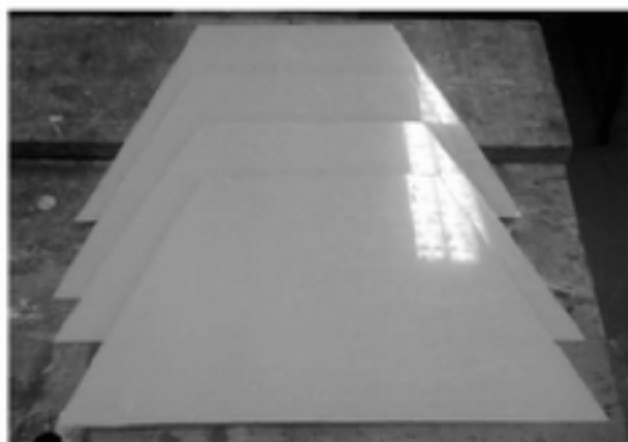


Figure 6-8 *The mirrored reflectors cut ready.*

the shortest side is equal to the length of the inside of the box cooker (Figure 6-8).

Now take the mirrored reflectors, and on the nonreflective side, use Duck Tape to join them together to form the reflector which will sit on the top. Using Duck Tape allows you to make flexible hinges, which allow the reflector to be folded and stored out of the way.



Figure 6-9 *The solar cooker ready and complete.*

When the cooker is finished it will look like Figure 6-9. It is now ready for cooking!

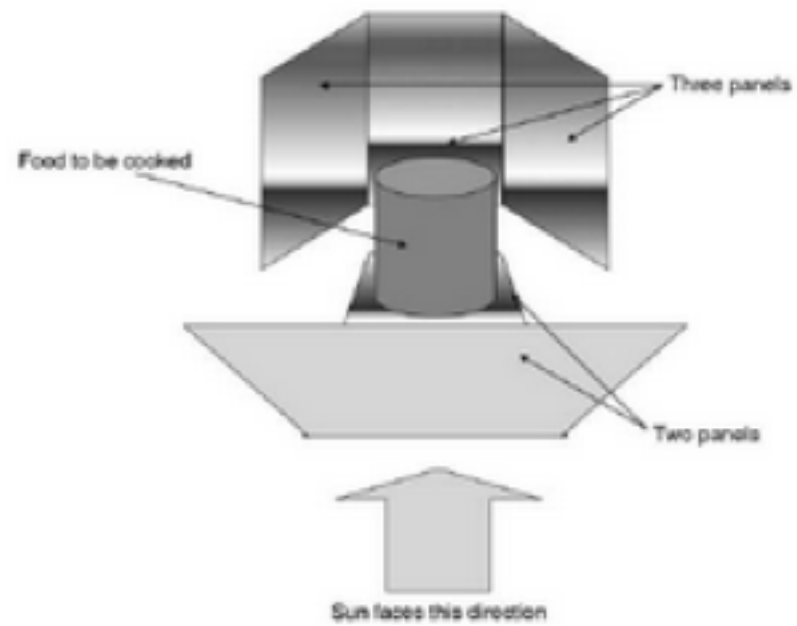


Figure 6-10 *The set-up solar stove.*

[Solar Cookers International](http://video.nationalgeographic.com/video/environment/energy-environment/solar-cooking/) (<http://video.nationalgeographic.com/video/environment/energy-environment/solar-cooking/>)



Advanced Energy Systems

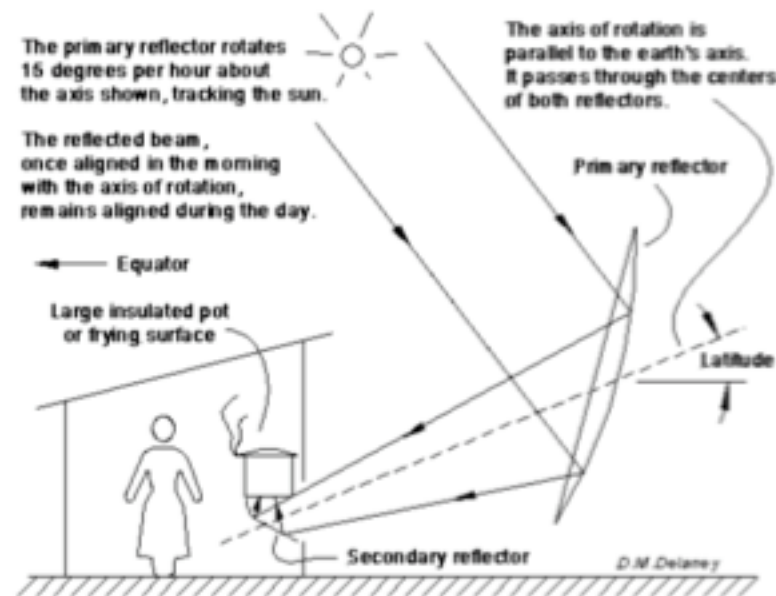


BIG TIME COOKING IN A SMALL PACKAGE - SOELOV 100



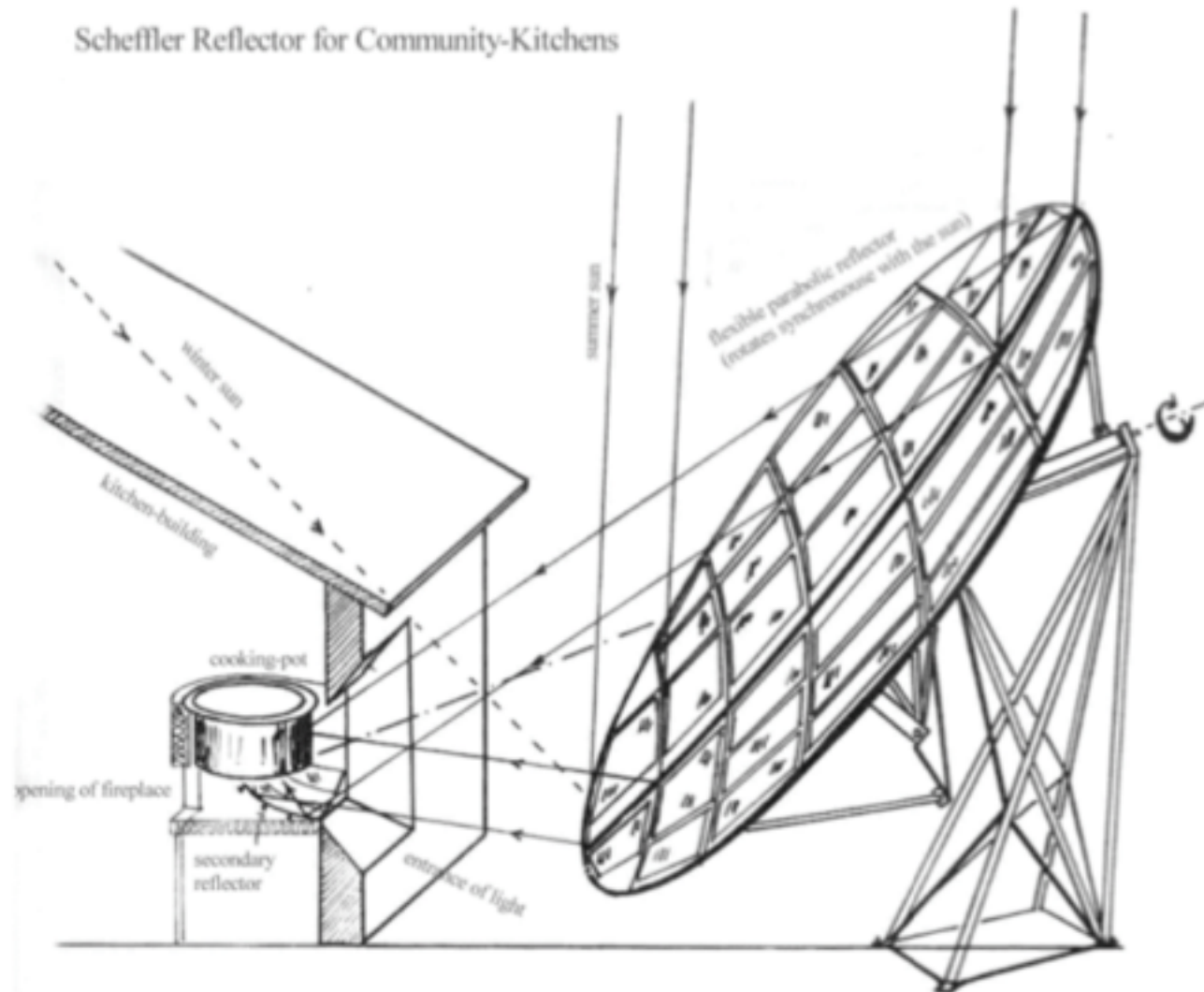


Figure 4: "Rose Bud" Solar Cooker



How a Scheffler reflector used for cooking keeps its focus on the cooking place as the sun moves.

Scheffler Reflector for Community-Kitchens





for [18]

Figure V.i.4 Scheffeler solar
community collector [19]

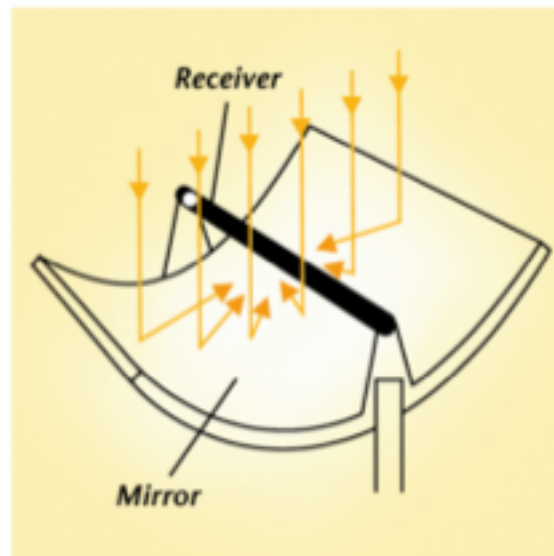


Figure 5: Parabolic Trough Design Overview

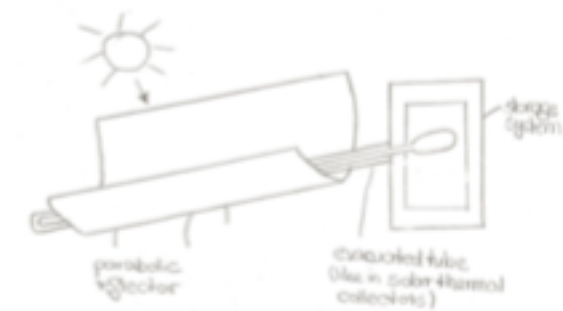


Fig. 2.1: Heat pipe collection system.

Figure V.iv.2: Berkley's Blazing Tube solar collector

To Cook at Night

- Large collection area focused to an insulated heat storage material
1500 W-hr/day delivered to food

- Heat storage materials: NaCl; Bricks; Ceramic tiles; Silicon oil; Water; Sand;
Combinations of heat storage and heat transfer materials

- Insulation

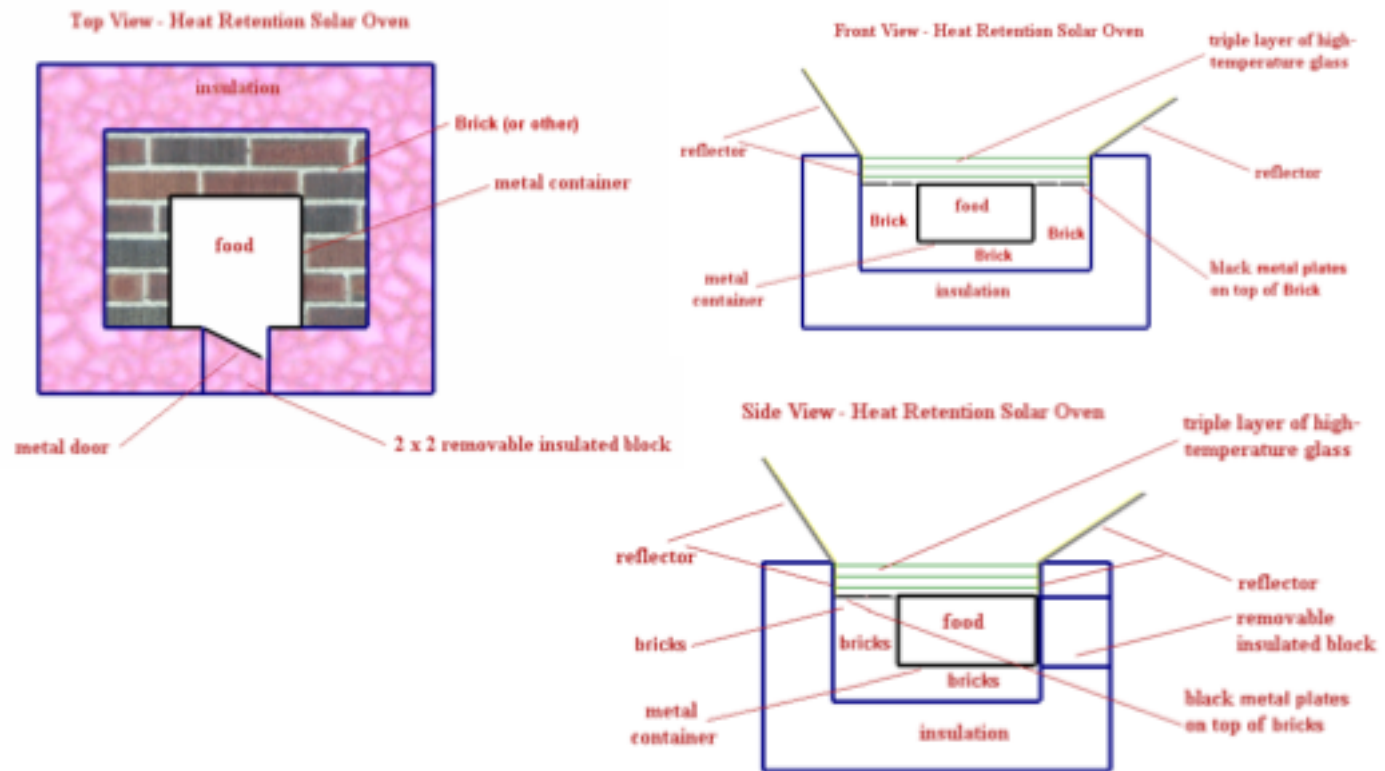
- Ideally you would cook indoors, collect heat outdoors

- Ideally the heat supplied to food would be adjustable

<http://www.webplaces.org/solaroven/design.htm>

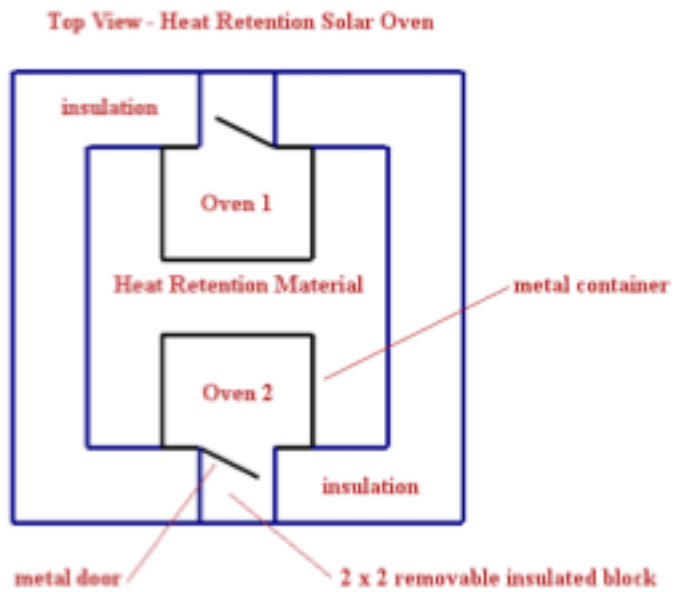
To Cook at Night

<http://www.webplaces.org/solaroven/design.htm>



To Cook at Night

<http://www.webplaces.org/solaroven/design.htm>



To Cook at Night

<http://www.webplaces.org/solaroven/design.htm>

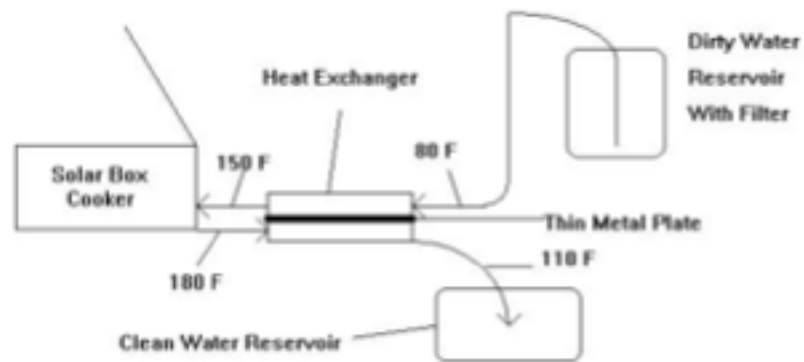


Figure 3: PAX -style water pasteurizer with heat exchanger. Typical temperatures are shown in degrees Fahrenheit.

To Cook at Night

<http://www.webplaces.org/solaroven/design.htm>

New Solar Stove Is Capable of Cooking at Night

Joshua Krause
Ready Nutrition
0 Comments



If there's one technology preppers love, it's solar panels. They're an essential piece of equipment if you're planning on living off the grid, and they're getting cheaper and more efficient every year. But while they're an excellent choice for running lights and electronics, they tend to fall short when it comes to heating (especially cooking).

That's because solar panels only convert roughly 15% of the sun's energy into electricity, and there are additional losses when that electricity is converted back into heat. Heating always requires way more energy than electronics, so that means you're either going to need more solar panels, or find an additional source of energy.

<https://www.engineeringforchange.org/10-solar-cookers-that-work-at-night/>

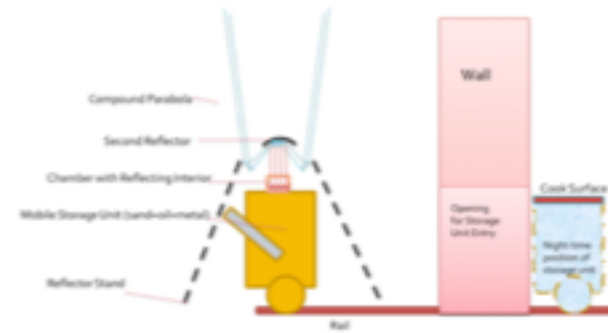
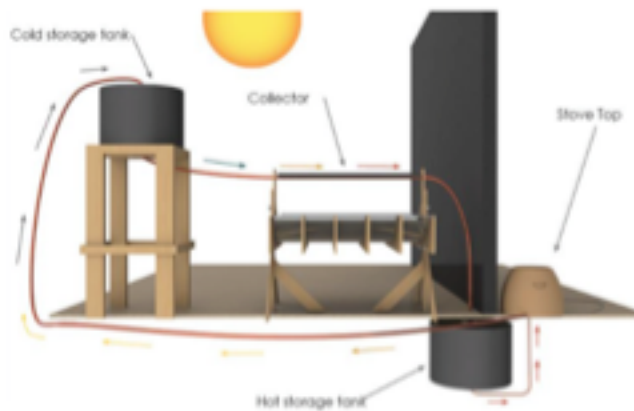


Figure V.Iv.3: Iowa Design Side View

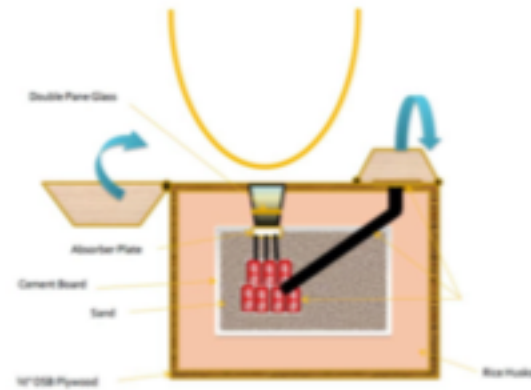


Figure V.Iv.4: Iowa Design Interior View[31]

https://www.engineeringforchange.org/wp-content/uploads/2015/10/solar_final_report.pdf

https://www.engineeringforchange.org/wp-content/uploads/2015/10/medp_final_report_2011.pdf



The iHawk Cooker prototype. Photo courtesy of H. S. Udaykumar

Heat transfer fluid is air
Heat storage material is Sand
Large parabolic collector
Also uses metal heat transfer plate

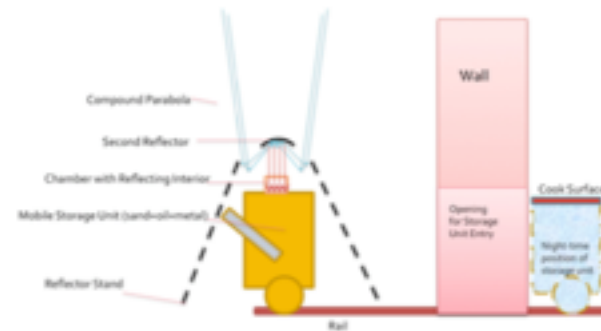


Figure V.iv.3: Iowa Design Side View

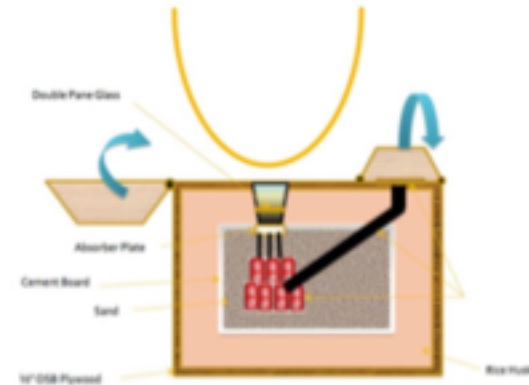


Figure V.iv.4: Iowa Design Interior View[31]

https://www.engineeringforchange.org/wp-content/uploads/2015/10/medp_final_report_2011.pdf



The Brass Cooker prototype. Photo courtesy of H. S. Udaykumar

Transfer to cook indoors by wheels

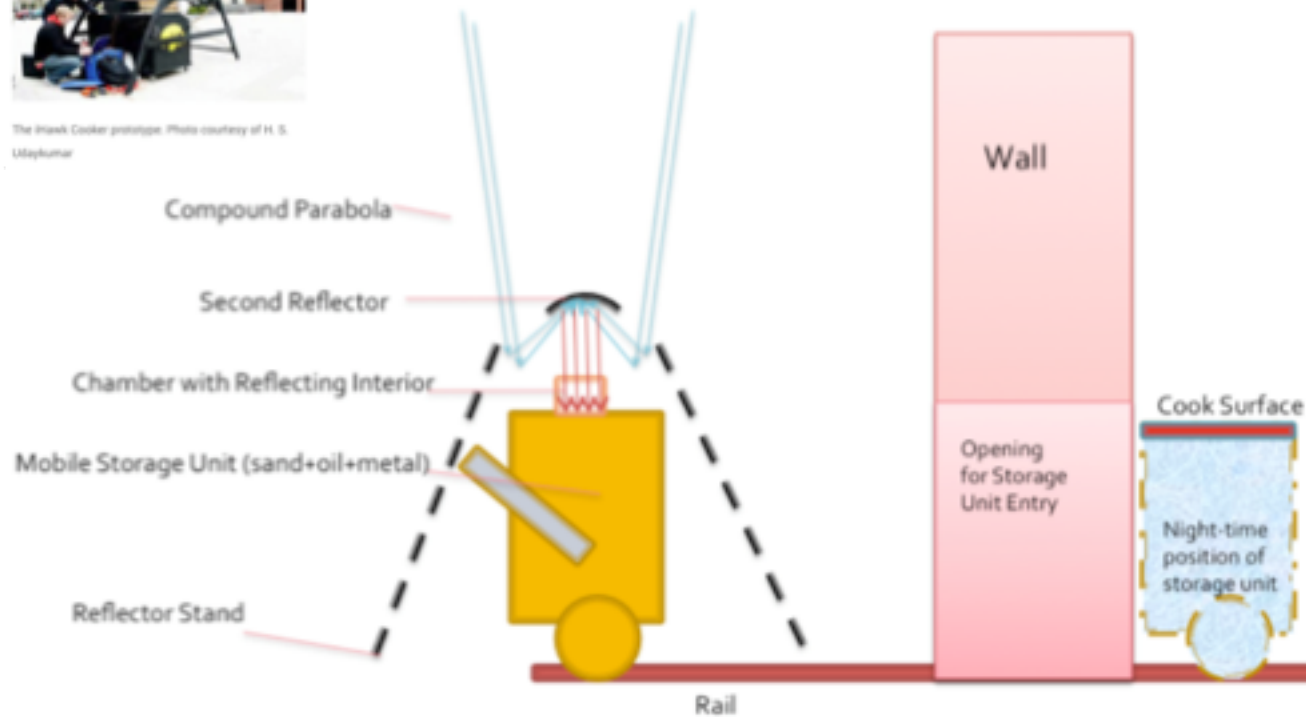


Figure 7: Side View Preliminary Design Overview

https://www.engineeringforchange.org/wp-content/uploads/2015/10/medp_final_report_2011.pdf



The Biomass Cooker prototype. Photo courtesy of H. S. Udaykumar

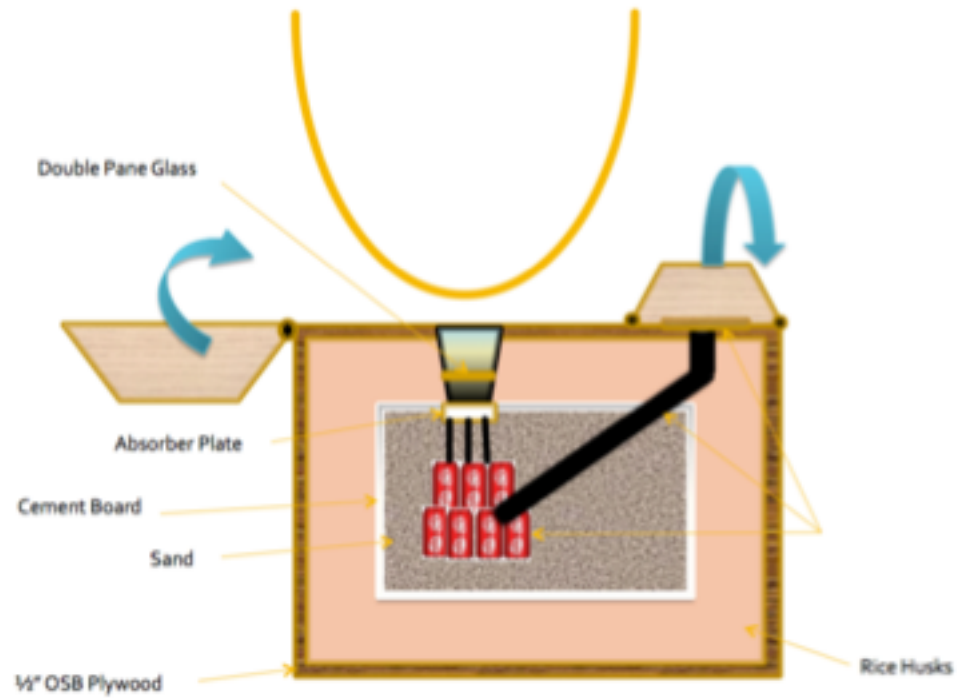


Figure 8: Preliminary Design Interior Overview

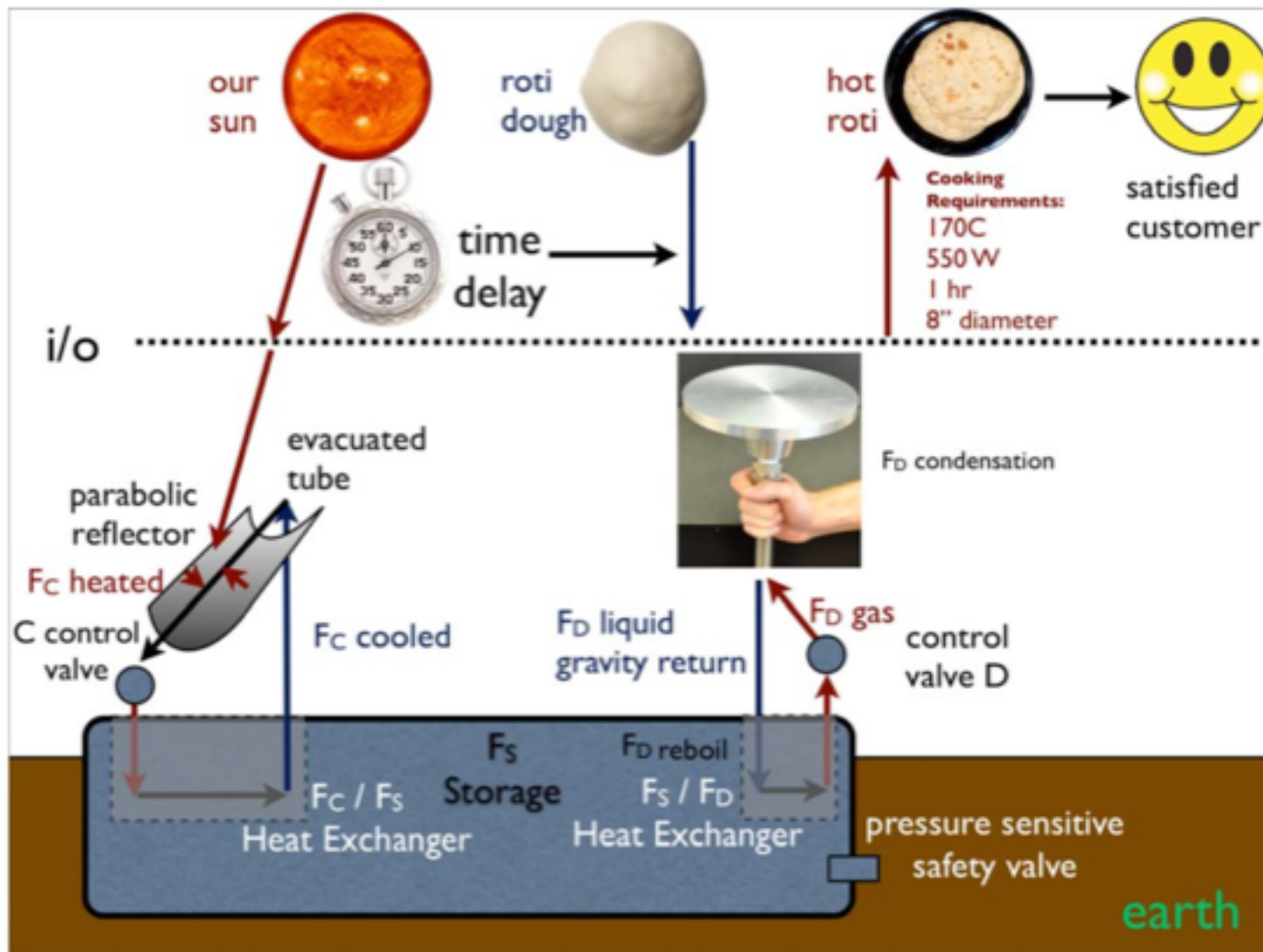
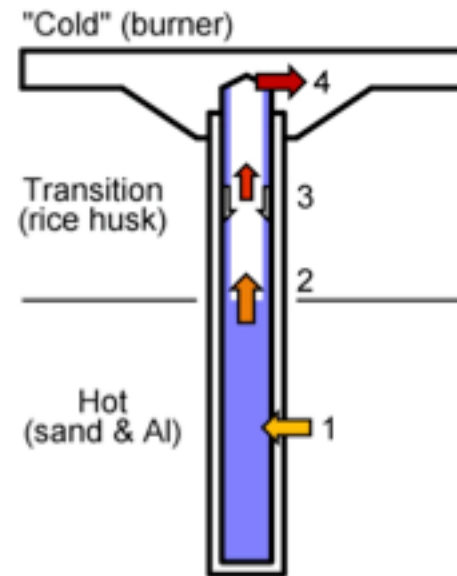
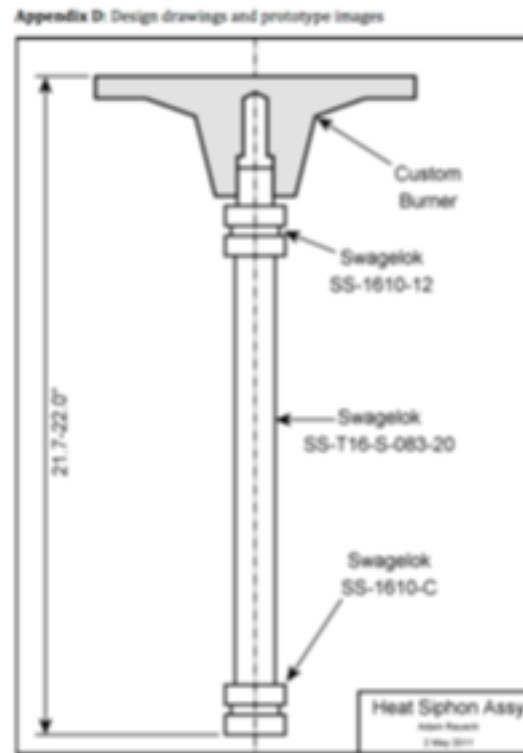


Figure 6.3. All-Fluid Design.

https://www.engineeringforchange.org/wp-content/uploads/2015/10/Solar_Cookstove_Final_Report.pdf



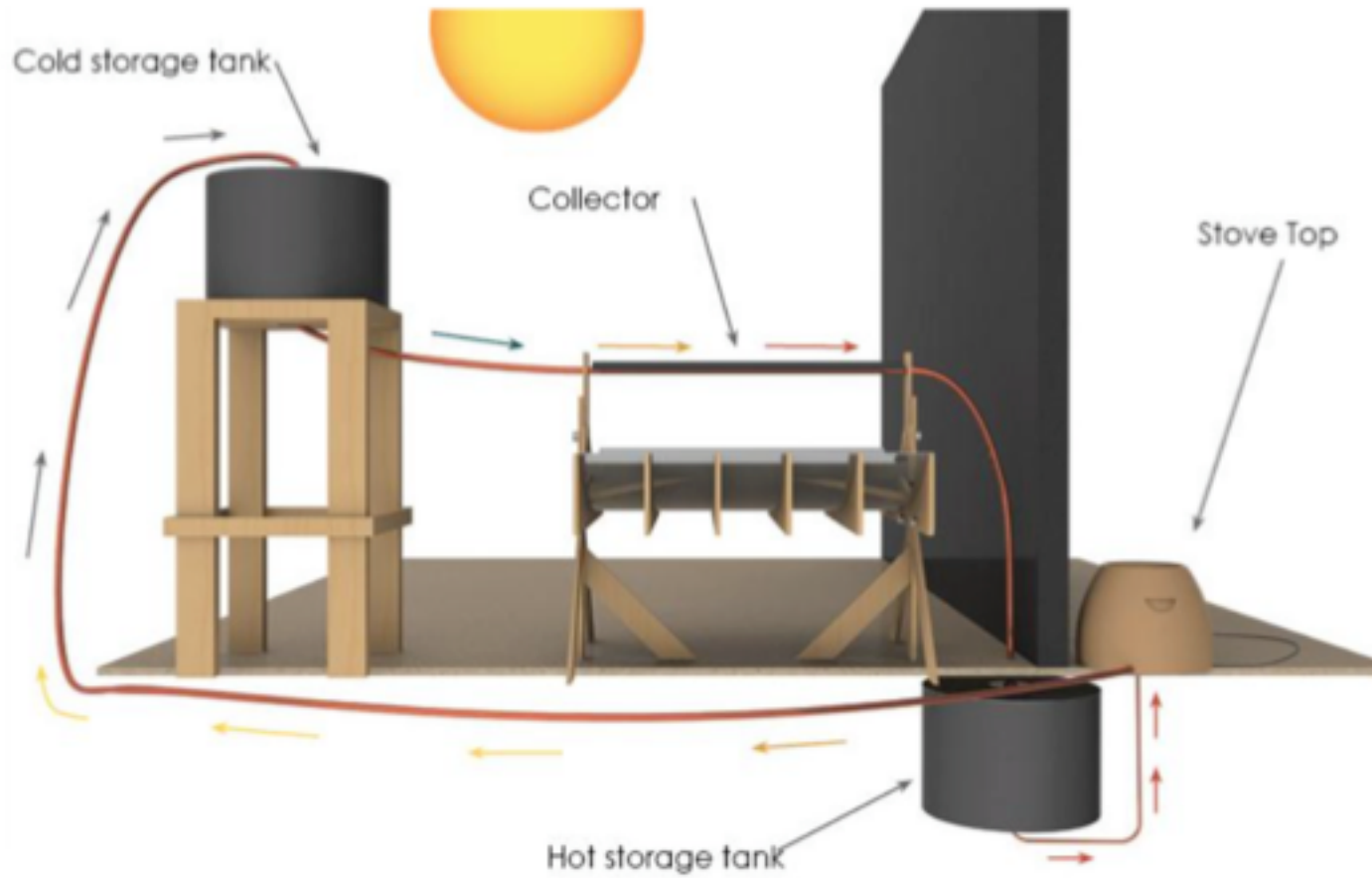


Figure VII.1. Depiction of the entire system

User Interface



Figure VII.iii.1 Schematic of heat output subsystem

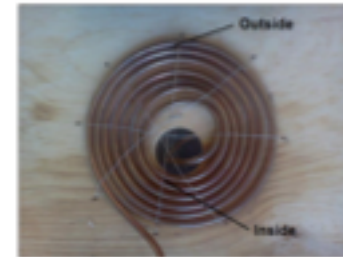


Figure VII.B.4 Thermometer placement inside and outside of the coil.

Figure VII.III.3 Heat dissipation coil experiment setup.

Table VII.III.1 Heat dissipation experimental results

Fluid	Flow Rate (cm ³ /s)	Fluid Inlet Temperature (°C)	Coil Steady State Maximum Temperature (°C)	Coil Steady State Minimum Temperature (°C)
Water	11.6	99.3	93.3	92.8
Olive Oil	6.9	204	187	158
Olive Oil	8.85	204	186	163
Olive Oil	10.4	204	195.6	156

Table IX.L1: Reflective Material Comparison

Material	Reflectivity [55], [56]	Price	Advantages	Disadvantages
Polished Anodized Aluminum	95.00%	\$75/m ²	Highly reflective for the price, lightweight, Durable and easily shaped.	Easily scratched.
Mylar	>98%	\$1.66/m ² [57]	Highly reflective, light, cheap	Not good at standing up to the elements, forms 'bubbles' if glue starts to give, requires a rigid backing
Aluminum Foil	88%	\$0.34/m ² [58]	Cheap and widely available	Not so reflective, corrodes when mixed with acidic juices, structurally weak
Can lids	70-80% (estimate)	Price of canned food	Common material and very cheap	Not very reflective, non-uniform shape is labor intensive to shape and use
Acrylic Mirror	99%	\$67.81/m ² [59]	Very reflective (nearly 100%), nearly unbreakable	Comes in plane, very difficult to fit to parabola as a sheet, More expensive than most but long lifespan
Glass Mirror	99%	\$122.0/m ² [60]	Very reflective	Expensive and comes in rigid plane, breakable and heavy
Astro-foil	76%	\$6.63/m ² [61]	Strong and Reliable	Not reflective Enough

Table IX.I.2: Piping Material Comparison

Piping	Material	Thermal Conductivity, k (W/mK) [63, 64]	Melting Point
Steel	Carbon Steel	54	1425-1540°C [65]
Copper	Copper	401	1084°C [65]
PEX	Cross-linked High-Density polyethylene	0.51	130°C [66]
CPVC	Chlorinated Polyvinyl Chloride	0.14	175°C [67]
PE	Polyethylene	0.38	110°C [66]
PVC	Polyvinyl Chloride	0.19	180°C [66]

Table IX.III.1: Breakdown of origin of materials of the Sol'Ar system.

Material/Component	Here/There?	Tools Needed (In Rajasthan)
Cold and Hot storage Tanks With Fittings	Built and sent from India	Shovel and wood for cold storage tank stand
Collector Shape	Cut and sent from India	None
Reflector: Mylar and Acrylic	Cut and sent from India	For application: Need polystyrene for collector surface, epoxy for application of Mylar and Acrylic panels
Solar collector stand	There	Saw & nails/screws
Piping for system	Piping in India	Expected to be Cut and soldered there. Portable Soldering iron will be sent.
Stovetop and Oven	Piping in India. Clay found there	Clay stoves can be built there individually, copper tubing to be installed by someone else.
Installation and Maintenance	There	Tools and Education provided for team of villagers on an installation and maintenance crew.

https://www.engineeringforchange.org/wp-content/uploads/2015/10/sol_r_final_report.pdf

Table IX.III.2: Material cost breakdown of the entire system

Item	Description	Unit Cost (\$)	Qty.	Total Cost (\$)	Here/There	References
UN-Compliant Steel Roll (Open Roll = 100)	Cold and Hot storage tanks	\$13.69	2	\$27.38	Here	[68]
Copper 90° Tube Fitting	Tube fitting for installation	\$1.12	5	\$5.60	Here	[22]
Anderson Fittings 4213SP1 5/16 Comp X 1/4 Comp Union	Compression Fittings on Tanks	\$3.00	2	\$6.00	Here	[69]
Ward 27-5/4G 3/4 Galv Metal Roof Flange	Pipe fitting (Flange) on Tanks	\$2.00	2	\$4.00	Here	[70]
Owens Corning R-6.7 Unfaced 2 in. x 14 in. x 48 in. Multi Purpose Continuous Roll Insulation	Insulation for collector olive oil heating pipe	\$3.94	2	\$7.88	Here	[71]
Plywood				\$0.00	There	
Olive Oil (13 gallons)	Energy Storage Material	\$20.40	13	\$265.20	There	[72]
Cooper Tools Cordless Soldering Iron, Battery-Powered	Soldering Iron for tube fittings	\$19.99	1	\$19.99	There	[73]
Solder-Joint Copper Tube Fitting for Water, Union, Socket (Female) X Socket (Female) for 3/4" Tube Size	Unions for ease of installation and maintenance	\$5.52	3.00	\$16.56	There	[70]
Mylar Sheeting (1.2m ²)	Reflective backing of solar collector	\$1.66	1.2	\$1.99	Here	[74]
Mirrored Acrylic (1.2m ²)	Reflective Strips for solar collector	\$67.81	1.2	\$81.37	Here	[75]
Copper Pipe (8ft)	Piping system for olive oil	\$1.70	12	\$20.40	There	[70]
Pemates High-Temperature RTV Silicone Gasket Maker 3-Ounce Tube	Sealant Silicone used on Storage Tanks (high temp)	\$6.41	2	\$12.82	Here	[76]
heavy Duty Metal Drum Pump Zinc-Plated 3" L 22 oz/Stroke 35-1/4" L Intake Tube	Shovel and storage tank pump	\$29.51	1	\$29.51	Here	[77]
620 Thick High Impact Styrene Sheet 40" x 72"	Styrene Sheet	\$3.39	1	\$3.39	Here	[78]
Clay	Shovel Base Material	0		\$0.00	There	
Total				\$502.89		

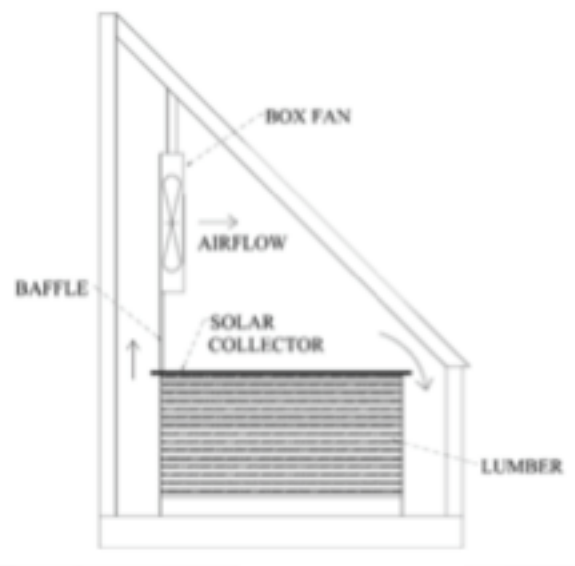
[Go Sun Stove](http://www.kickstarter.com/projects/707808908/gosun-stove-portable-high-efficiency-solar-cooker) (<http://www.kickstarter.com/projects/707808908/gosun-stove-portable-high-efficiency-solar-cooker>)



[Go Sun Fusion](#)

Solar Drying, Solar Kiln
Solar Baking
Solar Charcoal





https://pubs.ext.vt.edu/content/dam/pubs_ext_vt_edu/420/420-030/420-030_pdf.pdf

<http://solarfire.org/GoSol>

Bakers and Peanut Butter Producers Using our Tech in Kenya

In partnership with the NGO World Vision Finland and World Vision Kenya, GoSol has started a pilot project in the Western part of Kenya during Spring 2016. Through World Vision's Weconomy collaboration, GoSol has initiated and supported building of solar concentrators by local artisans using only available materials in Kisumu region, near lake Victoria. A local bakery has been able to reduce operating costs and can now produce and sell more baked goods to local schools and students. A peanut butter workshop in Karemo produces organic peanut butter with renewable energy. They have replaced the use of charcoal with solar thermal energy, which reduces cost and improves the taste of the end product.



2.5 The stages in charcoal formation

As the wood is heated in the retort it passes through definite stages on its way to conversion into charcoal. The formation of charcoal under laboratory conditions has been studied and the following stages in the conversion process have been recognised.

- at 20 to 110°C

The wood absorbs heat as it is dried giving off its moisture as water vapour (steam). The temperature remains at or slightly above 100°C until the wood is bone dry.

- at 110 to 270°C

Final traces of water are given off and the wood starts to decompose giving off some carbon monoxide, carbon dioxide, acetic acid and methanol. Heat is absorbed.

- at 270 to 290°C

This is the point at which exothermic decomposition of the wood starts. Heat is evolved and breakdown continues spontaneously providing the wood is not cooled below this decomposition temperature. Mixed gases and vapours continue to be given off together with some tar.

- at 290 to 400°C

As breakdown of the wood structure continues, the vapours given off comprise the combustible gases carbon monoxide, hydrogen and methane together with carbon dioxide gas and the condensable vapours: water, acetic acid, methanol, acetone, etc. and tars which begin to predominate as the temperature rises.

- at 400 to 500°C

At 400°C the transformation of the wood to charcoal is practically complete. The charcoal at this temperature still contains appreciable amounts of tar, perhaps 30% by weight trapped in the structure. This soft burned charcoal needs further heating to drive off more of the tar and thus raise the fixed carbon content of the charcoal to about 75% which is normal for good quality commercial charcoal.

To drive off this tar the charcoal is subject to further heat inputs to raise its temperature to about 500°C, thus completing the carbonisation stage.

<http://www.fao.org/docrep/x5555e/x5555e03.htm>

about 0.50 USD/kg in Tanzania

Design of semi-static solar concentrator for charcoal production

G. Ramos^{a*} and David Pérez-Márquez^a

a Instituto Politécnico Nacional, CICATA-IPN, Cerro Blanco 141, Col. Colinas del Cimatario, 76090 Querétaro, QRO, México

https://ac.els-cdn.com/S1876610214015501/1-s2.0-S1876610214015501-main.pdf?_tid=2825d798-b4f4-11e7-b1ff-0000aabb0f26&acdnat=1508434819_32b09327f2c7717ac422cf07c1e471ce

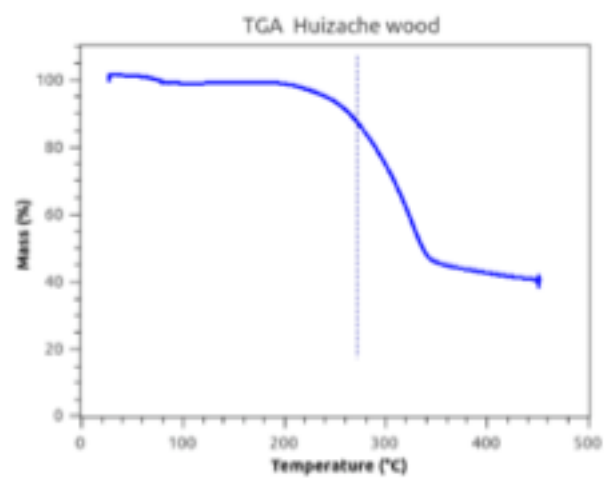


Figure 1. Thermogravimetric analysis of saw dust of *Vachellia farnesiana*.

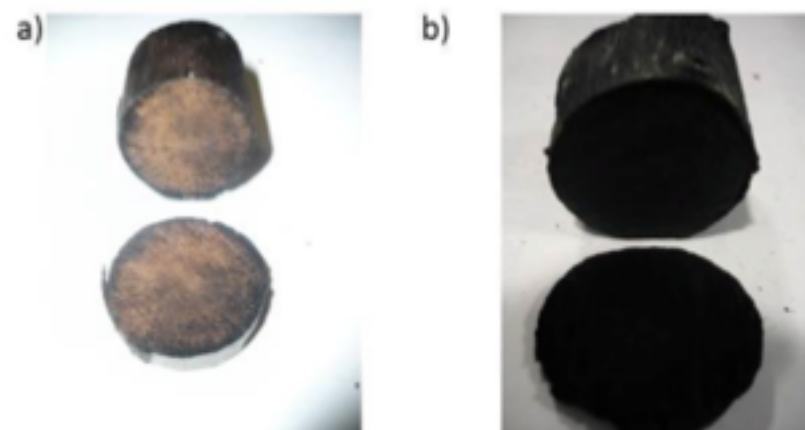


Figure 2. Pictures of Samples a) after 2 hours and b) 6 hours of carbonization at 275°C.



Figure 8 Picture of the prototype in its final version with the evacuated tube receiver.



Figure 9 Picture of the prototype in its final version with the evacuated tube receiver.

http://solarcooking.wikia.com/wiki/Solar_charcoal

The information below was provided by [Helen Dawson](#):

- Pack dry sticks in a metal tin as tightly as possible.
 - Heat wood in the closed tin to approximately 300 °C (572 °F) in a solar cooker.
 - (Somewhere between 200 °C (392 °F) for a couple of hours and 400 °C (752 °F) for half an hour will do).
- There is a good explanation of the overall benefits of turning woodchips or other biomass such as corn cobs to charcoal on the Solar Fire open source web page:

<http://www.solarfire.org/Solar-Charcoal> [®]

- The wood will give off smoke and water vapour below 200 °C (392 °F) unless the lid is very tight.
- Wipe the pyrex bowl lid to remove moisture and soot if its building up on the inside, before it gets too hot to handle.
- Over 200 °C (392 °F) approx. the wood is carbonizing.
- The time and temperature needed to turn the entire contents to charcoal depend on the wood used, the size of the sticks and the solar variables like cloud cover.
- Over 400 °C (752 °F) approx. the wood which is now charcoal ignites and burns to ash.
- Best to leave one set up for a whole day first time, with enough mirror capacity to get over 200 °C (392 °F) for a couple of hours, but less than what it would take to set it alight. Same as with cooking food, you're cooking the wood.
- This is the solar pyrolysis process.
- The wood doesn't create embers, when there is no air flow in the tin, there isn't enough oxygen for it to burn, and under 400 °C (752 °F) it is less likely to ignite.
- Sit an oven thermometer on top of the tin under the pyrex, so you can see the temp climb.
- Remove tin from pyrex bowls in the evening or next morning, when cooled.
- When you open the cooled tin the heat from the sun has turned the sticks to charcoal.
- You can do a drawing with them, and/or the following project.
- Solar cooked charcoal retains the tar in the tin and on the charcoal, making it a bit sticky to handle. As the temperature increases the stickiness decreases. Many Australian seed pods such as gumnuts and banksias, are germinated by fire, so putting them in the solar cooker will result in seedlings in the PET moss garden.
- Charcoal improves the soils ability to grow plants AND captures carbon dioxide, it is carbon sequestration.
- You can help cool the planet by putting charcoal in the soil.
- **Terra preta** owes its name to its very high charcoal content, and was made by adding a mixture of charcoal, bone, and manure to the otherwise relatively infertile Amazonian soil. It is very stable and remains in the soil for thousands of years. Its called Biochar in English speaking countries.



Pyrex bowls trap heat stop wind loss



Solar Cooker two mirrors and aluminium reflector base

200°C water vapor

Above 200 below 400 wood gas

Charcoal in about 2 hours from sticks

Small solar charcoal kiln for cloth


<https://www.youtube.com/watch?v=8Makaciz3Xc>

Fresnel Lens

<https://www.bladesmithsforum.com/index.php?/topic/32781-charcoal-through-solar-power/>

Home Solar Charcoal Distiller

Pollution free charcoal generation - at home!

 [vote for, against] (+12)

Charcoal has been used for fuel for millenia. Produced by heating wood in the absence of oxygen, it is nearly pure carbon, without the water or volatiles that cause smoky,uneven combustion in wood. As currently done, charcoal production is wasteful, burning some charcoal to produce more. Many operations also pollute heavily, discharging the tar and turpentine distilled from the wood into the air.

The Solar Charcoal Distiller allows you to make your own charcoal at home, without bathing your neighbors in clouds of turpentine. The SCD kit (from BUNGCO!) comes with a large plastic Fresnel lens and a special top designed to fit on a standard Weber Kettle. Simply load your Weber with branches and sticks from your neighborhood, put on the special lid, close those air intakes at the bottom, and set up the Fresnel to bathe your grill in concentrated rays (you will want to remove the wooden handles first). Already painted black with heat resistant paint, it will only be a few moments before your kettle glows cheery red and your wood begins to cook. Cook it all day, and then when the sun gets low you will have a kettle full of warm charcoal, ready for grilling dinner!

The special lid is fitted with a metal hose on the top. Place the end of this hose in a bucket of water. Operating on the same principle as a hookah, the steam and volatiles cooked off the wood are cooled and left in the water, for you to use later as you see fit. In our test runs here at BUNGCO we used a lot of eucalyptus and pine - the distilled products proved excellent for treating the bottom of the BUNGCO yacht!

—bungston, Nov 20 2005

Homemade solar charcoal

<http://www.youtube.com/watch?v=8Makaciz3Xc>
Giant lens - check. Backyard - check. [bungston, Jul 01 2013]

http://www.halfbakery.com/idea/Home_20Solar_20Charcoal_20Distiller

Design and Testing of a Solar Torrefaction Unit to Produce Charcoal

Rajaram Swaminathan*, Frans Nelongo Pandeni Nandjembo

Department of Mechanical and marine Engineering, Namibia University of Science and Technology, Windhoek, Namibia

https://file.scirp.org/pdf/JSBS_2016081016170057.pdf

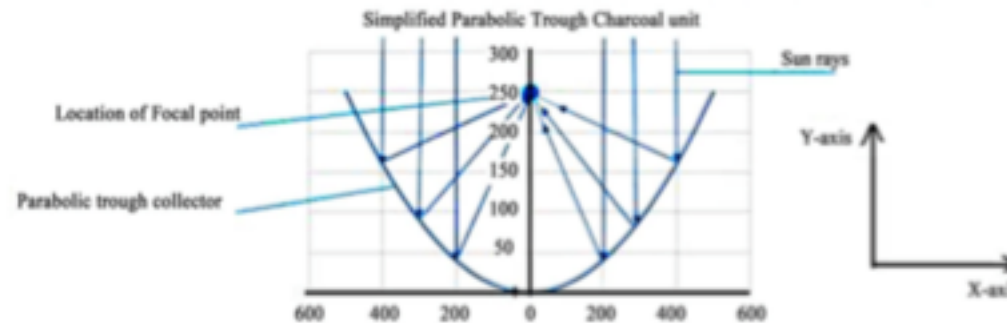


Figure 1. Indicates the focal point in the parabolic trough collector.

Design and Testing of a Solar Torrefaction Unit to Produce Charcoal

Rajaram Swaminathan*, Frans Nelongo Pandeni Nandjembo

Department of Mechanical and marine Engineering, Namibia University of Science and Technology, Windhoek, Namibia

<https://>



Figure 3. The unit.

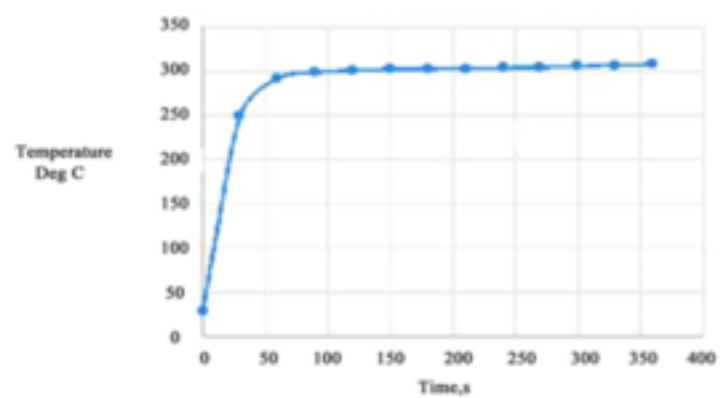


Figure 4. The tube inside temperature recorded at regular interval starting at 9AM.



Figure 5. Shows the different woods tested and the charcoal obtained.

Type of wood	Time for charcoal production (h)	Charcoal yield %
White Oak Charcoal	01; 30	21
Berchemia discolor	01; 30	35
Acacia	01; 30	28

The time taken for these types of wood is the same [Figure 5](#). The yield ranges from 21% - 35% depending on the wood. It is observed that the charcoal of white oak is lighter than those of Acacia and Berchemia.

<http://www.scienceforums.com/topic/6307-solar-parabolic-trough-charcoal-oven/page-18>



Like 0

☆☆☆☆☆

Solar Parabolic Trough Charcoal Oven

Started By Turtle, May 04 2008 02:16 PM

PREV

Page 18 of 19

16

17

18

19

NEXT

Please log in to reply

306 replies to this topic

Nitack

#230 <

Understanding



Members
447 posts

Posted 12 March 2009 - 01:14 PM

So this may be the most lowtech idea of making my frasnol lens actually make charcoal, but I actually think it might work. This came to me as I was testing out a traditional burner and retort (which did not work because I used unseasoned, large pieces of wood). I never got the retort to fire, but I came up with an idea. I am going to take apple sauce jars, the big mothers, punch a few holes in the top, pack them with mulch, and then sit them in the fire to char and eventually give off wood gas to help fuel the burn for my 55 gallon drum.

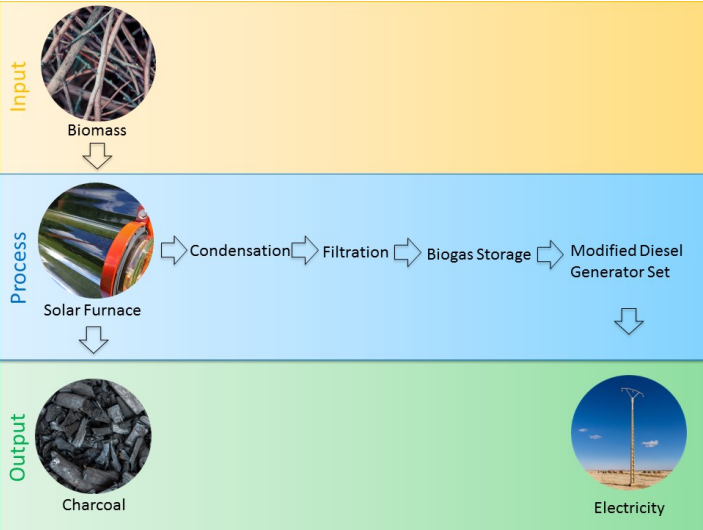
But I was thinking, why wouldn't that also work with a Fresnel directly on the mulch in the jar? As long as I pack the much there should be relatively low oxygen. Additionally, as long as I don't completely focus the beam, it should get hot enough to char everything. The stuff towards the inside may not get hot enough for long enough, but the stuff around the outside should all char right? 💡

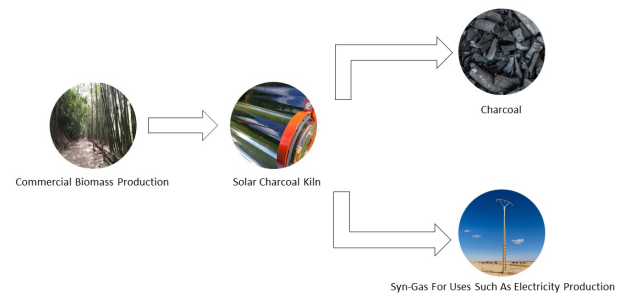
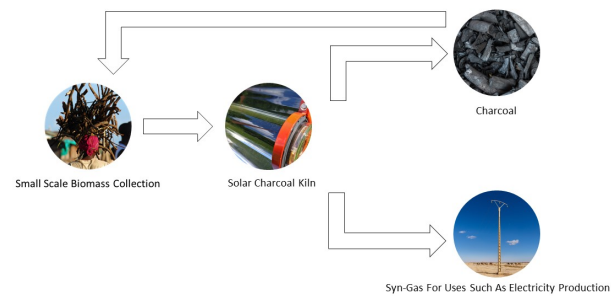
I think the biggest mistake I was making with the Fresnel was to just try to make one point supper hot and then have conduction/convection heat the material. Too damn much heat was being lost to the air around me. Thoughts?

Edit: finding the most long and skinny jar I can should probably help as well.

Turtle

#231 <





Kinetic Study on Bamboo Pyrolysis

Edward L. K. Mui, W. H. Cheung, Vinci K. C. Lee, and Gordon McKay*

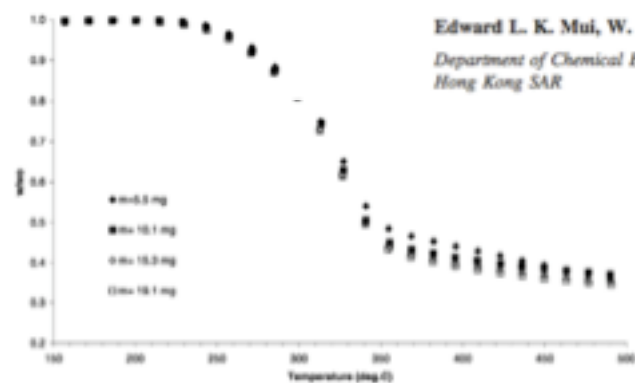
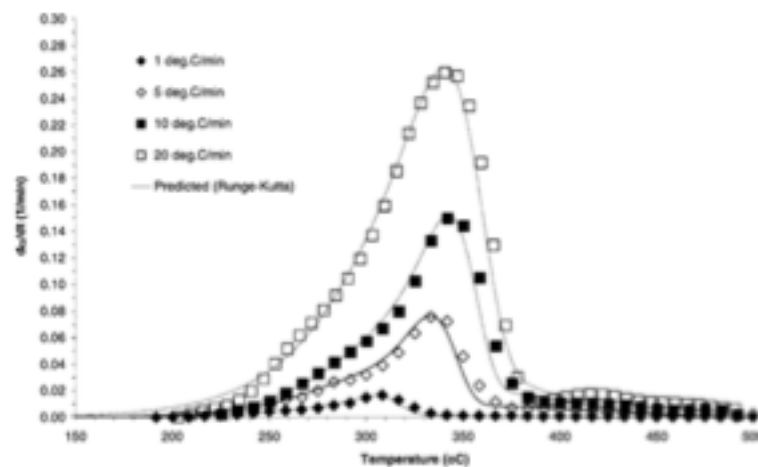
Department of Chemical Engineering, Hong Kong University of Science and Technology, Clear Water Bay, Hong Kong SARFigure 2. Thermograms of raw bamboo (710–500 μm) with different initial mass pyrolyzed under flowing nitrogen at 5 $^{\circ}\text{C}/\text{min}$.

Figure 3. Comparison between experimental data and predicted values (three-component model).



Review

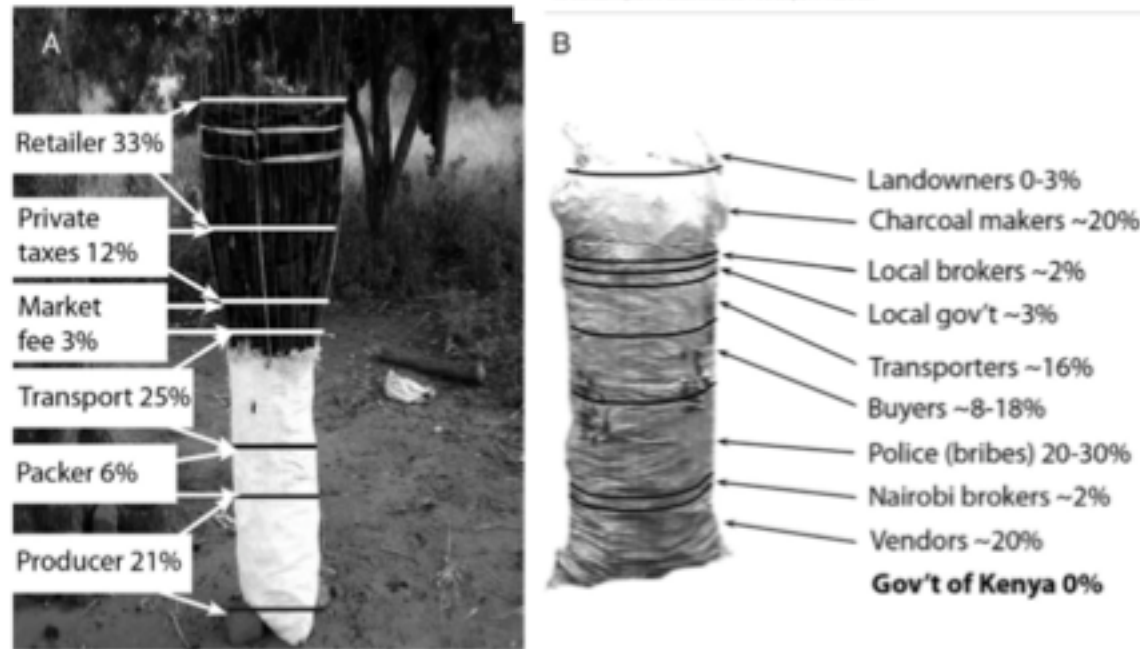
Dispelling common misconceptions to improve attitudes and policy outlook on charcoal in developing countries[☆]Tuyeni H. Mwampamba^{a,*}, Adrián Ghilardi^{b,c}, Klas Sander^d, Kim Jean Chaix^e^a Centro de Investigaciones en Ecosistemas (CIE), Universidad Nacional Autónoma de México, antigua carretera a Pátzcuaro #791, Morelia, Michoacán 58190, México^b Centro de Investigaciones en Geografía Ambiental (CIGA), Universidad Nacional Autónoma de México, antigua carretera a Pátzcuaro #791, Morelia, Michoacán 58190, México^c School of Forestry & Environmental Studies, Yale University, 100 Prospect Street, New Haven, CT 06511, USA^d Woods Hole Center for Coastal Studies, 100 West Main Street, Woods Hole, MA 02543, USA^e The Charcoal Project, 378 Clinton Street, 4th Fl., Brooklyn, NY 11231, USA

Fig. 3. The proportion of revenue captured by different stakeholders along the charcoal commodity chain in Malawi (A) and Kenya (B). Note how in both cases, the government captures none of the charcoal revenue, yet 12% to 30% is captured by “private taxes” otherwise known as bribes. Legalizing and regulating the charcoal sector could divert revenue from bribes to government coffers without affecting charcoal prices for consumers [Rights to reprint from original sources pending].



Opportunities, challenges and way forward for the charcoal briquette industry in Sub-Saharan Africa

Tuyeni H. Mwanpamba ^{a,*}, Matthew Owen ^b, Maurice Pigabe ^c

^a Centre de Développement en Économie, Université National Autonome de Malawi, Campus Main, Angwe Campus, Malawi, No. 475, 121, De l'Académie de la Justice de la République

C.P. 30190, Morija, Malawi

^b Charbon Ltd, P.O. Box 24071, Dar es Salaam, Tanzania

^c BM&F Consulting, Peter-Hofe-Strasse 13, 80509 Frankfurt, Germany

166

T.H. Mwanpamba et al. / Energy for Sustainable Development 17 (2013) 158–170

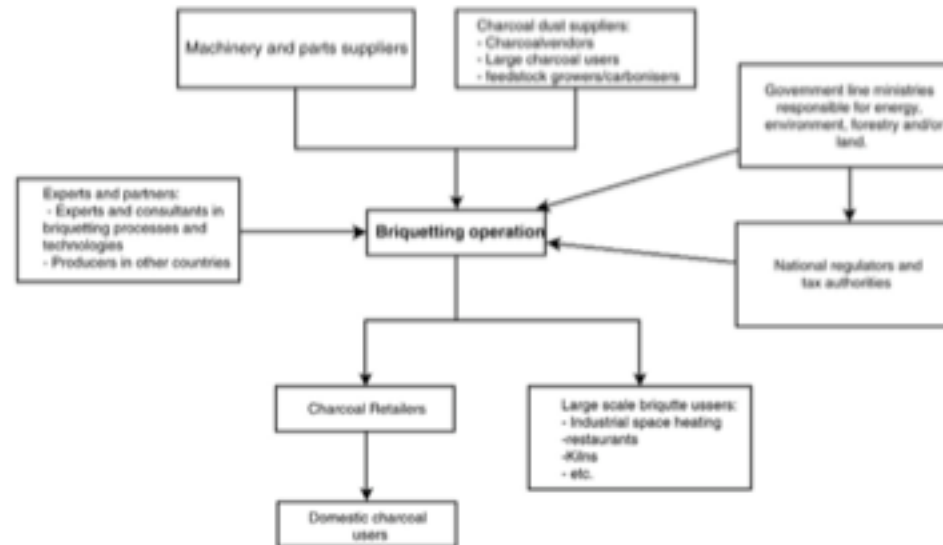


Fig. 3. Stakeholder analysis revealing the central role of the briquetting operation along the briquette value chain. A briquetting operation is influenced by several actors. Through sale of briquettes, however, the briquetting operation ultimately influences briquette retailers and consumers and is highly dependent on the willingness of end-users to accept and incorporate charcoal briquettes into their energy portfolios. Balancing the pressures and requirements of different stakeholders has made briquetting in East Africa a constant juggling of different stakeholder interests.



Fig. 2. Schematic diagram of "carbonize-first" briquetting method, in which raw biomass is carbonized (or salvaged in carbonized form) before it undergoes the densification process to form uniformly shaped briquettes.

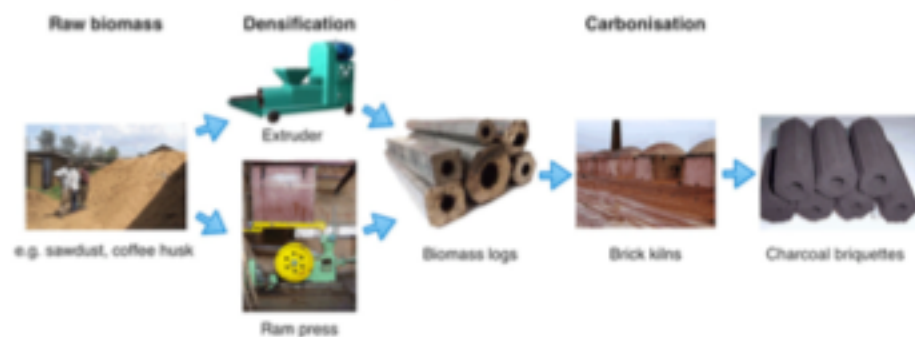


Fig. 3. Schematic diagram of "densify-first" briquetting method, in which raw biomass is densified into uniformly shaped masses before it is carbonized to form charcoal briquettes.

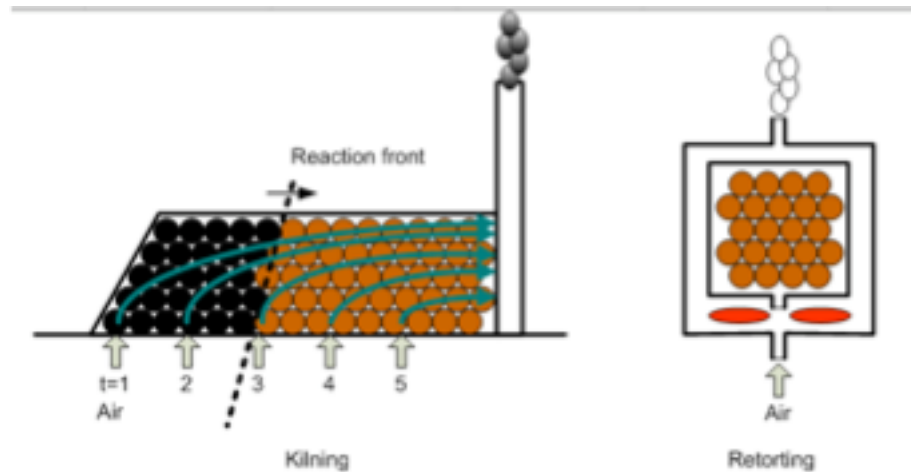
UDSM Charcoal briquette production Dr. Hassan M. Rajabu



Dr Hassan M. Rajabu's briquette equipment UDSM







Kilning: The reaction front moves gradually from one side to the other during interval $1 < t < 5$. Air valves are controlled to provide combustion air at the required place and time. Uncombusted vapour cools down on the heating load. The cooled vapour cannot ignite and gives dirty emissions.

Retorting: Released vapour is combusted to 1/ indirectly provide heat to the load, and 2/ to prevent dirty emissions.

Illustration: © Clean Fuels B.V. www.cleanfuels.nl

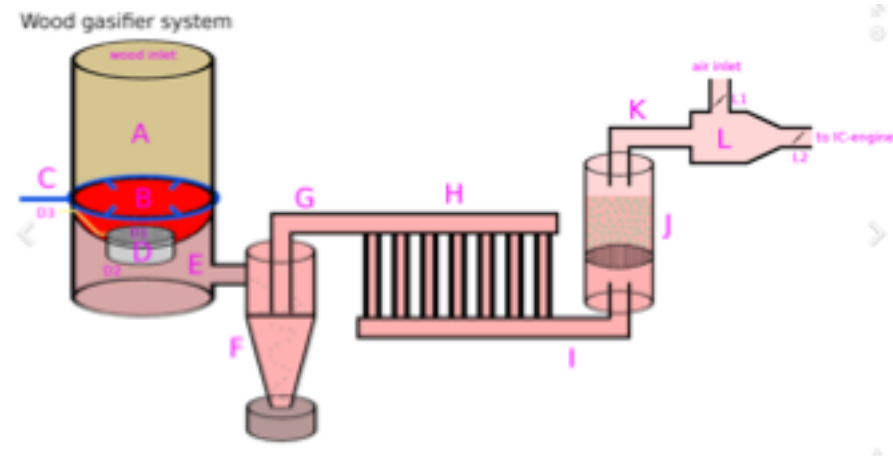
<http://www.cleanfuels.nl/Sitepics/Kilning-principle.png>

Wood Gas Byproduct

<https://www.youtube.com/watch?v=fBYaP5K0AkE>

A retort kiln using wood gas



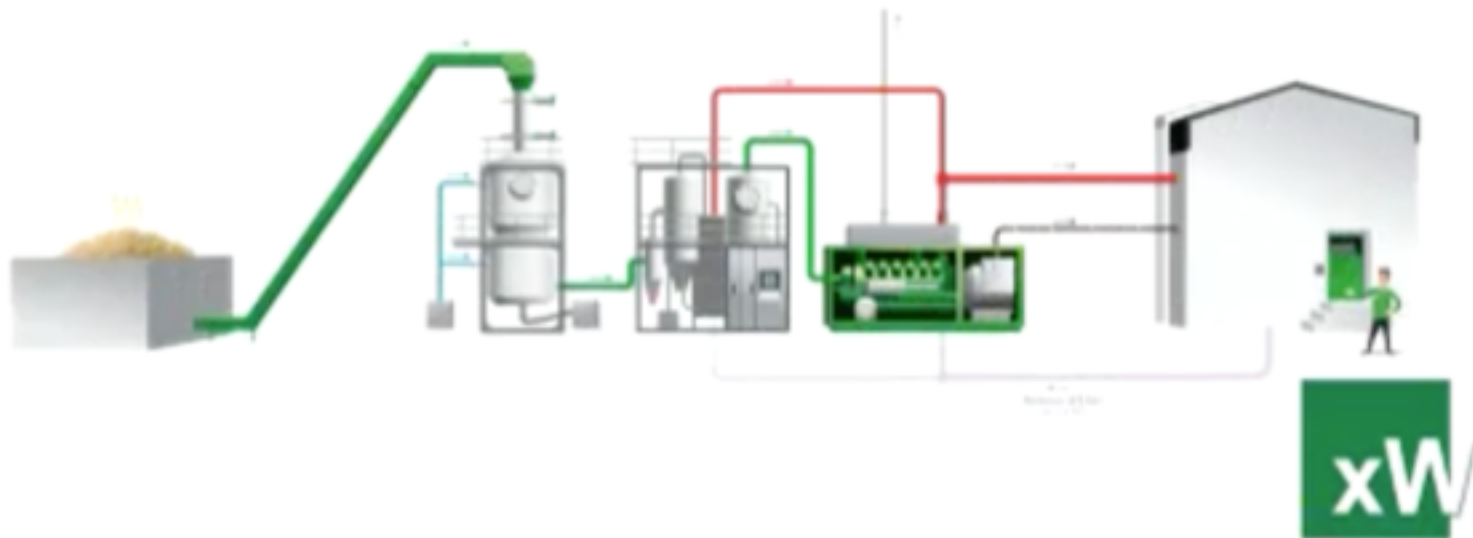


A schematic showing the wood gasifier built by Dick Strawbridge and Jem Stansfield for the show "Planet Mechanics". Parts: A: wood B: fire C: air inlet (air going to 4 nozzles) D: reduction zone; contains charcoal; smoke goes through the accumulated charcoal and reacts with it. H_2O and CO_2 becomes H_2 and CO D1: top grating (movable) D2: lower grating (not movable) D3: handle: used to stir up the wood to provide evenly high temperature over top grating E: smoke F: single-cyclone separator (coarse filter) G: partially filtered smoke H: radiator (reduces heat of gas and hence condenses the gas, making it more flammable/potent) I: cooled, partially filtered smoke J: fine filter (consisting of clay balls on top of a grating) K: wood gas (= fully filtered, cooled smoke) L: air/gas mixer (replaces IC engine carburetor) L1: air inlet valve (operated via handle mounted to gear stick) L2: choke valve

https://en.wikipedia.org/wiki/Wood_gas#/media/File:Planet_Mechanics_wood_gasifier.png

Biomass/Syngas/Wood Gas

[Moderate Scale Plant](http://www.dailymotion.com/video/xit4aj_xylowatt-biomass-gasification-renewable-syngas_tech) (http://www.dailymotion.com/video/xit4aj_xylowatt-biomass-gasification-renewable-syngas_tech)



Home » A charcoal production plant that also generates heat and electricity from the by-product gas

A charcoal production plant that also generates heat and electricity from the by-product gas

Author: Heggie

Post date: Saturday, November 8, 2008 - 8:02am

Tom Miles

[Log in to post comments](#)

A charcoal production plant that also generates heat and electricity from the by-product gas
Biofuel Energy Systems, Sustainable Energy Ltd., UK, 2004



In 2004 Biofuel Energy Systems Ltd. developed a plant for charcoal production, which uses the gases given off during production to drive a gas turbine, generating heat and electricity. The electricity generated can be used on site (especially useful in remote areas with no electrical grid connection) or sold back to the grid for additional profit.

Conventional charcoal production is very inefficient and wastes half of the energy within the wood. Biofuel Energy Systems' unique plant, however, uses 90% of the wood's energy and uses a totally clean, emission-free process. See the diagram on the Biofuel Energy Systems website that shows the steps involved in simplified terms. This represents a huge advancement in the efficiency and cleanliness of charcoal production.

« 1 2 3 4 5 6 7 8 9 10 11 12 »

<https://terrapreta.bioenergylists.org/biofuelenergysystems>

Cogenerating electricity from charcoaling: A promising new advanced technology[☆]Rogério Carneiro de Miranda^{a,*}, Rob Ballis^b, Adriana de Oliveira Vilela^c^a Proleto, Brazil^b School of Forestry and Environment, Yale University, USA^c Alcoa Industrial, SA, Brazil

172

R.C. de Miranda et al. / Energy for Susta

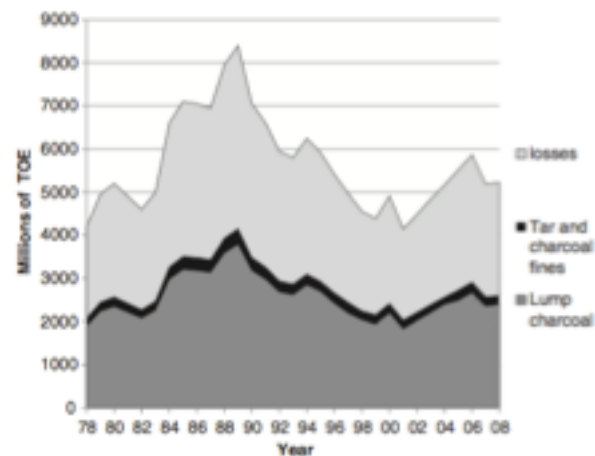


Fig. 1. Total energy breakdown from charcoal production in Minas Gerais, Brazil from 1978 to 2008, as lump charcoal, other sub-products (charcoal fines and tar), and losses (smoke). (Source: BEEMG, 2009).

Table 1

Characteristic temperatures, carbonization and gas content in each phase of wood pyrolysis.

Parameters	Drying	Pre-carbonization	Beginning of tars phase	Tars phase
Process temperature (°C)	150–200	200–280	280–380	380–500
Carbon content of charcoal (%) ^a	60	68	78	84
NCG (%) ^b				
CO ₂	68	66.5	35.5	31.5
CO	30	30	20.5	12.3
H ₂	–	0.2	6.5	7.5
Hydrocarbons (mainly CH ₄)	2	3.3	37.5	48.7
NCG heat value (kcal/Nm ³) ^c	1100	1210	3920	4780

^a (%) percentage based on dry mass of charcoal.

^b (%) percentage based on dry mass of non-condensable gases (NCG).

^c Based on NCG mass balance (Brito and Barrichelo, 1981).



Fig. 2. View of the Barreiro power plant boiler (left photo) and detail view of the fuel feeding system in the boiler (right photo), with the central hole (open tube) used for wood tar injection, and the main round tube used for steel furnace gas injection.

2009 the Minas Gerais state power utility (CEMIG)² operated a 15 MW power plant designed to use tar as complementary fuel to hot exhaust gases from steel furnaces (Fig. 2). The plant used tar at the rate of 500 kg per hour. It required a tar filter and a heater to reduce the viscosity of the tar before it was injected under pressure inside the boiler. However after 2009 CEMIG stopped using tar because the supplier found a more lucrative market (Miranda, 2012).

Brazil

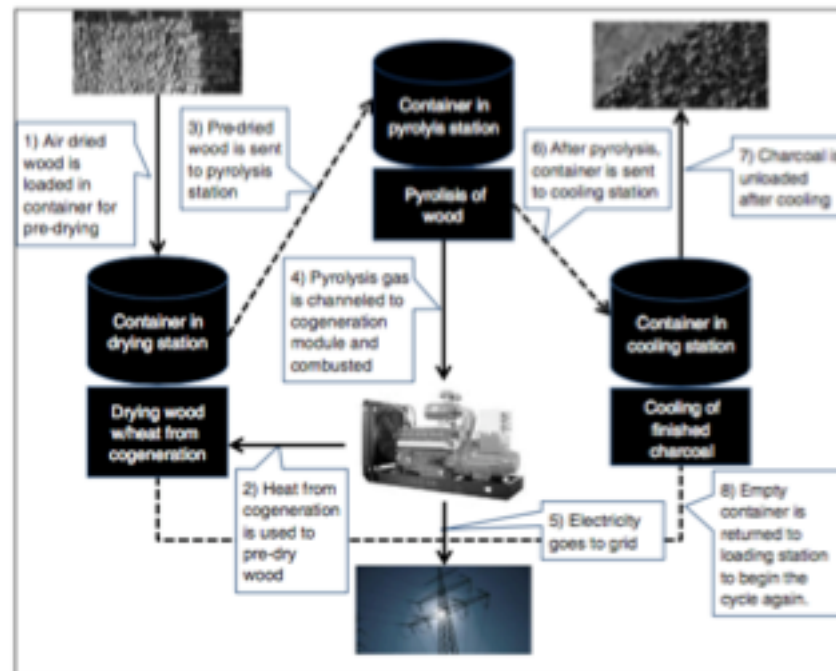


Fig. 3. An example of a charcoal cogeneration cycle utilizing waste heat for pre-drying.

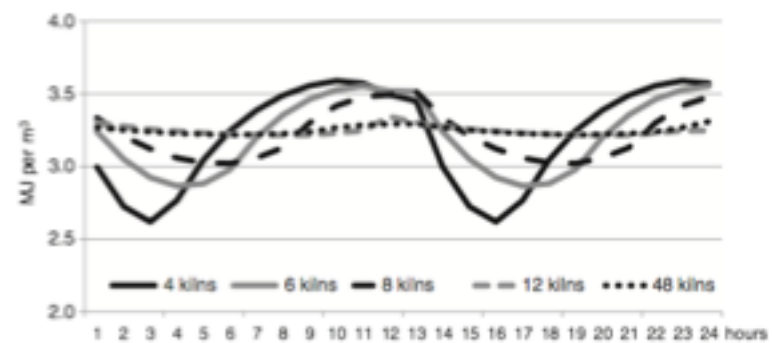


Fig. 4. Variation in calorific value of pyrolysis gas with variation of number of kilns in series (Vilela, 2010).



Fig. 5. Biochar plant in Denmark, with 35 KWe cogeneration capacity, powered by Stirling engine.

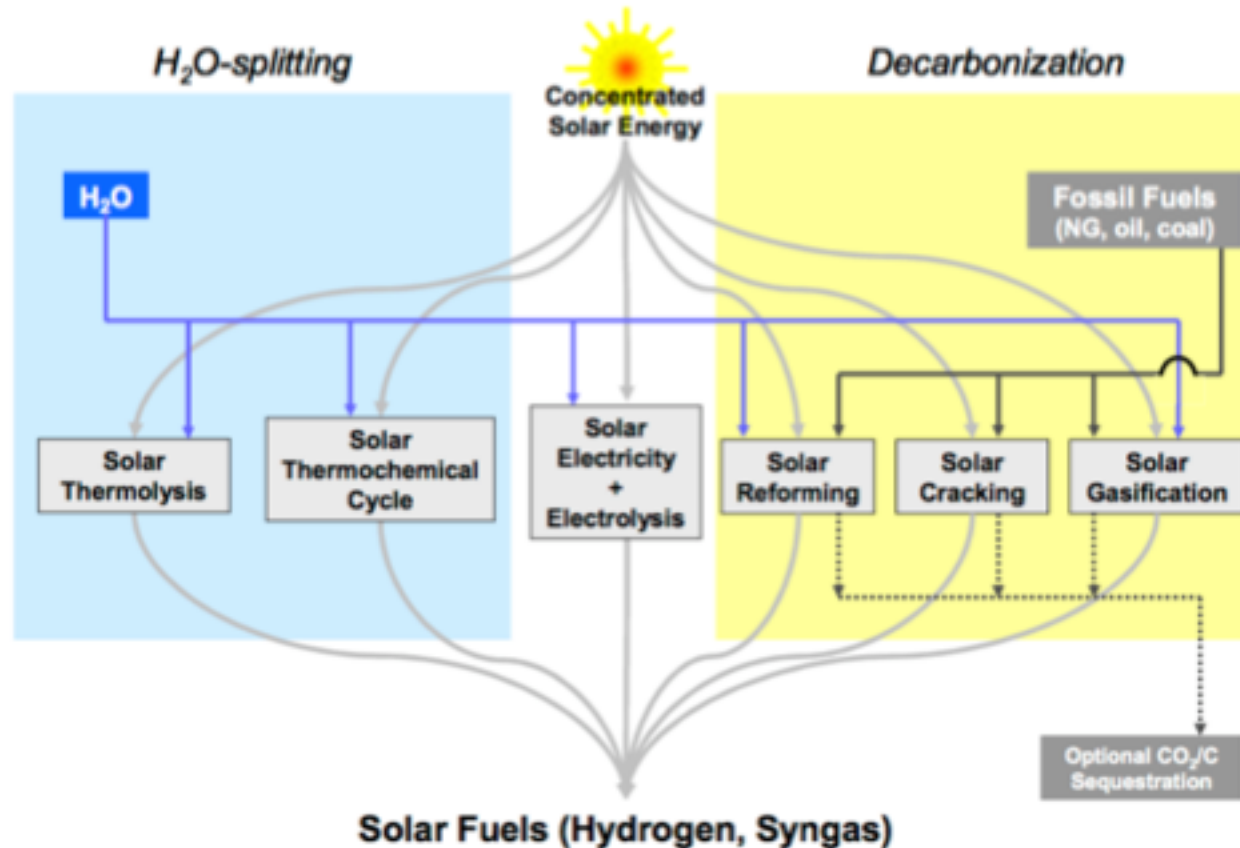


Fig. 2: Thermochemical routes for solar hydrogen production – Indicated is the chemical source of H₂: H₂O for the solar thermolysis and the solar thermochemical cycles; fossil fuels for the solar cracking, and a combination of fossil fuels and H₂O for the solar reforming and gasification. For the solar decarbonization processes, optional CO₂/C sequestration is considered. All of those routes involve energy consuming (endothermic) reactions that make use of concentrated solar radiation as the energy source of high-temperature process heat. Adapted from [1,2].

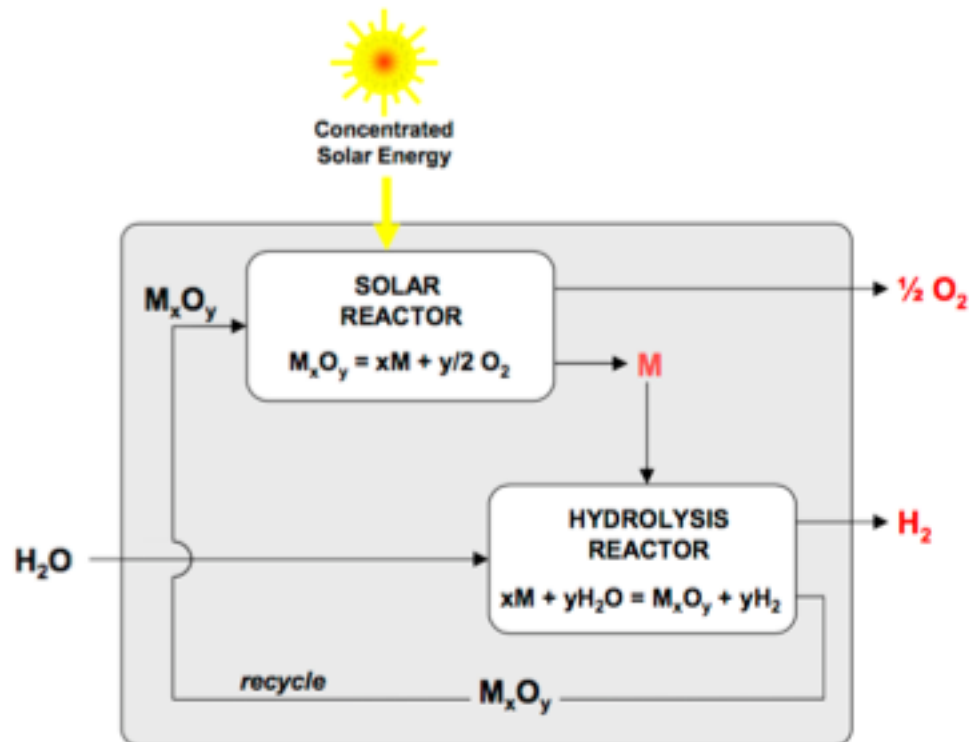
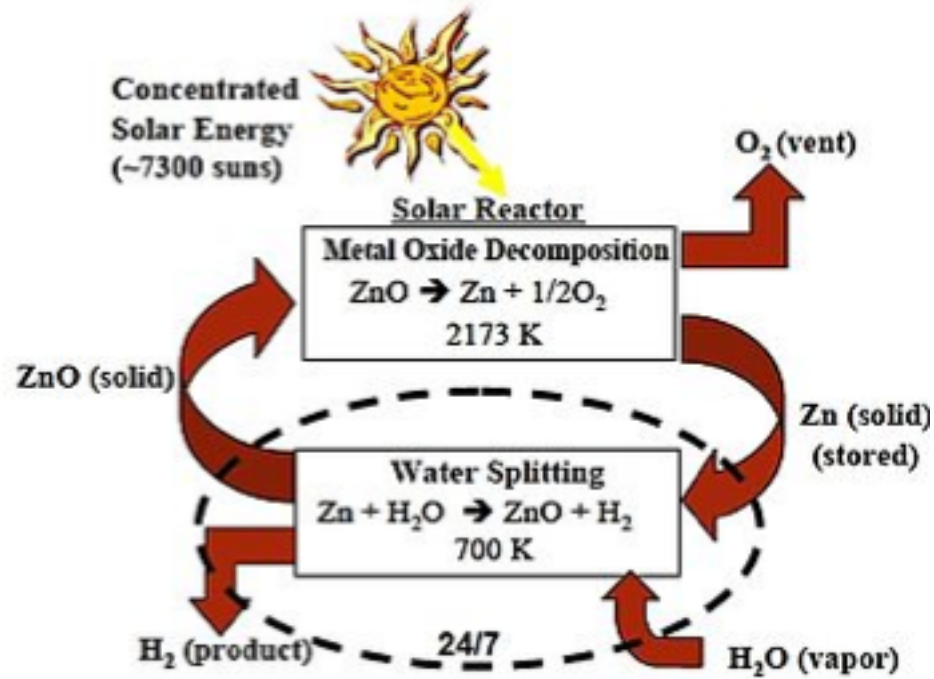


Fig. 3: Thermochemical route based on metal oxide redox reactions – The first step of the cycle is the solar thermal release of O_2 from the metal oxide (M_xO_y). This step requires very high temperatures. The second step is the reaction of the metal (M) with H_2O to form H_2 and the corresponding M_xO_y . This step proceeds at lower temperatures and does not require additional heating in some cases. Since H_2 and O_2 are formed in different steps, the need for high-temperature gas separation is thereby eliminated. This cycle was originally proposed for an iron oxide FeO/Fe_3O_4 redox system. Adapted from [1].

[Zn => ZnO Cycle](http://en.wikipedia.org/wiki/Zinc%E2%80%93zinc_oxide_cycle) (http://en.wikipedia.org/wiki/Zinc%E2%80%93zinc_oxide_cycle)

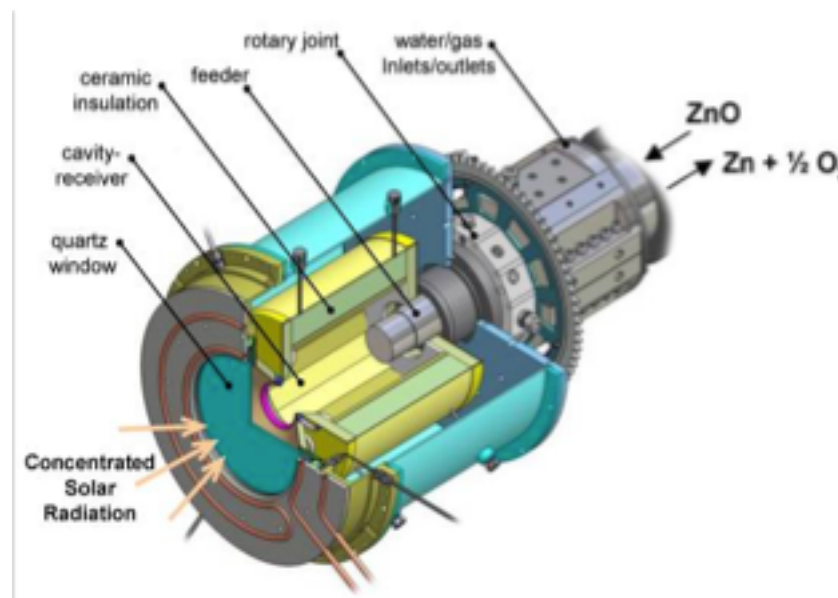


[UNIV](http://www.hydrogen.energy.gov/pdfs/review06/pd_10_weimer.pdf) (http://www.hydrogen.energy.gov/pdfs/review06/pd_10_weimer.pdf)

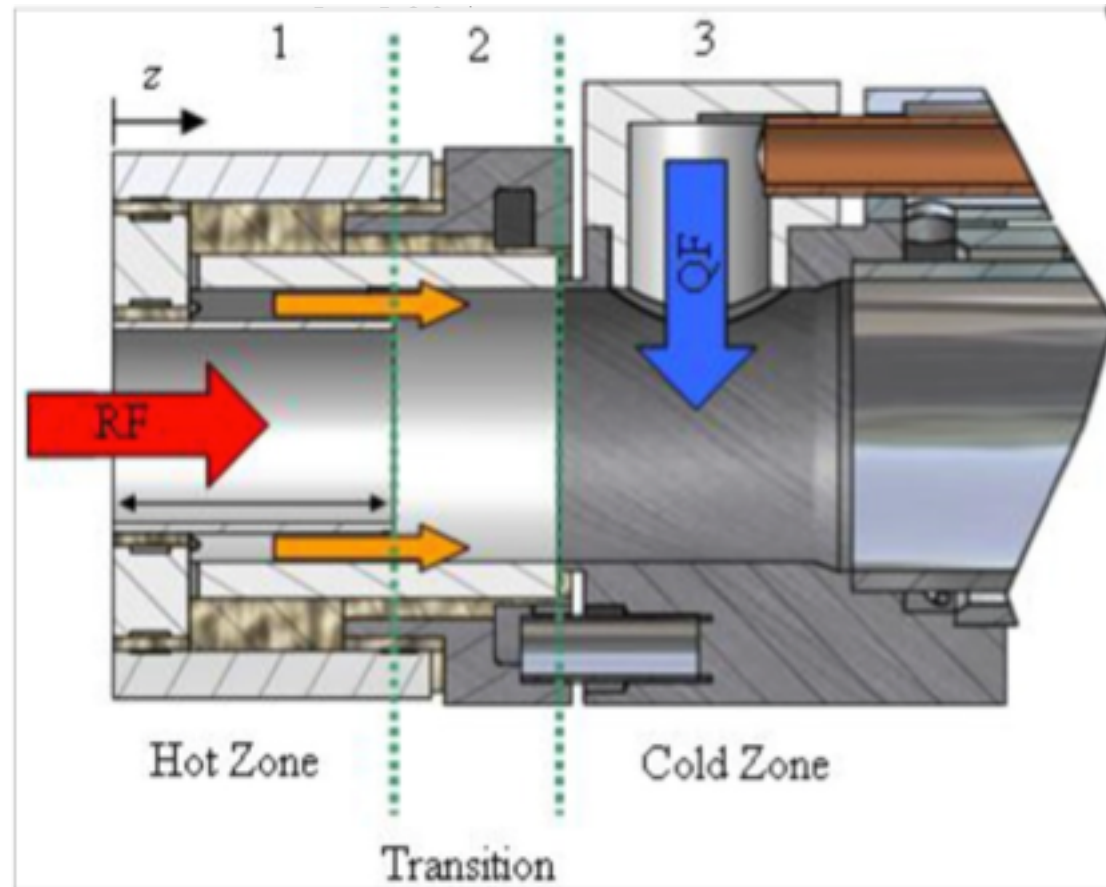
[PSI/ETHZ](https://www.psi.ch/media/producing-pure-recycling-zinc-with-concentrated-solar-energy) (<https://www.psi.ch/media/producing-pure-recycling-zinc-with-concentrated-solar-energy>)

[France Solar Furnace Talk](http://sfera.sollab.eu/downloads/Conferences/SolarPACES_2012_SFERA_Meier.pdf) (http://sfera.sollab.eu/downloads/Conferences/SolarPACES_2012_SFERA_Meier.pdf)

Zn => ZnO Cycle
(Solar Driven Redox Reactions)



Need to rapidly quench and dilute Zn + O₂ mixture



http://sfera.sollab.eu/downloads/Conferences/SolarPACES_2012_SFERA_Meier.pdf

Outline

100 kW Pilot Plant at MWSF

- Installation
- Commissioning

Scientific Background

- Solar ZnO dissociation at 2000 K
- Solar reactor technology

Experimental Results

- Solar reactor experiments
- Flux measurements

Outlook / Acknowledgements



CNRS 1 MW Solar Furnace
Odeillo, France

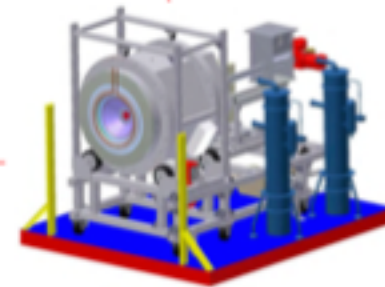


Table 1. Major assumptions and findings for cost and efficiency of the Zn/ZnO cycle from Steinfeld [5] and Charvin et al. [22].

	Steinfeld (792 kg/hr) [5]	Charvin et al., (250 kg/hr) [22]	Charvin et al., (50 kg/hr) [22]
<i>Plant size, energy and mass flows</i>			
Concentration ratio, C	5,000 suns	5,000 suns	5,000 suns
Solar plant size (power input to solar reactor) [MW _{th}]	90	55	11
Beam irradiation [kWh _{th} /m ² ·yr]	2300	2000	2000
Heliostat area [m ²]	155,172	54,800	10,960
<i>Efficiencies</i>			
Optical efficiency of solar concentration system, η_{optics}	58%	48.4%	not included
Cycle efficiency, η_{cycle}	29%	30.4%	not included
Global efficiency, η_{global}	17%	20.8%	not included
<i>Assumptions</i>			
Pump or work input	none	none	none
Solar step temperature [K]	2300	2000	2000
Reactor re-radiation losses	accounted for	accounted for	accounted for
Endothermic reaction losses	accounted for	accounted for	accounted for
Heat recovery from quenching after first step	no heat recovery	heat recovery	heat recovery
Recovery of heat of exothermic reaction	no heat recovery	complete heat recovery	complete heat recovery
Efficiency of separation of Zn & O ₂	no recombination	20% recombination	20% recombination
Efficiency of hydrolysis step	complete hydrolysis	complete hydrolysis	complete hydrolysis
Hydrogen energy content [kJ/mol]	241 (LHV)	286 (HHV)	286 (HHV)
<i>Costs</i>			
Heliostat field [M\$, assuming \$150/m ²]	23.28	8.22	1.65
Land [M\$, assuming \$1/m ²]	not included	0.28	0.06
Tower [M\$]	3.60	1.50	1.00
Tower reflector and CPCs [M\$]	5.30	not included	not included
Solar receiver-reactor + periphery [M\$]	7.00	2.00	1.00
Quencher [M\$]	3.00	not included	not included
Hydrolyser [M\$]	4.00	1.00	0.50
Balance of plant, indirects, contingency [M\$]	8.90	2.00	1.00
H ₂ storage [M\$]	not included	1.00	0.50
Total capital cost for solar H ₂ [M\$]	55.08	16.00	5.70
<i>Annual Cost</i>			
Annual fixed charge rate [M\$]	15%	not included	not included
Capital cost for solar H ₂ [M\$]	8.26	not included	not included
O&M cost for solar H ₂ [M\$]	1.10	1.01	0.42
Total annual cost for solar H ₂ [M\$]	9.36	1.01	0.42
<i>Hydrogen production rate [kg/hr]</i>			
Hydrogen production rate [kg/hr]	792	250	50
Hydrogen cost [\$/kg]	5.02	7.98	14.75

ES2010- 0

RENEWABLE HYDROGEN FROM THE Zn/ZnO SOLAR THERMOCHEMICAL CYCLE: A COST AND POLICY ANALYSIS

Julia F. Hattwanger^{*}
Mechanical Engineering
University of Minnesota
Minneapolis, Minnesota 55457

Jane M. Davidson
Mechanical Engineering
University of Minnesota
Minneapolis, Minnesota 55457

Elizabeth J. Wilson
Humphrey Institute of Public Affairs
University of Minnesota
Minneapolis, Minnesota 55457

^{*}steam methane reforming (SMR).

Prior work projects that hydrogen produced by the zinc/zinc-oxide cycle will cost between \$5.02 and \$14.75/kg, compared to \$2.40 to \$3.60/kg for steam methane reforming. Overcoming this cost difference would require a carbon tax of \$119 to \$987/tCO₂, which is significantly higher than is likely to be implemented in most countries. For the technology to become cost competitive, incentive policies that lead to early implementation of solar hydrogen plants will be necessary to allow the experience effect to draw down the price. Under such policies, a

Zn \Rightarrow ZnO Cycle
(Solar Driven Redox Reactions)

Julia Halvorsen Nicodemus
Engineering Studies
Lafayette College
Easton, PA
Email: nicodemj@lafayette.edu

Morgan McGuinness
Physics and Math
Lafayette College
Easton, PA

To put these costs in perspective, comparison to the cost of natural gas is appropriate. The industrial cost of natural gas is \$0.246/kg, or, on an energy basis, \$0.0046/MJ¹. Because the heating value of natural gas is about twice that of syngas, costs are better compared on an energy basis. Table 2 lists the costs of solar syngas for 100MW_{th} and 500MW_{th} plants, for low cost water (\$0.01/L) and high cost water (\$0.1/L) for all six carbon pricing scenarios. Assuming low cost water and CO₂ captured from a power plant with no additional costs, the cost of solar syngas is 4 and 5 times the cost of natural gas for the 100MW_{th} and 500MW_{th} plants, respectively.

In this analysis, we will consider six possible scenarios for pricing CO₂: carbon capture from a power plant (CC), carbon capture plus the social cost of carbon (CC+SCC), carbon capture plus a carbon tax (CC+tax), CO₂ supplied by a chemical supplier (Chem), CO₂ from a chemical supplier plus the social cost of carbon (Chem+SCC), and CO₂ from a chemical supplier plus a carbon tax (Chem+tax).

TABLE 2: SYNGAS COST PER MEGAJOULE (MJ)

	100MW _{th}		500MW _{th}	
	low H ₂ O cost	high H ₂ O cost	low H ₂ O cost	high H ₂ O cost
CC	\$0.0246	\$0.0282	\$0.0190	\$0.0226
CC + SCC	\$0.0252	\$0.0288	\$0.0196	\$0.0232
CC + tax	\$0.0354	\$0.0390	\$0.0299	\$0.0334
Chem	\$0.0257	\$0.0293	\$0.0201	\$0.0237
Chem + SCC	\$0.0263	\$0.0299	\$0.0207	\$0.0243
Chem + tax	\$0.0365	\$0.0401	\$0.0310	\$0.0345

Cite this: *Energy Environ. Sci.*, 2011, **4**, 73

www.rsc.org/ees

REVIEW

Solar-driven gasification of carbonaceous feedstock—a review

Nicolas Piatkowski,^a Christian Wieckert,^b Alan W. Weimer^c and Aldo Steinfeld^{*a,b}

Received 28th July 2010, Accepted 28th September 2010

DOI: 10.1039/c0ee00312e

Given the future importance of solid carbonaceous feedstocks such as coal, coke, biomass, bitumen, and carbon-containing wastes for the power and chemical industries, gasification technologies for their thermochemical conversion into fluid fuels are developing rapidly. Solar-driven gasification, in which concentrated solar radiation is supplied as the energy source of high-temperature process heat to the endothermic reactions, offers an attractive alternative to conventional autothermal processes. It has the potential to produce high-quality synthesis gas with higher output per unit of feedstock and lower specific CO₂ emissions, as the calorific value of the feedstock is upgraded through the solar energy input by an amount equal to the enthalpy change of the reaction. The elimination of an air separation unit further facilitates economic competitiveness. Ultimately, solar-driven gasification is an efficient means of storing intermittent solar energy in a transportable and dispatchable chemical form. This review article develops some of the underlying science, examines the thermodynamics and kinetics of the pertinent reactions, and describes the latest advances in solar thermochemical reactor technology.

Alan W. Weimer

Sears Professor • C2B2 Executive Director

✉ alan.weimer@colorado.edu

☎ (303) 492-3759

📄 [Curriculum Vitae](#)

🔍 [Google Scholar Profile](#)

👤 [Weimer Research Group](#)

JSCBB C224

Education

B.S., University of Cincinnati (1976)

M.S., Ph.D., University of Colorado (1978, 1980)

Dow Chemical Company (1980-1996)



Solar Thermochemical Production of Fuels

Anton Meier^{1, a} and Aldo Steinfeld^{1, 2, b}

¹Solar Technology Laboratory, Paul Scherrer Institute, 5232 Villigen PSI, Switzerland

²Department of Mechanical and Process Engineering, ETH Zurich, 8092 Zurich, Switzerland

^aanton.meier@psi.ch, ^baldo.steinfeld@ethz.ch

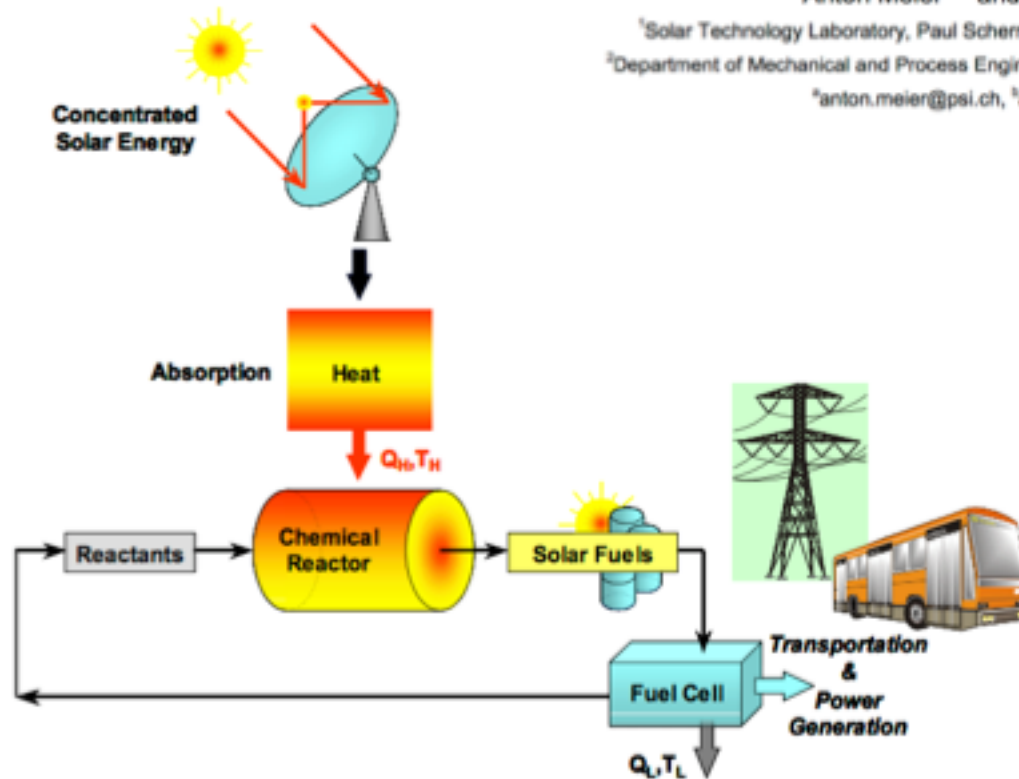


Fig. 1: Energy conversion into solar fuels for transportation and power generation – Concentrated solar radiation is used as the energy source of high-temperature process heat for driving thermochemical reactions towards the production of storable and transportable fuels. Adapted from [1].



Fig. 8: 1 MW_{th} solar plant in Broomfield, Colorado – The plant uses an array of 2700 mirrors to concentrate sunlight on a 20-meter-tall solar tower to produce heat needed to drive the chemical reactor. From [43].



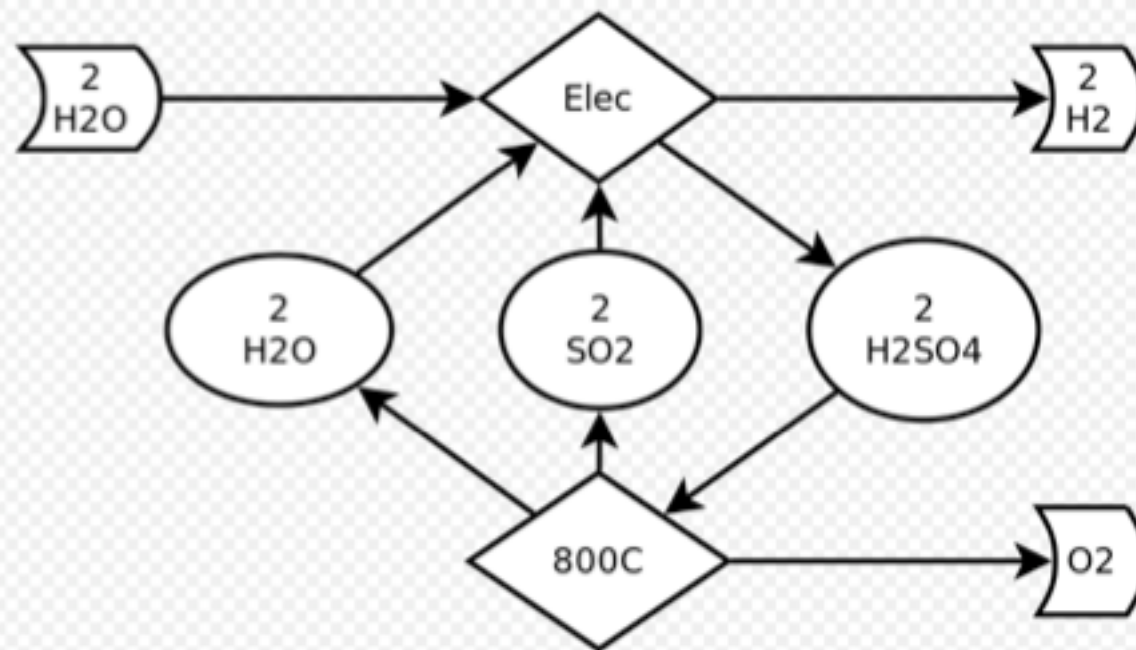
California Mojave Desert



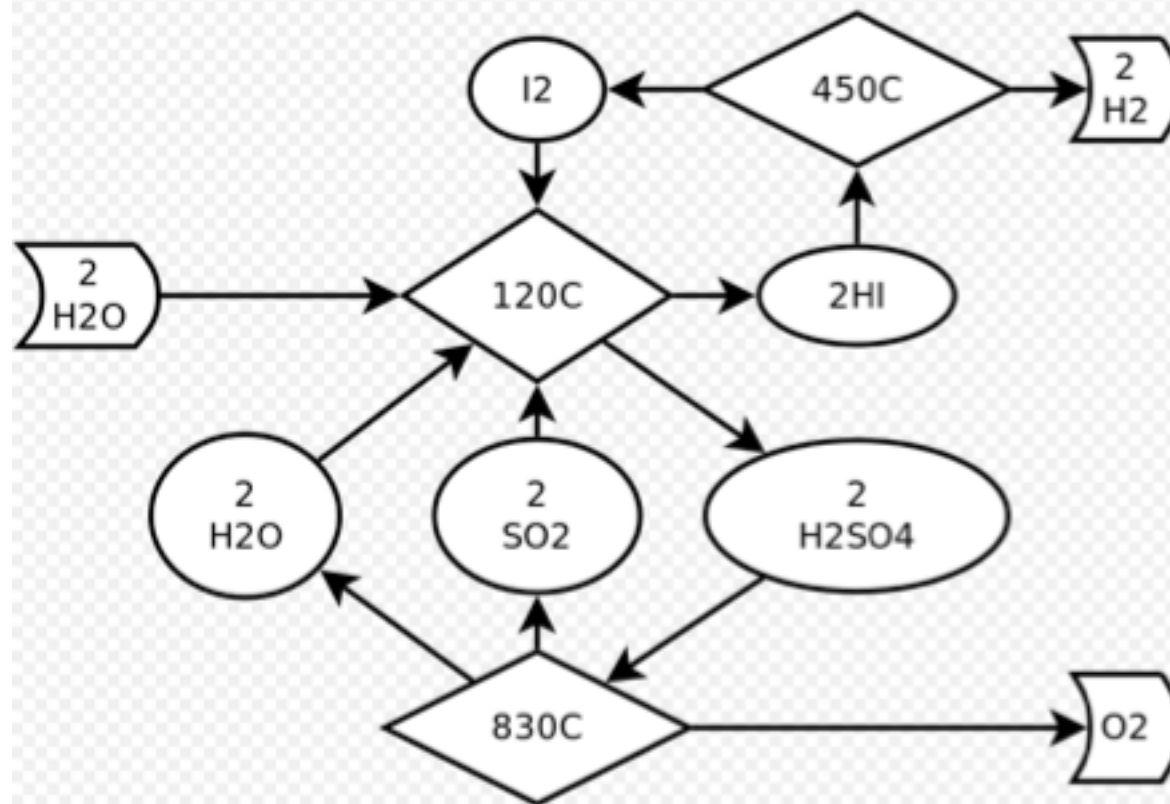
Elevation view of the Odeillo MWSF facility

Odeillo, France

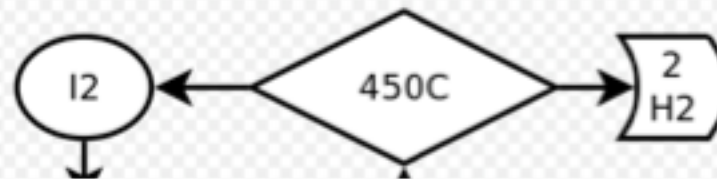
Hybrid Sulfur Cycle



Sulfur-Iodine Cycle



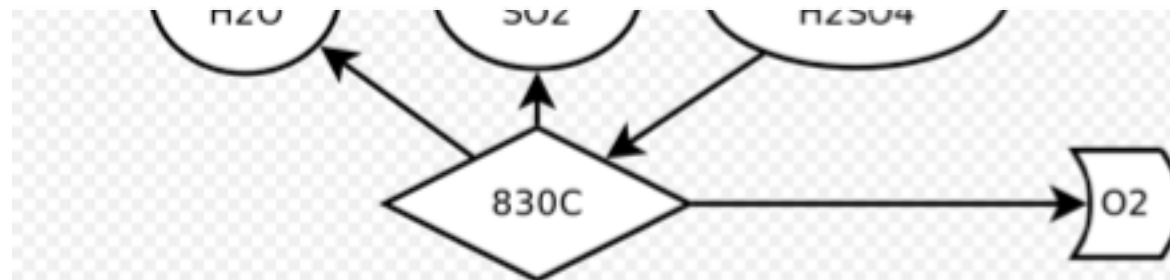
Sulfur-Iodine Cycle



Advantages and disadvantages [\[edit \]](#)

The characteristics of the S-I process can be described as follows:

- All fluid (liquids, gases) process, therefore well suited for continuous operation;
- High utilization of heat predicted (about 50%), but very high temperatures required (at least 850 °C);
- Completely closed system without byproducts or effluents (besides hydrogen and oxygen);
- Corrosive reagents used as intermediaries (iodine, sulfur dioxide, hydriodic acid, sulfuric acid); therefore, advanced materials needed for construction of process apparatus;
- Suitable for application with solar, nuclear, and hybrid (e.g., solar-fossil) sources of heat;
- More developed than competitive thermochemical processes (but still requiring significant development to be feasible on large scale).

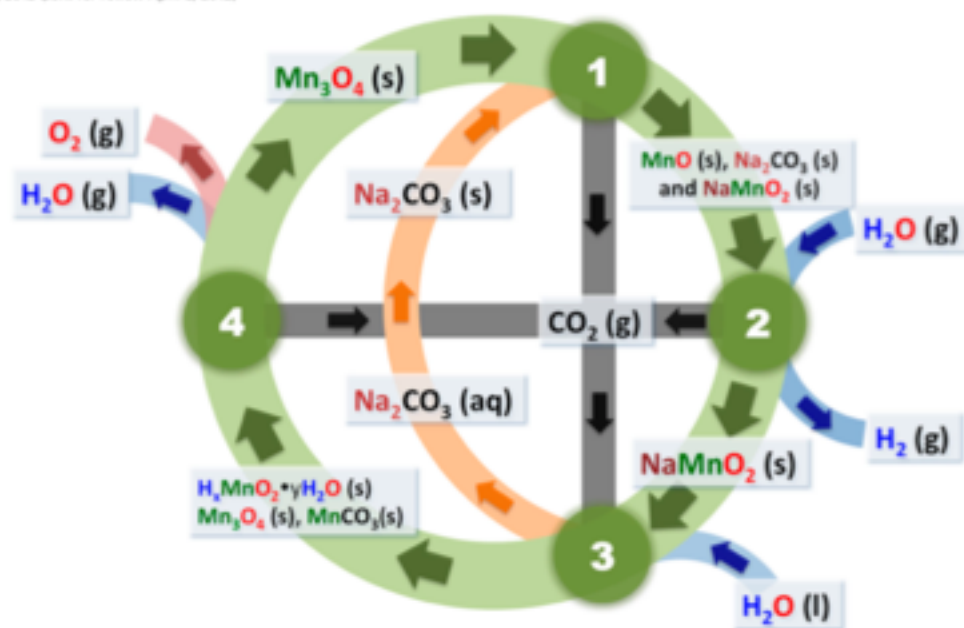


Low-temperature, manganese oxide-based, thermochemical water splitting cycle

Bingjun Xu, Yashodhan Bhawe, and Mark E. Davis^{*}

Chemical Engineering, California Institute of Technology, Pasadena, CA 91125

Contributed by Mark E. Davis, April 17, 2012 (sent for review April 5, 2012)



Step	Reaction	Temp (°C)
1	$3\text{Na}_2\text{CO}_3(\text{s}) + 2\text{Mn}_3\text{O}_4(\text{s}) \rightarrow 4\text{NaMnO}_2(\text{s}) + 2\text{CO}_2(\text{g}) + 2\text{MnO}(\text{s}) + \text{Na}_2\text{CO}_3$	850
2	$2\text{MnO}(\text{s}) + \text{Na}_2\text{CO}_3(\text{s}) + \text{H}_2\text{O}(\text{g}) \rightarrow \text{H}_2(\text{g}) + \text{CO}_2(\text{g}) + 2\text{NaMnO}_2(\text{s})$	850
3	$6\text{NaMnO}_2(\text{s}) + a\text{yH}_2\text{O}(\text{l}) + (3 + b)\text{CO}_2(\text{g}) \rightarrow 3\text{Na}_2\text{CO}_3(\text{aq}) + a\text{H}_2\text{MnO}_2 \cdot \text{yH}_2\text{O}(\text{s}) + b\text{MnCO}_3(\text{s}) + c\text{Mn}_3\text{O}_4(\text{s})$	80
4	$a\text{H}_2\text{MnO}_2 \cdot \text{yH}_2\text{O}(\text{s}) + b\text{MnCO}_3 + \rightarrow (2-c)\text{Mn}_3\text{O}_4(\text{s}) + a\text{yH}_2\text{O}(\text{g}) + b\text{CO}_2(\text{g}) + 0.5\text{O}_2(\text{g})$	850
Net	$\text{H}_2\text{O}(\text{g}) \rightarrow \text{H}_2(\text{g}) + 0.5\text{O}_2(\text{g})$	

a , b and c satisfy following relations: $a + b + 3c = 6$ and $(4-x)a + 2b + 8c = 18$

Fig. 2. Schematic representation of the low-temperature, Mn-based thermochemical cycle.

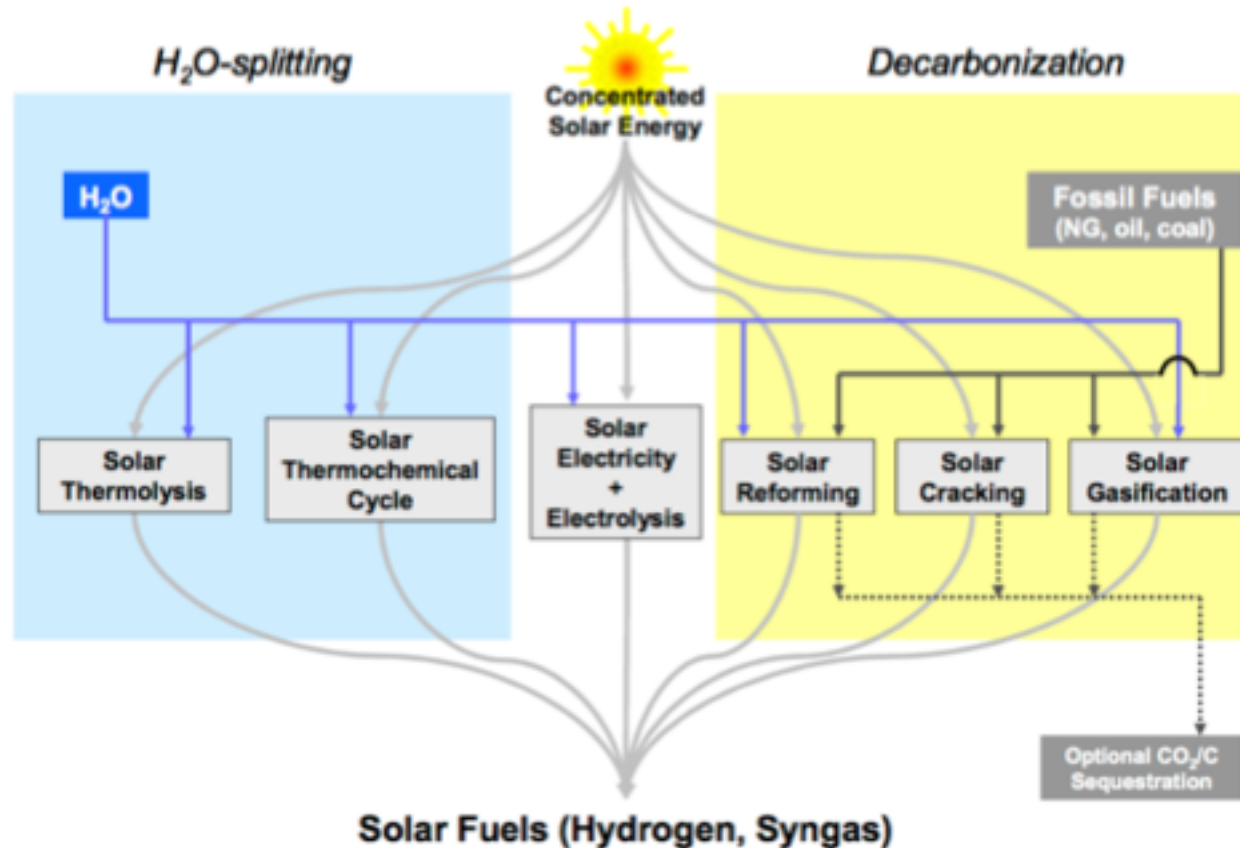


Fig. 2: Thermochemical routes for solar hydrogen production – Indicated is the chemical source of H₂: H₂O for the solar thermolysis and the solar thermochemical cycles; fossil fuels for the solar cracking, and a combination of fossil fuels and H₂O for the solar reforming and gasification. For the solar decarbonization processes, optional CO₂/C sequestration is considered. All of those routes involve energy consuming (endothermic) reactions that make use of concentrated solar radiation as the energy source of high-temperature process heat. Adapted from [1,2].

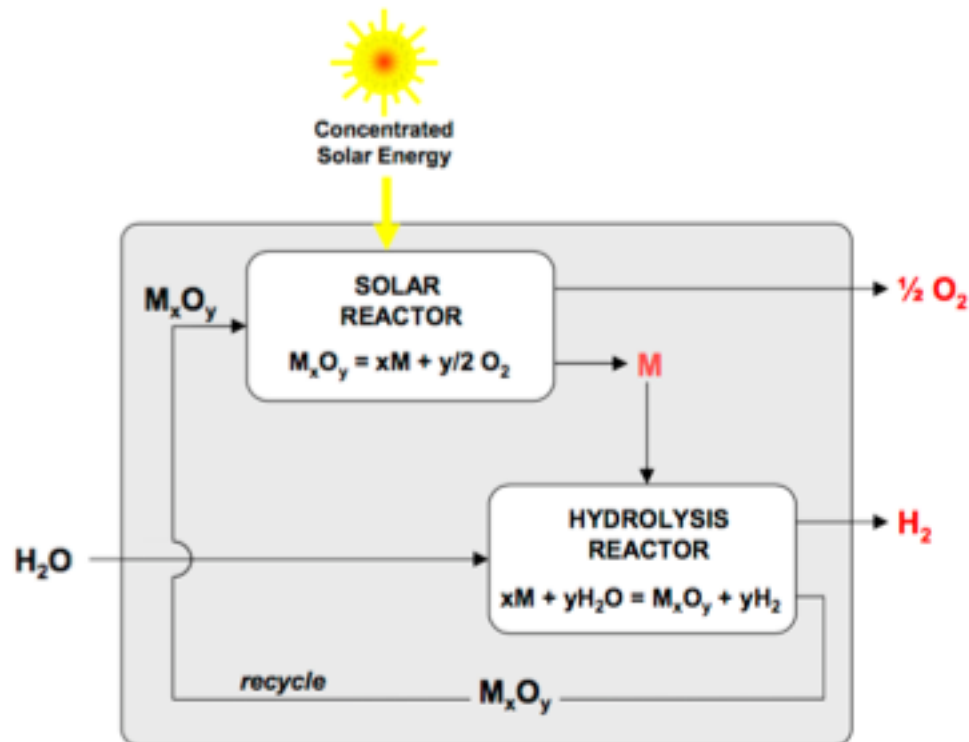


Fig. 3: Thermochemical route based on metal oxide redox reactions – The first step of the cycle is the solar thermal release of O_2 from the metal oxide (M_xO_y). This step requires very high temperatures. The second step is the reaction of the metal (M) with H_2O to form H_2 and the corresponding M_xO_y . This step proceeds at lower temperatures and does not require additional heating in some cases. Since H_2 and O_2 are formed in different steps, the need for high-temperature gas separation is thereby eliminated. This cycle was originally proposed for an iron oxide FeO/Fe_3O_4 redox system. Adapted from [1].

Mixed Iron Oxide Cycle. Other metal oxides such as manganese oxide or cobalt oxide, as well as mixed oxides redox pairs – mainly based on iron – have also been considered [17-20]. For example, a mixed iron oxide cycle was demonstrated within the European P&D project *HYDROSOL-2* [21]. Figure 5 depicts the monolithic dual chamber solar reactor. A quasi-continuous H_2 flow is produced by cyclic operation of the two reaction chambers through sequential oxidation and reduction steps at 800°C and 1200°C , respectively.

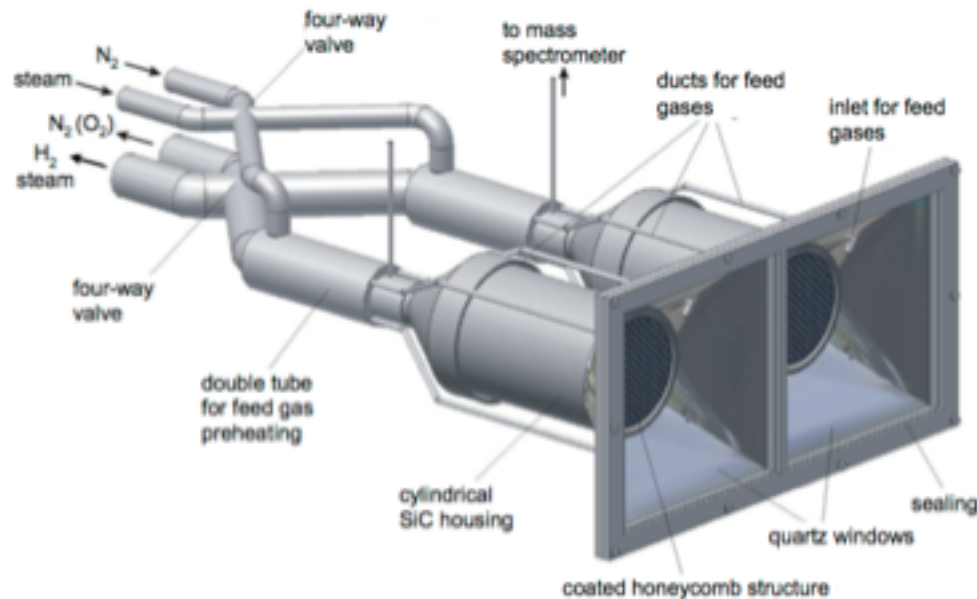


Fig. 5: Monolithic dual chamber solar receiver-reactor for continuous H_2 production – The concept features a closed receiver-reactor constructed from ceramic multi-channeled monoliths. Cyclic operation of the water-splitting and regeneration steps is established in two reaction chambers. Their individual temperature levels are controlled by focusing and defocusing heliostats. Adapted from [21].

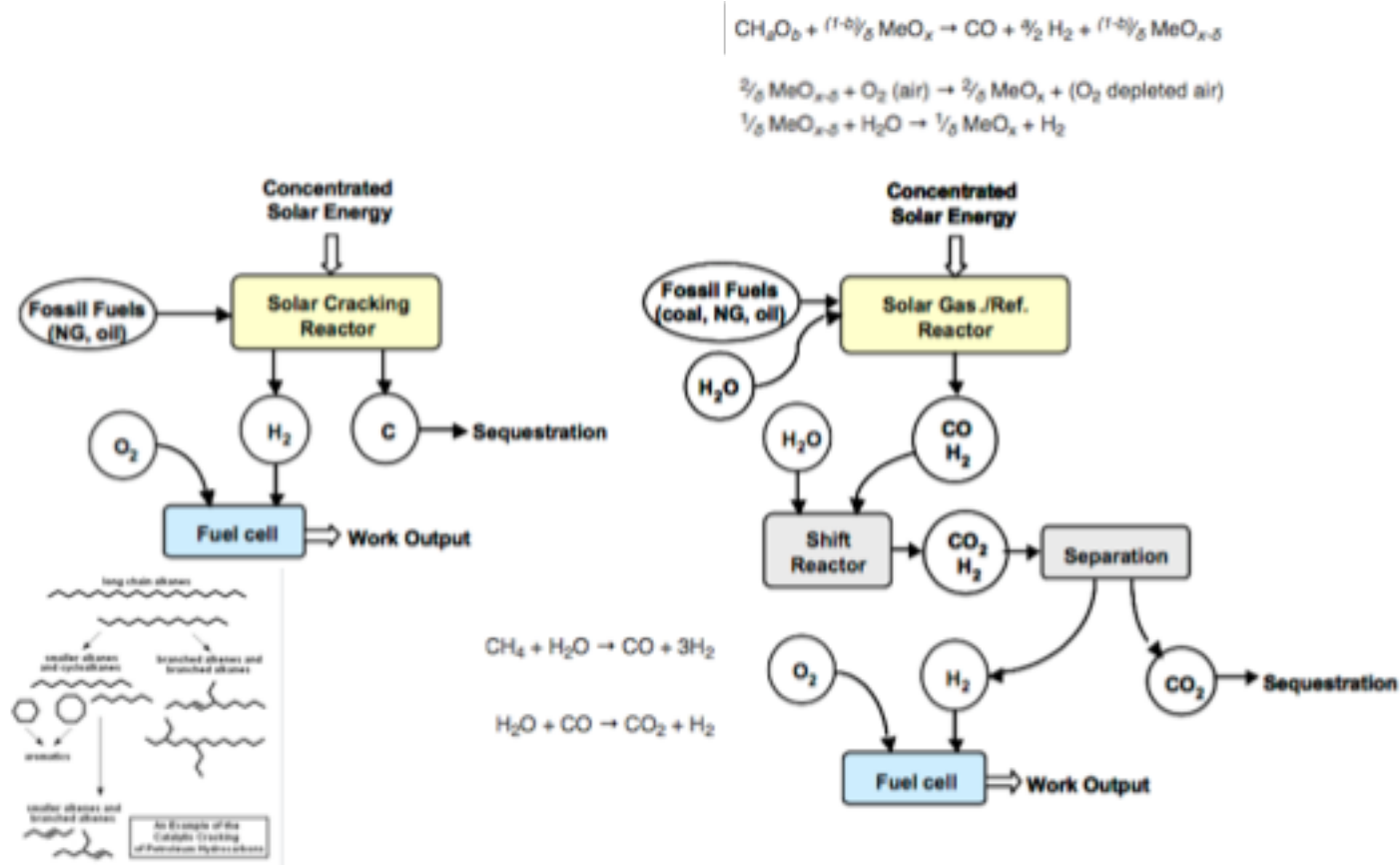


Fig. 7: Solar thermochemical routes for H_2 production using fossil fuels and H_2O as the chemical source – Solar cracking (left), and solar reforming and gasification (right). From [1].



Round-the-clock power supply and a sustainable economy via synergistic integration of solar thermal power and hydrogen processes

Emre Gençer^a, Dharik S. Mallapragada^a, François Maréchal^b, Mohit Tawarmalani^c, and Rakesh Agrawal^{a,1}

^aSchool of Chemical Engineering, Purdue University, West Lafayette, IN 47907; ^bIndustrial Process and Energy Systems Engineering Group, École Polytechnique Fédérale de Lausanne, CH-1951 Sion, Switzerland; and ^cKrannert School of Management, Purdue University, West Lafayette, IN 47907

Edited by Hans Joachim Schellnhuber, Potsdam Institute for Climate Impact Research (PIK), Potsdam, Germany, and approved November 17, 2015 (received for review July 12, 2015)

We introduce a paradigm—"hydricity"—that involves the coproduction of hydrogen and electricity from solar thermal energy and their judicious use to enable a sustainable economy. We identify and implement synergistic integrations while improving each of the two individual processes. When the proposed integrated process is operated in a standalone, solely power production mode, the resulting solar water power cycle can generate electricity with unprecedented efficiencies of 40–46%. Similarly, in standalone hydrogen mode, pressurized hydrogen is produced at efficiencies approaching ~50%. In the coproduction mode, the coproduced hydrogen is stored for uninterrupted solar power production. When sunlight is unavailable, we envision that the stored hydrogen is used in a "turbine"-based hydrogen water power (H₂WP) cycle with the calculated hydrogen-to-electricity efficiency of 65–70%, which is comparable to the fuel cell efficiencies. The H₂WP cycle uses much of the same equipment as the solar water power cycle, reducing capital outlays. The overall sun-to-electricity efficiency of the hydricity process, averaged over a 24-h cycle, is shown to approach ~35%, which is nearly the efficiency attained by using the best multijunction photovoltaic cells along with batteries. In comparison, our proposed process has the following advantages: (i) It stores energy thermochemically with a two- to three-fold higher density, (ii) coproduced hydrogen has alternate uses in transportation/chemical/petrochemical industries, and (iii) unlike batteries, the stored energy does not discharge over time and the storage medium does not degrade with repeated uses.

solar | electricity | hydrogen | solar thermal power | process synthesis

metrics of interest. The STE efficiency refers to the fraction of incident solar energy that is recovered as the net electricity output and accounts for the losses in the solar concentrators and blackbody collection system. Heat-to-electricity efficiency refers to the fraction of process heat input that is recovered as the net electricity output and is a true measure of the efficiency of the power cycle. The third metric, OST efficiency (SI Appendix, Eq. S4), is the net STE efficiency for a constant power delivery round-the-clock—that is, over the average 24-h production accounting for energy storage and delivery of the stored energy. Hydrogen production cycles are evaluated based on sun-to-hydrogen efficiency, which refers to the fraction of incident solar energy that is recovered as the net hydrogen output based on its lower heating value (SI Appendix, Eq. S10).

Solar photovoltaic (PV) and solar thermal are the two main methods of solar power generation. Solar PV systems generate electricity using only a portion of the solar spectrum (7). However, PV systems are suitable for both diffuse and direct sunlight applications (8). To date, the maximum reported STE efficiencies for silicon-crystalline PV is 27.6%, single-junction gallium arsenide PV is 29.1%, and concentrator four-junction PV is 44.7% (9). Solar thermal systems use concentrators to absorb photons of all wavelengths in the incident spectrum as high-temperature heat (10, 11). Due to the use of optical concentrators, these systems can only be operated under direct sunlight, which imposes geographical limitations (12). Further, these systems are anticipated to be cost-effective only as large-scale power plants, owing to the capital costs of installing solar concentrators (12, 13). However, the highest STE

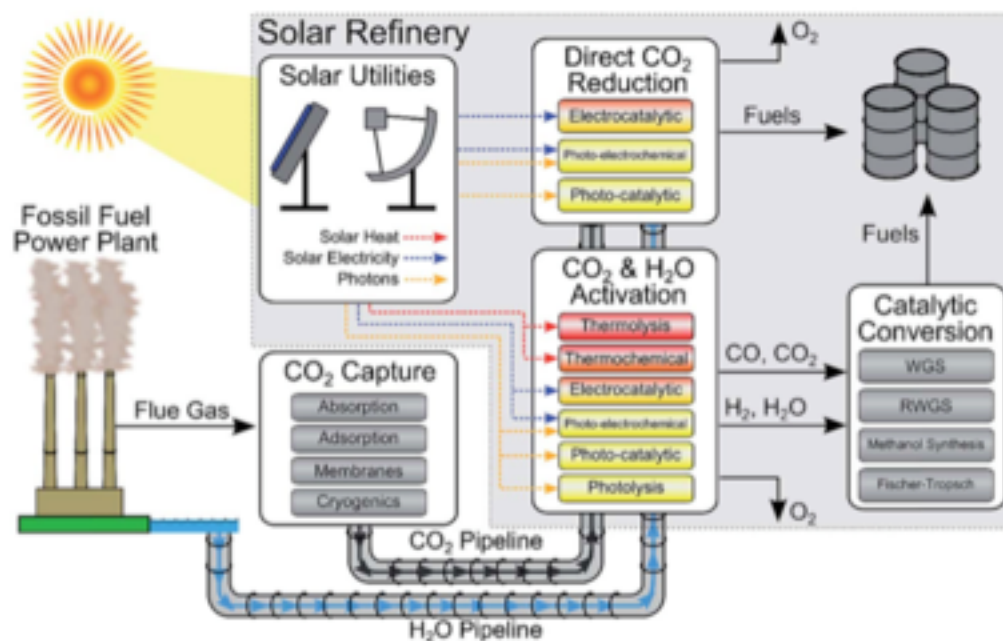


Fig. 1 Schematic for solar fuels production. Solar fuel feedstocks (CO₂, H₂O, and solar energy) are captured on-site and/or transported to the solar refinery. Solar energy provides solar utilities in the form of heating, electricity, and photons which are used in the solar refinery to convert CO₂ and H₂O into fuels. CO₂ and H₂O are converted to fuels through two principal routes: (1) direct solar-driven CO₂ reduction by H₂O to fuels or (2) solar activation of CO₂/H₂O to CO/H₂, respectively, and subsequent catalytic conversion to fuels via traditional processing (i.e. methanol synthesis or Fischer-Tropsch). The approximate temperature requirements for the solar-driven conversion processes are color-coded (red = high temperature, yellow = ambient temperature).

ANALYSIS

[View Article Online](#)

[View Journal](#) | [View Issue](#)



Cite this: *Energy Environ. Sci.*, 2015, 8, 126

A general framework for the assessment of solar fuel technologies†

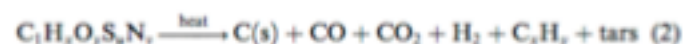
Jeffrey A. Herron, Jiyong Kim,‡ Aniruddha A. Upadhye, George W. Huber and Christos T. Maravelias*

The conversion of carbon dioxide and water into fuels in a solar refinery presents a potential solution for reducing greenhouse gas emissions, while providing a sustainable source of fuels and chemicals. Towards realizing such a solar refinery, there are many technological advances that must be met in terms of capturing and sourcing the feedstocks (namely CO_2 , H_2O , and solar energy) and in catalytically converting CO_2 and H_2O . In the first part of this paper, we review the state-of-the-art in solar energy collection and conversion to solar utilities (heat, electricity, and as a photon source for photo-chemical reactions), CO_2 capture and separation technology, and non-biological methods for converting CO_2 and H_2O to fuels. The two principal methods for CO_2 conversion include (1) catalytic conversion using solar-derived hydrogen and (2) direct reduction of CO_2 using H_2O and solar energy. Both hydrogen production and direct CO_2 reduction can be performed electro-catalytically, photo-electrochemically, photo-catalytically, and thermochemically. All four of these methods are discussed. In the second part of this paper, we utilize process modeling to assess the energy efficiency and economic feasibility of a generic solar refinery. The analysis demonstrates that the realization of a solar refinery is contingent upon significant technological improvements in all areas described above (solar energy capture and conversion, CO_2 capture, and catalytic conversion processes).

Received 25th June 2014
Accepted 1st October 2014

DOI: 10.1039/c4ee01958j

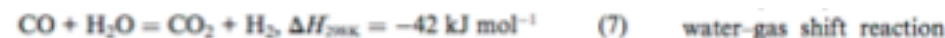
www.rsc.org/ees



Pyrolysis has been extensively studied empirically for various coal ranks ranging from anthracite (~10 wt% volatile matter) to peat (>65 wt% volatile matter), as well as for scrap tires, plastics, biomass, and refuse derived fuels.¹³⁻¹⁷ Solar-driven pyrolysis was investigated in early studies on biomass and coal.¹⁸⁻²¹ Subsequent to pyrolysis, char serves as the reactant for the highly endothermic carbon-steam gasification reaction,



Favorable conditions for this reaction are temperatures above 1100 K, where the reaction kinetics is fast and equilibrium is entirely on the side of the products. Eqn (3) summarizes the overall reaction, but a number of intermediate competing reactions need to be considered:



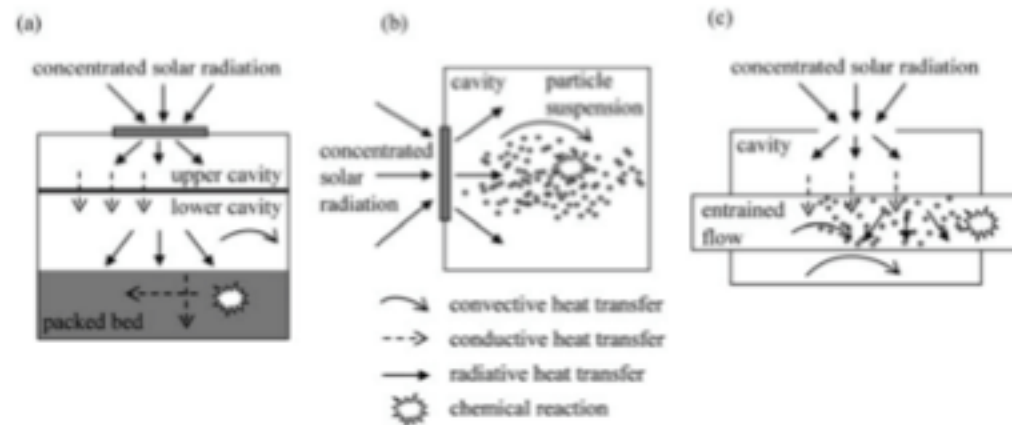


Fig. 10 Modeling schematics for the three solar reactor concepts: (a) indirectly irradiated packed-bed; (b) directly irradiated vortex-flow, and (c) indirectly irradiated entrained flow.

Directly irradiated vortex-flow reactor

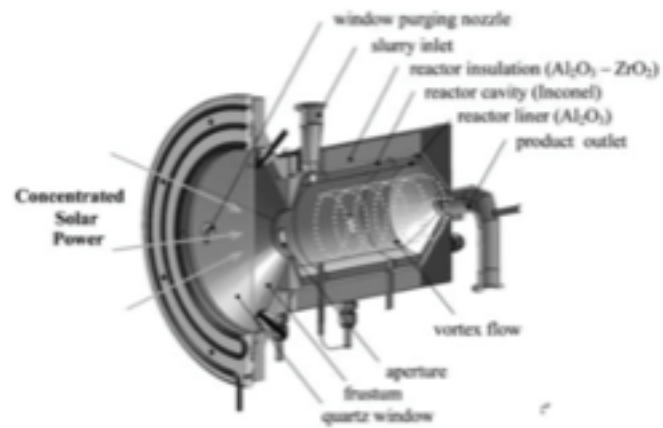


Fig. 6 Scheme of the directly irradiated vortex-flow solar reactor configuration, featuring a helical flow of carbonaceous particles and steam confined to a cavity-receiver and directly exposed to concentrated solar radiation.

Indirectly irradiated packed-bed reactor

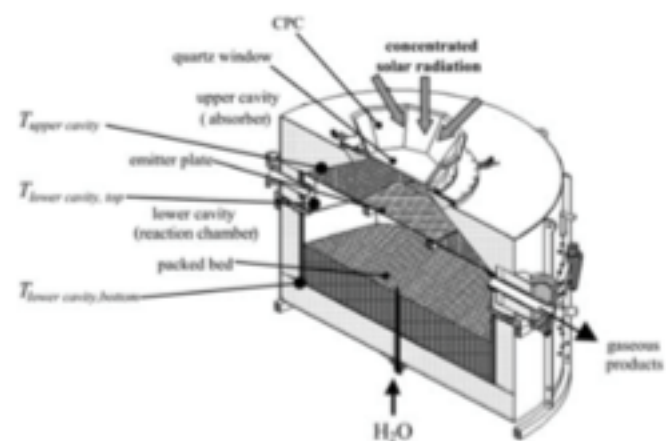


Fig. 4 Scheme of the indirectly irradiated packed-bed solar reactor configuration, featuring two cavities separated by an emitter plate, with the upper one serving as the radiative absorber and the lower one containing the reacting packed bed that shrinks as the reaction progresses.

Indirectly irradiated entrained-flow reactor

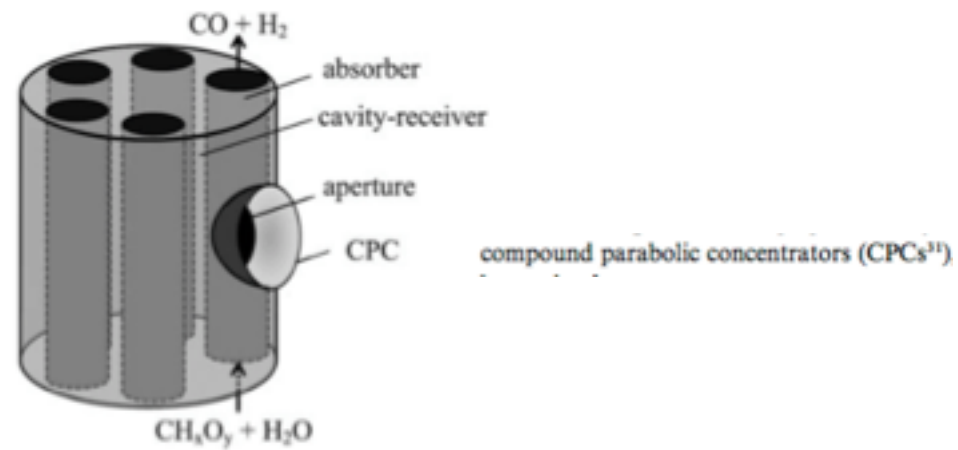


Fig. 8 Scheme of the indirectly irradiated entrained-flow solar reactor configuration, featuring a cylindrical cavity-receiver containing an array of tubular absorbers through which a continuous flow of water vapor laden with carbonaceous particles reacts to form syngas.

Need to rapidly quench and dilute Zn + O₂ mixture

Zn => ZnO Cycle
(Solar Driven Redox Reactions)

fossil-based fuels in sustainable future transportation systems. Economic analyses have been carried out to determine the long-term potential of the Zn/ZnO-cycle realized in a solar tower system. The cost of H₂ ranged between 0.10 and 0.15 \$/kWh (based on its LHV and a heliostat field cost at 100 to 150 \$/m²), and thus might become competitive *vis-à-vis* other paths for producing solar H₂ from H₂O [15,72,73,74]. Credit for pollution abatement and CO₂ mitigation can accelerate the deployment of the solar thermochemical technology. A comparison of H₂ produced via steam methane reforming and the Zn/ZnO cycle concluded that a significantly higher carbon tax is required to make the Zn/ZnO competitive than is likely to be implemented [75]. Therefore, the economic viability of the Zn/ZnO cycle must also include competitive, incentive policies that lead to early implementation of solar H₂ plants. On the other hand, the Zn/ZnO cycle can be applied to split both H₂O and CO₂ and produce both H₂ and CO, thereby laying the path to the solar production of synthetic liquid hydrocarbons for fueling the transportation sector and the existing massive global infrastructure.

Two Other Redox Systems (<http://energy.gov/eere/fuelcells/hydrogen-production-thermochemical-water-splitting>)

2 Cycle Inventory Development and Initial Selection

Many hydrogen producing thermochemical cycles have been proposed over the last 40 years. A literature search was performed to identify all published cycles¹⁻⁵⁸. These were added to an

Table 2.4. Listing of non-zero efficiencies for top-scoring cycles.

PID	Cycle Name	Eff. (LHV)	PID	Cycle Name	Eff. (LHV)
110	Sodium-Mn-3	50.0	184	Hybrid Antimony-Br	30.6
106	High T Electrolysis	49.1	134	Cobalt Sulfate	29.9
147	Cadmium Sulfate	46.5	56	Cu Chloride	29.2
5	Hybrid Cd	45.1	114	Hybrid N-I	28.2
6	Zinc Oxide	45.0	62	Iron Bromide	27.7
182	Cadmium Carbonate	44.3	23	Mn-Chloride-1	26.6
2	Ni-Mn Ferrite	44.0	51	K-Peroxide	23.5
194	Zn-Mn Ferrite	44.0	61	Sodium-Iron	22.8
67	Hybrid Sulfur	43.1	185	Hybrid Cobalt Br-2	21.7
7	Iron Oxide	42.3	53	Hybrid Chlorine	21.6
191	Hybrid Copper Chloride	41.6	160	Arsenic-Iodine	21.2
149	Ba-Mo-Sulfate	39.5	152	Iron-Zinc	19.9
1	Sulfur-Iodine	38.1	103	Cerium Chloride	18.0
193	Multivalent Sulfur-3	35.5	26	Cu-Mg Chloride	17.4
131	Mn Sulfate	35.4	199	Iron Chloride-11	16.9
72	Ca-Fe-Br-2	33.8	200	Iron Chloride-12	16.9
79	Hybrid S-Br	33.4	104	Mg-Ce-Chloride	15.1
24	Hybrid Li-NO ₂	32.8	132	Ferrous Sulfate-3	14.4
201	Carbon Oxides	31.4	68	As-Ammonium-I	6.7
22	Fe-Chloride-4	31.0	129	Mg Sulfate	5.1

Table 2.5. Cycles that could move to Phase 3 detailed theoretical and experimental study.

Cycle	PID	Efficiency %	Estimated Max T
Sulfuric Acid Cycles			
Hybrid Sulfur	67	43	900
Sulfur Iodine	1	45	900
Multivalent Sulfur	193	42	1570
Metal Sulfate Cycles			
Cadmium Sulfate	147	55	1200
Barium Sulfate	149	47	1200
Manganese Sulfate	131	42	1200
Volatile Metal Oxides			
Zinc Oxide	6	53	2200
Cadmium-Carbonate: Cadmium Oxide	182: 213	52: 59	1600: 1450
Hybrid-Cadmium	5	53	1600
Non-volatile Metal Oxides			
Iron Oxide	7	50	2200
Mixed Metal Sodium Manganese; Sodium Manganese	110	59	1560
Nickel Manganese Ferrite	2	52	1800
Zinc Manganese Ferrite	194	52	1800
Hybrid Cycles			
Hybrid Copper Chloride	191	49	580

Table 3.1. Cycles considered in the formal evaluation process.

Class	Cycle	Lead Organization
Sulfuric Acid Cycles	Sulfur Iodine	General Atomics, Sandia National Labs, CEA
	Hybrid Sulfur	Savannah River National Laboratory
Volatile Metal Oxide Cycles	Zinc Oxide	University of Colorado
	Cadmium Oxide	General Atomics
Non-volatile Metal Oxide Cycles	Sodium Manganese and Sodium Manganate	University of Colorado
	Reactive Ferrite	Sandia National Laboratories
	ALD Ferrite	University of Colorado
Hybrid Cycles	Hybrid Copper Chloride	Argonne National Laboratory
	Photolytic Sulfur Ammonia	SAIC

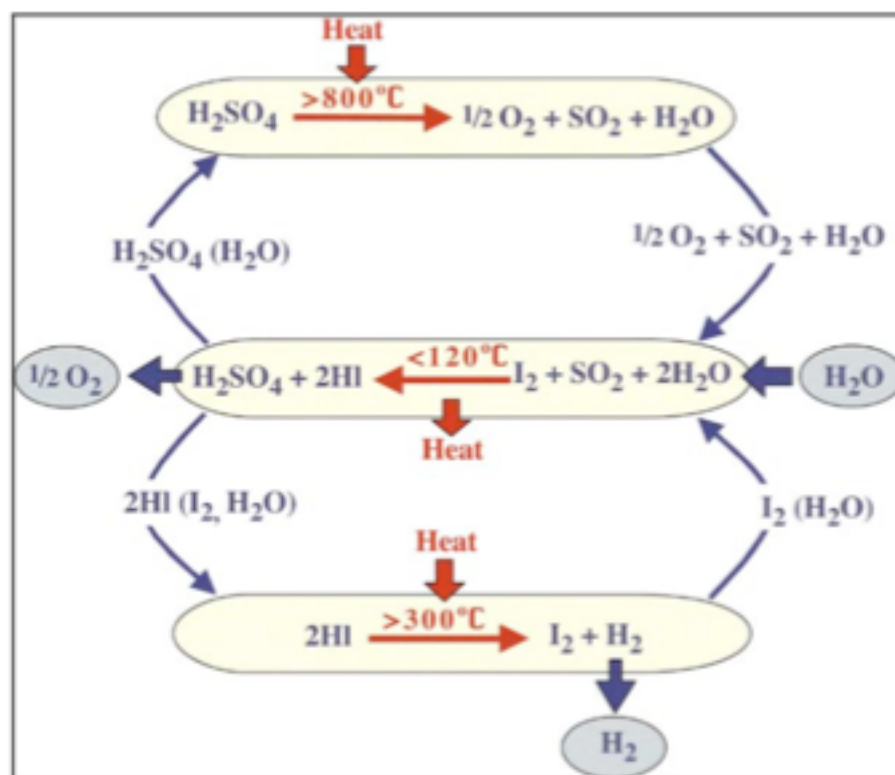


Figure 4.1.1. Sulfur iodine three-step cycle.

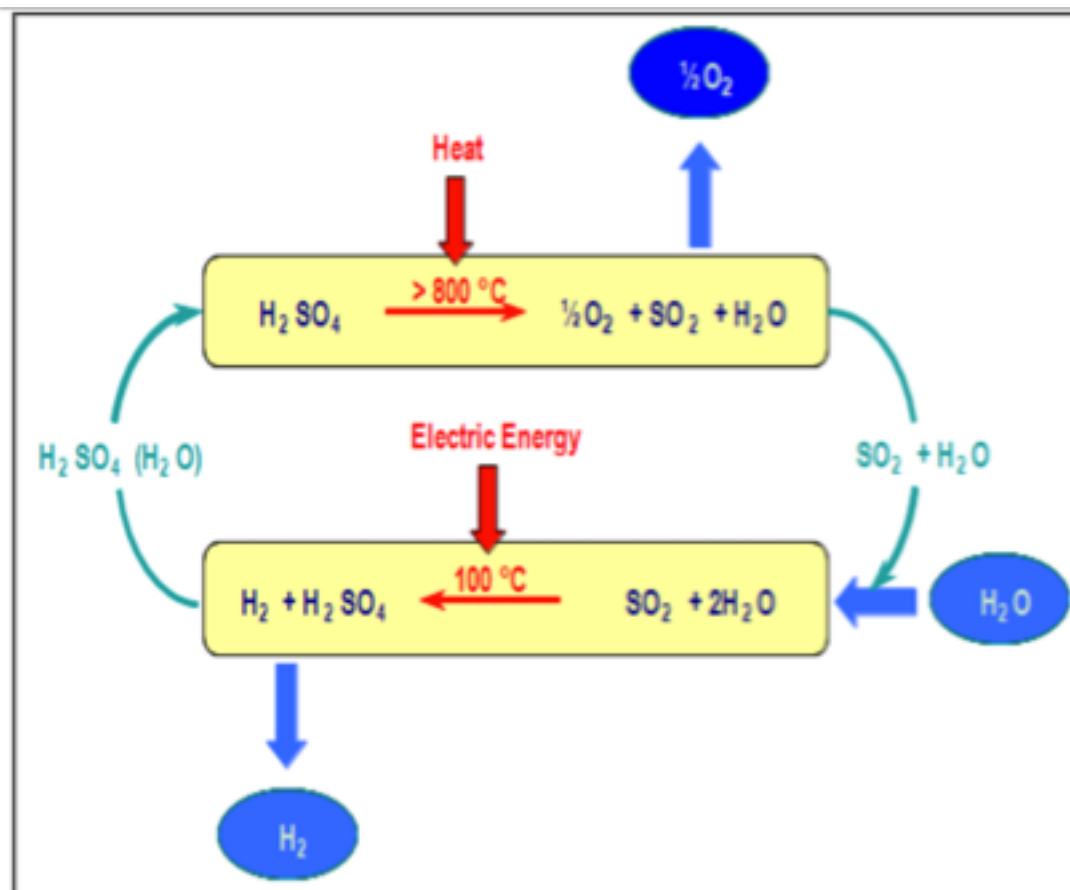


Figure 4.2.1. The Hybrid Sulfur cycle.

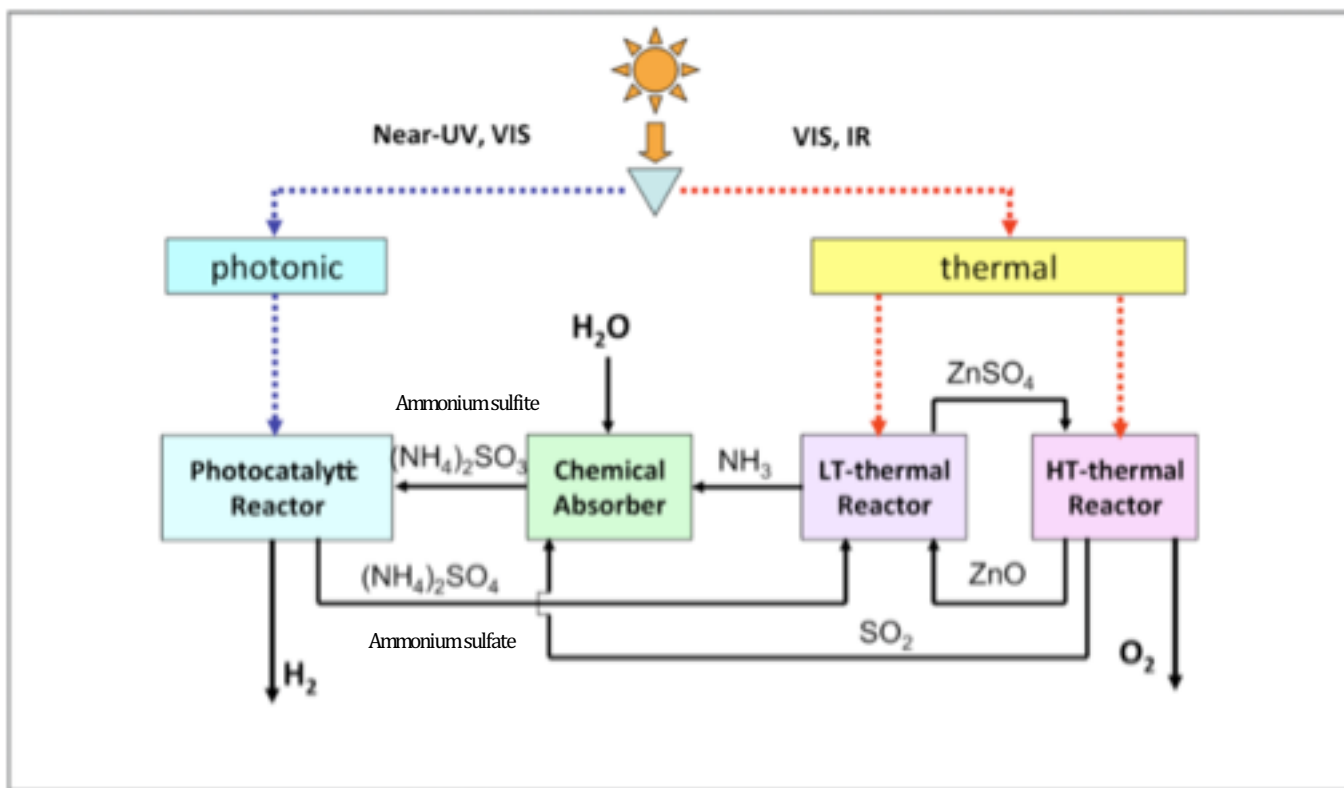


Figure 4.3.1. Photolytic Sulfur Ammonia schematic process.

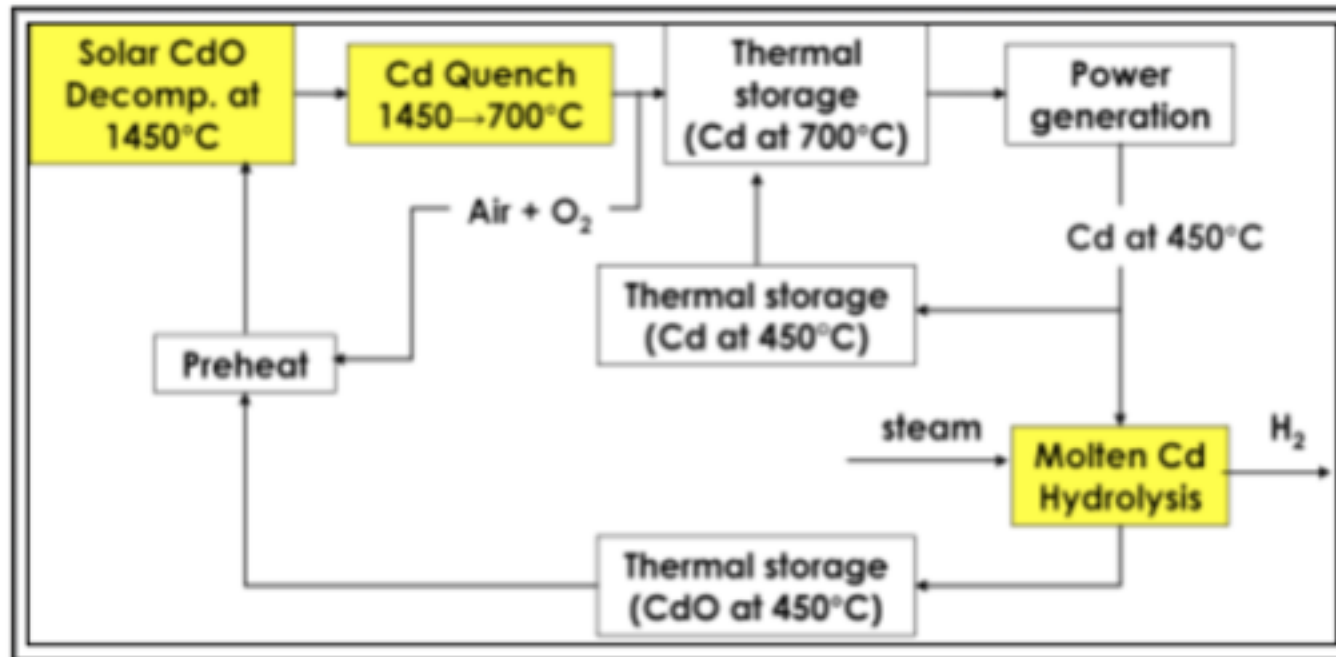


Figure 4.5.2. Process flow for a diurnal solar cadmium oxide hydrogen cycle.

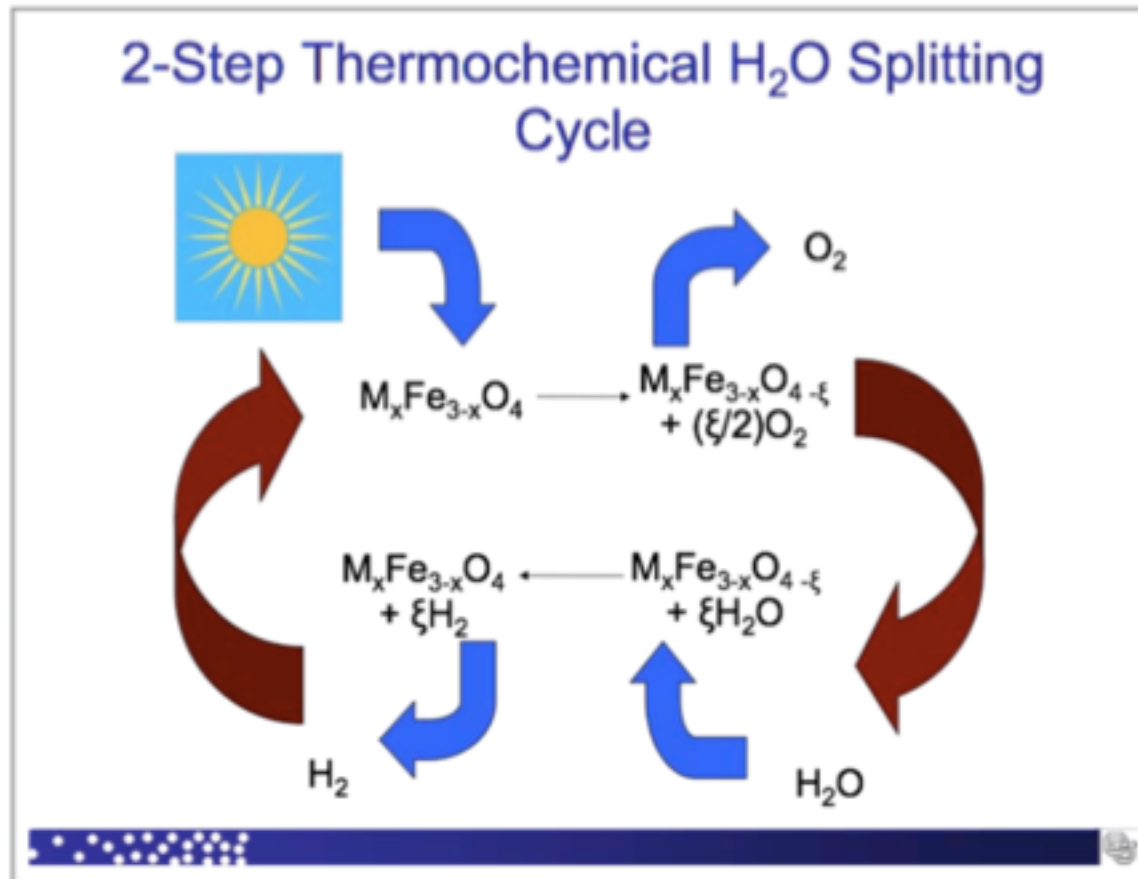


Figure 4.8.1. Schematic chemistry of a water-splitting ferrite cycle.

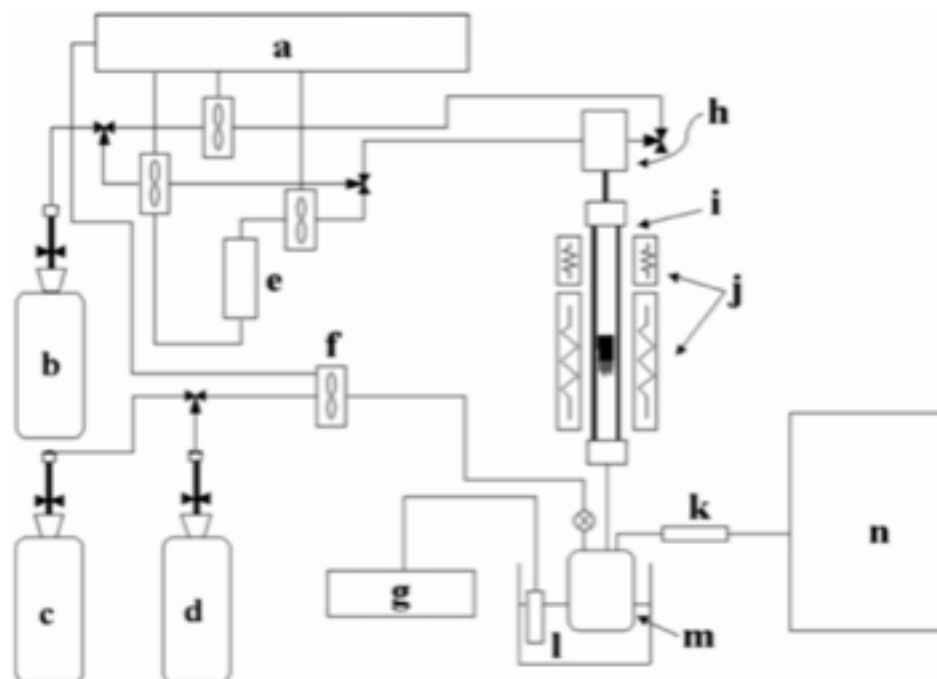


Fig. 1. Experimental apparatus for H₂O decomposition: (a) MFC & Temperature controller, (b) He, (c) H₂, (d) O₂, (e) water, (f) MFC, (g) Condenser, (h) Controlled evaporator mixer, (i) Reactor, (j) Furnace, (k) Silica-gel, (l) Ethanol, (m) Water trap, and (n) Mass.



Hydrogen generation through cuprous chloride-hydrochloric acid electrolysis

**Natarajan Sathaiyan^{1,*}, Venkataraman Nandakumar¹, Ganapathy Sozhan²,
Jegan Gandhibha Packiaraj¹, Elumalai Thambuswamy Devakumar¹, Damaraju Parvatalu³,
Anil Bhardwaj³, Bantwal Narayana Prabhu³**

¹Electro Hydro Metallurgy Division, CSIR-Central Electro-Chemical Research Institute, Karaikudi, India

²Electro Inorganic Chemicals Division, CSIR-Central Electro-Chemical Research Institute, Karaikudi, India

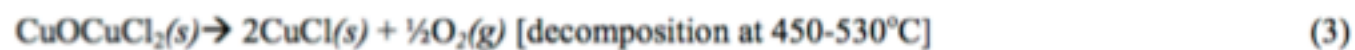
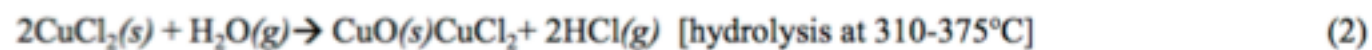
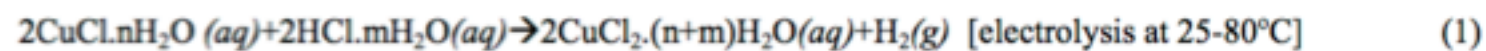
³ONGC Energy Centre, IEOT, Panvel, Navi Mumbai, India

Email address:

enes@rediffmail.com (N. Sathaiyan)

To cite this article:

Natarajan Sathaiyan, Venkataraman Nandakumar, Ganapathy Sozhan, Jegan Gandhibha Packiaraj, Elumalai Thambuswamy Devakumar, Damaraju Parvatalu, Anil Bhardwaj, Bantwal Narayana Prabhu. Hydrogen Generation through Cuprous Chloride-Hydrochloric Acid Electrolysis. *International Journal of Energy and Power Engineering*. Vol. 4, No. 1, 2015, pp. 15-22. doi: 10.11648/j.ijepe.20150401.13



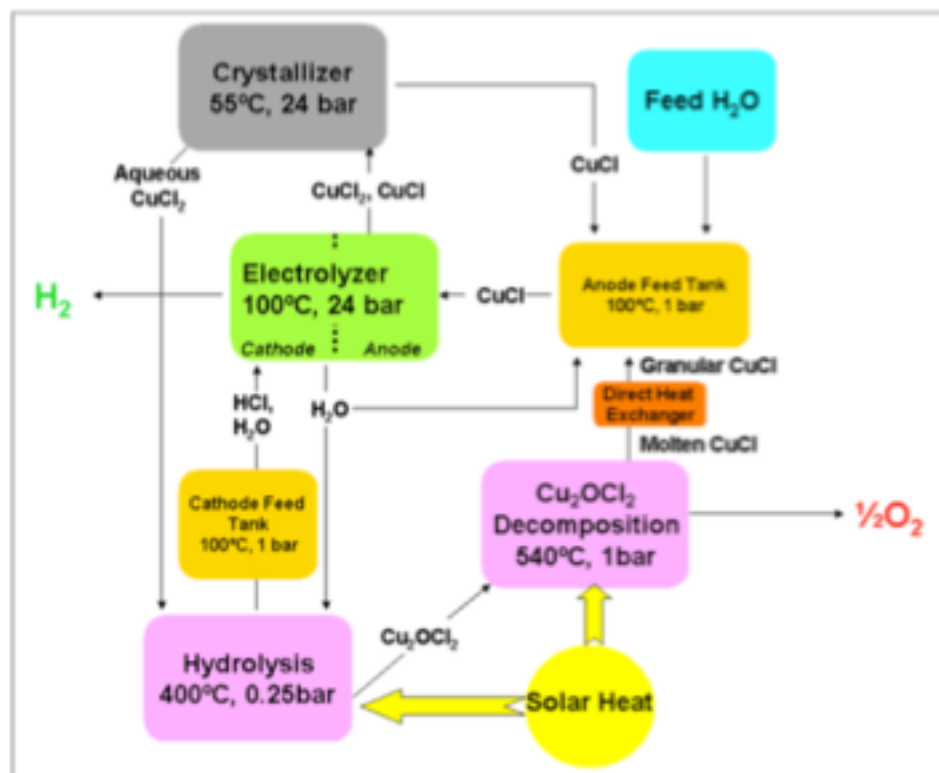


Figure 4.9.2. Hy-CuCl conceptual block flow chart.

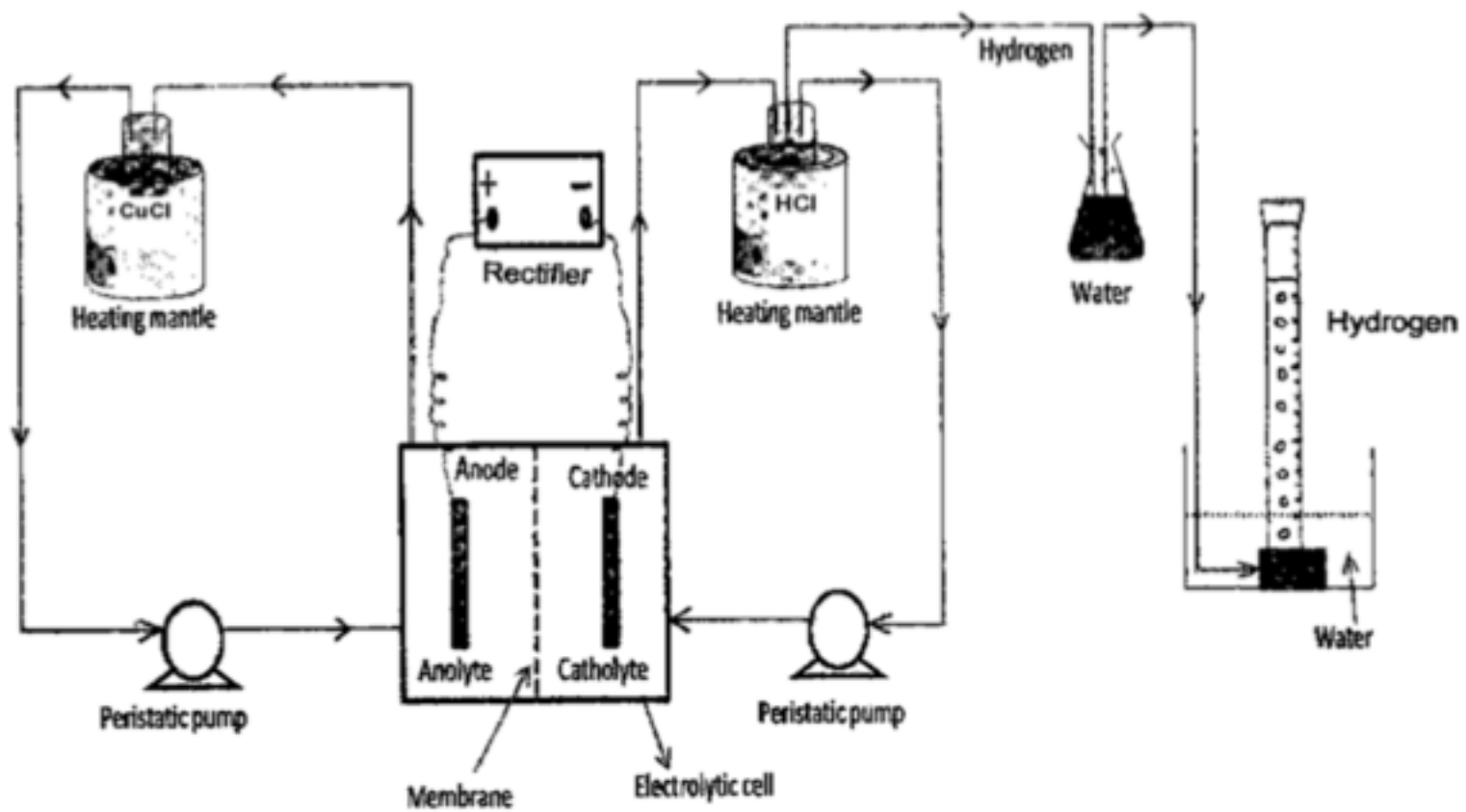
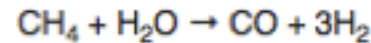


Fig 1. Cell Set-Up for the hydrogen generation through CuCl-HCl electrolysis

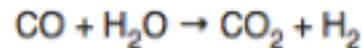
Biomass/Syngas

Steam Reforming Reaction: CH₄ to H₂ and CO



At high temperatures (700 – 1100 °C) and in the presence of a metal-based catalyst (nickel), **steam** reacts with methane to yield carbon monoxide and hydrogen. ...

Water Shift Gas Reaction: CO to H₂



The shift reaction will operate with a variety of catalysts between 400°F and 900

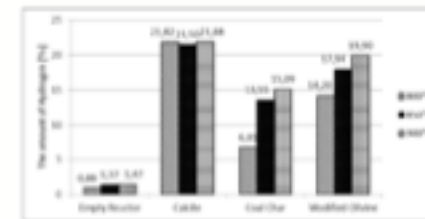
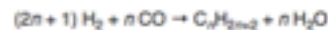


Fig. 3. Average percentage representation of hydrogen for the studied catalysts at 400, 600 and 800°C

Fischer-Tropsch Reaction: H₂ and CO to Liquid Fuel

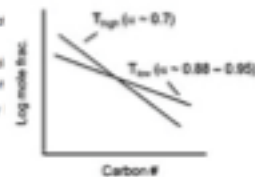
Reaction mechanism [\[edit \]](#)

The Fischer–Tropsch process involves a series of chemical reactions that produce a variety of hydrocarbons, ideally having the formula (C_nH_{2n+2}). The more useful reactions produce **alkanes** as follows:



where *n* is typically 10–20. The formation of methane (*n* = 1) is unwanted. Most of the alkanes produced tend to be straight-chain, suitable as **diesel fuel**. In addition to alkane formation, competing reactions give small amounts of **alkenes**, as well as **alcohols** and other oxygenated hydrocarbons.^[4]

- Nickel (Ni) tends to promote methane formation, as in a [methanation process](#); thus generally it is not desirable
- Iron (Fe) is relatively low cost and has a higher water-gas-shift activity, and is therefore more suitable a lower hydrogen/carbon monoxide ratio (H₂/CO) syngas such as those derived from coal gasification
- Cobalt (Co) is more active, and generally preferred over ruthenium (Ru) because of the prohibitively cost of Ru
- In comparison to iron, Co has much less water-gas-shift activity, and is much more costly.



Low T	Sasol Arge	High T	Sasol Synthol
- low C ₁ - C ₆	13.3	- higher C ₁ - C ₆	43.0
- low C ₇ - C ₁₀	17.9	- higher C ₇ - C ₁₀	40.0
- low C ₁₁ - C ₁₅	13.9	- less C ₁₁ - C ₁₅	7.0
- 50-70% wax	51.7	- low wax	4.0
- 225-270°C		- 325 - 350°C	
- α: 0.87*		- α: -0.7	
- gasoline/diesel: 1:2		- gasoline/diesel: 2:1	
- 80° Octane #		- 50-60 Octane #	
- 0-20 Octane #		- 0-40 Octane #	

Dependency of Fischer-Tropsch synthesis ASF distribution on temperature: Product selectivities (in %) of the Sasol Arge (220 °C) and Sasol Synthol (340 °C) processes are also plotted. Source: [Biomass to liquid: sustainable energy from biomass](#), 2010

Biomass/Syngas

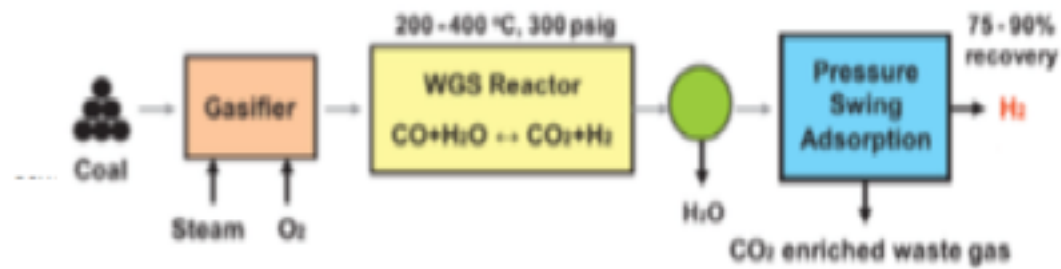


Figure1: Conventional process flow sheet for the production of hydrogen from coal gasification (Bell et al., 2011)

More Polar Molecules will Adsorb



More Polar Molecules will Adsorb

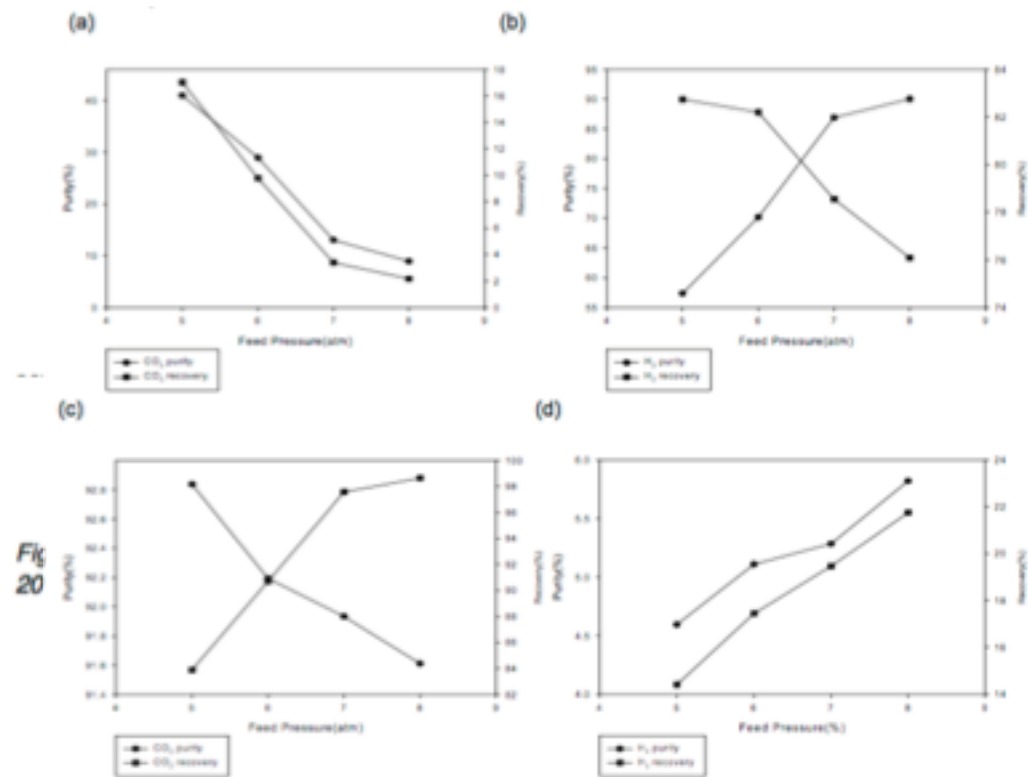


Fig
20

Figure 4: Effect of feed pressure at CO_2 -PSA on (a) CO_2 in top product (b) H_2 in top product (c) CO_2 in bottom product (d) H_2 in bottom product

Beil et al.,

Biological Digestion

[India Biogas Reactor](https://www.youtube.com/watch?v=9kKRdlAFuZw) (https://www.youtube.com/watch?v=9kKRdlAFuZw)



Biogas Reactor for the Developing World (<https://www.youtube.com/watch?v=Cwm5Rm8uIsk>)



Biomass/Syngas

[Single House Biogas](http://www.youtube.com/watch?v=3th2bcqHbsk) (<http://www.youtube.com/watch?v=3th2bcqHbsk>)



Biomass/Syngas

[Biogas in Kenya](http://www.youtube.com/watch?v=qh3mmgiybTw) (<http://www.youtube.com/watch?v=qh3mmgiybTw>)



Photocatalysis

Titania as a photocatalyst

- *Irradiation of semiconductors having a band gap (2 - 4 eV) with UV light energy \geq energy of the band gap E_g*

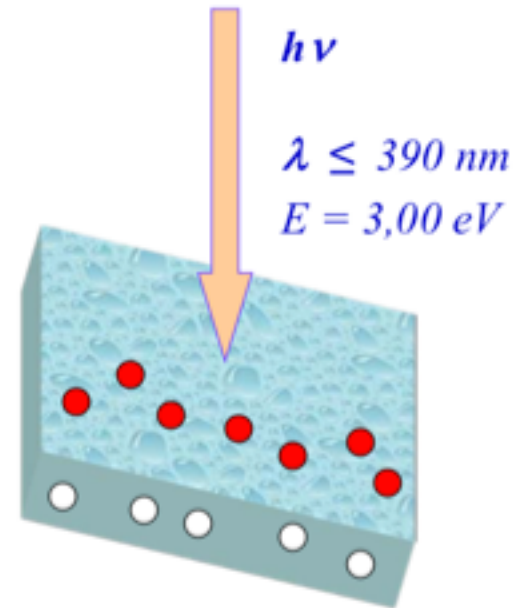
- *Generation of charge carriers*



- *Formation of active radicals (OH^* , O_2^*)*



- *Recombination process*



Titania as a photocatalyst

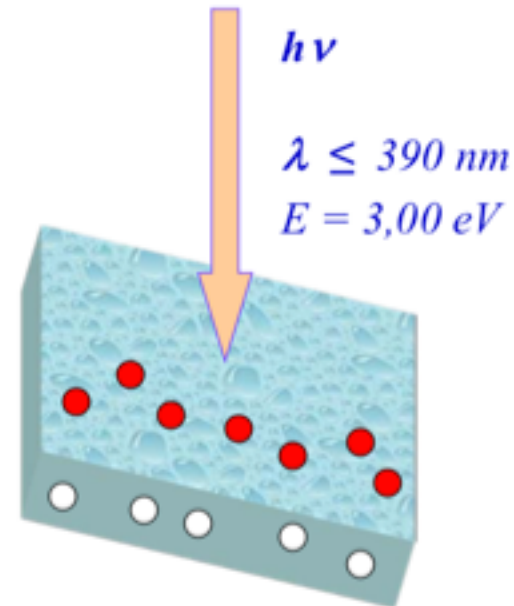
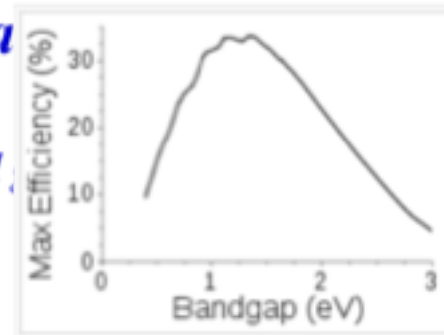
- Irradiation of semiconductors having a band gap, light energy \geq energy of the band gap E_g*
- Generation of charge carriers*



- Formation of active radicals (OH^* , O_2^*)*



- Recombination process*



Water is decomposed using only light

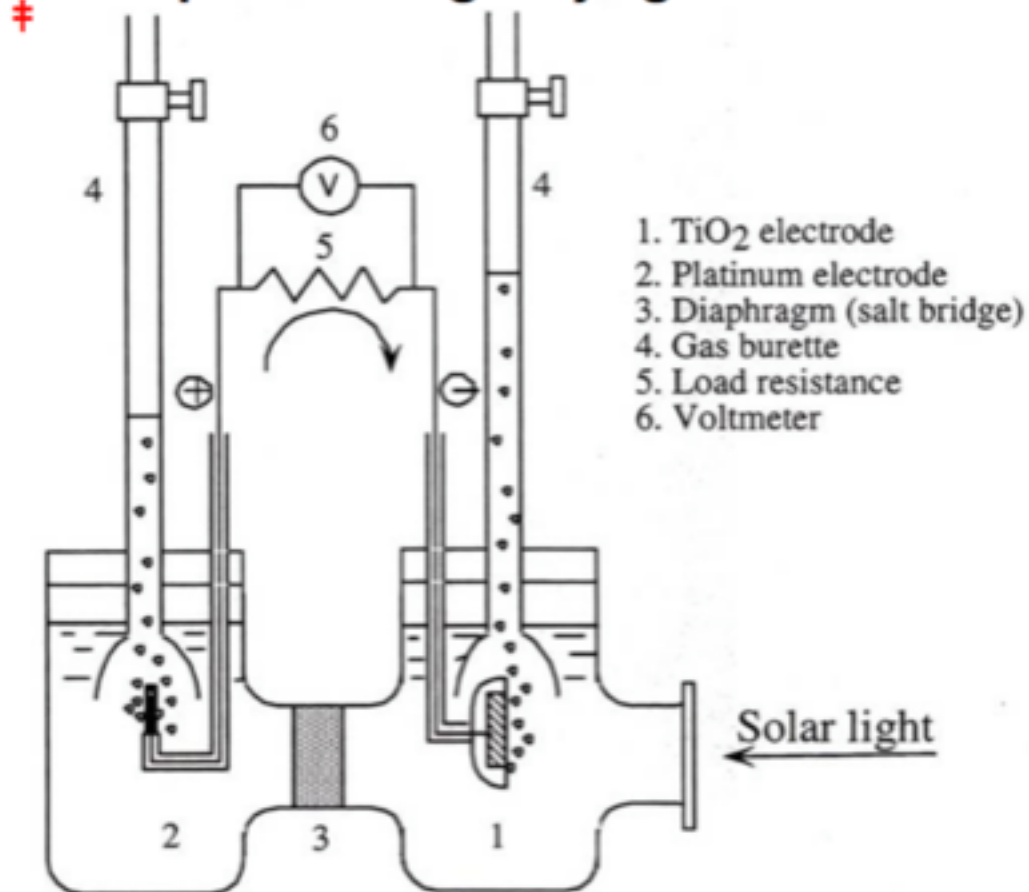
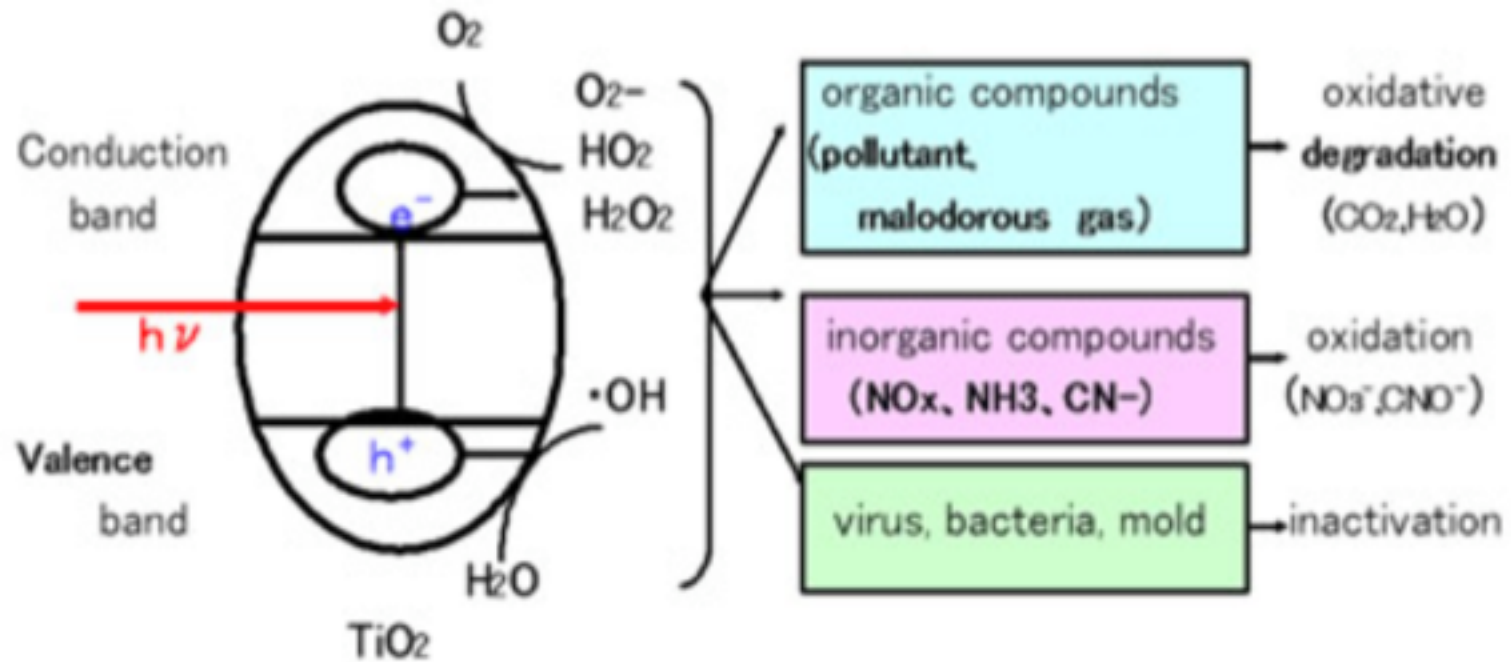


Figure reprinted from;

AKIRA FUJISHIMA, KENICHI HONDA "Electrochemical Photolysis of Water at a Semiconductor Electrode"
Nature 238, 37-38 (1972)

Reaction mechanism of TiO_2 photocatalysis



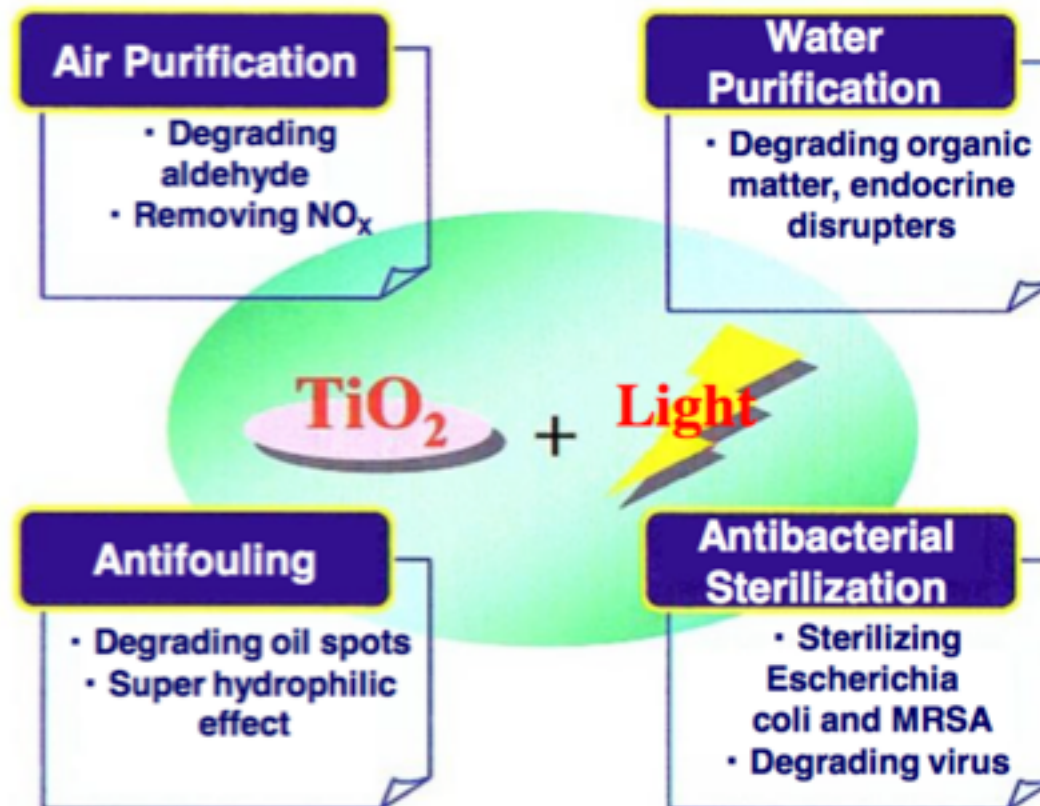
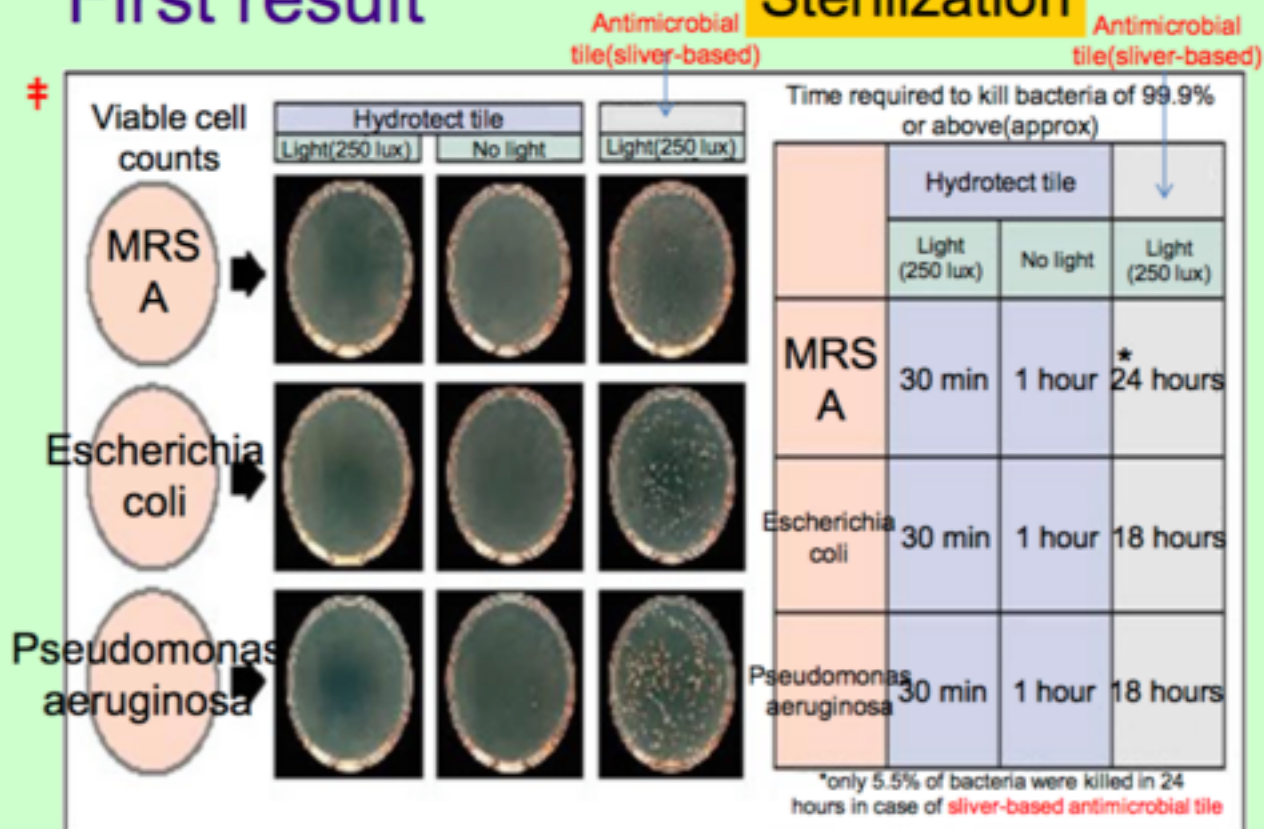


Fig.1 Area of Photocatalyst

Degradation of Bacteria

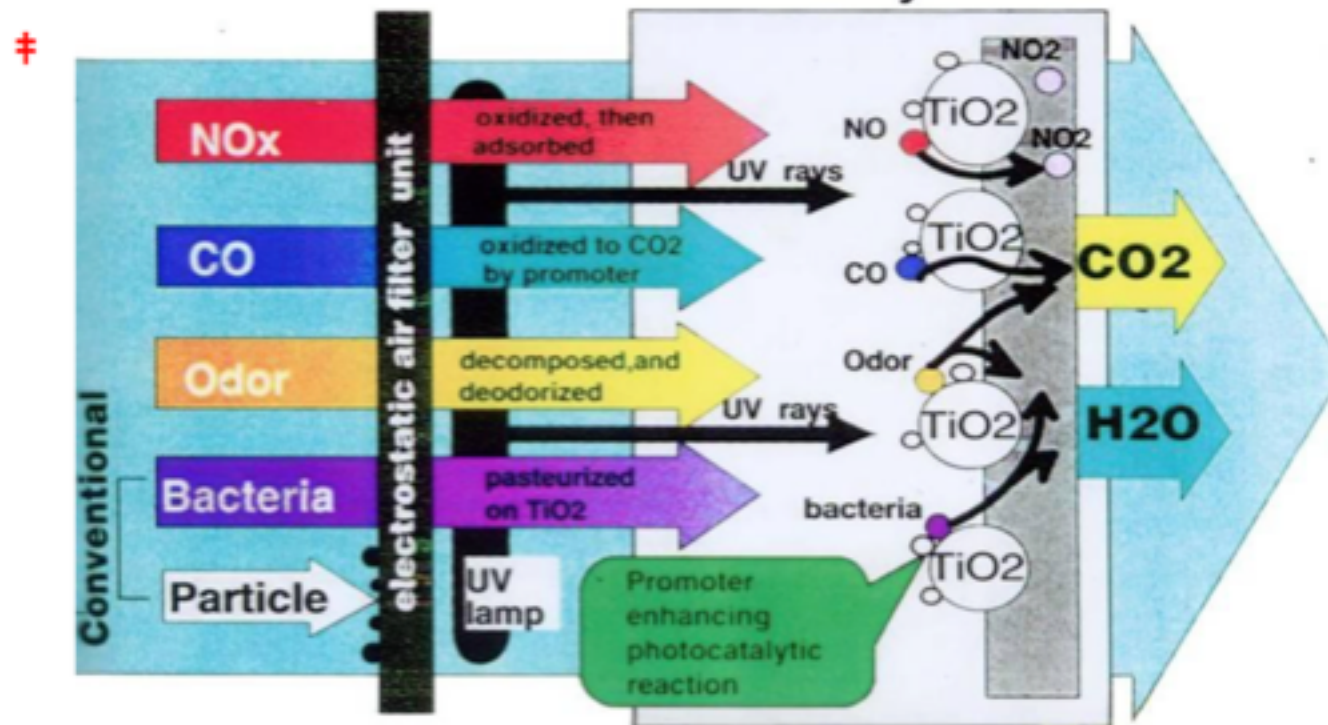
First result

Sterilization



Courtesy of TOTO Ltd.

Photocatalyst Filter



Deodorizing, Sterilization, Degradation

Nano-Catalyst Synthesized by Flame Spray Pyrolysis (FSP) for visible light Photocatalysis

A dissertation submitted to the Division of Research and
Advanced Studies of the University of Cincinnati

In partial fulfillment of the
requirement for the degree of

DOCTOR OF PHILOSOPHY

In the Chemical Engineering Program of School of Energy, Environmental,
Biological and Medical Engineering

by

Siva Nagi Reddy Inturi

Committee:

Professor Panagiotis (Peter) G. Smirniotis (Chair)

Professor Makram Suidan

Professor Vesselin Shanov

Professor Gregory Beaucage

Assoc. Professor Anastasios Angelopoulos

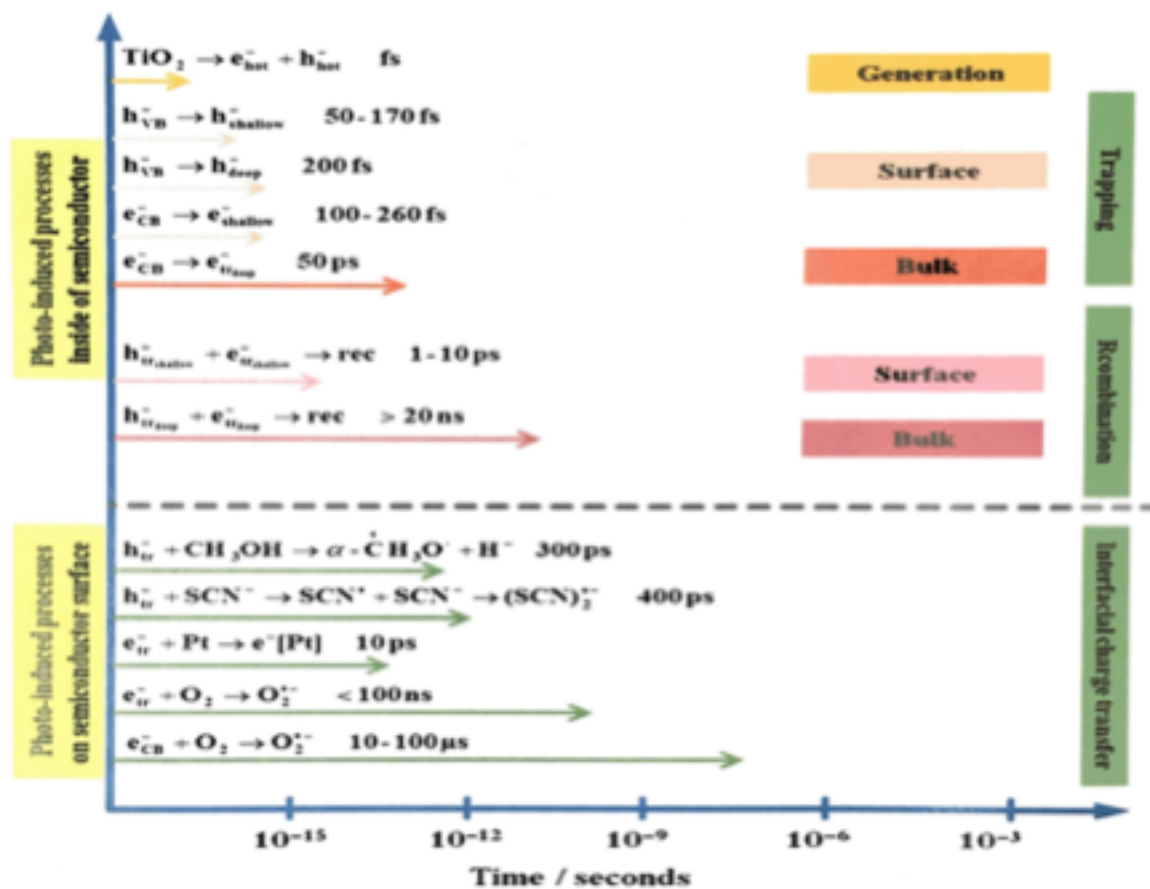


Figure 1.2: The general mechanism for heterogeneous photocatalysis on TiO₂.

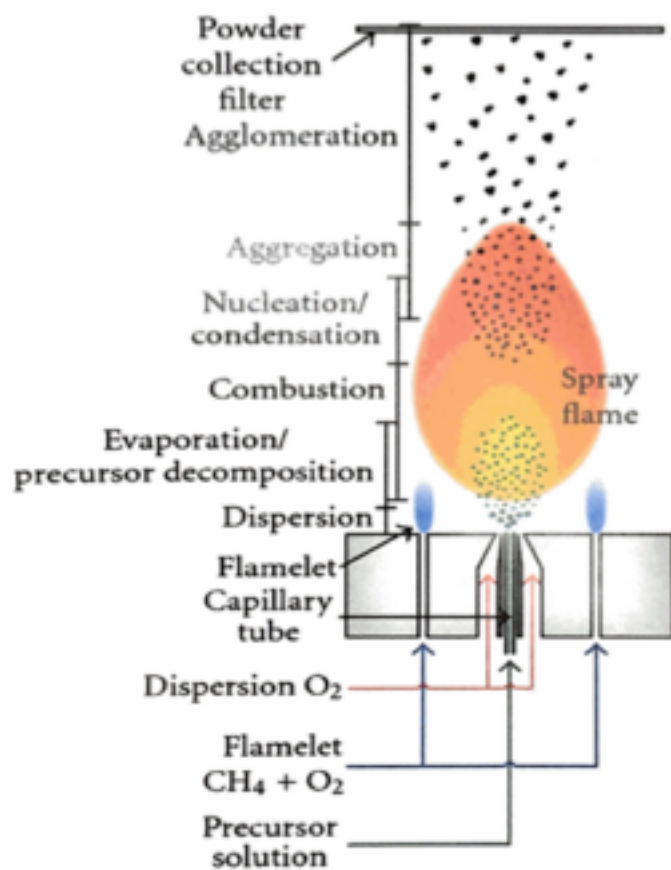


Table 2-5: Photocatalytic activity of the catalyst used in the present study

Catalyst	Absorption region	Band gap (eV)	K_A ($\text{m}^3\text{g}^{-1}\text{s}^{-1}$)
P25	UV	3.11	0.051
FSP TiO ₂	UV	3.08	0.098
Ce/TiO ₂	UV	3.13	0.014
Co/TiO ₂	Visible	2.54	0.021
Cr/TiO ₂	Visible	2.82	0.616
Cu/TiO ₂	Visible	2.86	0.010
Fe/TiO ₂	Visible	2.69	0.152
Mn/TiO ₂	Visible	2.86	0.006
Mo/TiO ₂	UV	3.19	0.004
Ni/TiO ₂	Visible	2.37	0.019
V/TiO ₂	Visible	2.63	0.165
Y/TiO ₂	UV	3.20	0.004
Zr/TiO ₂	UV	3.21	0.008

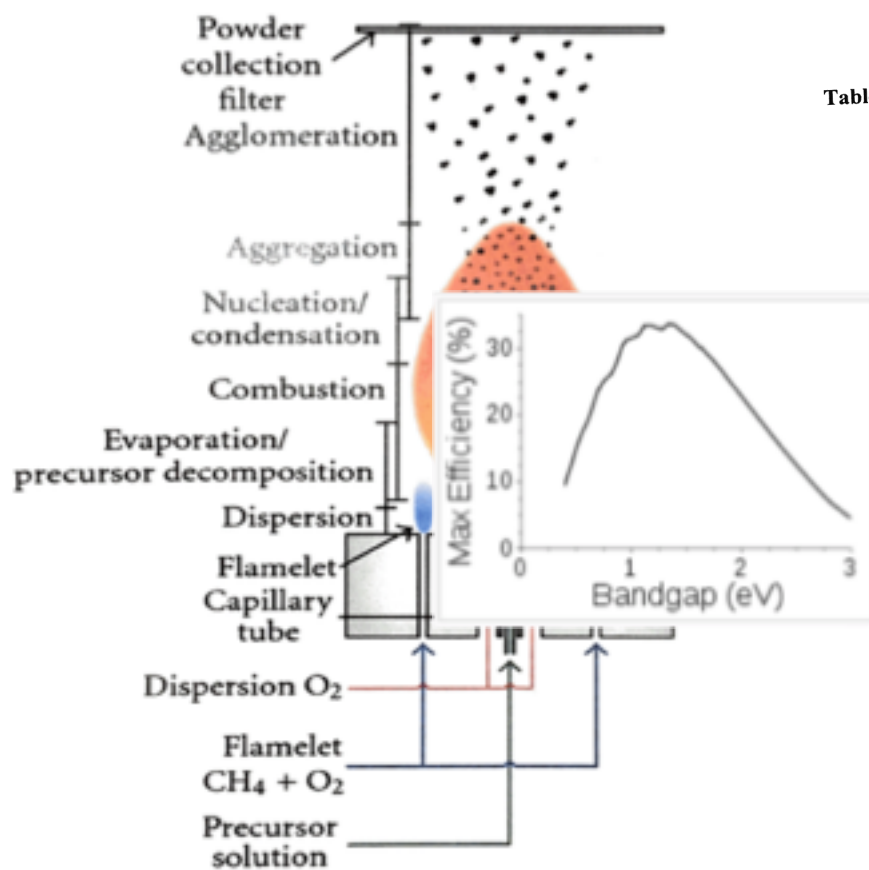


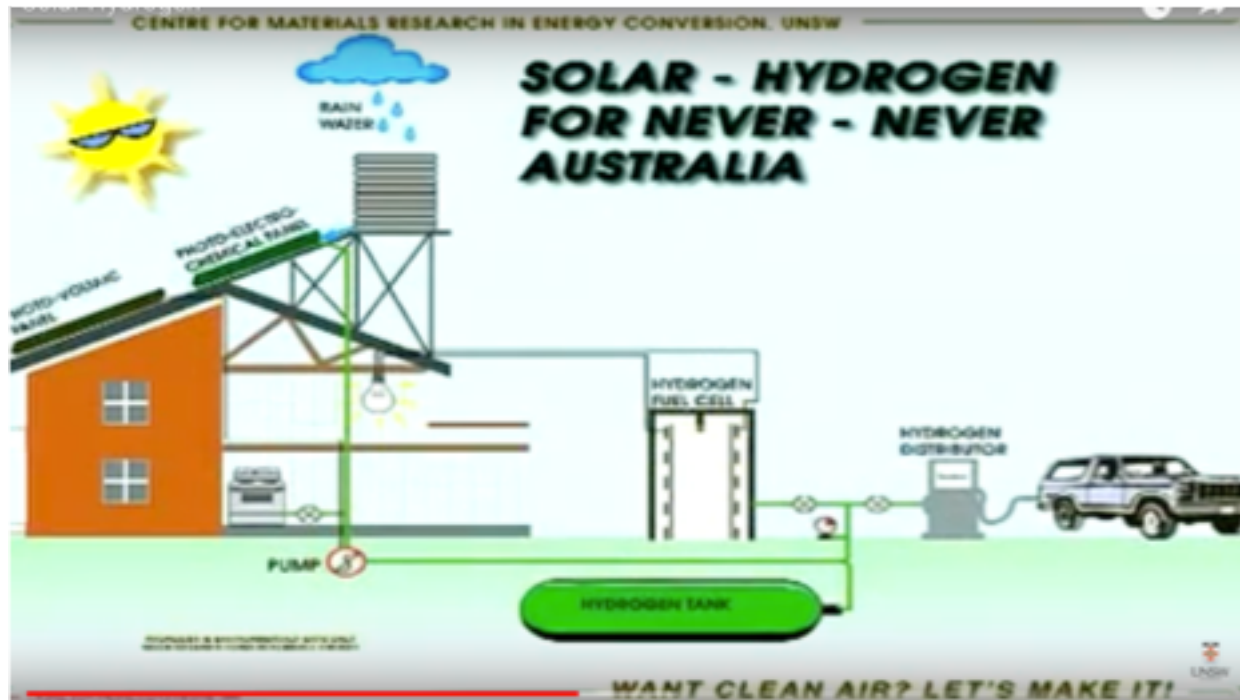
Table 2-5: Photocatalytic activity of the catalyst used in the present study

Catalyst	Absorption region	Band gap (eV)	K_A ($\text{m}^3\text{g}^{-1}\text{s}^{-1}$)
P25	UV	3.11	0.051
FSP TiO ₂	UV	3.08	0.098
Ce/TiO ₂	UV	3.13	0.014
Co/TiO ₂	Visible	2.54	0.021
Cr/TiO ₂	Visible	2.82	0.616
Cu/TiO ₂	Visible	2.86	0.010
Fe/TiO ₂	Visible	2.69	0.152
Mn/TiO ₂	Visible	2.86	0.006
Mo/TiO ₂	UV	3.19	0.004
Ni/TiO ₂	Visible	2.37	0.019
V/TiO ₂	Visible	2.63	0.165
Y/TiO ₂	UV	3.20	0.004
Zr/TiO ₂	UV	3.21	0.008

Solar Thermolysis

[Direct solar thermolysis](http://www.youtube.com/watch?v=fBLGIvm-B2A) (<http://www.youtube.com/watch?v=fBLGIvm-B2A>)

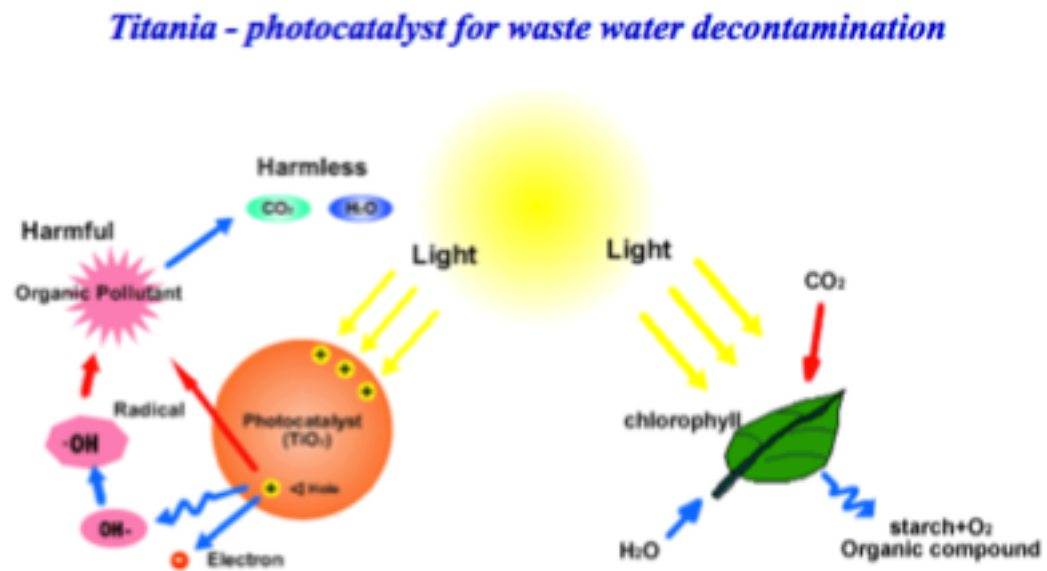
[Titania Catalyst](http://www.youtube.com/watch?v=8kJqsDh8cs0) (<http://www.youtube.com/watch?v=8kJqsDh8cs0>)



Solar Thermolysis

Titania as a photocatalyst

http://www.mvt.ovgu.de/mvt_media/Vorlesungen/VO_ENAP/Folien_ENAP_10.pdf



Titania as a photocatalyst

<https://cdn.intechopen.com/pdfs-wm/51861.pdf>

Chapter 7

Concretes with Photocatalytic Activity

Magdalena Janus and Kamila Zajęc

Additional information is available at the end of the chapter

<http://dx.doi.org/10.5772/64779>

Solar Thermolysis

Titania as a photocatalyst

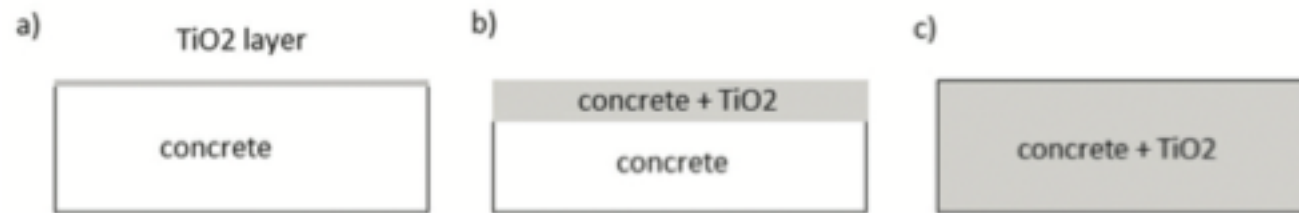


Figure 2. Scheme of possible ways for concrete modification by photocatalysts.

Solar Thermolysis

Titania as a photocatalyst

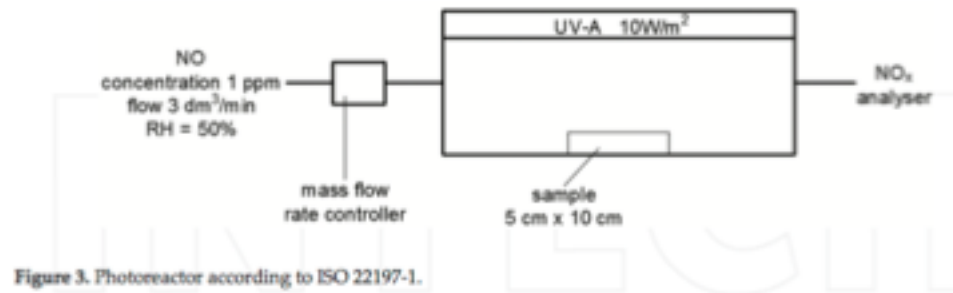


Figure 4. Separate parking lanes at the Leien of Antwerp with photocatalytic pavement blocks [15].

Solar Thermolysis

Titania as a photocatalyst

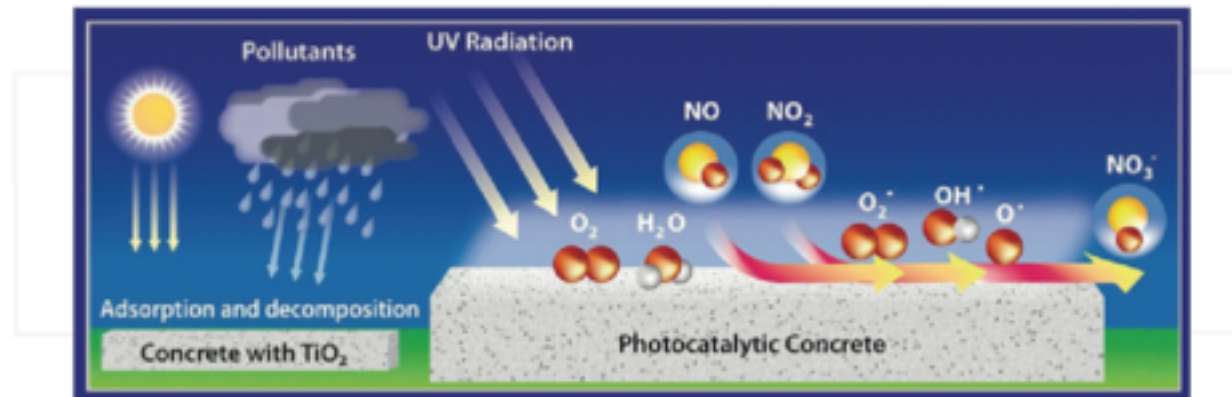


Figure 6. Scheme of photocatalytic air purifying pavement [15].

Solar Thermolysis

Titania as a photocatalyst

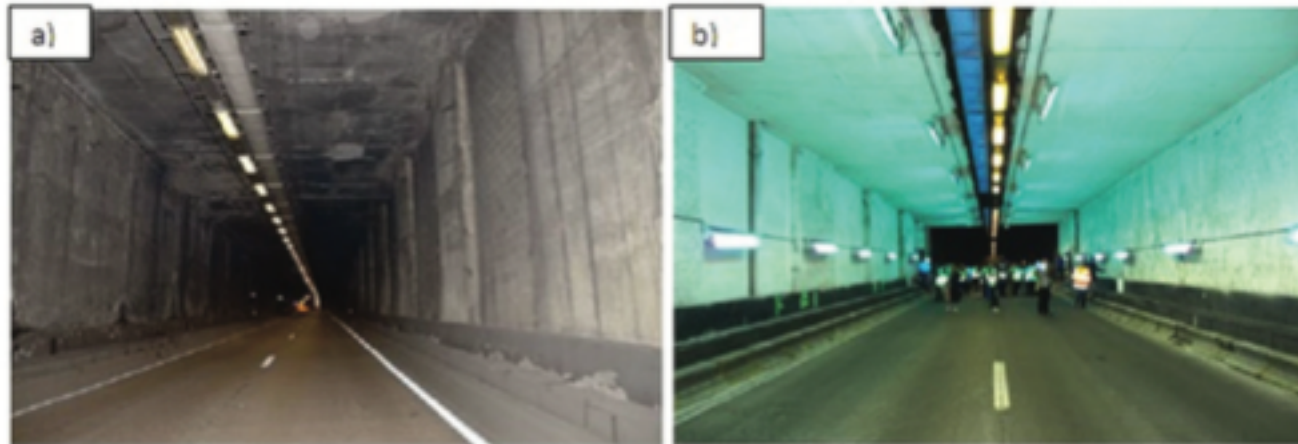


Figure 7. Inside view of test site within Leopold II tunnel in Brussels (a) before renovation, (b) after renovation with using photocatalytic walls [15].

Solar Thermolysis

Titania as a photocatalyst

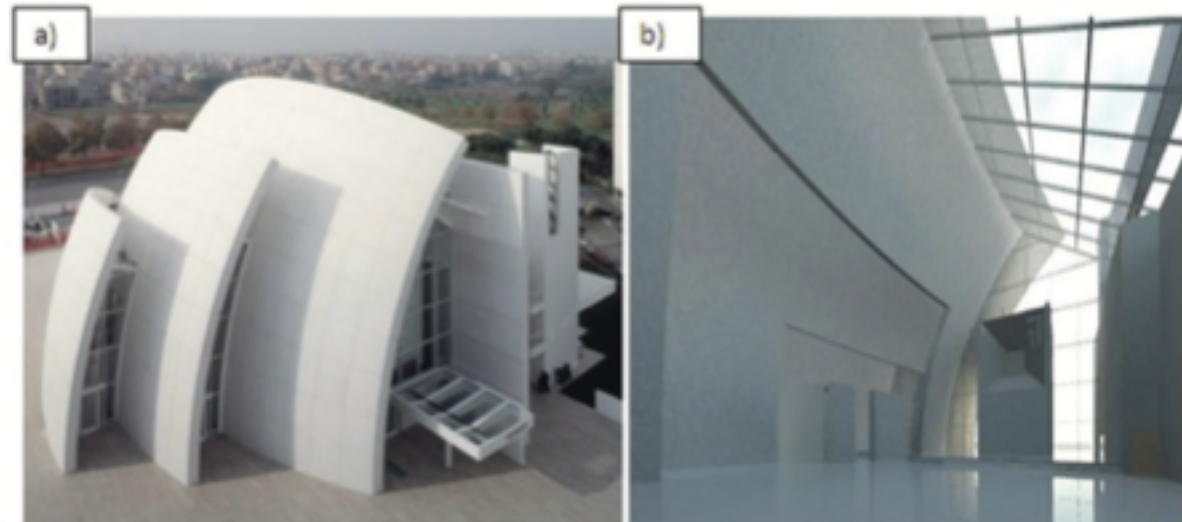


Figure 8. Dives in Misericordia Church in Rome (a), zoom insight (b) [41].

Solar Thermolysis

Titania as a photocatalyst

[42, 43]. It is impressive that according to Fujishima and Zhang [44] by 2003, self-cleaning TiO_2 -based tiles had been used in over 5000 buildings in Japan. Among them the most famous is the Maru Building, located in Tokyo's main business district.

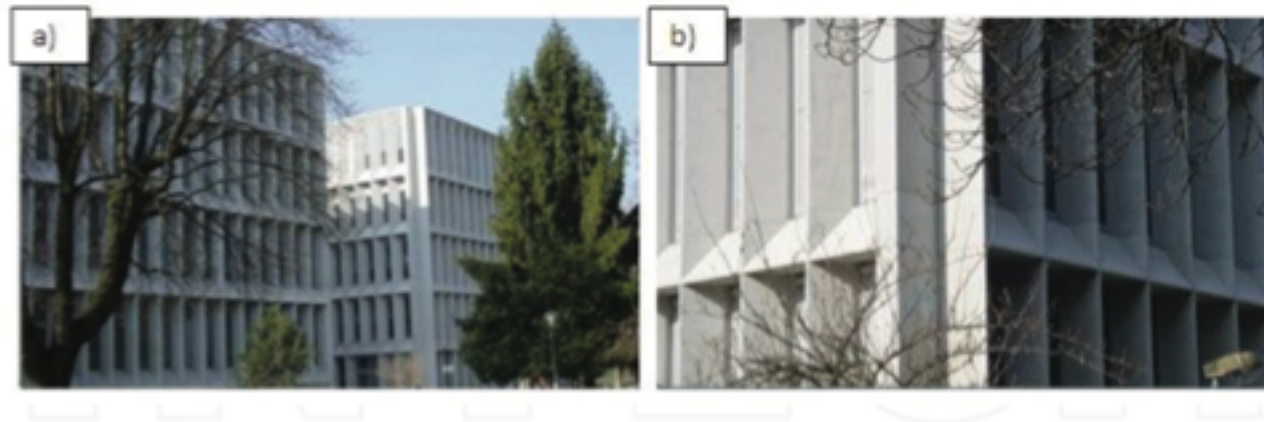


Figure 9. Cité de la Musique et des Beaux- Arts in Chambéry [45].

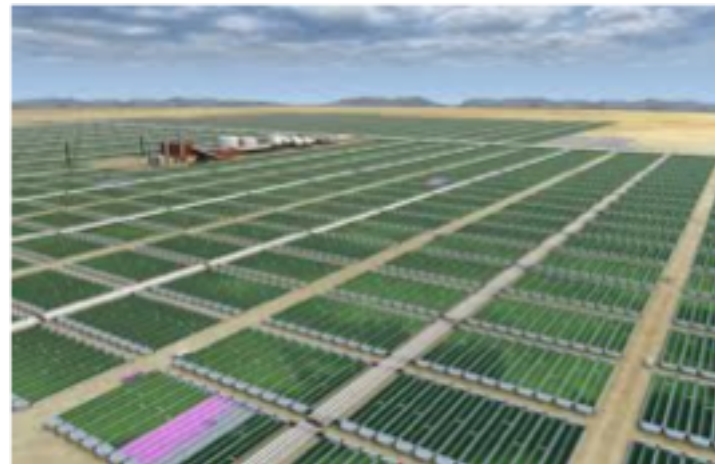
Algae

Algae:

Food

Diesel Fuel

Hydrogen



Spirulina Summary

<http://wellnessmama.com/4738/spirulina-benefits/>

Algae:

Food

Diesel Fuel

Hyd



Spirulina Summary

<http://wellnessmama.com/4738/spirulina-benefits/>

Algae It also contains (per Tablespoon):

Food

Hydrc



[Spirulina Algae in West Africa](https://www.youtube.com/watch?v=CxSA5iiGgiY) (<https://www.youtube.com/watch?v=CxSA5iiGgiY>)



Grow Spirulina in Northern California
<https://www.youtube.com/watch?v=16KfzWau08>

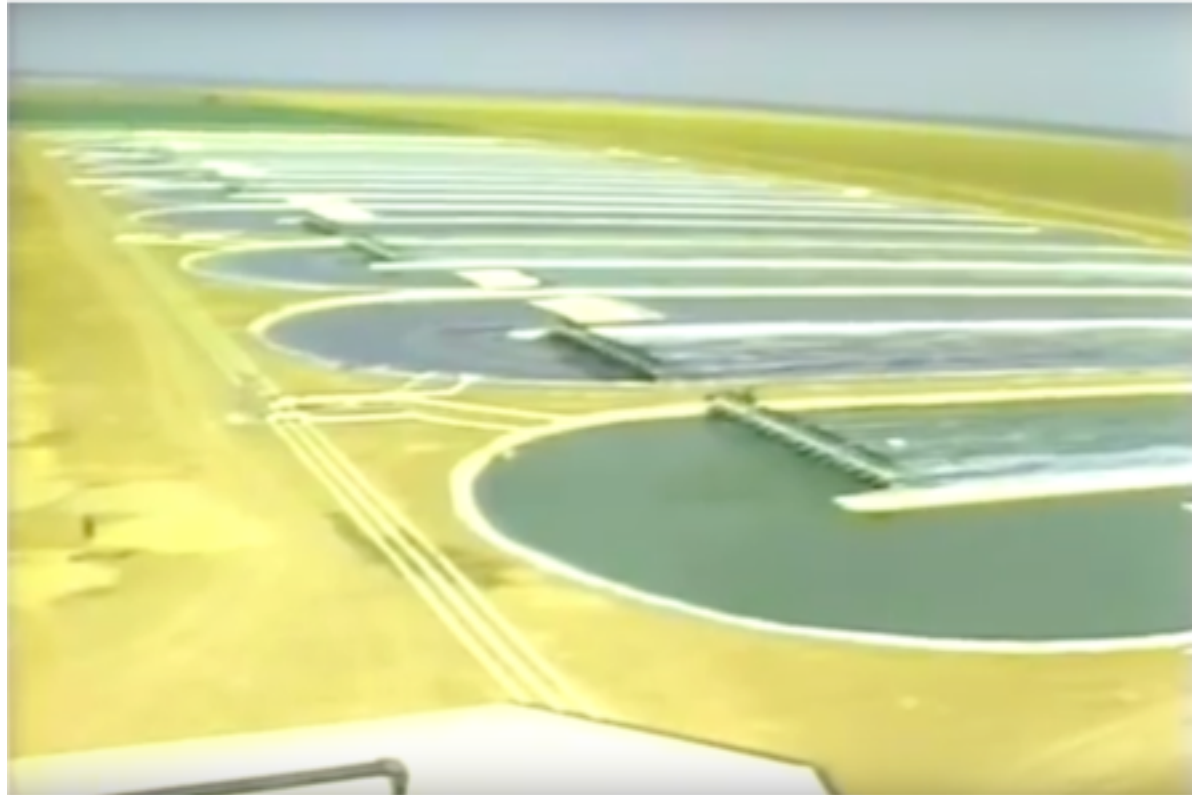


Spirulina in France (<https://www.youtube.com/watch?v=qfCBDyPITS4>)



California (<https://www.youtube.com/watch?v=DpQgNLASec>)

<http://earthrise.com>



[Cooking with Spirulina](https://www.youtube.com/watch?v=_UVMlmlk6Vw) (https://www.youtube.com/watch?v=_UVMlmlk6Vw)



Hydrogen from Algae

Simple schematic for biological hydrogen production

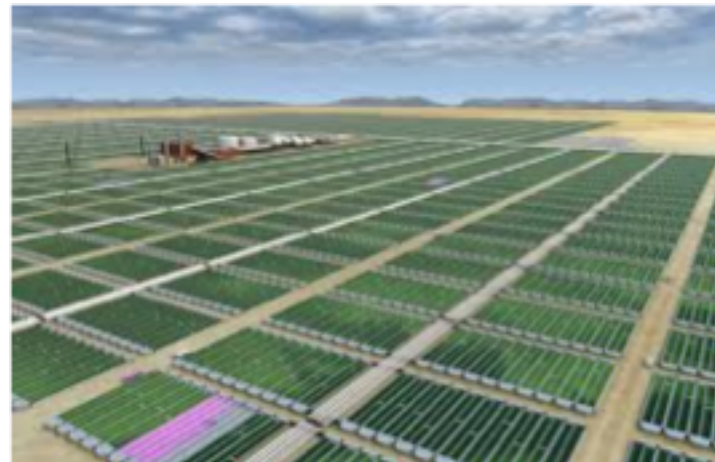
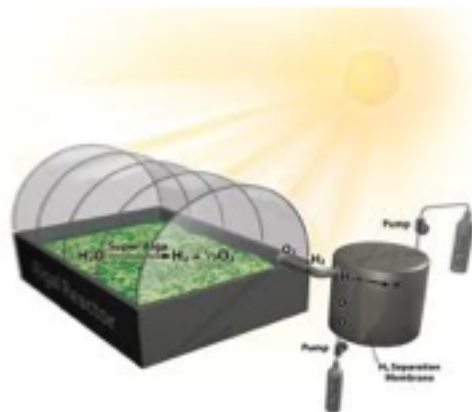
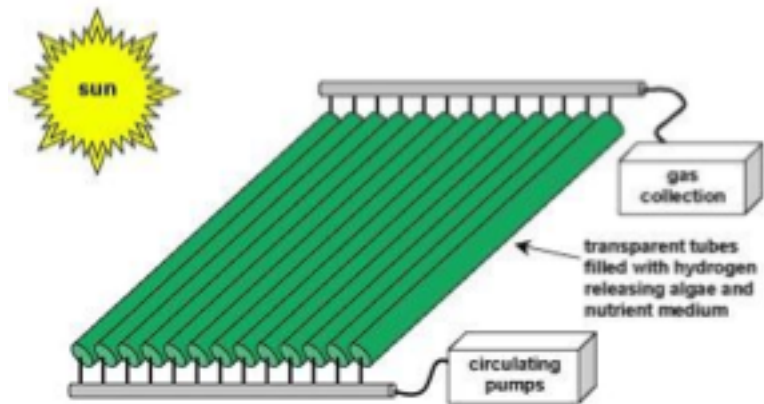


Table 1

Microorganisms used in hydrogen production.

Microorganism	Mode of Operation	References
<i>C. reinhardtii</i> <i>Phaeodactylum tricornutum</i>	Genetic engineering using expressed sequence tags (ESTs)	[30]
<i>Thalassiosira pseudonana</i>		
<i>Cyanidiosclerotium merolae</i>		
<i>Ostreococcus lucimarinus</i>		
<i>Ostreococcus tauri</i>		
<i>Micromonas pusilla</i>		
<i>Fragilariaopsis cylindrus</i>		
<i>Pseudo-nitzschia</i>		
<i>Thalassiosira rotula</i>		
<i>Chlorella vulgaris</i>		
<i>Dunaliella salina</i>		
<i>Micromonas pusilla</i>		
<i>Galdieria sulphuraria</i>		
<i>Porphyra purpurea</i>		
<i>Hibiscus carteri</i>		
<i>Aureococcus anophagefferens</i>		
<i>Chlorella pyrenoidosa</i>	Lipid Biosynthesis	[31]
<i>Chlamydomonas moewusii</i>	Anaerobic Fermentation	[32]
<i>Scenedesmus obliquus</i>	Anaerobic Fermentation	[33]
<i>Anabaena variabilis</i>	Photo-Fermentation	[34]
<i>Rhodobacter sphaeroides</i>	Transcriptional analysis	[29]
<i>Enterobacter aerogenes</i>	Batch Fermentation	[35]
<i>Clostridium butyricum</i>	Anaerobic Fermentation	[36]
<i>Bacillus coagulans</i>	Anaerobic Fermentation	[10]
<i>Clostridium acetobutylicum</i> ATCC 824	Anaerobic Fermentation	[37]
<i>Laminaria japonica</i>	Anaerobic Fermentation	[38]
<i>Gelidium amansii</i>	Dark Fermentation	[39]

Silicon Clusters to Produce H₂



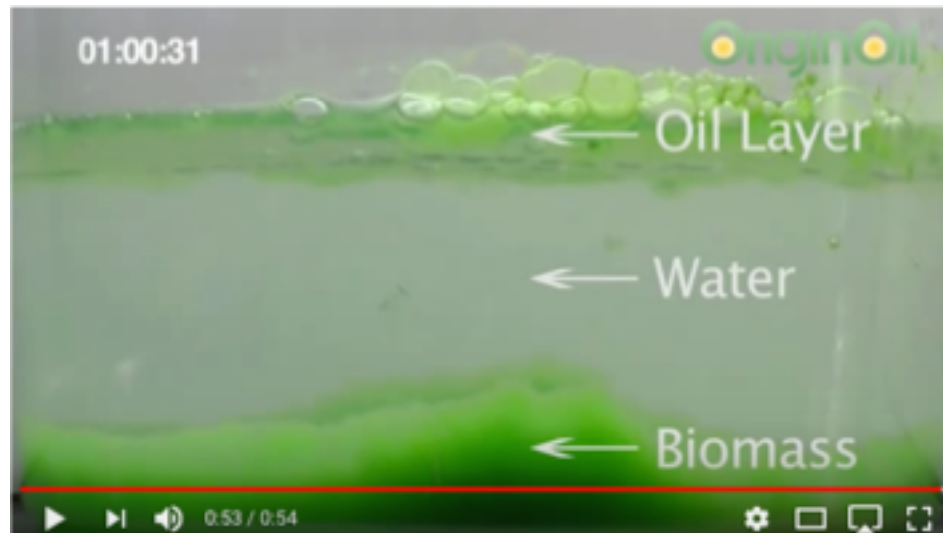
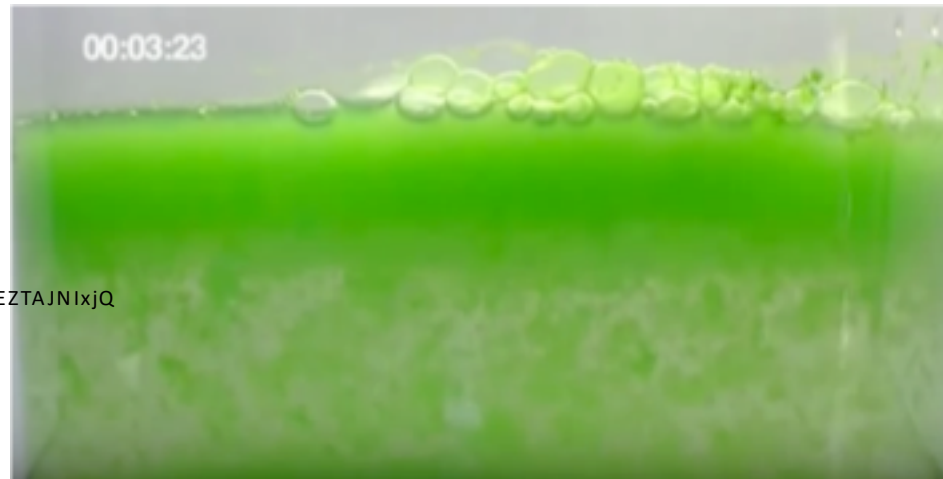
Two stage algae reactor for hydrogen production



Oil from Algae

[Algae oil extraction](https://www.youtube.com/watch?v=aEZTAJNixjQ)

<https://www.youtube.com/watch?v=aEZTAJNixjQ>





Oil from Algae in lab



<https://www.youtube.com/watch?v=oQqlsk3cuWY>

Biofuel from Algae in Vermont



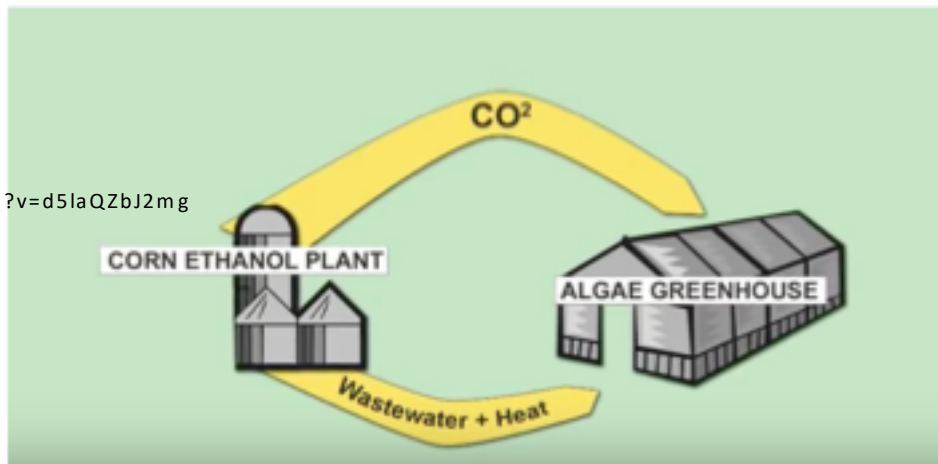
[US DOE Algae to Fuel Promo Video](#)

<https://www.youtube.com/watch?v=IxyvVkeW7Nk>



[Iowa Algae farm](#)

<https://www.youtube.com/watch?v=d5laQZbJ2mg>

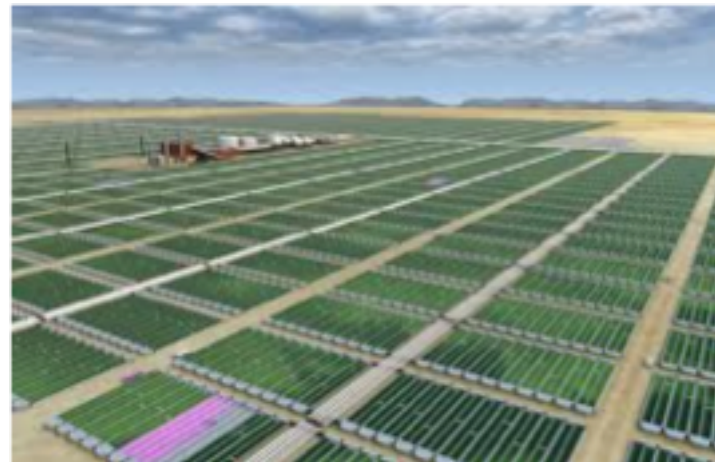
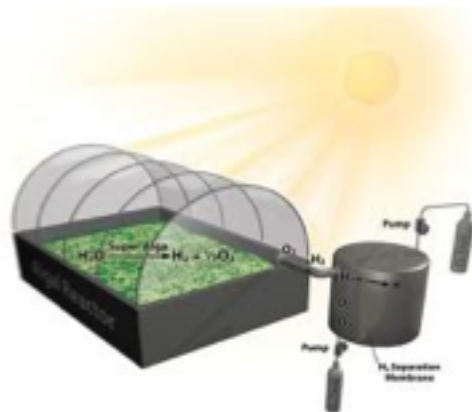
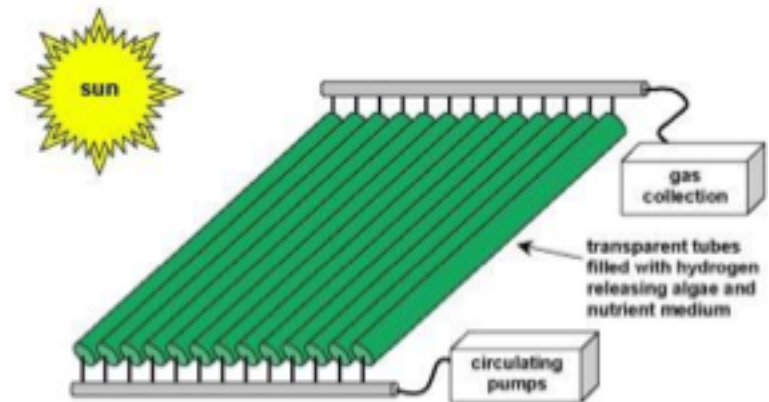


[Algae Tower](#)

[Algae Building in Germany](#)

[NASA Floating Algae Farm Project](#)
(<http://www.youtube.com/watch?v=c7Goyg12Reg>)

Simple schematic for biological hydrogen production



Algae Tower



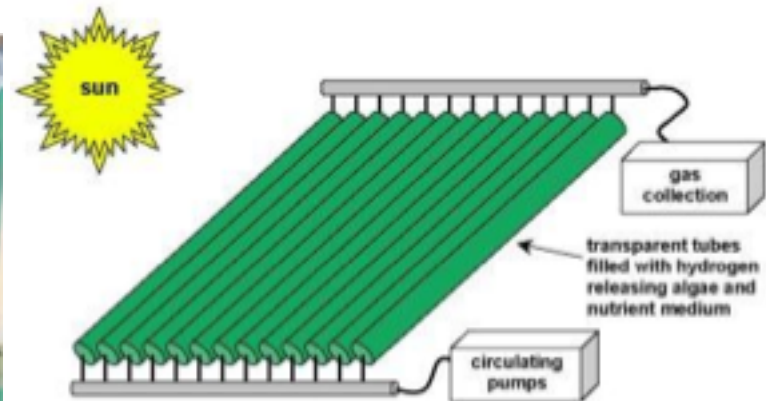
[Hydrogen from Algae](http://www.youtube.com/watch?v=Or_F6qC0sK4)

(http://www.youtube.com/watch?v=Or_F6qC0sK4)

[Hydrogen from Algae Imperial College](https://www.youtube.com/watch?v=OFByDIVRbuc)

(<https://www.youtube.com/watch?v=OFByDIVRbuc>)

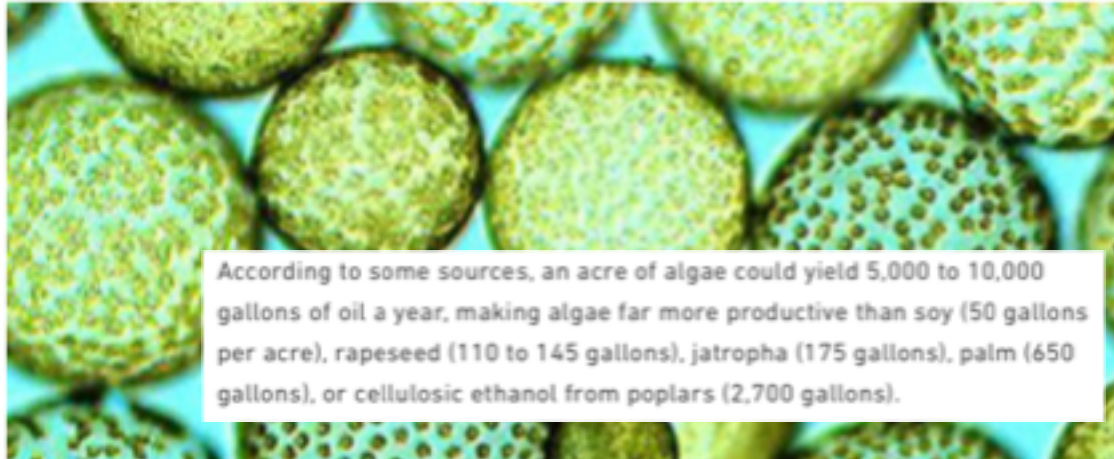
Simple schematic for biological hydrogen production



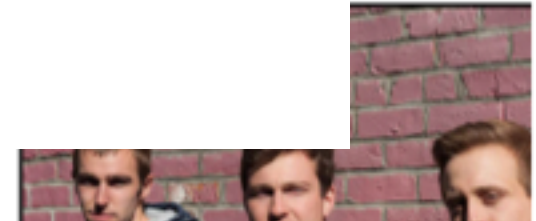
<https://www.greentechmedia.com/articles/read/lessons-from-the-great-algae-biofuel-bubble#gs.PJr1F3k>

Entrepreneurs can have tunnel vision. VC herd mentality doesn't produce results. Physics and thermodynamics are fairly important in energy applications.

ERIC WESOFF | APRIL 19, 2017



According to some sources, an acre of algae could yield 5,000 to 10,000 gallons of oil a year, making algae far more productive than soy (50 gallons per acre), rapeseed (110 to 145 gallons), jatropha (175 gallons), palm (650 gallons), or cellulosic ethanol from poplars (2,700 gallons).



Jim Lane of *Biofuels Digest* authored what was possibly history's least accurate market forecast, projecting that algal biofuel capacity would reach 1 billion gallons by 2014. In 2009, Solazyme promised competitively priced fuel from algae by 2012. Algenol planned to make 100 million gallons of ethanol annually in Mexico's Sonoran Desert by the end of 2009 and 1 billion gallons by the end of 2012 at a production rate of 10,000 gallons per acre. PetroSun looked to develop an algae farm network of 1,100 acres of saltwater ponds that could produce 4.4 million gallons of algal oil and 110 million pounds of biomass per year.

Nothing close to 1 billion (or even 1 million) gallons has yet been achieved -- nor has competitive pricing.

Today, the few surviving algae companies have had no choice but to adopt new business plans that focus on the more expensive algae byproducts such as cosmetic supplements, nutraceuticals, pet food additives, animal feed, pigments and specialty oils. The rest have gone bankrupt or moved on to other markets.

- **Algae Floating Systems** is "temporarily shifting its focus away from fuel to nutraceutical and animal feed markets."
- **Algenol** intended to use nitrogen-fixing blue-green algae (cyanobacteria) in photobioreactors to produce ethanol directly. With tens of millions of dollars in public money and hundreds of millions in private-sector investment, **Algenol** once claimed its technology "enables the production of the four most important fuels (ethanol, gasoline, jet, and diesel fuel) for around \$1.30 per gallon each using proprietary algae, sunlight, carbon dioxide and saltwater at production levels of 8,000 total gallons of liquid fuel per acre per year." In 2015, the firm fired its CEO and shifted its focus to carbon capture and nutraceuticals.
- **Algae Tec**: An Australian PBR penny stock company with algae oil and algae byproduct dreams.
- **Algix** develops fish farms and algae harvest equipment.
- **AlgaeLink** was a sketchy retailer of photobioreactors and commercial algae cultivation equipment.
- **Alga Technologies** grows algae in closed bioreactors to harvest astaxanthin in Israel's Arava desert.
- **Aquaflow Bionomics** once intended to produce biofuel from wild algae harvested from open-air environments. The company is now a biofuel site developer called **NXT Fuels**.
- **Aurora Biofuels**: Aurora moved from fuel to food with its genetically modified algae in 2011. The firm went **bankrupt** in 2015 after winning more than \$23 million from Oak, Noventi Ventures and Gabriel Venture Partners.
- **Cellana** and its Hawaii-based algae feedstock production system received DOE funding to boost algae productivity as a way to reduce cost. The firm produces DHA and omega-3 EPA and DHA oils, animal feed/food, and biofuel feedstocks.
- **Global Algae Innovations** is exploring algal biofuels at a 3.2-acre algae farm co-located with a power plant in **Hawaii**. The firm has received \$11 million from the U.S. DOE.
- **GreenFuel Technologies**, long bankrupt, was backed with more than \$27 million in funding from Polaris Ventures, Draper Fisher Jurvetson and Access Private Equity.
- **Heliae** raised \$80 million from two \$20 billion food conglomerates in 2016, and has spent years developing a "platform technology" to produce nutraceuticals, personal care products and perhaps fuel through a mixture of phototrophic and fermentation processes.
- **LiveFuels** received \$10 million in funding from The Quercus Trust in 2007. Lissa Morgentahler-Jones and David Jones are still listed as officers of the firm on LinkedIn.
- **OriginOil** is now **OriginClear** and has shifted to water decontamination.
- **PetroAlgae** changed its name to **Parabel** as it shifted from fuel to foods in 2012.

- **Phycal** received significant DOE funding to design a high-yield algae farm and biorefinery in Hawaii.
- **Pond Technologies** is cultivating algae for carbon capture and nutraceuticals.
- **Renewable Algal Energy** is a microalgae products company that received DOE funding to prove out its algal oil harvesting and extraction technologies.
- **Sapphire Energy** produces omega-3 oils and animal feed ingredients. Sapphire raised more than \$100 million from Bill Gates' Cascade Investments and ARCH Venture Partners.
- **Seambiotic** uses raceway/paddle-wheel open pond algae cultivation. According to Israel 21C, Seambiotic "recently launched a commercial algae farm in China" to produce a "valuable nutraceutical food additive."
- **Solix**, once a well-funded algae fuel aspirant, repositioned itself as an astaxanthin, DHA, and omega-3 supplier.
- **Synthetic Genomics**, founded by Craig Venter and ExxonMobil, announced earlier this year that it has extended its agreement on joint research into advanced algae biofuels "after making significant progress in understanding algae genetics, growth characteristics and increasing oil production."
- **TerraVia** (formerly Solazyme) shifted from supplying fuels to oils, algal flour and proteins with a heterotrophic process that ferments genetically modified algae fed sugars.
- **XL Renewables** developed algal production systems using dairy waste streams, then changed its name to Phyco Biosciences and went out of business.

Considering the immense technical risks and daunting capital costs of building an algae fuel company, it doesn't seem like a reasonable venture capital play. And most — if not all — of the VCs I've spoken with categorize these investments as the longer-term, long-shot bets in their portfolio. But given the size of the liquid fuels market, measured in trillions of dollars, not the customary billions of dollars, it makes some sense to occasionally take the low-percentage shot.

Vertical Farming in Cincinnati

